Hybrid Cold-Formed Steel Structural Systems for Buildings

A Thesis submitted in fulfilment for the degree of

Doctoral of Philosophy

By

Nima Usefi

WESTERN SYDNEY UNIVERSITY

Centre for Infrastructure Engineering,
Western Sydney University

September 2020

ABSTRACT

Cold-formed steel (CFS) shear walls or strap-braced walls are the primary lateral load resisting components in light-weight steel framed (LSF) structures. Despite the increasing demand on the application of CFS systems in mid-rise construction, the relatively low lateral load resistance capacity of these systems has remained one of the major obstacles for further growth, as this low resistance becomes problematic in their use in cyclonic wind regions or highly seismic zones. In this thesis, in order to address this issue, a new Hybrid CFS wall composed of CFS open sections and square hollow sections (SHS) is developed and investigated. The proposed hybrid system is suitable for light-weight steel structures for mid- to high-rise construction, due to its satisfactory lateral load resistance. The thesis presented provides the results of the study which contains experimental and numerical investigation as outlined in the following.

In the first stage of this study, a comprehensive literature review was conducted to reveal the existing gaps in the previous studies on CFS structures under lateral loads. It was found that various research studies have been undertaken in order to improve the behaviour of CFS wall frames in compliance with increased demands for mid-rise construction. Although some of these new systems can improve the seismic performance of shear walls by providing superior shear resistance, the mass of the entire wall is much higher than that of CFS frames, which increases the dead load of the shear wall and consequently the seismic base shear of the building during an earthquake. Besides, the design procedures for stronger CFS walls is not provided in the available CFS provisions; and therefore, the development of new CFS wall panels with a higher strength to weight ratio is deemed necessary.

In the second stage, a series of full-scale experimental tests were performed on seventeen hybrid CFS wall panels in order to investigate their lateral performance, shear resistance, failure modes and energy absorption. The behaviour of the proposed hybrid wall panels was evaluated through both cyclic and monotonic loading protocols. The design parameters of the wall panels were also obtained using Equivalent Energy Elastic-Plastic (EEEP) curve and some seismic characteristics such as ductility, stiffness and response modification factors were evaluated. A comparison between hybrid CFS walls in this study and 87 previously tested CFS wall panels from 28

references in terms of strength to weight ratio was also conducted.

In the third stage of this thesis, a comprehensive study was performed on the theories and applications of the numerical models for analysis of the lateral behaviour of CFS wall systems during the past several decades, and all existing numerical methods for simulating the behaviour of CFS shear walls were accordingly classified. The study looked at the challenges and gaps that need to be addressed in future numerical research studies. The numerical models for analysing the lateral behaviour of CFS shear walls including their strengths, weaknesses, limitations of the employed behavioural models, contributing factors, and parameters and functions influencing their performance were discussed and compared with each other. The existing models were grouped into two categories: micro modelling methods, which simulate fine-scale details; and macro modelling methods, which amalgamate details into selected categories for further simplification. Also, a numerical study was performed to compare the results of micro and macro modelling of CFS wall panels under lateral load using ABAQUS and Opensees programs, respectively.

In stage four of this study, proposed hybrid wall panel was further developed, and twenty new wall configurations were evaluated using non-linear finite element analysis, aiming to further investigate the seismic performance of CFS hybrid walls. The numerical modelling approach including material modelling, connection modelling, interactions, shell details, solvers, boundary condition modelling were described in details. The numerical models were first verified against the experimental test results. Then the new hybrid wall panels were analysed and the results were compared with each other. It was found that the developed numerical models of hybrid CFS wall panels are efficient systems proven to be able to enhance the lateral performance of light-weight steel structures for mid- to high-rise construction.

Finally, in the last stage, a sustainability analysis was performed which could be of interest to all stakeholders including owners, builders and investors, when assessing the potential use of hybrid CFS systems, in particular for mid-rise buildings. In addition of the sustainability analysis, economic and social costs of hybrid CFS building were evaluated since these parameters are of great importance to decision-makers when it comes to deciding on promoting this system in comparison with the conventional systems. At this stage, the performance of a hybrid CFS system for structural frames

of North American buildings was evaluated and a multidimensional comparison between this system and conventional hot-rolled steel (HRS) structural frames in terms of structural behaviour, environmental impact (sustainability), construction cost and social impacts was provided.

ACKNOWLEDGMENTS

Statement of Authentication

The work presented in this thesis is, to the best of my knowledge and belief, original except as acknowledged in the text. I hereby declare that I have not submitted this material, either in full or in part, for a degree at this or any other institution.
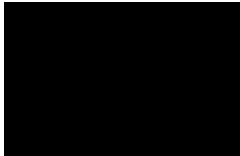
Nima Usefi

PUBLICATIONS DURING CANDIDATURE

Publications made during the PhD candidature (March 2017- September 2020) are listed below. Each publication covers a chapter in this thesis. In addition, articles not entirely related to the thesis topic are also included in this list.

Journal papers	Related Chapter	Year	Journal
Pezhman Sharafi, Mina Mortazavi, **Nima Usefi**, Kamyar Kildashti, Hamid Ronagh, and Bijan Samali. "Lateral force resisting systems in lightweight steel frames: Recent research advances." **Thin-Walled Structures,** 130 (2018): 231-253. https://doi.org/10.1016/j.tws.2018.04.019 (Contribution: Investigation, Resources, Methodology Writing - Original Draft, Visualization, Writing - Review & Editing)	Chapter 2	2018	Q1
Nima Usefi, Hamid Ronagh, and Pezhman Sharafi. "Lateral performance of a new hybrid CFS shear wall panel for mid-rise construction." **Journal of Constructional Steel Research,** 168 (2020): 106000. https://doi.org/10.1016/j.jcsr.2020.106000	Chapter 3	2020	Q1
Nima Usefi, and Hamid Ronagh. "Seismic characteristics of hybrid cold-formed steel wall panels." In **Structures**, vol. 27, pp. 718-731. Elsevier, 2020. https://doi.org/10.1016/j.istruc.2020.06.033	Chapter 4	2020	Q1
Nima Usefi, Pezhman Sharafi, and Hamid Ronagh. "Numerical models for lateral behaviour analysis of cold-formed steel framed walls: State of the art, evaluation and challenges." **Thin-Walled Structures,** 138 (2019): 252-285. https://doi.org/10.1016/j.tws.2019.02.019	Chapter 5	2019	Q1
Nima Usefi, Hamid Ronagh, Pezhman Sharafi, "Modelling and design of hybrid cold-formed steel shear wall panel", **Thin-Walled Structures,** 157 (2020): 107084. https://doi.org/10.1016/j.tws.2020.107084	Chapter 7	2020	Q1
Nima Usefi, Pezhman Sharafi, Mina Mortazavi, Hamid Ronagh, Bijan Samali, "Structural performance and sustainability assessment of hybrid-cold formed modular steel frame", **Journal of Building Engineering**, *Inpress*, 2020.	Chapter 8	2020	Q1
Reza Ayatollahi, **Nima Usefi**, Hamid Ronagh, Mohsen Izadinia, and Mohammad Reza Javaheri. "Performance of gypsum sheathed CFS panels under combined lateral and gravity loading." **Journal of Constructional Steel Research** 170 (2020): 106125. https://doi.org/10.1016/j.jcsr.2020.106125	-	2020	Q1
Shahrzad Kasaeian, **Nima Usefi**, Hamid Ronagh, Saeed Dareshiri, "Seismic performance of CFS strap braced walls using capacity-based design approach", **Journal of Constructional Steel Research**, https://doi.org/10.1016/j.jcsr.2020.106317	-	2020	Q1

Ehsan Taheri, Ahmad Firouzianhaji, **Nima Usefi**, Peyman Mehrabi, Hamid Ronagh, and Bijan Samali. "Investigation of a Method for Strengthening Perforated Cold-Formed Steel Profiles under Compression Loads." <u>**Applied Sciences**</u>, 9, no. 23 (2019): 5085. https://doi.org/10.3390/app9235085	'	2019	Q1
Foad Mohajeri Nav, **Nima Usefi**, and Reza Abbasnia. "Analytical investigation of reinforced concrete frames under middle column removal scenario." <u>**Advances in Structural Engineering**</u> 21, no. 9 (2018): 1388-1401. https://doi.org/10.1177/1369433217746343	'	2018	Q1
Mohammad Bahrani, Amin Nooralizadeh, **Nima Usefi**, and Majid Zargaran. "Seismic evaluation and partial retrofitting of concrete bridge bents with defect details." <u>**Latin American Journal of Solids and Structures**</u>, 16, no. 8 (2019). https://doi.org/10.1590/1679-78255158	'	2019	Q2
Majidi, Leila, **Nima Usefi**, and Reza Abbasnia. "Numerical study of RC beams under various loading rates with LS-DYNA." <u>**Journal of Central South University**</u> 25, no. 5 (2018): 1226-1239. https://doi.org/10.1007/s11771-018-3820-x	'	2018	Q2

Conference papers	Related Chapter	Year
Nima Usefi, Hamid Ronagh, Kamyar Kildashti, and Bijan Samali. "Macro/micro analysis of cold-formed steel members using ABAQUS and OPENSEES." In *Volume of Abstracts, Proceedings of the 13th International Conference on Steel, Space and Composite Structures (SS18)*. 2018.	Chapter 6	2018
Nima Usefi, Hamid R. Ronagh, and Masoud Mohammadi. "Finite element analysis of hybrid cold-formed steel shear wall panels." In *Streamlining Information Transfer between Construction and Structural Engineering: Proceedings of the Fourth Australasia and South-East Asia Structural Engineering and Construction Conference, Brisbane, Australia, December 3-5, 2018*, pp. STR-41. 2018. https://doi.org/10.14455/ISEC.res.2018.148	Chapter 7	2018
Shahab Shafaei, Hamid Ronagh, and **Nima Usefi**. "Experimental evaluation of CFS braced-truss shear wall under cyclic loading." In *Advances in Engineering Materials, Structures and Systems: Innovations, Mechanics and Applications, (SEMC 2019), September 2-4, 2019, Cape Town, South Africa*, p. 192. CRC Press, 2019. https://doi.org/10.1201/9780429426506-32	'	2019
Nima Usefi, Nariman Saeed, and Hamid Ronagh. "Analysis of rehabilitated steel pipes subjected to impact loading using finite element framework." In *Volume of Abstracts: 13th International Conference on Steel, Space and Composite Structures (SS18), 31 January-2 February 2018, The University of Western Australia, Perth, Australia*. 2018.	'	2020

LIST OF ABBREVIATIONS

AISI: American Iron and Steel Institute

BMB: Bolivian Magnesium Board

CFS: Cold-Formed Steel

CSB: Calcium Silicate Board

FCB: Fibre Cement Board

FE: Finite Element

FEM: Finite Element Method

GWB: Gypsum Wall Board

GWP: Global Warming Potential

HLFC: High-Strength Lightweight Foamed Concrete

HRS: Hot-Rolled Steel

HW: Hybrid Wall

LCA: Life Cycle Assessment

LFRS: Lateral Force Resisting System

LSF: Lightweight Steel Framed

MOR: Model Order Reduction

OMRF: Ordinary Moment Resisting Frames

OSB: Oriented Strand Board

SHS: Square Hollow Sections

SLM: Sprayed Lightweight Mortar

Table of Contents

List of tables:

List of figures:

XVI

XVII

XVIII

Chapter 1 Introduction

1.1 General background and problem overview

Cold-formed steel (CFS) structures have been used extensively in construction industry due to their unique advantages such as being cost-effective, lightweight, easy to install, low maintenance and recyclable. In the context of building frames for low rise and mid-rise construction, the CFS structures are often classified as lightweight steel framed (LSF). LSFs have enjoyed a greater market share in high seismic areas compared to their other counterparts [1] in particular due to their light weight as well as economical and environmental advantages they possess. In addition, over the past few years, the development in building automation has led to the invention of many prefabricated CFS wall panels as one of the leading products of modular lightweight steel structures, particularly in mid-rise buildings which has increased the market share of LSF even further. Due to the limited lateral load capacity of these systems when acting as shear wall, further growth has been hindered and highest usage is low rise construction market.

CFS walls are classified as shear walls and strap-braced walls to provide a lateral resisting mechanism in LSF construction. These systems can be used in the low to moderate seismicity zones, when they are designed according to relevant standards [2-15]. Despite the extensive development of research programs on CFS walls in the literature, the current CFS provisions are only limited to shear walls which are only suitable for low-rise buildings. For example, North American standard for seismic design of CFS structural frame (AISI-S400) [16], as the main reference for designing CFS wall panels, only provides guidelines for CFS panels which are restricted by sheathing and framing thicknesses, fastener spacing, screw sizes, and aspect ratio. In addition, the nominal design values tabulated in the current standards are not adequate to be employed for design of a mid-rise CFS building. Therefore, to improve the relevant design codes towards mid-rise construction, development of stronger CFS shear walls with higher shear resistance and ductility is deemed necessary.

The increasing demand for stronger shear walls in CFS mid-rise construction in recent years has led to numerous research activities to enhance the performance of CFS

framed systems. Different systems with high shear capacities such as CFS walls with lightweight mortar [17], foamed concrete-filled CFS shear walls [18], and CFS walls with concrete-filled rectangular steel [19] are recently proposed by various researchers to be used for mid-rise structures. Although these new systems have shown to be able to improve the seismic performance of shear walls through providing higher shear resistance, they significantly increase the weight of walls that negatively affect the seismic base shear of building during an earthquake or extreme action [20, 21].

Based on the abovementioned problems of the existing CFS shear walls as well as the lack of design guidelines for the stronger CFS shear walls in the current regulations, a new hybrid CFS wall, composed of square hollow sections (SHS) and CFS open sections, is proposed in this study. This new hybrid system can offer great advantages with respect to the lateral performance of light steel frames, in particular for application in mid-rise construction. This system is a relatively new lightweight system, which is developed at Western Sydney University (WSU) and allows taking advantage of both components' strengths (CFS open section and SHS element) minimising their limitations as stand alone systems.

1.2 Concept of the proposed hybrid CFS wall

A typical CFS wall is generally fabricated from open CFS sections (U and C section profiles). However, it is well acknowledged that the implementation of open CFS sections for lateral bearing systems would result in many types of instabilities during seismic action and consequently reduces the lateral resistance of system [1, 22]. Therefore, innovative systems such as the proposed hybrid CFS wall in this study needs to be developed in response to the needs of CFS provisions as well as lightweight steel industry in mid-rise construction.

As shown in Figure 1.1, the proposed hybrid system combines CFS open sections with SHS elements, which allows taking advantage of the mechanical characteristics of each system while providing a unified wall panel. The SHS provides higher buckling capacity compared to the CFS open sections, which is effective in controlling the buckling failures in a shear wall. Besides, SHS can provide more tilting and bearing resistance of screws when sheathing is employed, because of its higher thickness compared to CFS members. On the other hand, the open CFS sections are relatively lighter than SHS, which helps with lifting and installation of the prefabricated panels.

2

Due to the truss-bracing configuration of the SHS part, the frame is offering relatively higher resistance compared to heavy CFS shear walls tested in the literature. This truss is employed to improve the shear resistance of CFS shear walls through absorbing more energy and to prevent the buckling of the end studs, which is one main failure mode of traditional CFS walls. In this system, the structural elements possess different functions: SHS elements support both lateral and vertical loads, while the CFS profiles provide resistance only against vertical loads. This load sharing can enhance the buckling resistance level for all the components in the proposed system. Various configurations and detailing were considered for the design of this hybrid system, with the aim of addressing both structural and constructional needs.
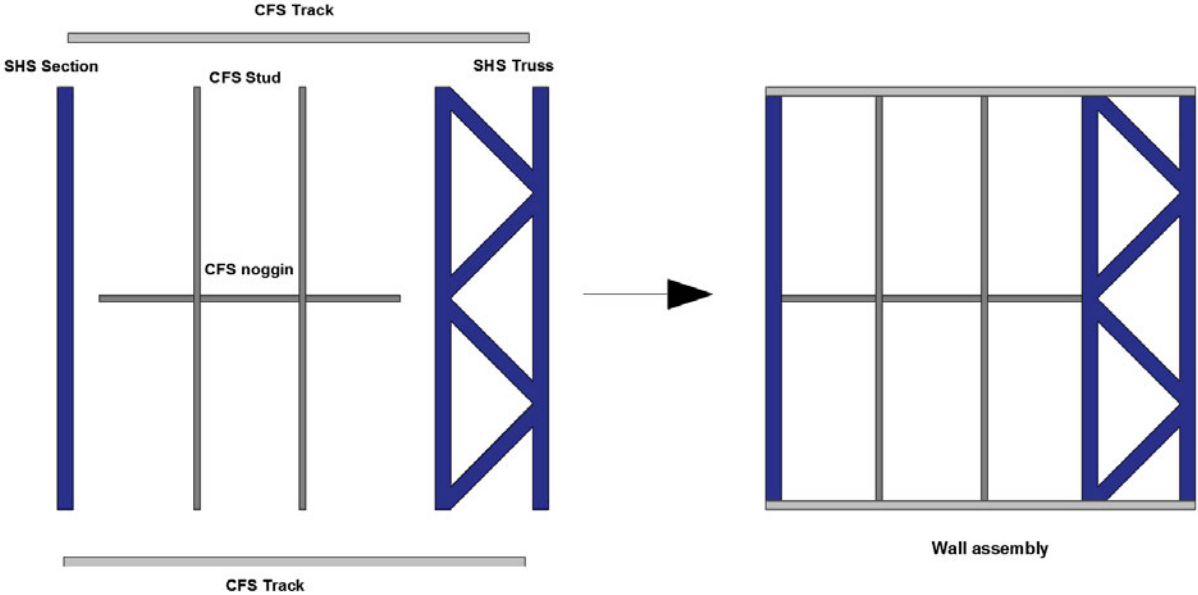
Figure 1.1. Components of hybrid wall panel

1.3 Objectives of the research

This study aims to enhance the lateral load resistance capacity of the CFS buildings by employing a hybrid shear wall with combination performance of open CFS profiles and SHS elements in lateral load. The following are some of the specific objectives of this particular study:

- Increasing the lateral resistance of the CFS shear walls by proposing a hybrid CFS system

3

- Enhancing the energy absorption, ductility and obtaining higher Response modification factor

- Conducting full-scale experimental testing on the hybrid CFS panels in order to compare the pros and cons of the proposed system with the previously tested CFS walls

- Addressing the issues of numerical modelling of CFS structures under lateral load and classifying all existing models.

- Developing numerical methods such as ABAQUS and OpenSees for micro and macro analysis of the proposed hybrid shear wall and employing the proposed panel for mid-rise buildings.

- Performing sustainability and cost analysis of the proposed hybrid system and comparing the results with hot rolled steel (HRS) buildings.

1.4 Organisation of the thesis

This study is a comprehensive experimental and numerical research on the hybrid CFS systems aiming to improve the lateral resistance of a CFS shear panel. The study is provided in nine chapters:

In Chapter 1, the general background, problem overview, the concept of hybrid panel and the objectives of the study are introduced.

In Chapter 2, a comprehensive literature review on CFS lateral load resisting systems is presented. The study describes different CFS lateral load resisting systems including CFS shear walls with various sheathing, CFS strap-braced wall panels, CFS walls with mixed sheathing and bracing techniques and hybrid CFS walls.

In Chapter 3, the capability of the innovative low-weight hybrid shear wall for achieving high strength, ductility and energy absorption is assessed through testing eleven full-scale wall specimens under lateral monotonic loads. The performance of the hybrid walls is evaluated in terms of shear resistance, stiffness, ductility parameters and energy absorption capacity.

In Chapter 4, an experimental program is developed to test six hybrid CFS wall specimens under reversed cyclic loading to promote the use of CFS lateral systems in mid-rise buildings. A comparison between the monotonic tests from Chapter 3 and the cyclic tests of this chapter is also provided. The cyclic results of the hybrid CFS wall

panels in this chapter are analysed, and the response modification factor of the system is determined. In addition, the hybrid CFS walls in this study are compared against 87 previously tested CFS wall panels from 28 references in terms of strength to weight ratio.

In Chapter 5, the numerical methods used for modelling the lateral performance of CFS framed wall structures in the literature are classified, and their positive and negative aspects, limitations, their applicable software, and challenges for simulation of different scenarios are discussed. The existing models are classified into macro modelling and micro modelling methods, and each is discussed within their own context. Then a comparative discussion on both macro and micro categories is carried out in order to evaluate their effectiveness, positive and negative aspects, and their accuracy.

In Chapter 6, ABAQUS and OpenSees programs as separate tools for Micro-element and Macro-element modelling of CFS shear walls under lateral load are compared. Advantages and disadvantages of using different methods/software are then discussed.

In Chapter 7, the proposed hybrid wall system is modelled by a comprehensive finite element (FE) analysis, calibrated and validated based on the findings from Chapter 3. First, the numerical modelling procedure is presented in detail, and the model is verified by the test data of Chapter 3. The agreement of numerical and experimental results are checked in terms of load-displacement curve, failure mode, stiffness and drift ratio. Finally, using the validated numerical model, 20 new hybrid wall panels with various configuration of SHS truss-braced are proposed, and their performance is compared with each other.

In Chapter 8, the performance of a newly developed hybrid CFS system for structural frames of North American buildings is evaluated, and a multidimensional comparison between this system and conventional HRS structural frames in terms of structural behaviour, environmental effect (sustainability), construction cost and social impacts is provided.

In Chapter 9, a summary of the thesis is presented, and the conclusions for this study are drawn. Some recommendations for future research are also presented.

Chapter 2   Literature review

2.1 Introduction

The low lateral resistance of traditional CFS wall has persuaded many research groups to perform experimental, numerical and theoretical investigations aiming to improve the lateral performance of CFS walls. In the past decades, various strategies have been proposed to improve the seismic performance of CFS frames in seismic regions. The strap bracing system is one appropriate method which can meaningfully improve the lateral performance of CFS frames by transmitting the horizontal forces from the floor to the foundation. Sheathing the CFS panels by means of steel, wood, gypsum, etc is another approach to enhance seismic resistance of CFS structures. Combination of bracing and sheathing technique as well as hybrid methods are also considered as the potential approaches for increasing the lateral performance of the CFS walls. Review of the past studies on the lateral behaviour of CFS structures is carried out in this chapter. The review is performed in four categories of CFS structures with sheathing, bracing, mixed bracing and sheathing systems and hybrid systems. Classification of all the lateral force-resisting systems in the lightweight steel frames, along with their strengths and weaknesses is also presented in some recent studies [1, 22, 23].

2.2 CFS frames with sheathing

Sheathing can provide considerable strength and stiffness for CFS shear wall panels. A large number of studies have been carried out to evaluate the effect of different sheathing materials such as cement board, gypsum board, wood-based sheathing and steel on the lateral behaviour of CFS walls.

In a study by Liu et al. [17] sprayed lightweight mortar (SLM) was employed as a sheathing technique for CFS walls. Figure 2.1 illustrates the details of the wall specimens in their study. They observed that the local buckling of the end studs was the general failure mode of the specimens. Also, they reported that specimens having SLM sheathing on both sides were stronger than the specimens with calcium silicate and SLM. In addition, they concluded that the ductility and energy absorption were increased due to the slippage between the steel frame and the SLM layer. They stated that the lateral load capacity of the walls is also reduced by the increase of vertical load.
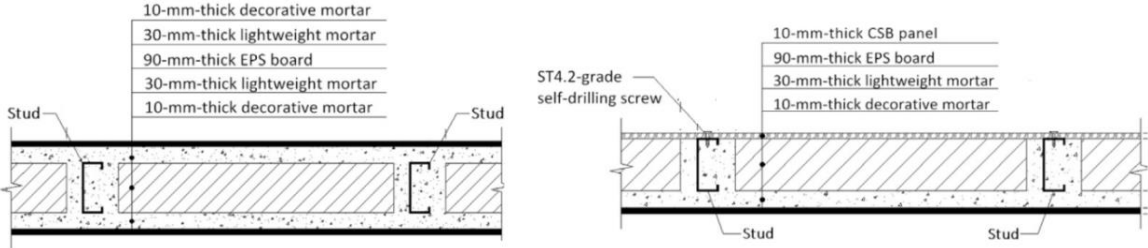
Figure 2.1. Details of wall specimens with SLM in one and both sides [17]

An experimental test for evaluating the effects of stud section, interlayer action, stud type and openings on the performance of sheathed CFS walls was conducted by Wang and Ye [24]. Figure 2.2a shows the two and three-storey frames of this study. Their results showed that the elastic stiffness of the lower storey was improved by increasing the web depth of columns. They also observed that the opening in shear walls, regardless of its position, could decrease the shear strength of the walls. In addition, they concluded that coupled C section could increase both non-deformability and shear strength of the specimens and better energy-dissipating capacity was gained for the specimens. Energy dissipation and failure modes of the specimens are presented in Figure 2.2b and Figure 2.3, respectively.
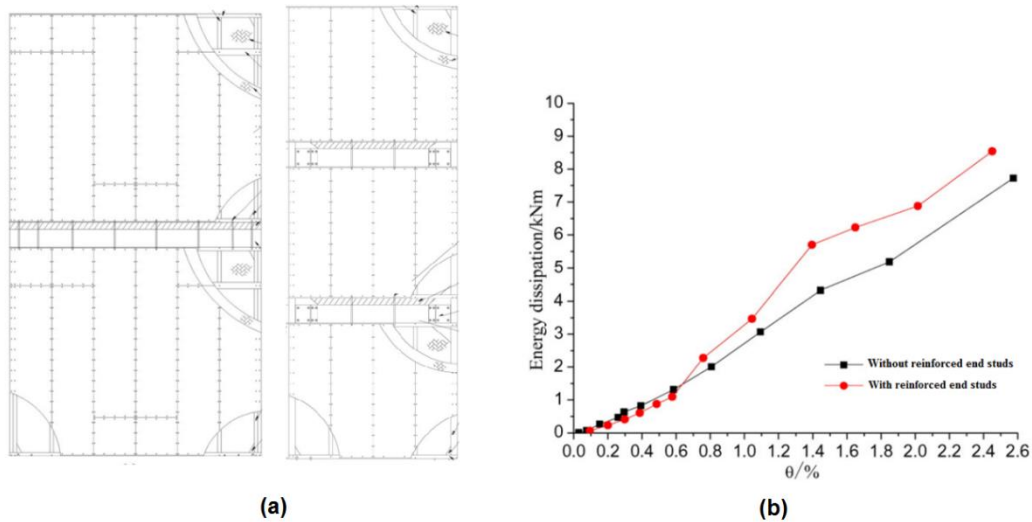
Figure 2.2. a) Configuration of two and three-storey frames, b) Energy dissipation [24]
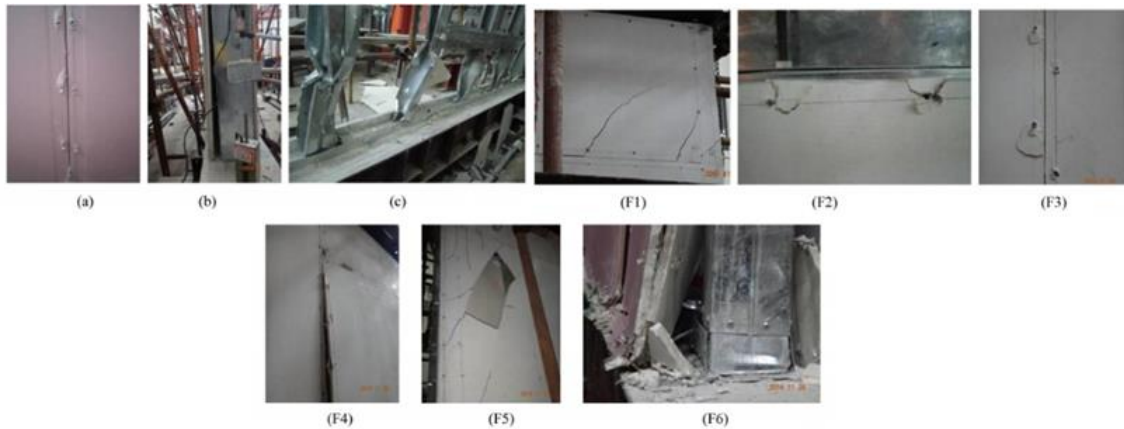
Figure 2.3. Failure modes of the specimens
(a) Pulling through (P); (b) shearing off (S); (c) deformation (D). (d) (F1) Cracks; (F2) splitting; (F3) bearing; (F4) bulging; (F5) shedding; (F6) crushing [24]

Karabulut and Soyoz [25] also carried out some experimental tests on different sheathed CFS shear walls in order to investigate the effects of steel thickness, board type, axial loads and screw spacing on lateral performance of walls. They also developed some analytical models suitable for seismic performance assessment of CFS walls. Based on their results, they concluded that by using Gypsum Wall Board (GWB) as a sheathing material, decreasing the screw spacing and increasing the vertical load, the lateral resistance capacity of the wall could increase.

For investigation of the seismic response of steel sheathed CFS shear walls, Mohebi et al. [26] utilized some experimental tests on steel sheathed, gypsum and fibre cement

board (FCB) claddings walls. They reported that energy dissipation, shear strength and lateral stiffness of the wall could increase using sheathing materials at either or both sides. Table 2.1 presents the types of the specimens and sheathing materials used in their study. Also, they concluded that by using double-sided claddings, the energy dissipation was increased by 37% and 76% compared to single-sided and walls with no cladding. This comparison is shown in Figure 2.4.

Table 2.1. Shear wall test specimens [26]

Specimen	Front side sheathing/cladding	Back side cladding
S	Steel sheet (S)	–
S-G	Steel sheet (S)	Gypsum board (G)
S-C	Steel sheet (S)	Fiber cement board (C)
GS-G	Gypsum board+Steel sheet (GS)	Gypsum board (G)
CS-G	Fiber cement board+Steel sheet (CS)	Gypsum board (G)
CS-C	Fiber cement board+Steel sheet (CS)	Fiber cement board (C)
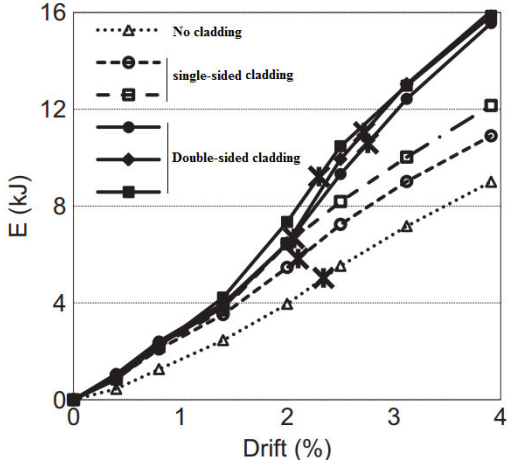
Figure 2.4. Cumulative hysteretic energy dissipation's comparison [26]

Extensive experimental program on CFS shear walls sheathed by steel sheet was conducted by Yu et al. [27-29]. They utilized both monotonic and cyclic loading to evaluate the performance of the walls. They observed that the primary failure modes for steel sheathed CFS shear walls are pullout of sheathing screws and the buckling of the steel sheathing; however, the failure mechanism did not occur by the failure of the fasteners. Peck et al. [30] implemented experimental tests on 21 shear walls in order to evaluate the effect of some parameters on the gypsum board shear wall performance. They reported that wall capacity was increased by reducing the stud spacing; however, this reduction could cause an increase in numbers of fasteners. Also, they stated that by reducing the fastener spacing, the wall lateral strength was increased. In addition, it was mentioned that blocked walls have 15% to 20% better capacities than unblock walls. An experimental program concerning the influence of

the sheathing types, fastener, steel thicknesses and stud spacing was conducted by Serrette and Nolan [31]. They concluded that increasing the stud spacing had a little effect on enhancing the lateral capacity of walls.

A study on CFS walls sheathed by Calcium Silicate Boards (CSB) was conducted by Lin et al. [32]. They stated that due to the large deformation of the track, the common failure mode occurred at the bottom track. They also showed that sheathed boards on both sides of the wall provided higher resisting strength and stiffness than walls with one side sheathing. It was noted that the results of the cyclic test were less than those subjected to the monotonic test. In addition, coupled C section for studs, compared to single section, could provide higher energy absorption, stiffness and strength. Their results showed that sheathing thickness did not influence the shear capacity of the wall.

Vieira and Schafer [33] presented the strength and stiffness of the CFS walls sheathed by different materials. They showed that the lateral stiffness of the wall was separated into two parts of local and diaphragm. The parameters in their study consisted of fastener and stud spacing, sheathing type, construction flaws, edge distance and environmental conditions. In a theoretical analysis, Lang and Naujoks [34] developed a design procedure that allowed for the design of walls having both horizontal and vertical loads. They utilized their calculation model for the stabilising behaviour of a C section stud which is under compression.

Nithyadharan and Kalyanaraman [35] studied the performance of CFS walls sheathed by CSB subjected to monotonic and cyclic loading. They evaluated the effects of screws spacing, wallboard configurations and board thicknesses on the of the shear wall capacity and provided different limit states for screw failure. In another study [36], they utilized a constitutive model in order to investigate the energy dissipation of the shear walls sheathed by CSB. Based on their observation, this energy dissipation was due to the severe pinching behaviour in connections which caused degradation in stiffness and strength. The shear load transferred to the screw connection in a cyclic load was studied by the same authors [37]. The influence of the edge distance and the thickness of the boards on the energy dissipation and ultimate strength of screws were also reported in this study. They noted that increasing the sheathing thickness and edge distance could cause an increase in strength and stiffness in both monotonic and cyclic loading. Based on their results, the energy absorption and strength were lower

under cyclic loading compared to the monotonic values. It was also mentioned that by decreasing the board thickness, the ductility did not change significantly.

Castillo et al. [38] carried out an experimental and numerical study on CSB, GWB, Oriented Strand Board (OSB) and polystyrene sheathed CFS walls. They concluded that OSB sheathing material could provide the highest stiffness among all other sheathing materials. They also proposed that by having clad walls with polystyrene material, the damages caused by ground settlement due to land subsidence can be reduced. Figure 2.5 shows more details regarding different wall configurations in this study.
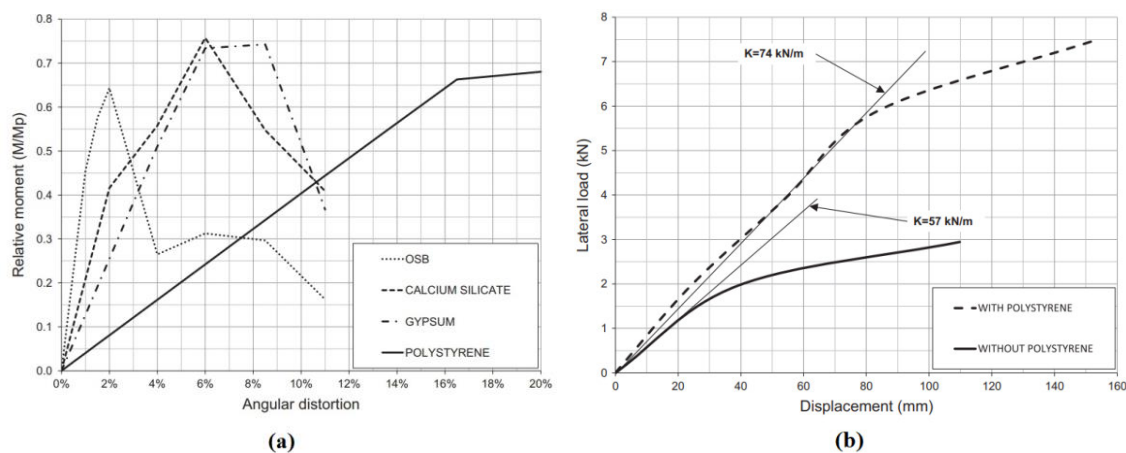
Figure 2.5. (a) Moment–angular distortion curves for wall frames with different sheathing materials, (b) Load–displacement curve for CFS wall frames with and without polystyrene sheathing [38]

Fiorino et al. [39] evaluated the screw connections of CFS walls sheathed by OSB and GWB with a series of experimental tests under cyclic loading protocol. Various configurations of walls, sheathing direction and the effects of edge distance were investigated to compare different wall capacities. It was noted that the response of the walls depended on the sheathing type. For example, higher absorbed energy and strength was obtained from OSB sheathing, while GWB provided more considerable ductility and stiffness. Fiorino et al. [40] also compared gypsum and cement-based screw connections used in common practice. They concluded that the gypsum fibreboard had the most strength compared to the standard gypsum board, which had the least strength. The rest of the connections showed similar values of resistance. In terms of ductility, they reported that the lowest and highest values were obtained from gypsum fibreboard and standard gypsum board, respectively.

11

Bian et al. [41] reported that the sheathing-to-steel connections had a strong influence on the lateral strength of CFS walls. A complex interaction between fastener, sheathing and CFS members was generated, which provided resistance for the wall. This interaction is of great importance as it is the main source of shear wall nonlinearity. They concluded that the nominal strengths for different shear wall configurations listed in the current design specifications, is not enough and variability of shear walls should also be considered.

Pan and Shan [42] worked on different sheathing materials such as OSB, GWB and CSB for evaluation of CFS walls under monotonic loads. It was reported that the primary failure mode was the separation of sheathing and screws and bearing of sheathing around the screw connections. They concluded that the aspect ratio of 1:0 provided 35% higher strength than the aspect ratio of 2:0. It was also noted that the energy absorption of CSB was higher than OSB and GWB with moderate and lowest values, respectively. Besides, the results showed that the screw arrangement and spacing, as well as the anchor condition, could influence the ductility of CFS wall. In terms of ductility, it was reported that the one-side sheathing wall was more ductile than two side sheathing wall.

A series of experiments were performed by Peterman et al. [43] in order to examine the hysteretic behaviour of the connection between CFS studs and sheathing. Fastener spacing, sheathing configuration, steel thickness and fastener types were the parameters evaluated in this study. They concluded that the sheathing type and steel thickness affected the failure mode, while the fastener spacing did not have a tangible effect on this value.

An experimental study on CFS walls sheathed by OSB was conducted by Baran and Alica [44]. They concluded that the overall behaviour of the wall depended on the geometry of hold-down employed at the base of CFS wall. It was noted that the diagonal struts could increase the load resistance and stiffness of the walls slightly. Figure 2.6 shows the location of struts and its effect on the wall.
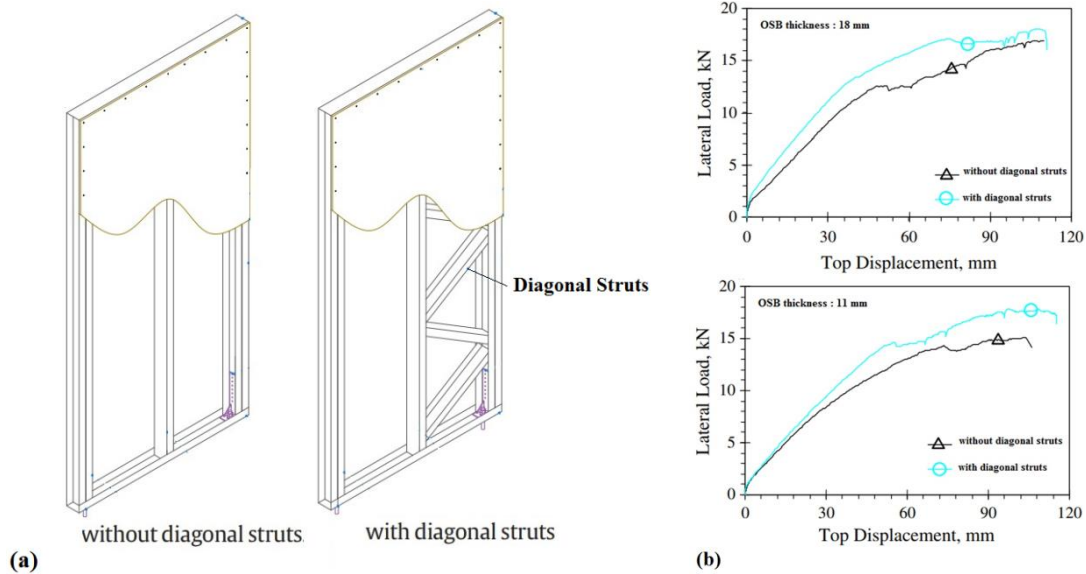
Figure 2.6. (a) Details of panels, (b) Effect of diagonal struts on wall performance [44]

Some parameters such as openings, configuration of the walls, stud thickness and spacing, screws spacing, top tracks and the wallboard thickness were examined in an experimental study by Restrepo and Bersofsky [45] and different damage states were observed in their experiments. Xu and Martinez [46] proposed an analytical approach in order to investigate the ultimate lateral resistance of the CFS wall by taking construction details, geometrical dimensions and material properties into account. A simplified model for analysing CFS buildings, with fewer numbers of elements was also proposed in this study to simulate the nonlinear behaviour of CFS walls. The proposed model was capable of evaluating the lateral resistance of CFS walls with different sheathing and framing materials.

A set of experimental tests on single and multi-storey CFS buildings were carried out by Fulop and Dubina [47, 48]. They reported that strengthening of the corner details with an ideal shape could stop failure at the bottom track in the anchor bolt region. This was due to the transmission of uplift force from brace to the anchoring bolt without enforcing bending in the bottom track. It was observed that the most sensitive region of the corrugated sheet specimens was the seam fastener in which damage was gently increased until their failure caused the overall failure of the wall.

Swensen et al. [49] also assessed the effect of screw type and adhesive in screw connections of GWB. Their results showed that enhanced screw could provide higher

strength than conventional screws; however, much more increase could be gained by employing adhesives. Figure 2.7 shows the effect of adhesives and type of screw on wall response.
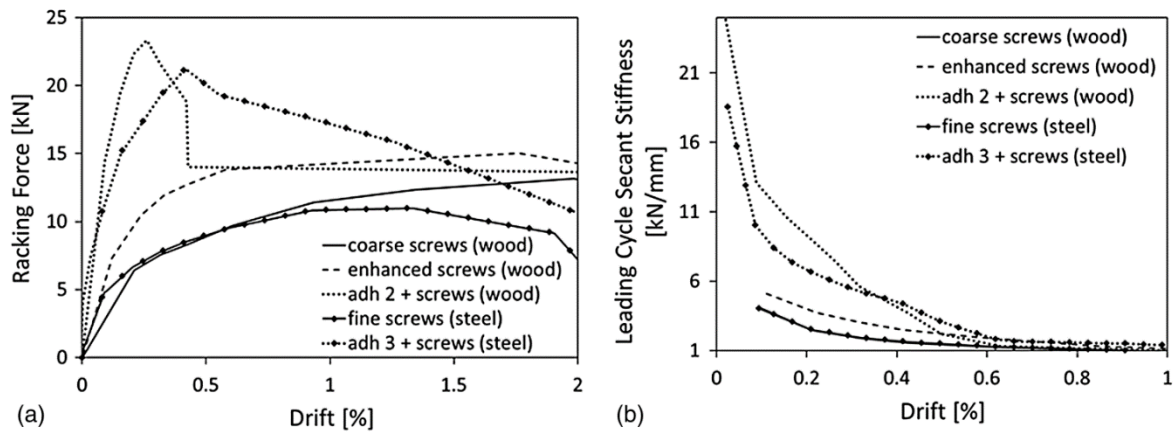
Figure 2.7. Impact of adhesives and enhanced screws on the wall performance: (a) backbone curve; (b) stiffness per cycle [49]

Shamim et al. [50, 51] [52] determined the level of damping, natural period of vibration and the effect of the second storey in the seismic performance of CFS shear walls. They reported that the general strength obtained from dynamic tests was not much different from the results tested under static loading. In a new study, some parameters such as sheathing thickness, various framing thickness, aspect ratio, screw fastener detailing and framing reinforcement were assessed by DaBreo et al. [53]. Their results showed that employing block studs could enhance the shear strength of the wall. Figure 2.8 shows the effect of blocking on the performance of the CFS walls. They also reported that the failure of chord stud could affect the performance of the wall directly.
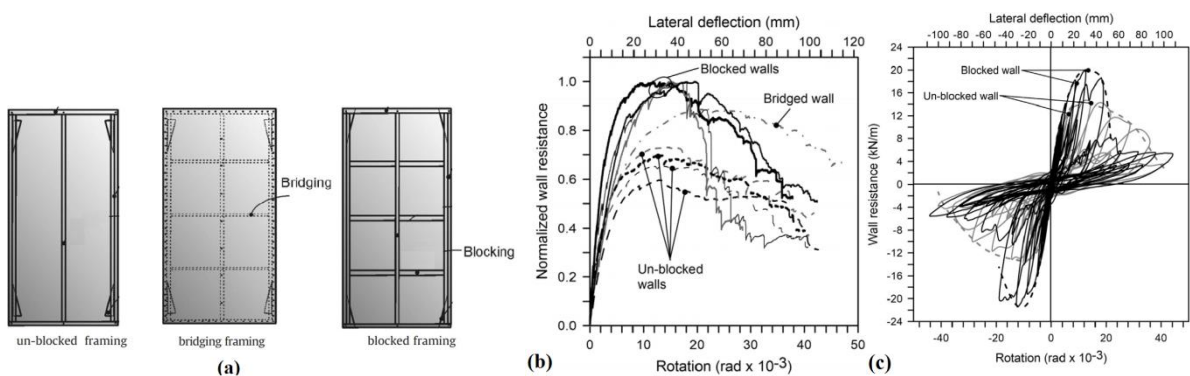
Figure 2.8. a) Details of the panels, b) comparison of monotonic results, c) comparison of cyclic results [53]

Attari et al. [54, 55] carried out some experimental tests on one- and two-side steel

14

sheeting CFS walls under cyclic loading. Their results showed that the thickness of steel sheathing and frame member, as well as the capacity of elements, could affect the performance of walls. They concluded that the strength of a two-side sheathed CFS wall was more than twice of strength for the one-sided sheathed wall. The effects of steel sheathing thickness and the number of layers of sheathings on the performance of CFS walls were investigated by Esmaeili et al. [56]. They concluded that having two-side sheathed walls could cause an increase in stiffness, higher ultimate strength and energy absorption compared to those having one-side sheathing. It was also reported that the stiffness and shear strength of the walls were increased by enlarging the sheathing thickness.

Landolfo et al. [57] conducted both experimental and numerical studies on the seismic performance of CFS shear walls and showed that walls sheathed with OSB, and GWB could be constructed in the low to medium seismic intensity zones when they are designed according to the related standards. It was noted that the failure mechanism was constant during applying the monotonic load; however, for the cyclic loading, some fluctuations occurred. Mohebbi et al. [58] also implemented some cyclic tests on CFS wall specimens. The failure modes in their study included fastener bearing/tilting, chord stud buckling and sheathing buckling. They also reported that having double-sided sheathing can enhance the energy dissipation, shear strength and the elastic stiffness; however, this could be gained only if the chord stud buckling is avoided and screw connection failure is dominant.

Different sheathing materials such as GWB, Bolivian Magnesium Board (BMB) and CSB were tested in a study by Ye et al. [59]. They concluded that the shear performance of screws was affected by differences in sheathing materials. It was also noted that the walls sheathed with BMB had higher ductility than the walls sheathed with CSB. They also suggested that the walls clad with CSB and GWB were preferred in areas of low seismicity.

Liu et al. [60] concluded that by having ledger track, the wall resistance enhances, while the energy dissipation declines. In addition, panel seams could decrease the strength and increase the flexibility of the wall. In an experimental study, Mowrtage [61] investigated the behaviour of ten full-scale CFS walls sheathed with four different materials including steel sheet, trapezoidal steel sheet, reinforced cement board, and thin-ribbed steel sheet shotcrete with cement mortar. They concluded that the

proposed sheathing materials could increase the strength of the walls around three times. Figure 2.9 and Figure 2.10 show the effects of various sheathing materials on the vertical and laterals load performance. In another study, Mowrtage et al. [62] carried out some experimental tests on a new sheathing material as shotcrete ribbed steel sheets. Their results showed that this new sheathing could increase the capacity of walls twice of the value of walls sheathed with traditional sheathings.
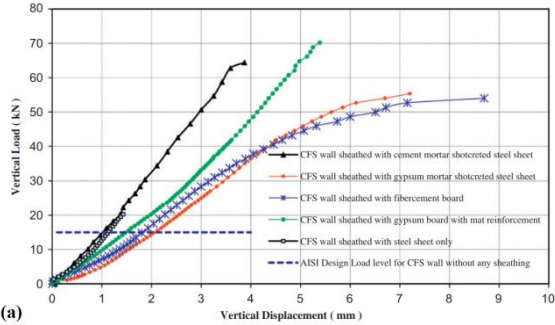
Figure 2.9. Effects of various sheathing materials on the vertical load performance
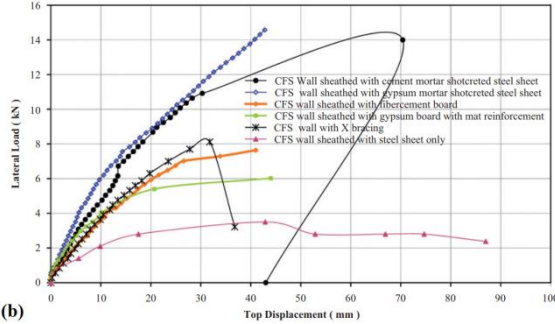
Figure 2.10. Effects of various sheathing materials on the lateral load performance [61]

Non-linear dynamic behaviour of CFS frames was investigated with both numerical and experimental methods by Kim et al. [63, 64]. Figure 2.11 shows a full-scale two-storey CFS building and the results of shake table tests. It was reported that the cross-bracing straps had very ductile but highly pinched hysteresis behaviour

16
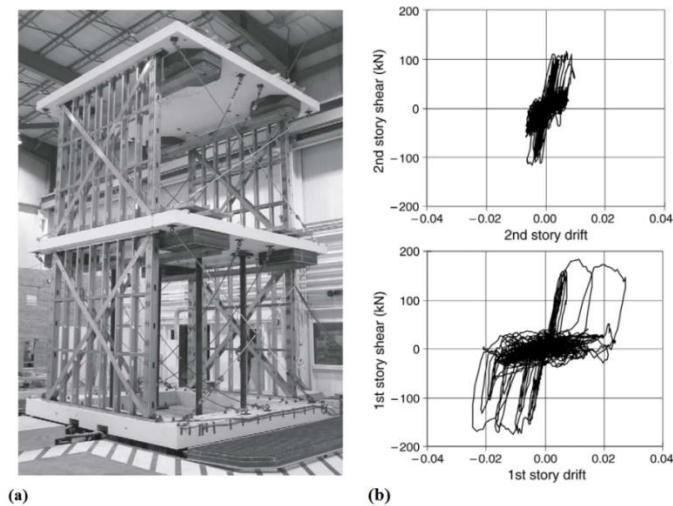
Figure 2.11. Shake table test: a) Test set up, (b) Storey shear vs drift [63, 64]

Zhang et al. [65, 66] utilized both experimental test and numerical methods and concluded that the gravity load of the frame could increase the lateral load capacity and stiffness of the wall. Gao and Xiao [67] conducted an experimental study on the monotonic and cyclic lateral loading performance of CFS walls sheathed with glued laminated bamboo panels. In this study, the strength capacity and deformability of ply-bamboo sheathed CFS walls were assessed and compared by ordinary wood sheathing panels. Telue and Mahendran [68, 69] also studied the performance of CFS walls sheathed with plasterboard in one side and both sides of the wall and employed Australian standard and the American specification for comparison of their results. Yu and Chen [70] investigated different wall configurations under monotonic and cyclic tests. Based on their results, it was noted that if the minimum framing needed by was used without additional detailing, the interior studs might buckle under cyclic lateral forces regardless of sheet buckling and screw pull out.

Stojadinovic and Tipping [71] tested some corrugated sheathed steel wall as an alternative lateral bracing system. Their results showed that corrugated steel sheet could increase the shear strength of the wall. They suggested that this system can be added to some regulations as a bearing wall system utilizing light-framed CFS walls sheathed with corrugated steel sheet. Yu and chen [72] created some openings in corrugated sheets to increase the ductility. They reported that by creating some circle holes in the corrugated sheathing, the failure occurred in the board instead of screw connections; however, this opening caused a significant reduction in the strength and stiffness. Hence, it was noted that the opening was not usable in such systems.

17

Javaheri-Tafti el al. [73] also carried out some experimental investigations on CFS frames sheathed by thin-galvanized steel plates. They showed that shear strength could be improved by decreasing the screw spacing; however, for specimens with double studs at the end, this improvement did not occur. They also made some recommendations in order to improve the R values in regulations.

In an experimental study, Zeynalian and Ronagh [74] worked on four full-scale FCB under cyclic lateral loading. Figure 2.12 shows the wall configurations and results for specimens of this study. Their study showed that double-sided FCB panels (H1) had approximately similar resistance to one-sided FCB panels (H3). They also reported that utilizing both FCB and X-strap lateral resistant systems in one shear wall was not suitable since they did not have similar stiffness and collapse at different loads.
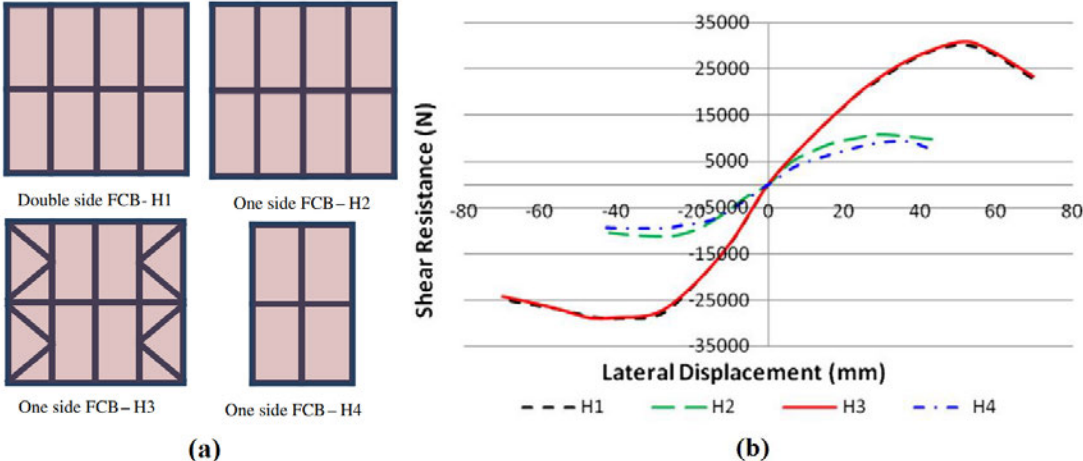
Figure 2.12. a) Specimens configurations, b) Hysteretic envelope curves [74]

Zeynalian et al. [75] tested a number of steel sheathed shear walls to assess the lateral seismic behaviour of the walls, and to propose a new configuration to the codes. They showed that double steel and thicker steel sheets could not necessarily increase the lateral resistance of wall due to the lack of adequate anchorage support, which induced the early failure in the frame by the screw tilting and hole bearing in the hold-down and tearing of the top track web. It was noted that the cyclic and monotonic loading results was similar and wall performance in both protocols was not different. Wang and Ye [19] conducted cyclic loading tests on CFS shear wall with concrete-filled rectangular steel tube columns. It was reported that the resistance of the wall is increased since the tilting of the screws was prevented by the concrete core. They also concluded that enlarging stud thickness could increase the ductility, while lateral

strength might not change by employing a coupled C section for the interior stud. Besides, the results showed that the strength of the wall reduced by increasing the size of the opening and this reduction depended on the location of opening. Gad et al. [76, 77] assessed the effect of using plasterboard on the seismic behaviour of CFS X-strap bracing walls using an experimental approach with shake-table and numerical studies. R factors between 4 and 29 were presented by the authors; however, they mentioned that many of these values were impractical and further research was required.

2.3 CFS frames with strap-brace

Strap brace is one conventional method of the bracing system for CFS walls where its application has been extensively investigated during recent years. Moghimi and Ronagh [78] carried out some experimental test focusing on the failure modes of different systems and ductile response of the CFS walls. The results showed that buckling failure could be prevented by employing double back-to-back studs as chord members. They noted that utilizing strap bracing in two sides could improve the lateral strength around twice of resistance for one side strap brace. They also pointed out that the bearing stress was reduced and the connection became stiffer due to the presence of these members. Figure 2.13 shows this proposed connection.
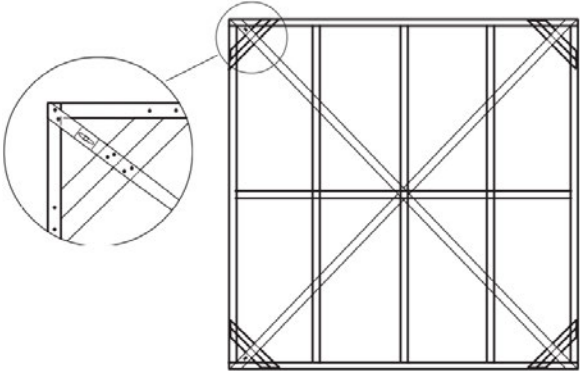
Figure 2.13 Proposed connection by Moghimi and Ronagh [78]

In a new study, the seismic performance of strap-braced stud walls was evaluated by Macillo et al. [79, 80]. They proposed some criteria for the design of strap-braced CFS structures and implemented a critical analysis of the requirements for CFS systems. It was noted that wall corners had a significant influence on the lateral performance of the wall; hence they should be well designed. In a theoretical study, Pastor et al. [81]

proposed a comprehensive model of the hysteretic performance of unsheathed x-braced frames which was able to consider the hardening plasticity and buckling of diagonal straps under tension and compression, respectively. In comparison to some theoretical studies, the order of time-integration was higher in their model.

There are also some new bracing systems such as K bracing [82] [83] proposed in the literature which have shown reasonable advantages in terms of ductility and energy absorption during lateral loading. The lateral performance of CFS knee-braced and K-braced CFS frames was investigated by Zeynalinan and Ronagh [83-85]. They concluded that by implementing brackets at corners of the panel, the lateral strength and ductility of the wall increased significantly. The bracing configurations and their hysteretic curves of both systems are shown in Figure 2.14 and Figure 2.15. Since the strength of Knee-bracing and K-bracing systems were much less than strap bracing, they suggested not using these systems for high and moderate seismic regions.
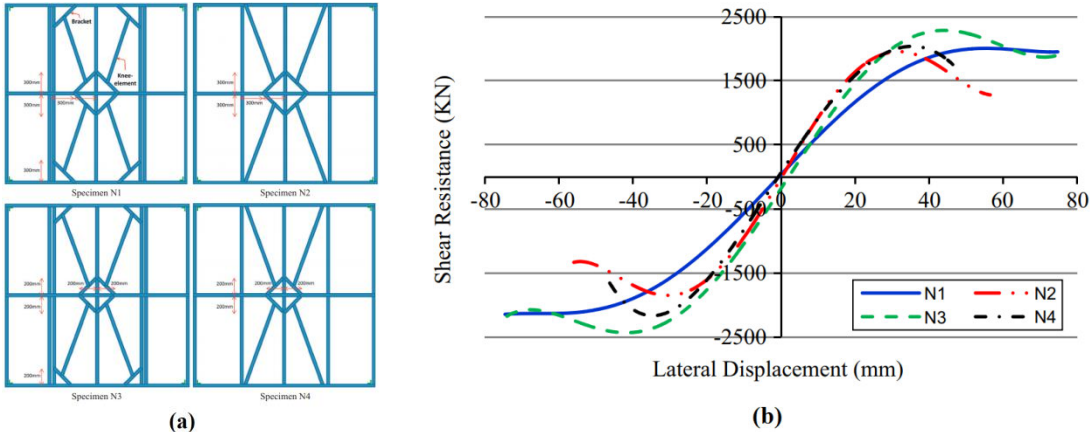
Figure 2.14. a) Panels with knee-bracing, b) envelope curves [83-85]
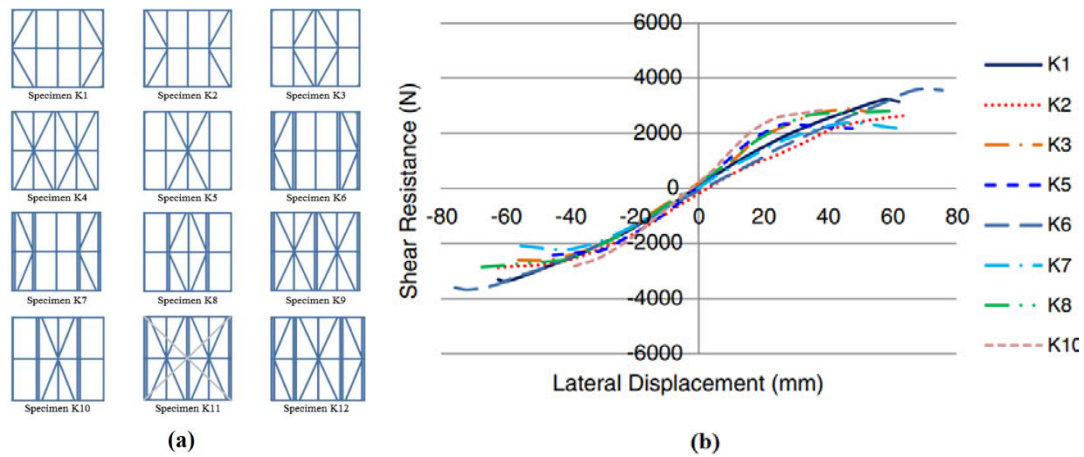
Figure 2.15. a) Panels with K-bracing, b) envelope curves [83-85]

The behaviour of k-braced CFS shear panels with improved connections was also evaluated by Pourabdollah et al. [82]. The configurations of the walls and brackets are shown in Table 2.2. Figure 2.16 also indicates that employing bracket can considerably enhance the shear resistance and ductility of the walls compared to the specimens with typical connections. It was also reported that coupled C section could improve the performance of the shear wall and both specimens K3 and K4 were suitable for high seismic regions.

Table 2.2 Modification of the K-braced connections [82]

Configuration				
Specimen	K1	K2	K3	K4
Description	Ordinary braced CFS	Change in brace configuration, double noggings and extra screws.	Gusset plates at the K-element to stud connections.	Gusset plates at connection with double chord studs.
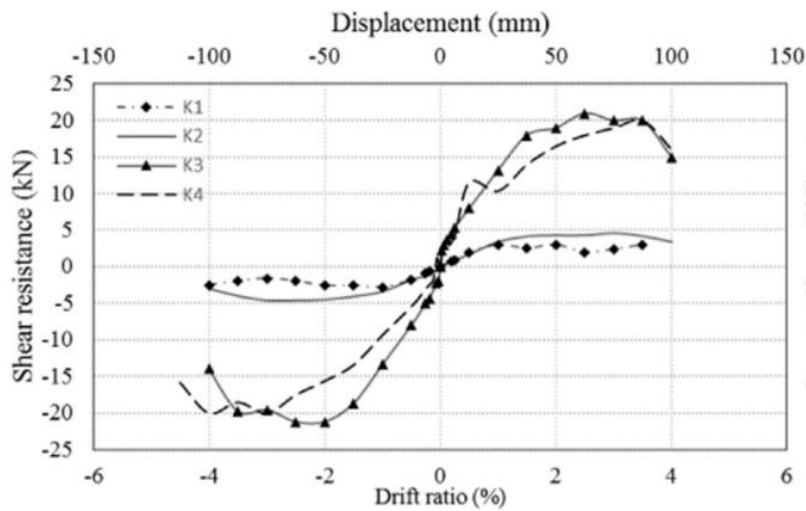
Figure 2.16. The backbone hysteretic curves for the modified K-braced connections [82]

In another work, Ronagh et al. [86] investigated the lateral performance of strap-braced CFS shear walls improved with brackets in the four corners of the wall. By comparing the results, they could find the optimum length of the brackets, which provided better performance for walls. Berman et al. [87] compared CFS braced frames and steel plate shear wall by some experimental tests. In their study, the larger initial stiffness and ductility were shown for the braced frame and steel sheet shear wall, respectively. It was found that both the energy dissipated and the cumulative energy dissipation was similar for steel sheet shear walls and braced frames. Fiorino et al. [88] indicated that the inelastic behaviour of CFS strap-braced stud walls could be influenced by non-ductile phenomena, such as the failure of gusset-to-track connection and combined compression and bending and axial load failure of the chord studs. Figure 2.17 shows the failures of strap-braced walls. It was noted that the wall corners must be accurately designed, as their response could considerably influence the overall wall performance.
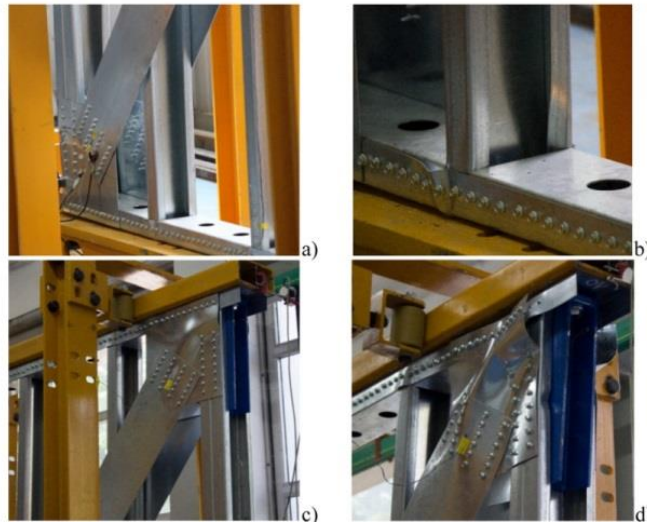
Figure 2.17. Failures walls: a) local buckling of the tracks; b) squashing of the stud ends; c) out-of-plane deformation of the gusset plate; d) gusset-to-track connection failure [88]

Al-Kharat et al. [89] assessed the inelastic behaviour of a strap-braced wall. Based on the results, punching shear failure of the track was seen in all tests. They also presented that due to the loss of compression resistance in the track and gusset plates after punching shear failure, the chord studs being pulled in towards the centre of the wall. Pull-out of the screws was also reported due to the large deformations of the walls.

2.4 CFS frames with mixed systems

There have also been several attempts to mix both strap brace and sheathing methods to improve the lateral behaviour of CFS walls and remedy the existing insufficiencies. Twenty one framing systems with vertical or diagonal studs and with opening were investigated by Accorti et al. [90]. Figure 2.18 shows four different walls used in this study. Based on their results, walls with diagonal bracing had better performance compared to the rest of the walls. It was noted that employing trussed members seemed to be adequate for moderate wind and/or seismic loads.
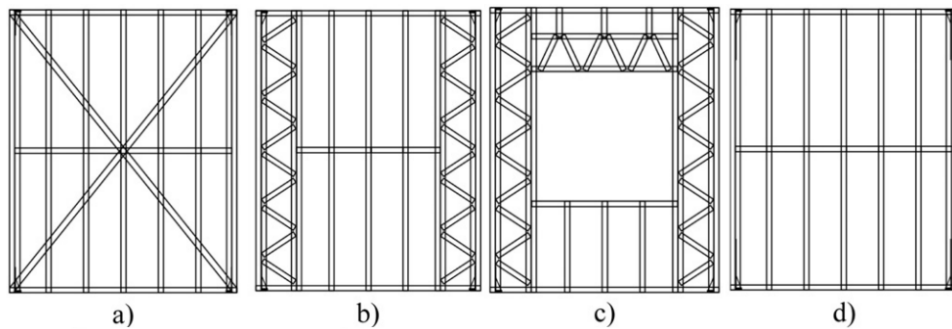
Figure 2.18. Four different configurations of walls [90]

Gerami et al. [91] carried out experimental tests on nine different frames with four different sheathings. The specimens used in their study are shown in Figure 2.19. They reported that the aspect ratio of the frame did not influence the sheathed wall panels performance, while the thickness of the sheathing had a significant effect on the behaviour of the wall.
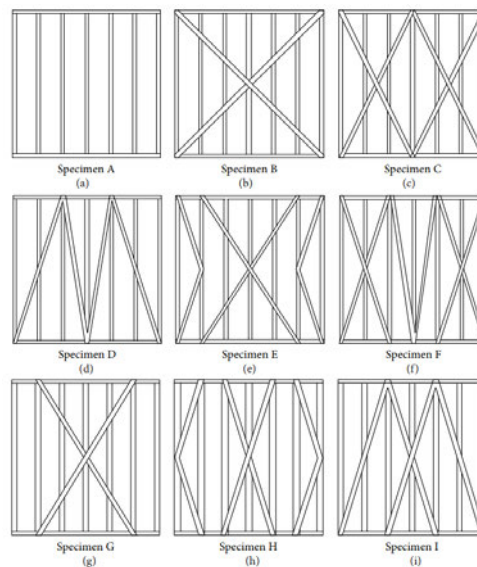
Figure 2.19. Specimens [91]

Serrette and Ogunfunmi [92] investigated the lateral performance of typical CFS steel walls for three different shear resisting systems. Figure 2.20 shows the configurations of walls in this study. For configurations B and C the maximum load was gained by the collapse of the wallboard along its edges. In addition, it was noted that by employing strap bracing for walls B and C, crack progression was avoided on the boards at the perimeter, and the lateral displacement of the wall was decreased.
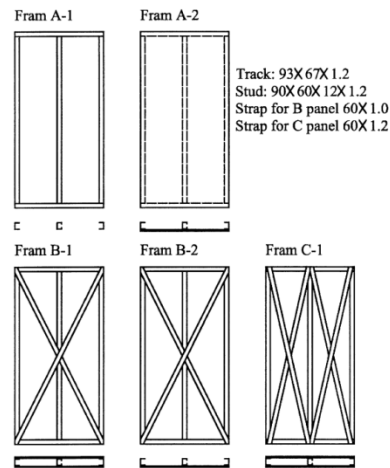
Figure 2.20. Frame bracing configuration [92]

In a similar study, composite panels with steel sheet and GWB investigated by Yu et al. [93]. They exhibited that these composite panels offered significantly better lateral resistance compared to the traditional wood sheathing. The proposed composite wall also had a similar failure scenario and post-peak behaviour as the steel sheet sheathing. In an experimental study, Xu et al. [18, 94] enhanced the lateral response of CFS walls by proposing high-strength lightweight foamed concrete (HLFC) shear walls (Figure 2.21). They showed that the new HLFC could considerably increase the performance of the wall and could also change the wall failure from brittle into ductile.
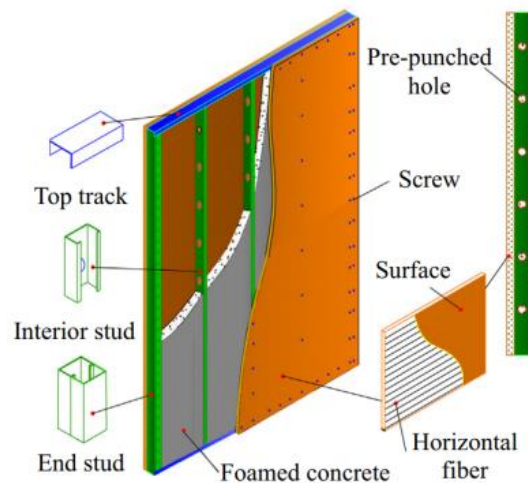
Figure 2.21. High-strength lightweight foamed concrete [18, 94]

2.5 CFS frames with hybrid system

Hybrid CFS system is a relatively new lightweight system, which is developed at Western Sydney University (WSU) and allows taking advantage of both open CFS sections and closed SHS elements. The first study on the hybrid CFS frames was conducted by Mortazavi et al. [95], where a number of hybrid CFS panels were tested under both monotonic and cyclic loads. Their results showed that the vertical load could be sustained by CFS open sections while the lateral load relied on the SHS elements. Although the strength to weight ratio of the hybrid panels of their study was relatively lower than the other traditional walls, they could obtain very high ductility values for their wall panel. The wall panels in this study are illustrated in Figure 2.22a. In another study by Kildashti el al.[96], the seismic collapse analysis of a six-storey hybrid CFS building was performed to determine the R factor through the proposed method of FEMA-P695. Based on their results, an R factor was proposed for constructions with hybrid CFS structural system. The simulated six-storey hybrid CFS building in this study is shown in Figure 2.22b.
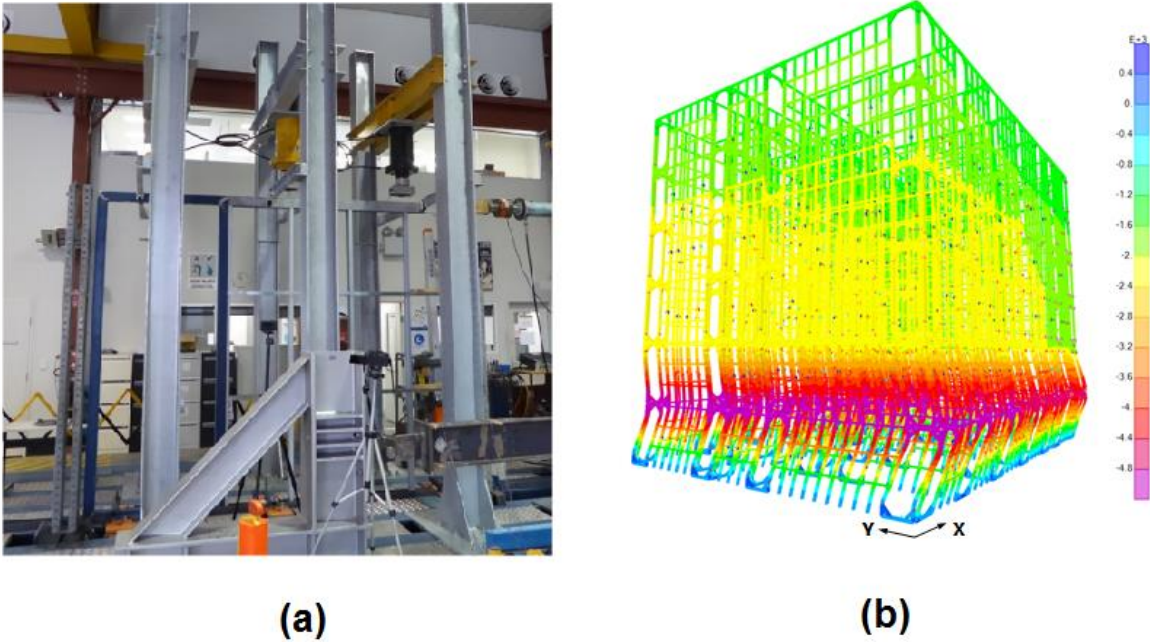
Figure 2.22. a) Hybrid CFS panel, b) Collapse analysis of a six-storey hybrid CFS building

2.6 Summary of literature review

By reviewing the past studies and their findings, it is concluded that although these

structural systems can play a role in improving the seismic performance of the CFS shear walls to some extent, the limited lateral load resistance capacity and poor energy dissipation of CFS frames is still one major problem for the application of these systems in mid-rise structures. Besides, the comprehensive review of the previous studies indicates that only a few investigations have been carried out on the performance of hybrid CFS shear walls. Therefore, more studies are required to evaluate the lateral performance of this new CFS shear wall. Consequently, the key objective of the current study is to investigate the lateral behaviour of the proposed hybrid panel.

The sheathing and bracing systems reviewed in this chapter are categorized in Figure 2.23. Furthermore, the parameters that can affect the performance of CFS shear wall are also obtained from different studies and listed in Table 2.3. The review of the literature also indicates that various factors can increase the lateral strength of the wall. These factors are also presented in Table 2.4.
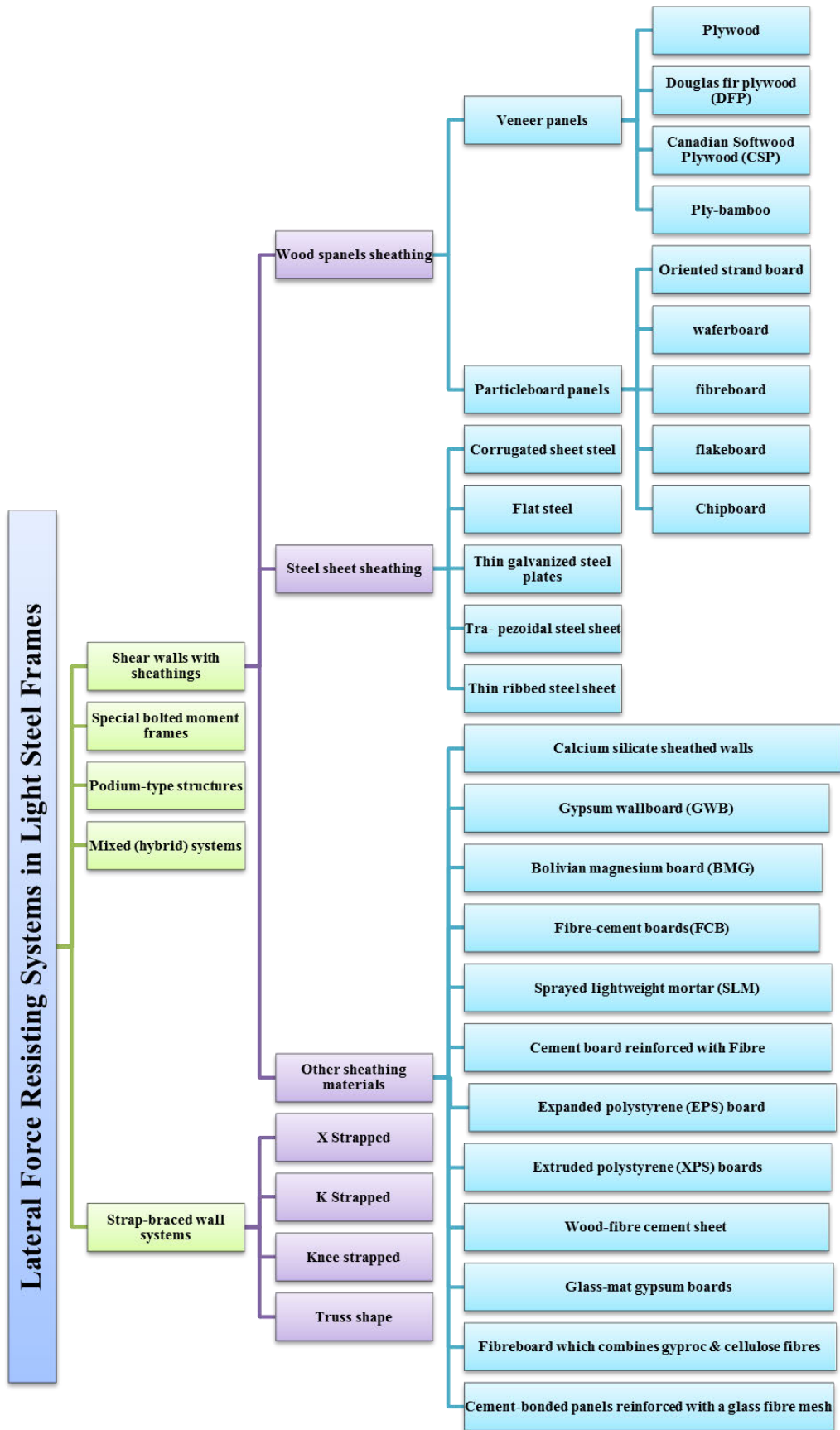
Figure 2.23. Classification of all sheathing and bracing systems for CFS framing

Table 2.3 Parameters that affect the performance of CFS shear wall

	Frame Properties	• Properties of framing members • Stud spacing & fixity • Hold down details
	Aspect Ratio	• Length to height ration
	Cladding	• Material properties • Thickness of cladding • Number of clad sides • Type & frequency of fasteners • Cladding orientation
Wall Panel Behaviour	Cladding & Braces Interaction	• Additive effects of cladding and diagonal bracing
	Diagonal Bracing	• Properties of braces • Fixity details • Initial tension level in strap braces
	Openings	• Size of openings Location of openings
	Boundary Conditions	• Set corner joints • Ceiling cornices • Skirting-boards • Vertical loads

Table 2.4. Factors that increase the lateral strength of CFS shear wall

Parameter	Reference
Applying double-sided sheathing	[17],[32] , [54],[55] ,[56],[58],[59],[74]
Increasing the vertical load	[17], [25], [65],[66], [24]
Increasing web depth of stud	[24]
Avoiding opening in wall	[24],[45] ,[72]
Decreasing the screw spacing	[25],[30],[41] ,[43] , [45],[73],[97]
Increasing the thickness of framing members	[27],[28], [29], [43], [45], [54],[55],[98]
Having blocks or diagonal struts	[30], [53], [44]
Decreasing the stud spacing	[30],[31],[45]
Using coupled C section	[24], [32],[78],[82],[99]
Applying monotonic load rather than cyclic	[32],[37]
Increasing the edge distance	[37]
Increasing the sheathing thickness	[37],[45] , [54],[55] ,[56],[91],[97]
Employing OSB rather than other materials	[38],[39] ,[42]
Using lower aspect ratio	[42],[100]
Improving geometry of hold-down	[44], [74]
Strengthening of the corner details	[47],[48], [78]
Employing adhesive for screw	[101],[49]
Enhancing screw type	[49] [83]
Adding ledger track for interior face of stud	[60]
Not using panel seams	[60]
Employing Corrugated steel sheet	[71],[102]
Using two sides strap	[78],[99],[97]
Limiting the use of Knee and K bracing	[84],[85] ,[83]
Using bracket at corner	[84],[85],[82],[99]
Infilling the stud	[18],[94] [19]

Chapter 3   Experimental program: Monotonic Investigation

3.1   Introduction

An experimental program, consisted of eleven full-scale specimens, was designed to examine the shear resistance and failure modes of a hybrid CFS wall subjected to monotonic loads. The wall panels were fabricated and tested in the Structural Engineering Laboratory of the Western Sydney University in a testing rig specifically made for this purpose. First, a monotonic test was conducted on three hybrid wall specimens with one specific type of connection. Then, based on the observations on the failure modes and location of weaknesses, the study was followed by proposing an improved type of connection. The analysis results can be used for the design of hybrid shear walls and provide an applicable database for engineering practice.

3.2   Experimental program

3.2.1   Specimen configuration

The lack of design guidelines for the hybrid CFS shear walls as well as the complicated structural analysis and design procedures associated with these systems greatly restrict the engineers' ability to design and determine the overall sizes and dimensions of the system. Therefore, the dimensions and sizes of the hybrid wall components were arbitrarily selected based on their availability in Australia's market with the aim of providing the required features of panelised buildings such as being light and liftable. Each wall specimen had an overall width and height of 2400 mm, in which the vertical elements were spaced at 600 mm. As GWB is normally available in a width of 1200 mm, this configuration for vertical elements was chosen to facilitate the installation of

GWB (screwing the mid vertical axis of GWB) on the wall panel. The truss profile was made of 89mm × 89mm × 2mm SHS. In the SHS truss, the diagonal elements were connected to vertical members through full fillet weld connection. The CFS part in the hybrid frame was composed of studs and blocking members (92mm web; 36mm flange; 10mm lip; and 0.55mm thickness) as well as tracks (92mm web; 50mm flange; and 1.15mm thickness). The self-drilling screw of 12-gauge diameter was also employed for the stud-to-track connections and connections of SHS elements to CFS track. The dimensions and construction details of a typical hybrid wall (HW4) are shown in Figure 3.1 and Figure 3.2, respectively.
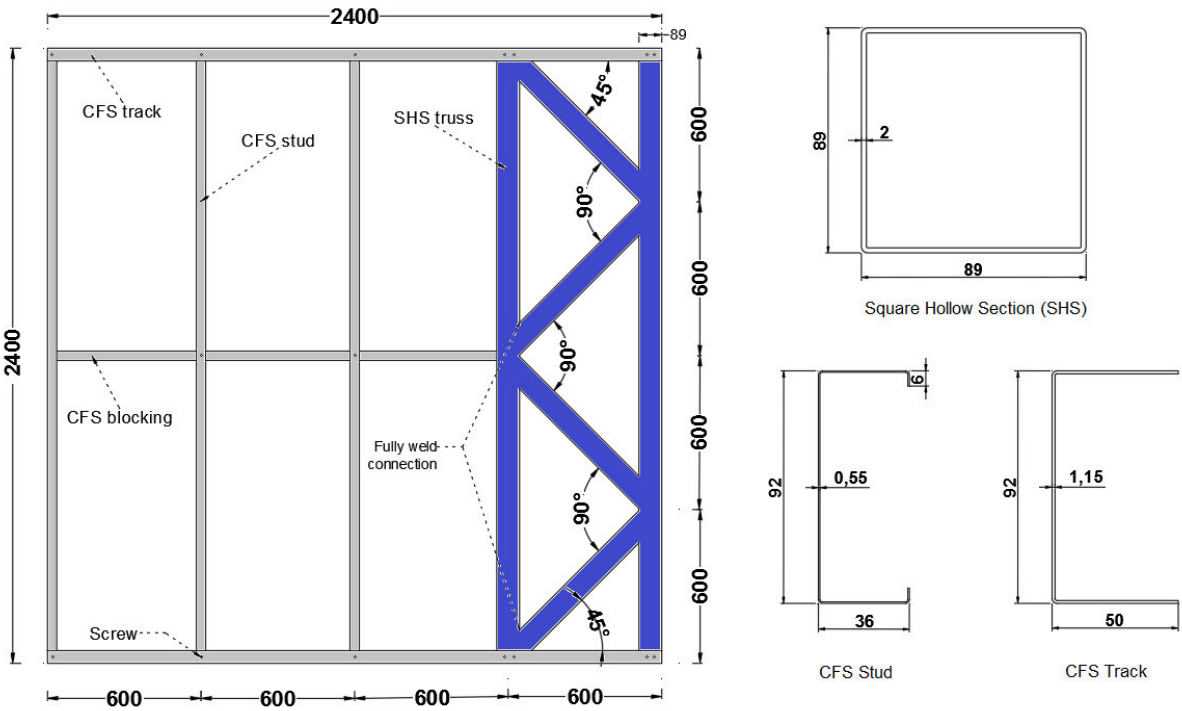
Figure 3.1. Detailed dimension of a typical hybrid wall in mm
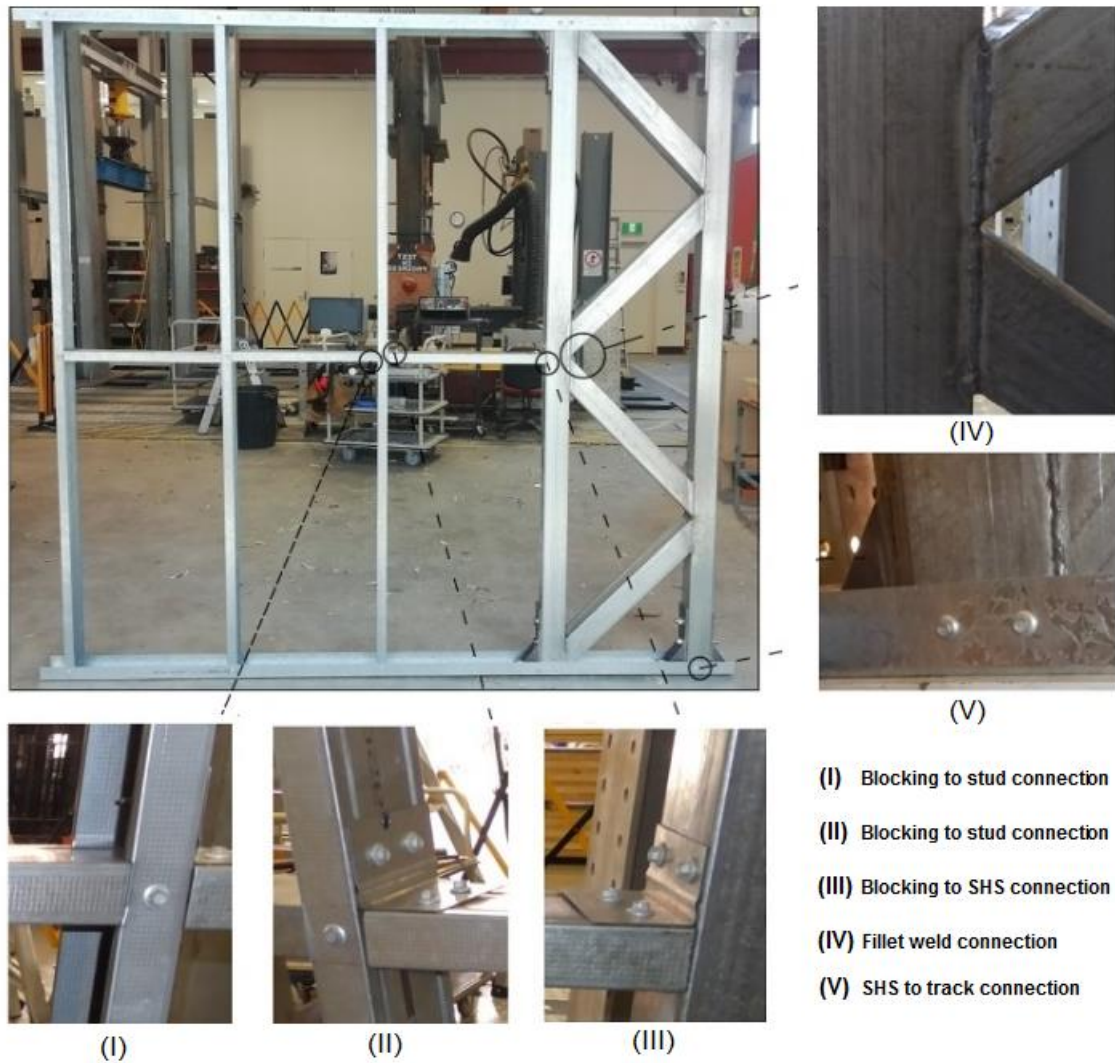
Figure 3.2. Construction details of the hybrid panels

(I) Blocking to stud connection
(II) Blocking to stud connection
(III) Blocking to SHS connection
(IV) Fillet weld connection
(V) SHS to track connection

As shown in

Table 3.1, seven different schemes were examined in this study through eleven tests. The test specimens were categorised into two groups according to the wall-to-floor connection; namely, connection type A and connection type B. First, specimen HW1 and HW2 were tested by connection type A and after observation of failure modes, the modified connection type B was proposed and utilized for all the other specimens.

Because of the asymmetric configuration of the walls, the performance of the panels was investigated through both pushing and pulling phases.

Table 3.1. Shear wall test matrix.

Test number	Specimen	Load direction	Connection type	GWB	SHS (mm)	CFS (mm)	
						Stud	Track
1	HW1	Push					
2		Pull	Connection type A				
3	HW2	Push					
4	HW3	Push					
5		Pull		-			
6		Push (a)			89×89×2	92×36×0.55	92×50×1.15
7	HW4	Push(B)	Connection type B				
8		Pull					
9	HW5	Push					
10	HW6	Push		✓			
11	HW7	Push		✓			

Different configurations of hybrid walls, tested in this study, are illustrated in Figure 3.3. The specimens HW1 and HW3 were constructed of the SHS truss skeleton and three CFS studs as the vertical members. For specimens HW2 and HW4, in order to improve the shear strength as well as preventing the system against the rigid body overturning of the panel, the end CFS stud was replaced by a single SHS element. This configuration also offers better weight distribution for lifting and installation of the shear wall in a real structure. In addition, this single SHS stud can improve the performance of GWB compared to when CFS stud is utilized, mainly due to the higher thickness of SHS. Specimen WH5 was assembled to investigate the effect of having single SHS elements as the chord stud of the wall and was considered as a reference to evaluate the influence of truss skeleton in the hybrid panel. Finally, specimens HW6 and HW7 were sheathed with GWB to examine the effect of sheathing material on the performance of the hybrid shear wall. The structure of the sheathed specimens was similar to specimens HW4 and HW5. For the sheathed specimens, the GWBs were attached to the frames using 12-gauge self-drilling screws that were 35 mm long. The screws were spaced at 300 mm on the CFS and SHS elements.
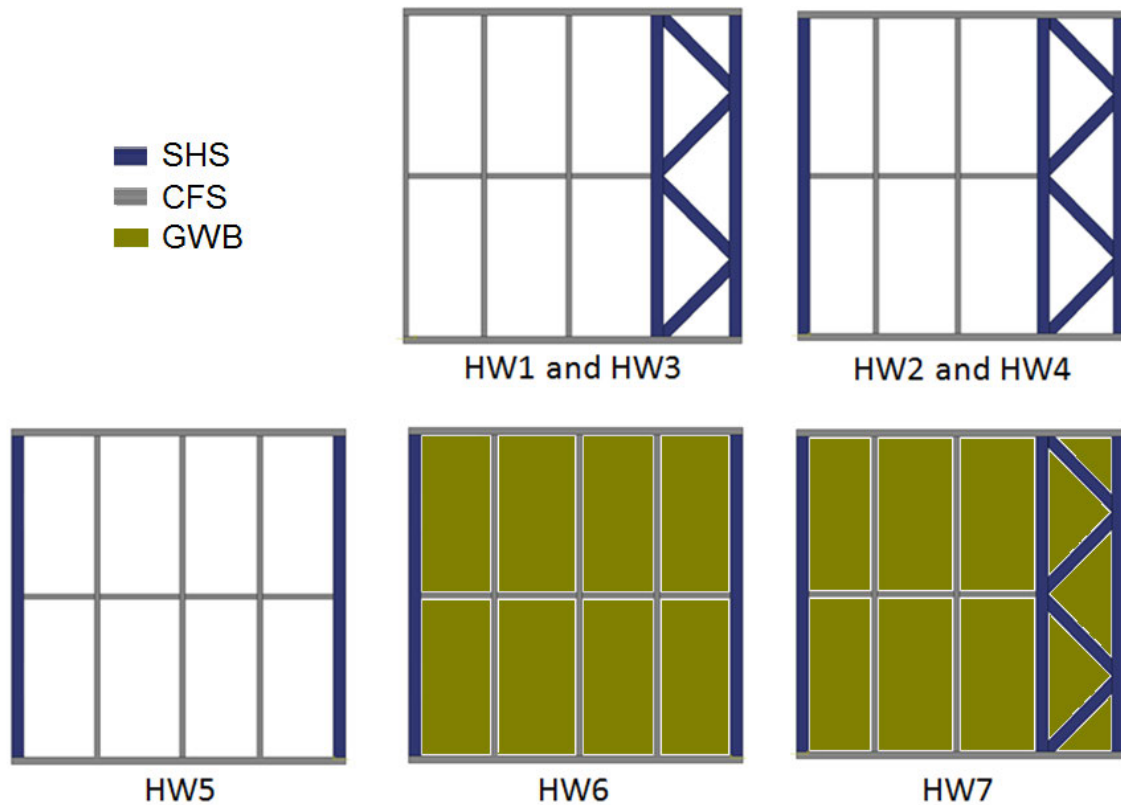
Figure 3.3. Different configurations of hybrid walls

3.2.2 Material properties

In order to determine the material properties of the wall components, coupon tests were performed following ASTM A370 ''Standard Test Methods and Definitions for Mechanical Testing of Steel Products'' [103]. The stresses and strains curves were captured from the coupon tests; then, the mean values of the material properties of wall components were obtained, as listed in Table 3.2. All the coupons meet the minimum ductility requirement by North American Specification for Design of Cold-Formed Steel Structural Members [104], which requires a tensile to yield strength ratio higher than 1.10, and an elongation greater than 7% for a 200 mm gauge length standard specimen.

Table 3.2. Material properties of the wall components

Section Type	Nominal thickness (mm)	Yield stress, f_y (MPa)	Ultimate stress, f_u (MPa)	Elongation (%)	Steel grade	Australian standard
SHS	2	352	438	15	C350	AS1163 [105]
CFS Stud	0.55	305	338	18	G2	AS1397

and Blocking					[106]
CFS Track	1.15	295	332	18	

3.2.3 Wall to floor connections

Generally, hold-down for wall to floor connection are used in two different ways. The first method is to have a fuse hold-down which provides more energy dissipation in the hold-down and the failure is intentionally concentrated in the hold-down. The other method is to have a rigid hold-down which causes failure in the wall and the hold-down remains intact until the end. The second method of hold-down connection was used in this study.

The behaviour of hybrid wall panels in this study depends on the connection of SHS elements to the top and bottom floor (top and bottom beams in the test). The hold-down connector plays two essential roles in the proposed hybrid wall panel. First, hold-downs are installed on the boundary elements to resist the overturning forces developed by the lateral load. Second, the hold-downs are employed to transfer the shear load from the top floor to the bottom floor through SHS elements preventing CFS sections from engaging in this mechanism. As shown in Figure 3.4, which indicates the force transition trend of a wall panel, the in-plane shear force applied to the top floor (loading beam in the test) is uniformly transferred to the wall panel through top hold-down brackets. The force is then distributed in the wall panel by SHS elements and then transferred to the bottom hold-downs. Finally, the forces are transferred to the lower foundation (bottom beam in the test) by the bottom hold-downs. Therefore, the load-carrying mechanism in a hybrid wall panel is somewhat different from CFS framed structure. In the hybrid wall panel, the CFS stud and noggins do not interact with the applied shear force and remain undamaged to the end of the test and their main application is only for bearing gravity loads.
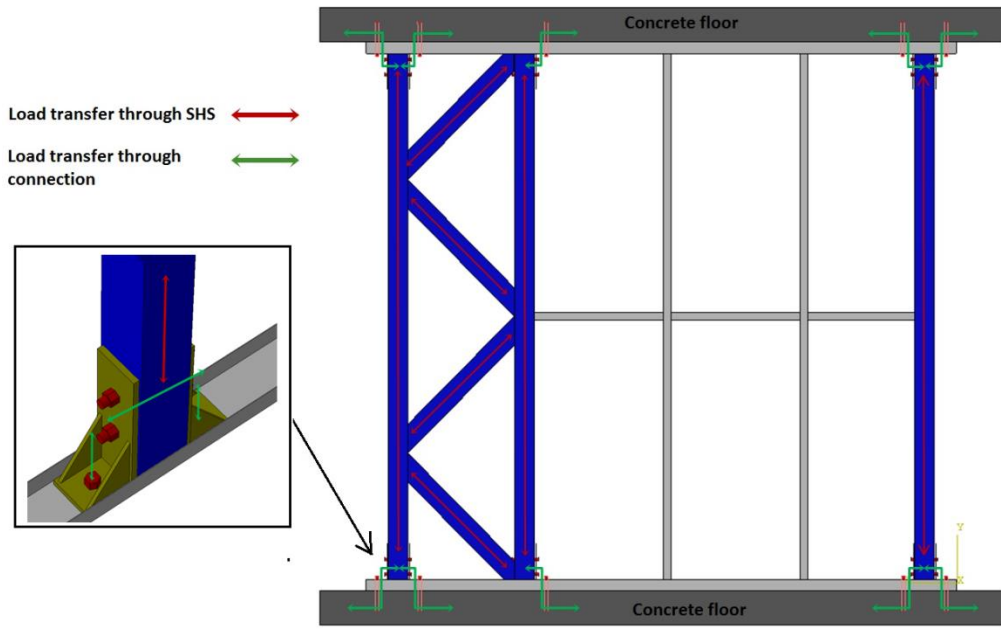
Figure 3.4. Load transition trend in a hybrid shear wall

As reported in several studies [19, 44, 90, 107], the unexpected failure of the hold-down and anchor rod negatively impact the overall performance of wall panels and thus the shear walls cannot reach their full capacity. Therefore, in this study, the hold-down dimensions were determined in a way to remain elastic and undamaged during the test to prevent any unfavourable failure in the wall. The anticipated uplift force for determining the hold-down dimensions was captured through numerical model of SHS truss under the lateral load. The dimension of the hold-down device is illustrated in Figure 3.5.
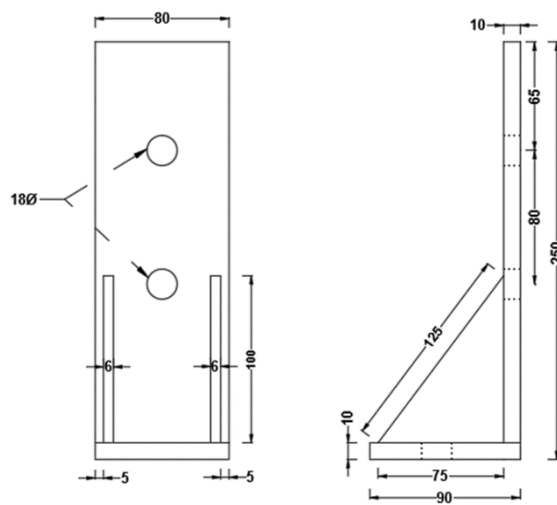
Figure 3.5. Details of hold-down device (measure in mm)

Two different types of wall-to-floor connections were employed in this study, as shown in Figure 3.6. For the specimens HW1 and HW2, the connection type A was used for connecting the wall panel to the top and bottom beams. In this type of connection, the hold-downs were attached to the wall using two 16-mm-diameter threaded-anchor rods and two nuts at both ends. The tension created by the tightening of the rods is also shown in Figure 3.6. For other specimens, HW3-HW7, the connection type B was utilized to connect the hold-down device to the SHS elements by four 18-mm-diameter bolts and four nuts. The friction and bearing capacity between the hold-down and the SHS elements in this type of connection is much higher than connection type A (due to tension created by four bolts and utilizing bigger bolts) which provides better uplift resistance for the wall. Although different types of wall-to-floor connectors can be employed for this system, it should be mentioned that this research only aims to evaluate the lateral behaviour of the proposed hybrid wall and therefore, the effects of connections on the performance of walls is out of the scope of this study.
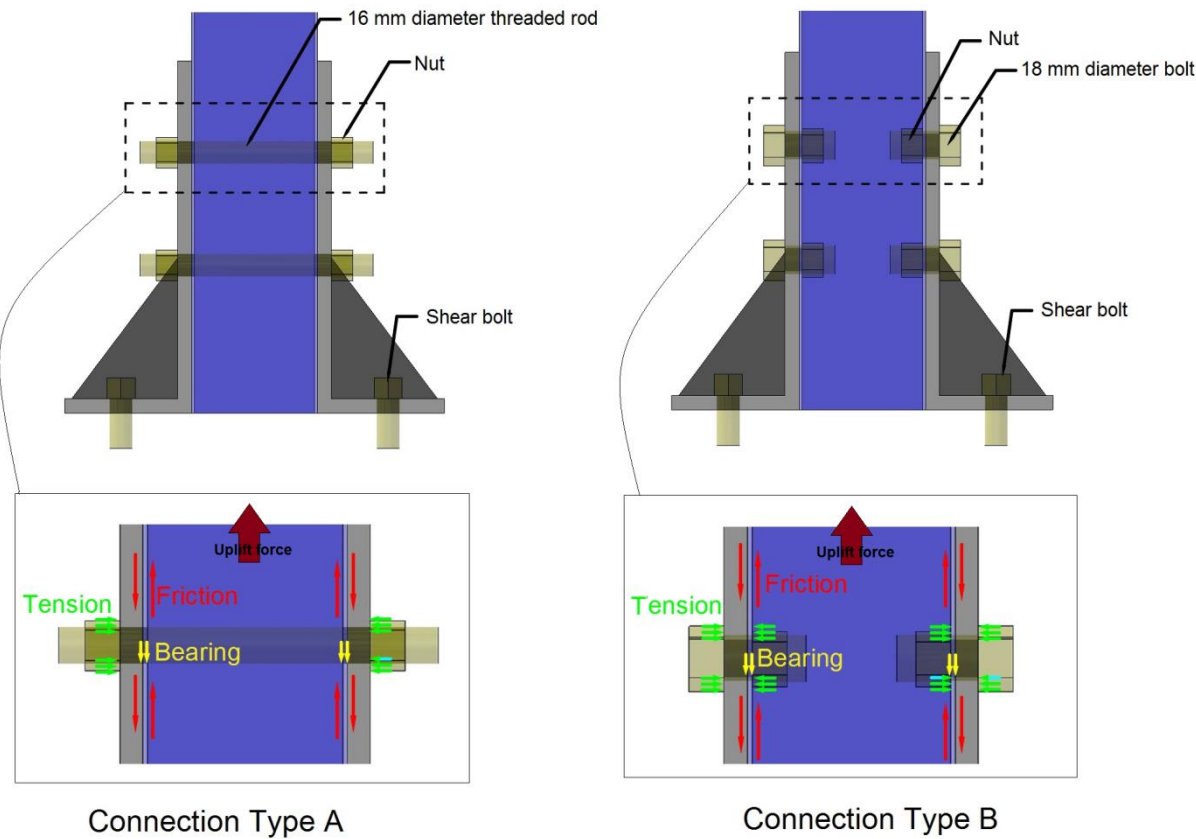
Figure 3.6. Connections used for the hybrid wall panels

3.2.4 Test setup

The general schematic of the testing rig, including frames, rigid floor, top and bottom beams, instrumentations, connectors, and lateral restraints, is illustrated in Figure 3.7. The reacting structure was a frame designed to be able to support the reaction with relatively negligible deformation. This frame was mounted on a multi-configurable strong floor.
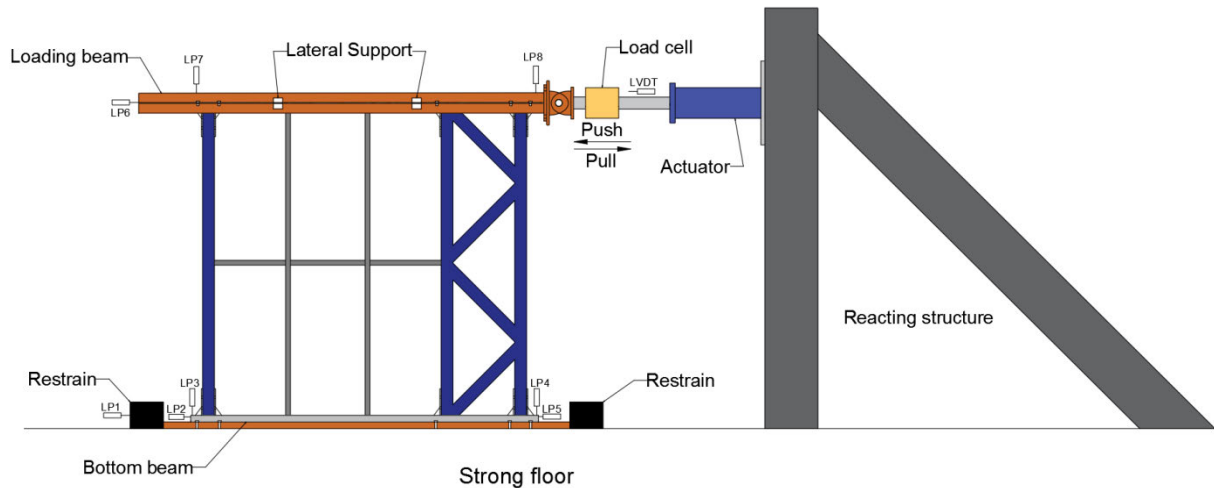
Figure 3.7. Test rig and instrumentation

The wall panels were positioned in the test rig between the bottom reaction beam and the top loading beam. The top track of each wall specimen was attached to the loading beam (which simulates the floor system in real structure) with 16 mm diameter bolts. The loading beam was made of H section steel (160 mm web height, 150mm flange width, 8 mm web thickness and 11 mm flange thickness), which was placed at the top of the shear wall. The hold-down brackets connected the wall panels to the top and bottom beams through M16 bolts, with A490 grade under the new ASTM-F3125 specification [108], to transmit the lateral force to the strong floor.

A Hydraulic actuator with a ±120mm stroke was utilised for shear wall tests. A 200 KN load cell capacity was also used to measure the applied load. Two sets of rollers were employed on both sides of the loading beam in order to restrain the out-of-plane deformation of the panel during the test. Figure 3.8 shows different experimental setups for the installation of the wall panels. The final hybrid wall panels placed in the testing rig are also shown in Figure 3.9. It is notable that due to limitation of laboratory equipment and difficulty of controlling the test, gravity load (vertical load) was not applied to the specimens.

(a)　　　　　　　　　　　(b)

(c)　　　　　　　　　　　(d)
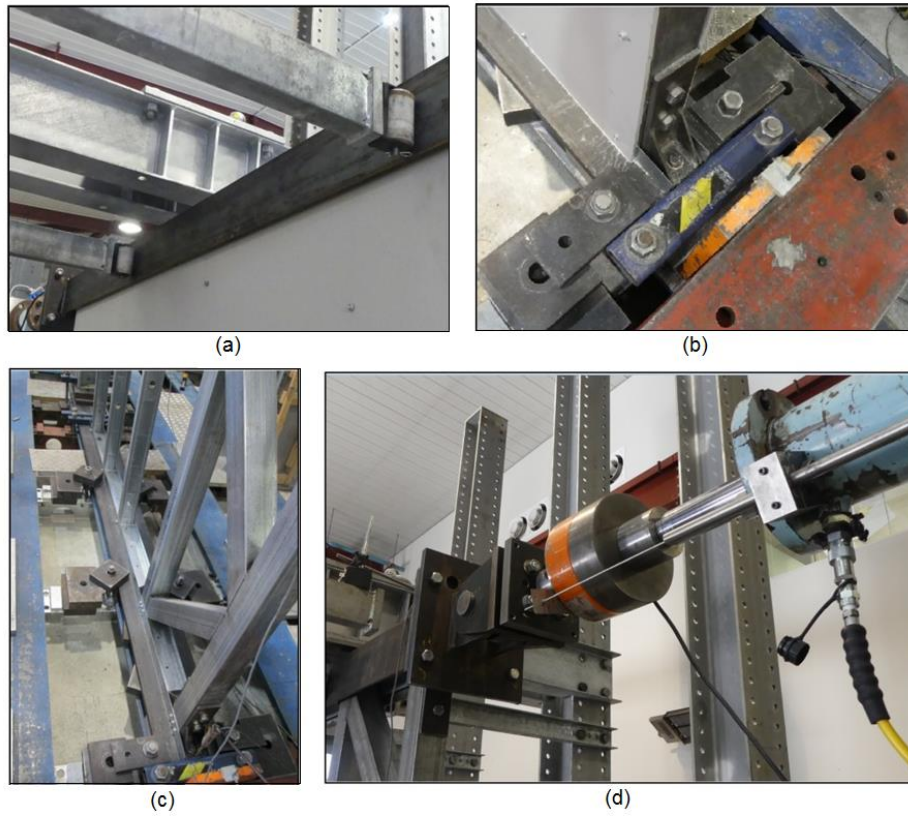
Figure 3.8. Experimental setup:　a) Lateral Support　b) End of wall restraint　c) Restraining of bottom beam d) Connection of actuator to the wall

(a)　　　　　　　　　　　　　　　　(b)

(c)　　　　　　　　　　　　　　　　(d)
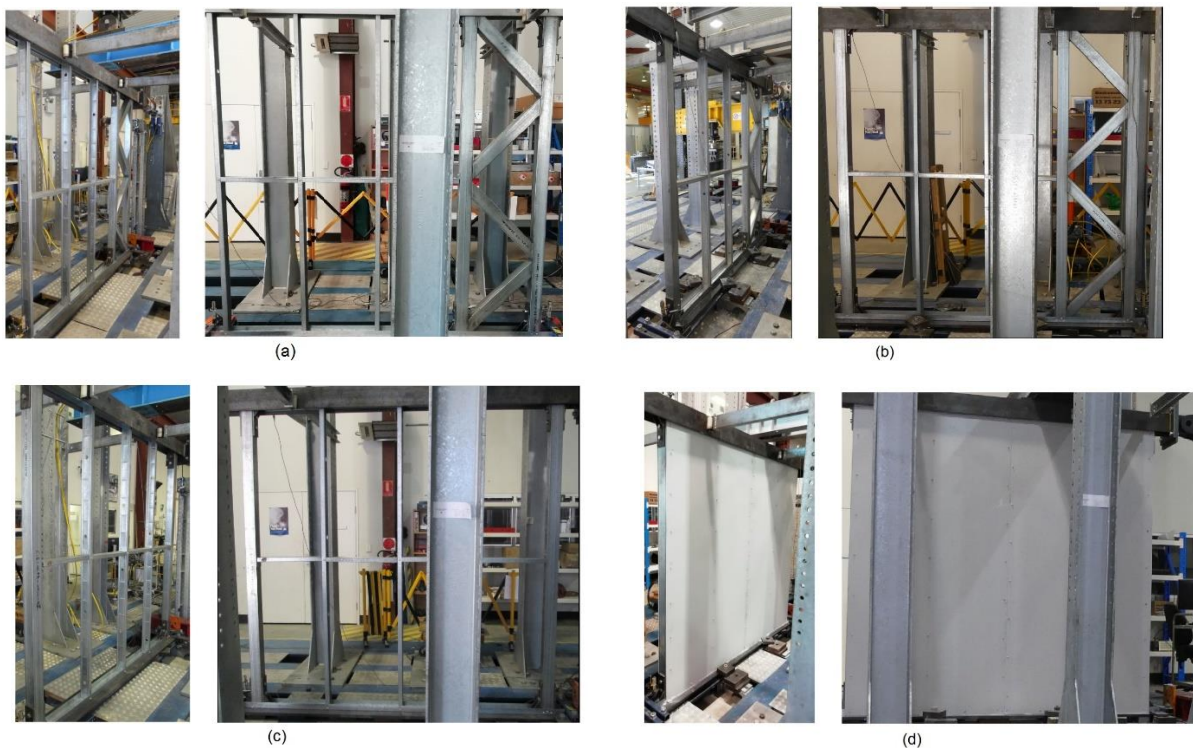
Figure 3.9. Hybrid wall assembly before the test a) HW1 and HW3, b) HW2 and HW4, c) HW5, d) HW6 and HW7

In order to measure the deformation of the walls in different locations, eight Linear Potentiometers (LP) were used in the tests, as shown in Figure 3.7. LP6 was installed at the end of the wall to measure the horizontal displacement. LP2 and LP5 were utilized to measure the relative slide between the wall specimen and the bottom reaction beam. LP3, LP4, LP7 and LP8 were used to measure the vertical displacements on the four corners of the wall panel. LP1 was used to measure the slippage of the bottom beam. One linear variable differential transformer (LVDT) was also connected to the load cell to measure the horizontal displacement of the wall at the connection of the wall to the actuator.

Monotonic loading protocol under a displacement-controlled regime with a rate of 0.1 mm/s was employed for testing of shear walls. Loading continued until an approximate displacement of 90 mm was reached, which is well beyond the allowable drift limit of 2.5% of wall height (60mm) as prescribed by the FEMA450 [109].

3.3 Experimental results

3.3.1 Load displacement curve

The lateral performance of a shear wall can be represented by the relationship between shear strength and lateral displacement of the wall panel. The load values are the lateral load measured by the load cell at the top of wall panels, while the displacement values are the net lateral displacement recorded with LPs placed at the top and base of the walls. As shown in Figure 3.10, the measured displacement (Δ_m) calculated by LP6 comprises three components: a) the net displacement (Δ_{net}), b) the horizontal deformation (Δ_s) because of the sliding between the panel and the bottom reaction beam, and c) the displacement due to the rotation of the wall (Δ_r). Hence, the net displacement (Δ_{net}), which can be used for the load-displacement curve of a wall specimen, is calculated as follows:

$$\Delta_n = \Delta_t - \Delta_s - \Delta_r \tag{3-1}$$
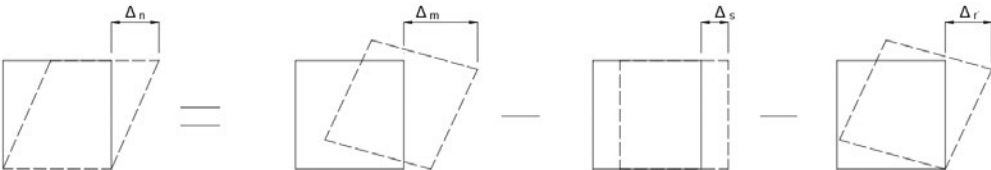
Figure 3.10. Measuring the net deformation

3.3.1.1 Results of specimens with connection type A (HW1, HW2)

Figure 3.11 shows the experimental responses for the specimens HW1 and HW2, in terms of lateral shear resistance vs lateral displacement. In these three specimens, the wall resistance started to decrease unexpectedly at 70-80 mm lateral drift. Specimen HW2 provided a maximum shear resistance of 38 KN, though the shear strength was still lower than the anticipated capacity of the frame. The main reason for this unfavourable behaviour can be attributed to the type of connection used for these panels, which was not designed properly to take the uplift. This factor resulted in a gradual decline in the shear resistance and stiffness of the walls.

In this connection, at the initial stages of loading, the major uplift force transfer between the SHS and hold down is by friction. The friction capacity depends on the normal force between the plates created by the rod tension. Once the applied force exceeds the nominal slip capacity, the connected elements slip relative to each other until SHS bear on the rod and hold down. After slip occurs, the force is then transferred by bearing between the edge of the SHS hole, the rod and the hold-down.
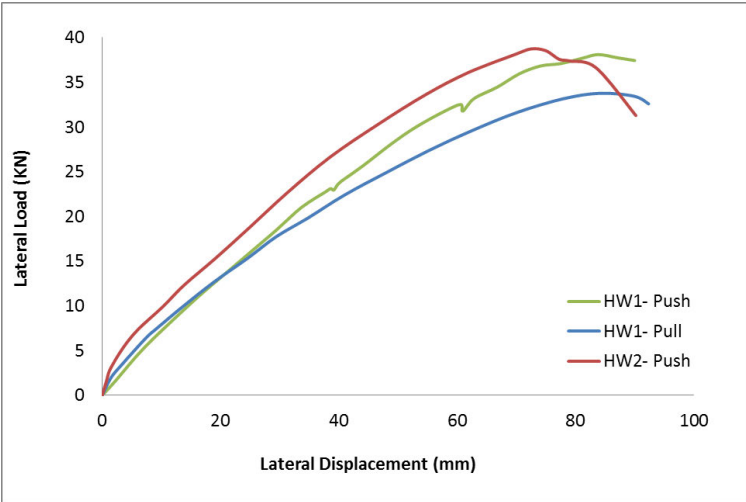
Figure 3.11. Lateral load-displacement of the Specimens HW1 and HW2

As shown in Figure 3.12 and Figure 3.13, the general failure mechanism of these three specimens was nearly similar; however, compared to specimen HW2-push, which comprised a single SHS element at the end of the wall, in specimen HW1-push, the lack of this single element caused damage at the location of the hold-down to SHS connection due to overturning of the wall. This failure was followed by a decrease in stiffness and strength capacity. Screw tilting failure was also observed in some parts

41

of the tracks the lateral displacement was increased. The bearing of track flange as well as the track local and distortional buckling were the other failure modes at this region, as shown in Figure 3.14. No further failure was observed in the SHS members and the SHS truss remained almost in elastic form with small plastic damages. Based on the observations made of the failure mode, an improvement was made when the second phase of tests were carried out on the walls with connection type B.

(a) (b)
(c) (d)
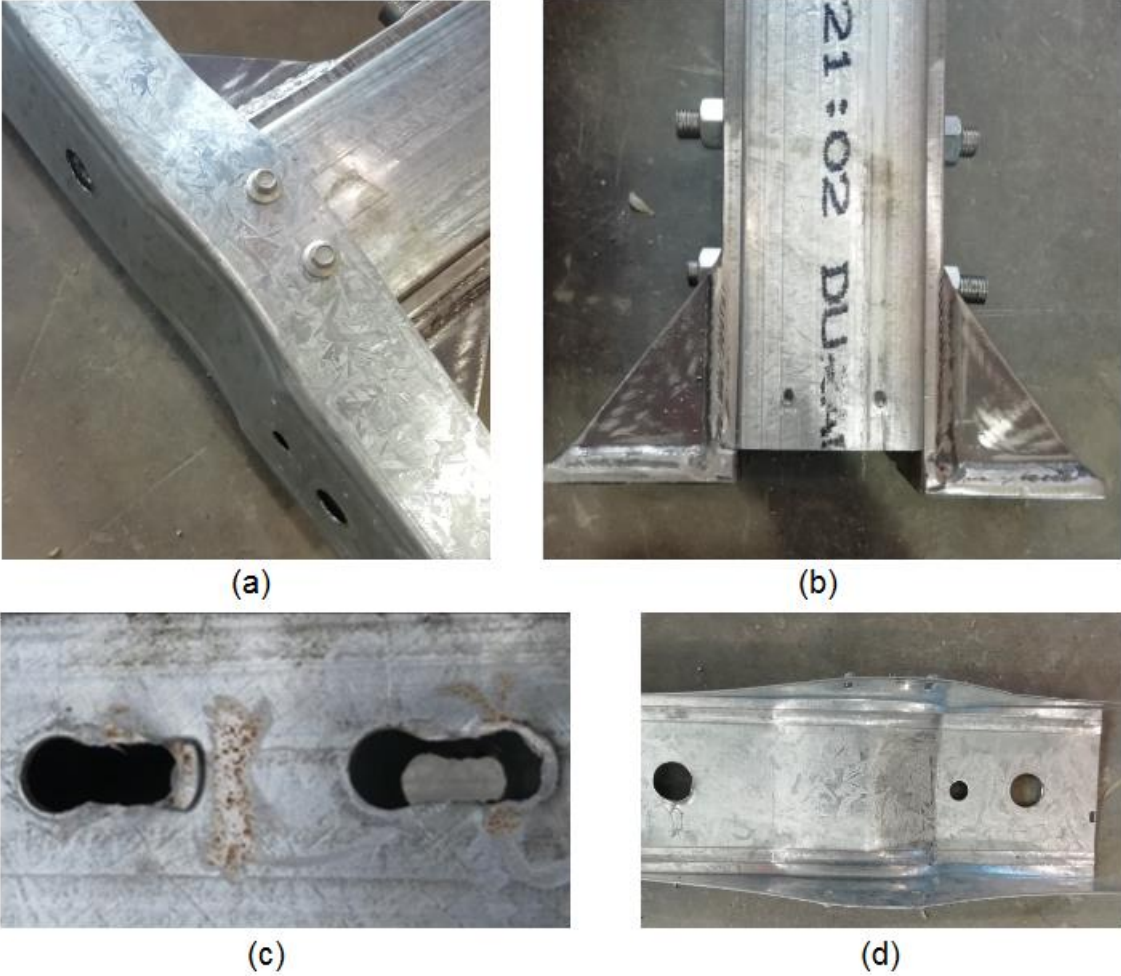
Figure 3.12. Failure modes of specimen HW1-Push: a) Deformation of track   b) Sliding of SHS element   c) Failure at the location of holes   d) Buckling in track
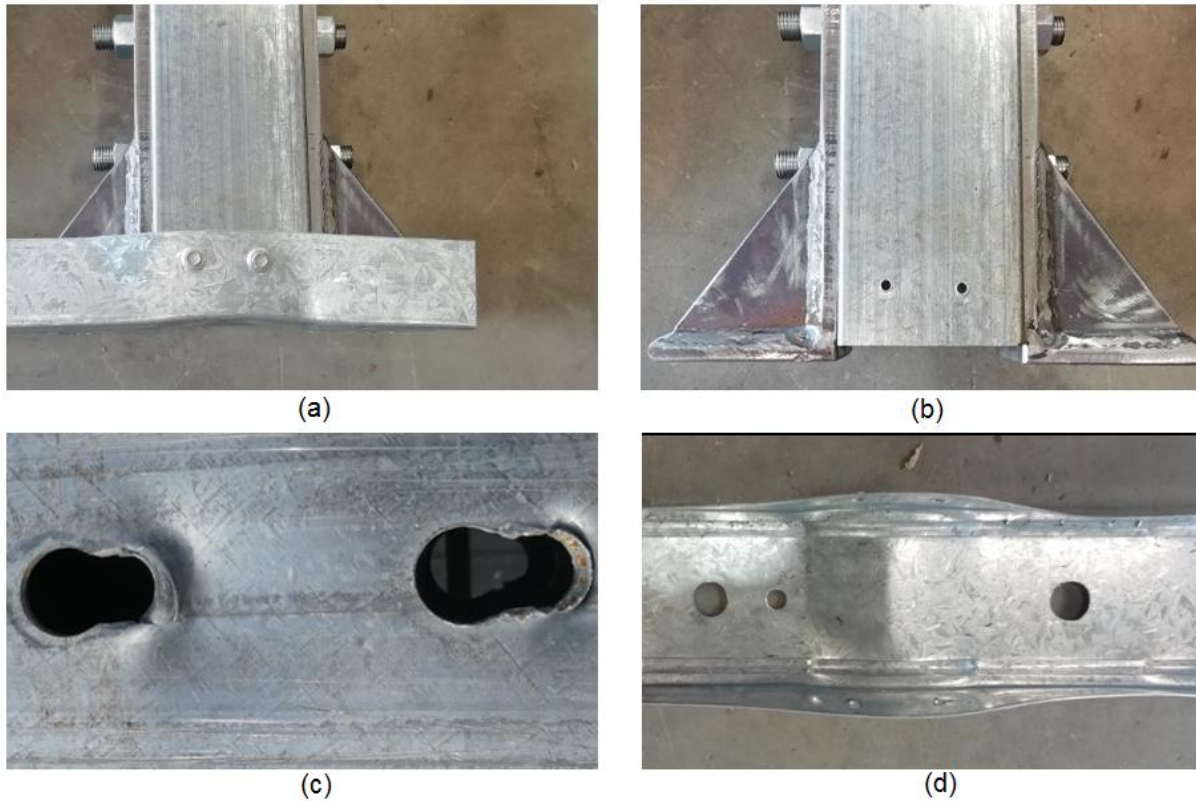
Figure 3.13. Failure modes of specimen HW2-Push: a) Deformation of track   b) Sliding of SHS element   c) Failure at the location of holes   d) Buckling in track

Figure 3.14. Failure modes of the track: a) Screw bearing, b) Track buckling

3.3.1.2 Results of specimens with connection type B, without sheathing (HW3-HW5)

The load-displacement curves for specimens HW3-HW5 are presented in Figure 3.15. In these specimens, due to the application of connection type B, both the load-resistance capacity and the lateral stiffness of the wall are much higher than corresponding values for walls with connection type A. As it is evident in Figure 3.15,

the hybrid wall with single SHS element at the other end of the wall (HW4) exhibited higher load capacity and stiffness compared to the similar wall but without single SHS chord stud at the end of wall (HW3). The higher capacity and stiffness of specimen HW4 was because of two main reasons: First, the single SHS chord stud at the end of the wall could offer higher lateral load resistance capacity for the wall; and second, the single SHS element prevented overturning of the wall during the loading procedure.
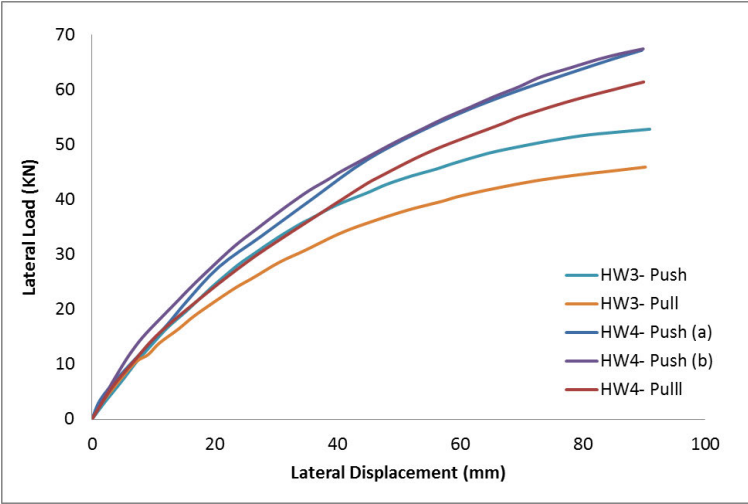
Figure 3.15. Lateral load-displacement curve of the specimens HW3-HW5

The difference between pushing and pulling phases for both HW3 and HW4 can be seen in Figure 3.15. The difference in lateral load-carrying capacity of specimens HW3 and HW4 in pushing and pulling phase is gradually enhancing by increasing displacement, indicating that walls in pulling phase demonstrate weaker performance than pushing phase. This difference is generally due to the asymmetric configuration of hybrid walls as well as SHS truss part. As shown in Figure 3.16, in the pushing phase, the SHS truss at the loading side is under tension force being restrained by two hold-down connectors, and the SHS element at the other side of truss is compressed to the bottom track due to the rigid body rotation of the wall. On the other hand, in the pulling phase, only one hold-down is restraining the SHS element in tension which gives lower stiffness and rigidity compared to the pushing phase.
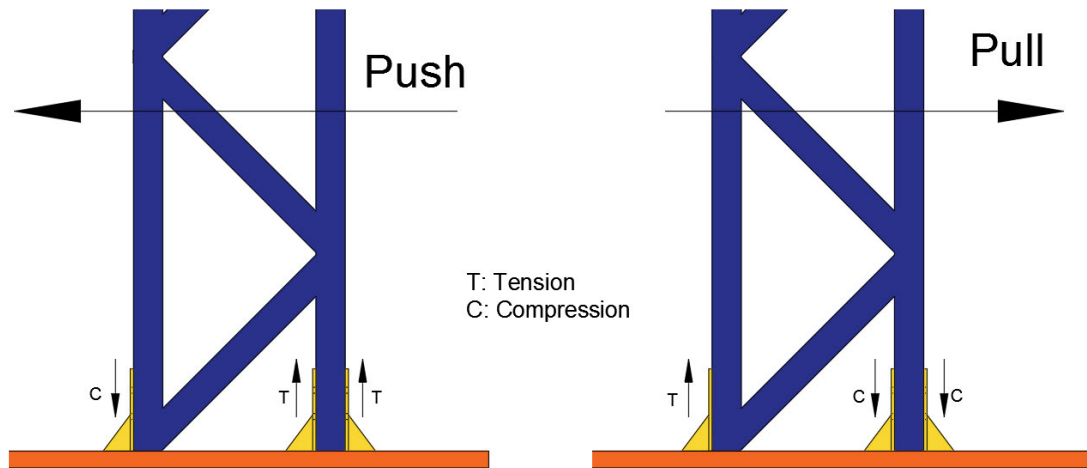
Figure 3.16. Higher stiffness for pushing phase

Figure 3.17 shows the deformation of a typical hybrid wall. As hinged screw connections were employed at the location of the stud to track connection, the CFS part barely resisted any lateral load. As a result, no failure was observed in the CFS sections and the shear strength of the wall can only be attributed to the SHS truss profile, as described in Figure 3.17. All shear walls exhibited elastic deformation in SHS members at small displacement amplitudes. By increasing the lateral displacement, the typical failure was localised at the connection point of the SHS elements to the hold-down devices for most of the specimens which was followed by a decrease in the stiffness of the wall panel, according to the observations made during the tests. Technically, the weakness of connection can be overcome with different methods; nevertheless, the stiffness difference between SHS elements and the strengthened connection would cause some local failure at the same location again. The failure modes of specimens HW3-pull, HW3-Push, HW4-Push are shown in Figure 3.18.
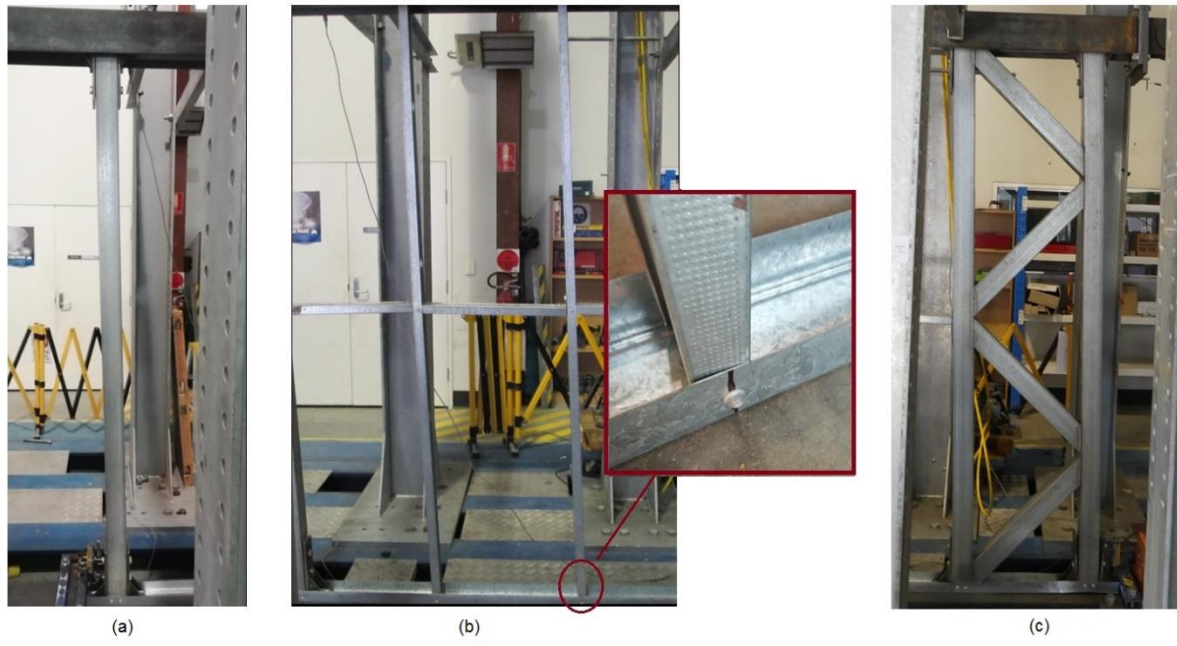
Figure 3.17. Typical deformation of a hybrid wall: a) Deformation of Single SHS element b) Deformation of CFS sections   d) Deformation of SHS truss
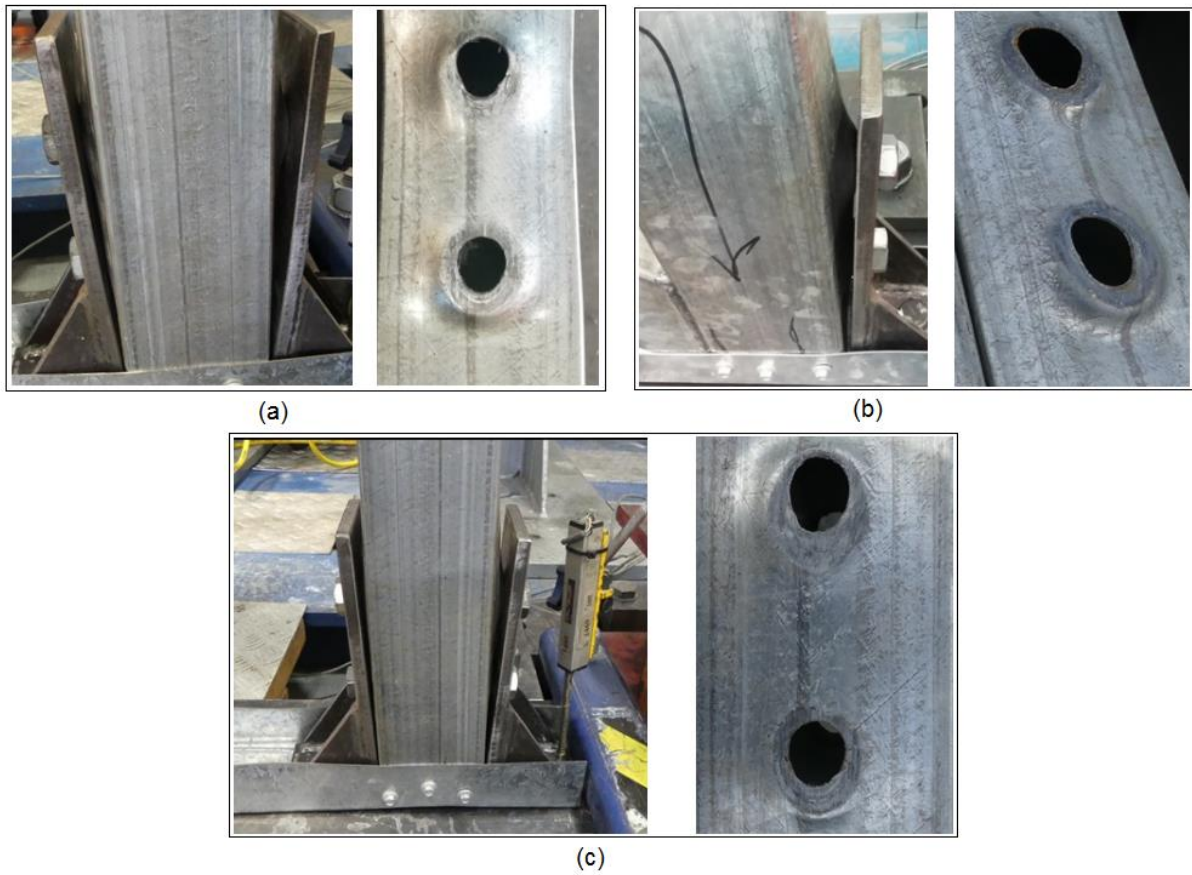
Figure 3.18. Failure modes of specimens: a) HW3-Pull   b) HW3-Push   c) HW4-Push

3.3.1.3 Results of specimens with connection type B and GWB (HW6- HW7)

To determine the effect of sheathing on lateral load performance of the hybrid walls, specimens HW6 and HW7 were tested with GWB under conditions similar to specimens HW5 and HW4, respectively. As shown in Figure 3.19, GWB can increase the lateral strength of specimens HW6 and HW7 by 16% and 50%, respectively, which is a remarkable progress in comparison with conventional CFS walls. The main reason for this increase can be justified by the higher thickness of SHS elements compared to CFS members, which can provide more surface interaction between screw, GWB and SHS, leading to higher tilting and bearing resistance of screw connections. Besides, SHS elements are stiffer than CFS members with a much lower chance of distortional buckling, causing sheathing board to remain undamaged on the wall for a longer time. Another benefit of GWB can be inferred from the area under the load-displacement curve, which shows higher energy absorption of sheathed hybrid wall panels compared to unsheathed specimens.

The considerable effect of GWB can also be derived from Figure 3.20 and Figure 3.21, showing the failure modes of sheathed hybrid walls. In comparison with unsheathed hybrid walls (HW4 and HW5), the sheathed walls experienced lower damage at the location of hold-down connections, mainly due to better load distribution and energy absorption of the gypsum panel. The pull-through sheathing mode of failure in specimen HW6 (the reason for the sudden drop in the curve) and tear-out and bearing sheathing failure for both sheathed specimens were the other types of failure occurred during the test.
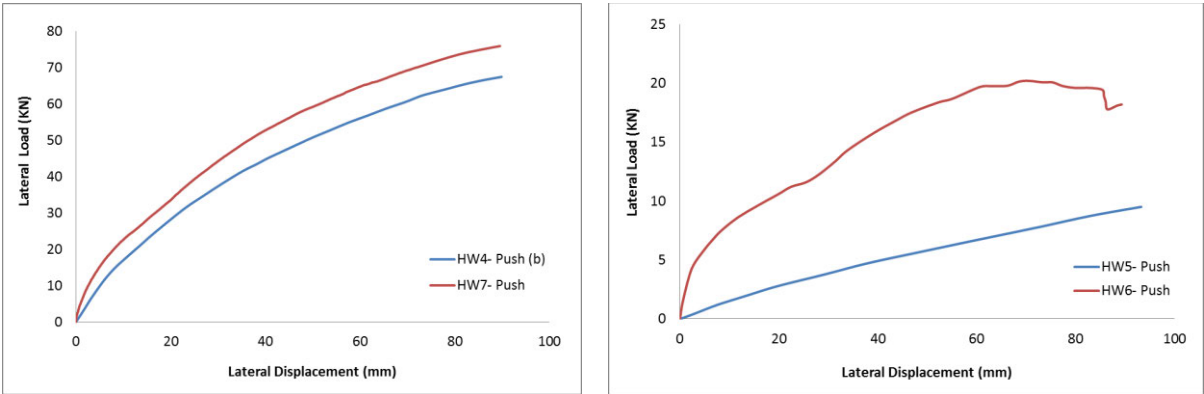
Figure 3.19. Effect of gypsum board on the load-displacement curve of hybrid wall panels (HW6 and HW7)
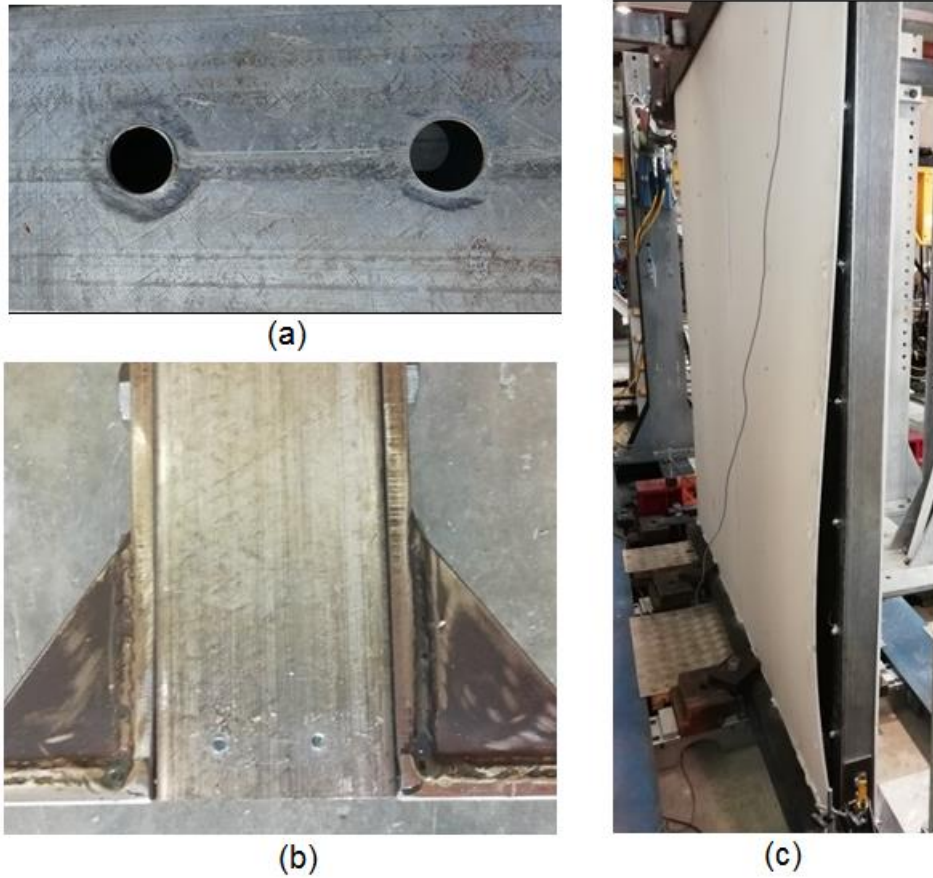
Figure 3.20. Failure modes for specimen HW6: a) Small local failure near the holes, b) Negligible sliding of SHS , c) Screw pull-through sheathing
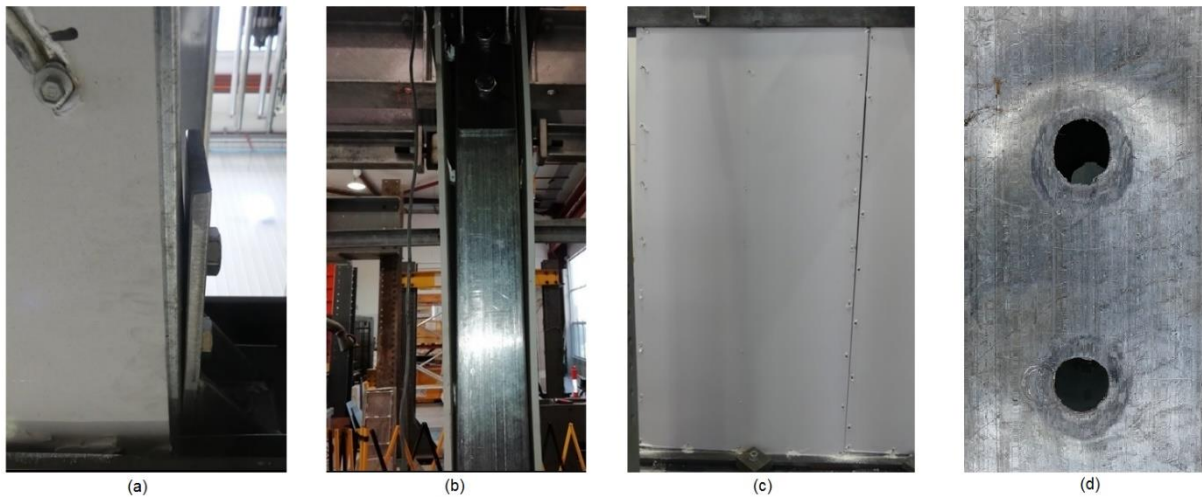
Figure 3.21. Failure modes for specimen HW7: a) bearing failure, b) screw pull-through sheathing, c) Detachment of the GWB d) buckling of SHS

3.3.2 Design values of loads and displacements

In order to develop design parameters of a system, experimental results need to be precisely analysed. Yield strength of the system is generally used for calculation of design parameters of CFS framed shear walls. Yet, determining yield strength value from a nonlinear load-displacement curve is complex in practice. The Equivalent Energy Elastic-Plastic (EEEP) model is a common approach suggested by AISI manual [110] for developing design parameters of CFS shear walls.

In this model, the dissipated energy measured by the monotonic or envelope load-displacement curve is equivalent to the energy found under the corresponding bi-linear elastic-plastic curve (areas A1 and A2 are equal), as shown in Figure 3.22. This bi-linear elastic-plastic model describes a wall panel with linear elastic behaviour until the yielding point. Once yielding is reached, a perfectly plastic behaviour is represented by shear wall, until the failure of specimen is occurred.

Using EEEP method based on the test results, the design parameters of shear walls including the elastic load (P_e), yield load (P_y), peak load (P_{max}), and ultimate load (P_u), as well as their corresponding lateral displacements (Δ_e, Δ_y, Δ_{max}, and Δ_u) can be obtained. The maximum point (Δ_{max}, P_{max}) is defined as the peak load and its corresponding displacement on the monotonic curves. The elastic point (Δ_e, P_e) is located at 0.4 P_{max}. Load and displacement at the point of the 80% post-peak load is also considered as the ultimate point (Δ_u, P_u). It should be mentioned that because of high shear resistance (ascending resistance behaviour) of walls in this study, measuring the 80% post-peak load in demand displacement range was not possible. Therefore, the maximum point was considered as the ultimate load and displacement for all hybrid walls.
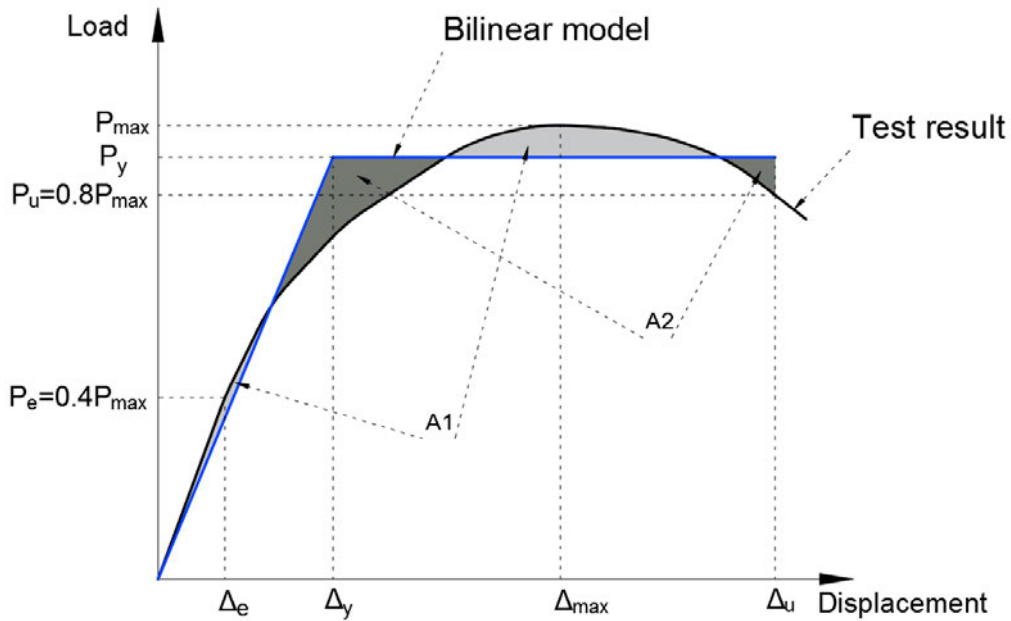
Figure 3.22. Graphical representation of the EEEP method

The yield point (Δ_y, P_y) is determined using the EEEP model. The yielding force and displacement (Δ_y, P_y) as well as the wall initial lateral stiffness (k_0) are determined as follows:

$$K_e = \frac{0.4P_{peak}}{\Delta_e} \qquad (3\text{-}2)$$

$$P_{yield} = \frac{-\Delta_u \pm \sqrt{\Delta_u^2 - \left(\frac{2A}{K_e}\right)}}{-\left(\frac{1}{K_e}\right)} \qquad (3\text{-}3)$$

$$\Delta_{Yield} = \frac{P_{yield}}{K_e} \qquad (3\text{-}4)$$

Where,

P_{yield} = Yielding shear resistance

Δ_{yield} = Yielding displacement at P_{yield}

P_{peak} = Ultimate shear resistance

Δ_u = Displacement at P_u = 0.8P_{peak}

Δ_e = EEEP wall displacement at 40% of ultimate load

50

A= Area under original curve at 80% post-peak load

K_e= Elastic stiffness

The limitation on the maximum inelastic lateral displacement of a shear wall can affect the general EEEP analysis procedure. According to the FEMA450 [109], for seismic design, the maximum acceptable inelastic inter-storey drift is equal to 2.5% of the storey height, which corresponds to a lateral displacement of 60 mm in the specimens tested. However, in some strong CFS shear walls, the ultimate resistance can reach after this lateral drift limit and shear walls can still dissipate a considerable amount of energy. Therefore, as recommended in the AISI report [111], higher lateral drifts can be also considered for these types of walls. That is the reason for choosing 90 mm lateral displacement for end of experiment which corresponds to the 3.75% storey-drift. Although all specimens with connection type B did not reach their ultimate resistance within this limit and the resistance was still increasing, taking a limit higher than 3.75% would not be realistic since no building is expected to undergo such large displacements during a seismic event. Table 3.3 and

Table 3.4 shows the EEEP results for all specimens calculated based on ultimate displacement (3.75% drift or 90 mm lateral displacement) and maximum allowable lateral drift (2.5% or 60 mm lateral displacement), respectively.

Table 3.3. EEEP values calculated based on 3.75% ultimate displacement drift (90 mm)

Specimen	Δ_e	P_e	Δ_y	P_y	$\Delta_{max}= \Delta_u$	$P_{max}= P_u$
HW1-Push	23.7	15.2	53.5	34.4	90	38.1
HW1-Pull	20.5	13.5	44.5	29.3	90	33.7
HW2-Push	19.5	15.5	43.6	34.7	90	38.7
HW3-Push	16.7	21.0	36.4	45.9	90	52.6
HW3-Pull	16.2	18.3	34.9	39.5	90	45.9
HW4-push (a)	20.5	26.9	42.8	56.2	90	67.3
HW4-Push (b)	18.9	26.9	39.3	56.1	90	67.4
HW4-Pull	20.4	24.4	43.0	51.6	90	61.1
HW5	28.8	3.7	59.3	7.6	90	9.3
HW6	10.0	8.1	21.2	17.1	90	20.2
HW7	17.1	30.3	36.1	64.0	90	75.9

Table 3.4. EEEP values calculated based on 2.5% maximum allowable drift (60 mm)

Specimen	Δ_e	P_e	Δ_y	P_y	$\Delta_{max} = \Delta_u$	$P_{max} = P_u$
HW1-Push	19.8	13.0	43.0	28.2	60	32.5
HW1-Pull	16.5	11.5	33.8	23.7	60	28.9
HW2-Push	17.2	14.2	36.7	30.3	60	35.5
HW3-Push	14.5	18.7	30.9	39.9	60	46.9
HW3-Pull	13.9	16.2	29.4	34.3	60	40.6
HW4-push (a)	16.2	22.2	33.7	46.4	60	55.7
HW4-Push (b)	14.7	22.4	30.3	46.3	60	56.0
HW4-Pull	15.9	20.4	32.7	42.0	60	51
HW5	18.9	2.68	38.8	5.5	60	6.7
HW6	9.3	7.8	17.8	15.1	60	19.7
HW7	13.1	25.8	26.7	53.1	60	64.7

3.3.2.1 Lateral stiffness and ductility ratio

According to the EEEP method, the stiffness is calculated based on secant stiffness, using the following equation:

$$\text{Stiffness} = \frac{P_e}{\Delta_e} \times \frac{H}{L} \tag{3-5}$$

where P_e and Δ_e are calculated according to the EEEP model and H/L is the aspect ratio of wall specimen which is 1 for all walls in this study. The calculated stiffness of each test specimen in respect to ultimate displacement (90 mm) as well as 2.5% allowable drift (60 mm) is represented in Figure 3.23.

The stiffness data shows that in general, the stiffness is more prominent for walls with connection type B compared to walls with connection type A. The main reason for higher stiffness of walls with connection type B is the higher friction and bearing capacity of this connection. Utilising GWB in the hybrid panel has also increased the stiffness of the wall panels dramatically. The lateral stiffness of specimens HW7 and HW5 with GWB is about 30% and 500% more than their counterparts without sheathing, HW4 and HW6, respectively. Specimen HW5 has the lowest stiffness among all hybrid walls in this study. Although the stiffness of this specimen enhanced by employing GWB (HW6), this is not still favourable for application in mid-rise structures. Comparing specimens HW4 and HW3 also shows that by using a single

SHS element at the end of the wall (HW4), one can increase the stiffness of wall panel by 16% and 10% for pushing and pulling respectively compared to the wall without SHS element at the wall end (HW3). It should be mentioned that the values of stiffness calculated according to 2.5% allowable drift (60 mm) is somewhat higher than the values calculated based on the ultimate displacement (90 mm), which gives a better choice for design procedure.
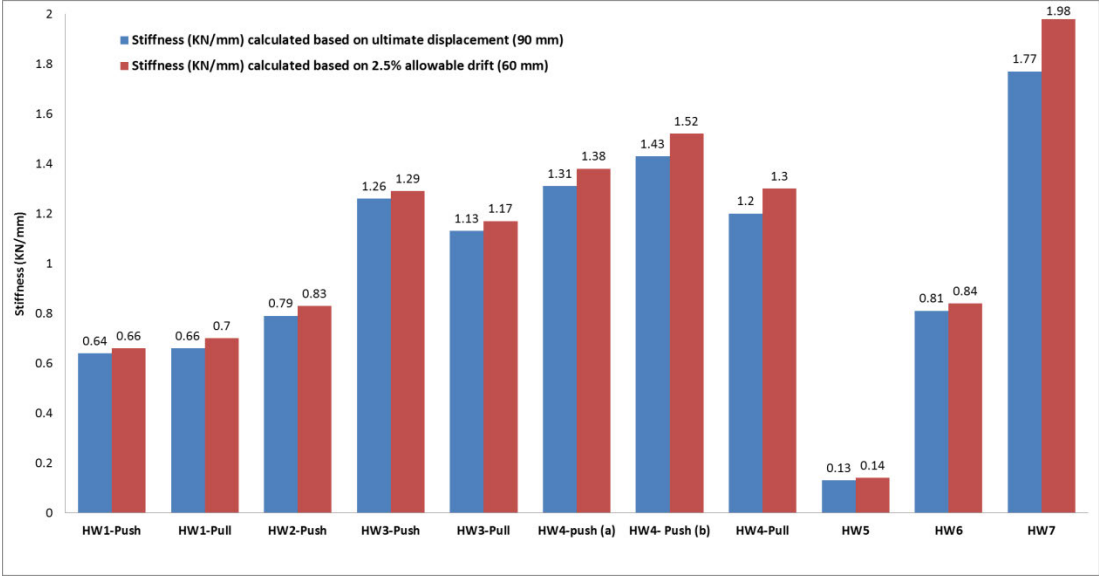
Figure 3.23. Stiffness of specimens

Ductility ratio is another important indicator for evaluating of shear walls, which shows the ability of walls to deform in the inelastic range. The ductility ratio (μ) is the ratio of the ultimate displacement Δ_u to the yield displacement Δ_y, where the displacements Δ_y and Δ_u are calculated using the EEEP method.

The calculated ductility ratio of each tested specimen in respect to the ultimate displacement (90 mm) as well as 2.5% allowable drift (60 mm) is summarised in Figure 3.24. According to the experimental results, it was observed that the specimens with GWB provide higher ductility ratio. This is due to the fact that the stiffness of GWB is significantly lower than steel components of the wall, so that allows for further displacement without a sudden drop in strength capacity. Although the application of GWB had a small effect on enhancing the ductility ratio of the full hybrid wall (comparing HW4 and HW7), the ductility ratio of the hybrid wall with only two single SHS elements with GWB was remarkably increased (comparing HW5 and HW6). This indicates that HW6 shear wall exhibited much better ductility than all other hybrid walls.

Ductility ratio was also reduced when single SHS element was used at the end of the walls with the SHS truss profile (HW4). This is because using single SHS element at the end of the hybrid wall increases the lateral rigidity of the wall and decreases the ultimate displacement, resulting in a reduction of the ductility ratio compared to its counterpart without single SHS element at the end (HW3).

Unlike the stiffness values, the ductility ratio for specimens in the pulling phase is higher compared to the values determined under the pushing phase. This difference is generally due to the asymmetric configuration of hybrid walls as well as SHS truss part which causes different resistance in pushing and pulling phases. The lower stiffness in pulling causes further inelastic displacement under the gradually increasing load. The walls with type B connection also exhibited higher ductility which is attributed to the plastic deformation of SHS elements at the location of connections.
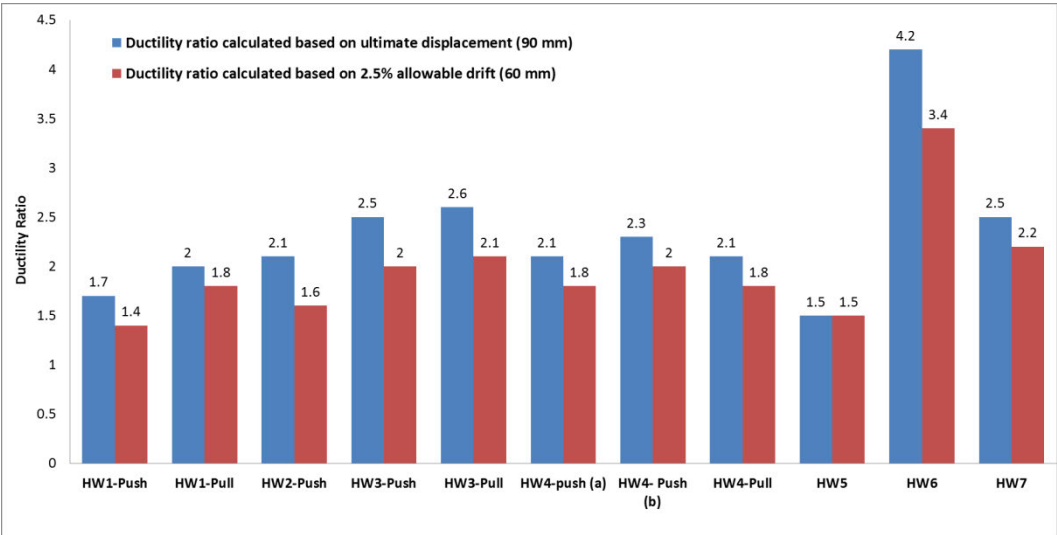
Figure 3.24. Ductility ratio of the hybrid wall panels

3.3.2.2 Energy absorption capacity

The area under load-displacement curve is used for measuring energy absorption of wall panels. Figure 3.25 shows the energy absorption of each test specimen corresponding to ultimate (90 mm) and maximum allowable drift ratio of 2.5% displacements (60mm). Based on the values, the following remarks can be obtained:

(1)   The energy absorption of specimens with GWB (HW6 and HW7) is higher than the energy absorption of specimens without GWB (HW5 and HW4), as expected. This is primarily due to the potential of GWS to dissipate energy by relative sliding that occurs between the board, SHS and studs as well as cracking of the board.

(2)   Because shear walls comprise lower rigidity in the pulling phase, the wall exhibits lower strength capacity compared to pushing of the same wall, which results in lower energy absorption in the pulling phase.

(3)   The relatively low shear capacity of the walls with connection type A resulted in lower energy absorption of these walls compared to energy absorption of walls with connection type B.

(4) The energy absorptions of hybrid shear walls with single SHS element at the end of the wall (HW2 and HW4) are evidently superior to that of hybrid walls without SHS element at the wall end (HW1 and HW3). This is because some more energy is absorbed through the SHS element and its connection to the top and bottom beams.

(5) The results for energy absorption evaluations indicate that the energy absorption calculated based on ultimate displacement (90 mm) is about twice the energy absorption calculated according to 2.5% allowable drift ratio (60 mm). This indicates that the hybrid walls can still absorb a considerable amount of energy beyond the lateral drift limit (2.5%), which can be accounted as a benefit for application in high seismic regions.
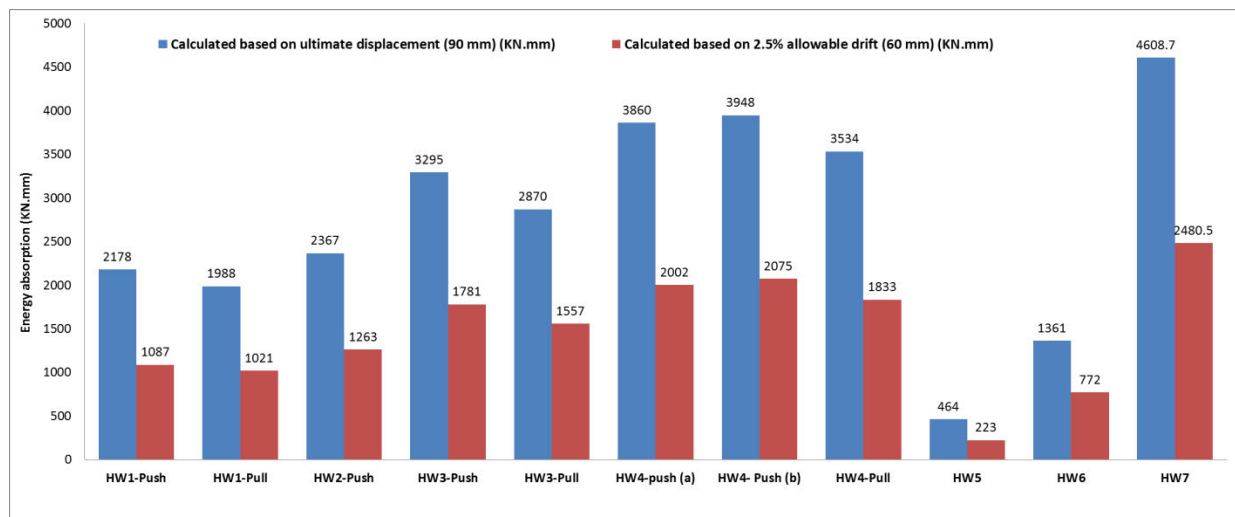
Figure 3.25. Energy absorption of the hybrid wall specimens

3.3.3 Comparison with other CFS walls proposed for mid-rise application

General comparison between hybrid shear walls in this study and other CFS walls is not reasonable due to the differences in the total weight of each wall. Different CFS

shear walls with high shear resistance have been proposed by researchers for application in mid-rise building [17-19]. Yet, the weight of wall panel in these studies is much higher than the hybrid walls in the current study, resulting in the increase of dead loads of whole structure and offering a high seismic base shear during an earthquake. Moreover, the higher weight prevents from prefabrication benefits and can also cause some problems during lifting and installation of walls.

The proposed panel in this study still offers the benefits of a light-weight CFS system by keeping the weight and size of the walls reasonably low. Therefore, panels can be conveniently handled, lifted, transported and installed. Under the same CFS frame and specimen size, the strength to total weight ratio of hybrid shear walls (HW3, HW4 and HW7) is relatively high compared to other shear walls, which shows the capability of application of hybrid walls in mid-rise structures. This can be interpreted by the fact that SHS elements in the form of truss skeleton can increase the lateral shear resistance and absorb more energy through diagonal elements. In addition, in terms of time-saving, it can also be said that construction with hybrid systems is more efficient than CFS shear walls infilled with concrete, foam and mortar. The installation of the panels can also be performed by labours without a need for heavy cranes, which can accelerate the installation process.

3.4 Conclusion

Eleven monotonic lateral load tests were conducted on seven types of hybrid wall panels with different configuration and connection details. Based on the test results, the following findings are concluded:

➢ Specimens HW1 and HW2 showed an undesirable shear performance and mode of failure due to the application of connection type A. Connection Type B was then proposed and utilised in order to improve the shear resistance of the wall. This type of connection provided much higher resistance and allowed shear walls to dissipate more energy in the lateral load path.

➢ Local failures at the location of the SHS element to hold-down connection were observed for all tests. This failure was improved for specimens HW7 with GWB. Although the connection weakness can be improved using different methods. Yet, local plastic failure can again occur between SHS element and hold-down due to the increased stiffness differences between them.

➢ The influence of GWB on the lateral resistance of hybrid panel, energy absorption, ductility and stiffness was significant, which is mainly due to the increased interaction area between screw, SHS elements and sheathing board. It also shows that the finished sheathed hybrid wall with GWB can offer some advantages compared to traditional CFS walls.

➢ Because of the asymmetric configuration of hybrid walls as well as SHS truss part, the lateral load-carrying capacity of the specimens in pushing and pulling phases was slightly different. Specimens in the pushing phase provided higher shear resistance compared to specimens in pulling phase primarily due to the higher stiffness of the wall in this direction.

➢ The specimen W4 exhibited higher load capacity and stiffness compared to the specimen HW3, which can be justified by this fact that single SHS chord stud at the end of the wall for specimen HW4 can provide an overall higher lateral load resistance capacity. In addition, the SHS section limits the overturning of the wall during the loading procedure.

➢ The total mass of the hybrid wall proposed in this study is relatively lower than walls infilled with concrete, foam and mortar. While it is offering a low weight assembly, it also provides high shear resistance and energy absorption, which is because of diagonal elements in SHS truss profile.

Cyclic test is required to be performed on hybrid walls to provide modifications such as ductility modification factor and response modification factor. Therefore, in the next chapter, the cyclic behaviour of the proposed hybrid wall panel is evaluated.

Chapter 4   Experimental program: Cyclic Investigation

4.1 Introduction

In the first phase of this study, the monotonic behaviour of the CFS hybrid panels was investigated through eleven full-scale specimens. However, it is also essential to carry out cyclic tests to derive seismic characteristics such as response modification factor (R factor) by establishing correct relationships. The tasks conducted in this chapter are included in the following steps:

i)   Testing full-scale single-storey hybrid CFS specimens, which can provide higher shear capacity and ductility than CFS walls listed in the CFS regulations,

ii)   Achieving preliminary design parameters and nominal shear resistance values.

iii) Comparing hybrid CFS walls in this study against 87 previously tested CFS wall panels from 28 references in terms of strength to weight ratio.

iv) Determining seismic force modification factors, Rd and Ro according to the Federal Emergency Management Agency (FEMA) FEMA356 [112] and FEMA P-1050 [113] methodologies.

4.2 Experimental program

4.2.1 Test Specimens

Six full-scale CFS wall panels with square geometry of 2400 mm were assembled for the experimental tests, as shown in Figure 4.1. The CFS tracks were selected of U channels with 92 mm web, 50 mm flange and 1.15 mm thickness. The lipped C channels with 92 mm web, 36 mm flange, 10 mm lip and 0.55 mm thickness were also

used as the CFS studs and noggins. The truss skeleton was made of SHS with a dimension of 89 mm × 89 mm × 2 mm. Table 4.1 summarizes the configuration details of the hybrid wall panels. The steel frame components were assembled with 5.5 mm thread diameter self-drilling screws. Three specimens were sheathed with 10 mm thick GWB to determine the influence of sheathing board on the seismic performance of the hybrid shear wall. The GWB was installed on the steel frame through 12-gauge self-drilling 35 mm long screws spaced at 300 mm centre to centre at the perimeter and field studs. The material properties of the wall components summarized in Table 4.2 were also obtained by tensile coupon tests. Three coupons were tested for each wall component and the mean values were then recorded. The screws shear and tensile strengths were 9.1 KN and 15.8 KN, respectively, which were obtained from screw technical guide [114].

Table 4.1. Test specimens

Specimen	GWB	SHS (mm)	CFS (mm)	
			Stud	Track
HW-C1				
HW-C2				
HW-C3		89×89×2	92×36×0.55	92×50×1.15
HW-C4	✓			
HW-C5	✓			
HW-C6	✓			

Table 4.2. Material properties

Section	Nominal thickness (mm)	Yield stress, f_y (MPa)	Ultimate stress, f_u (MPa)	F_u/F_y	Elongation (%)
SHS	2	352	438	1.2	15
CFS Stud and blocking	0.55	305	338	1.1	18
CFS track	1.15	295	332	1.1	18

As illustrated in Figure 4.1, specimens HW-C1 and HW-C2 (H for Hybrid, W for Wall, C for Cyclic test) were fabricated from one SHS truss frame and three open-section CFS studs. The unique difference between these two specimens is that the truss in the specimen HW-C2 is 180° turned over compared to HW-C1. Specimen HW-C3 is also similar to the specimen HW-C2, but in order to mitigate the overturning of the wall panel as well as to provide better seismic performance, SHS element was employed for the chord stud of the specimen HW-C3. GWB was also attached to the HW-C3 and tested as a new wall, HW-C4, to investigate the influence of finishing material on the cyclic

behaviour of the hybrid wall. Specimens HW-C5 and HW-C6 were fabricated to provide insight into the impact of using single SHS as the chord and field studs, and their results were only employed to demonstrate that the truss structure is the leading solution of the proposed hybrid panels. Hold-down device type B used for monotonic study in chapter 3 was also employed for cyclic tests where two 18 mm high strength bolts were utilized to connect the SHS members to the hold-down. The comprehensive details of the wall to floor connections (hold-down type B) as well as the discussion on the friction and bearing between the hold-down and the SHS element can be found in section 3.3 of chapter 3.
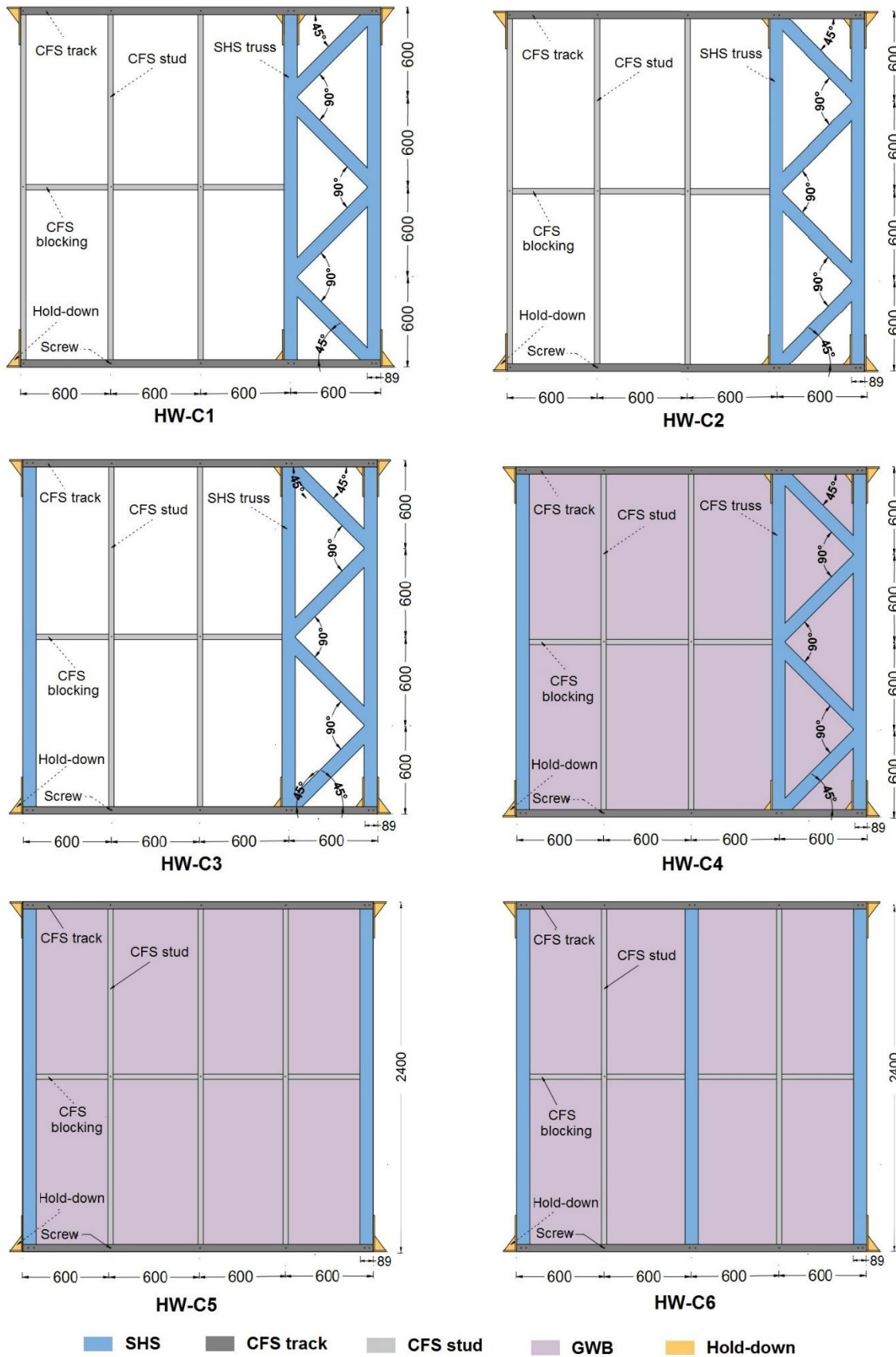
Figure 4.1. Schematic of hybrid walls (all dimensions in mm)

4.2.2 Test setup and loading protocol

The testing rig for performing the cyclic tests is displayed in Figure 4.2. The tracks of the wall specimens were attached to the loading and reaction beams of the testing rig using 18 mm diameter high-strength bolts. The rigid foundation was simulated by fixing the bottom reaction beam to floor. Four lateral supports were utilized at both sides of the loading beam (two at each side) to control the out of plane movement of wall panels. The lateral cyclic load was applied to the loading beam through a hydraulic jack with ±120 stroke and 500 KN capacity. This hydraulic jack was then equipped with a load cell of 200 kN capacity. A hinged connection was employed for connecting the loading beam to the hydraulic jack to prevent any undesirable damage on the load cell. Eight linear potentiometers (LP) were also placed at different locations to record the vertical and horizontal deformations of the wall panels, as illustrated in Figure 4.2. The lateral displacement of the actuator was recorded through a linear variable displacement transducer (LVDT).
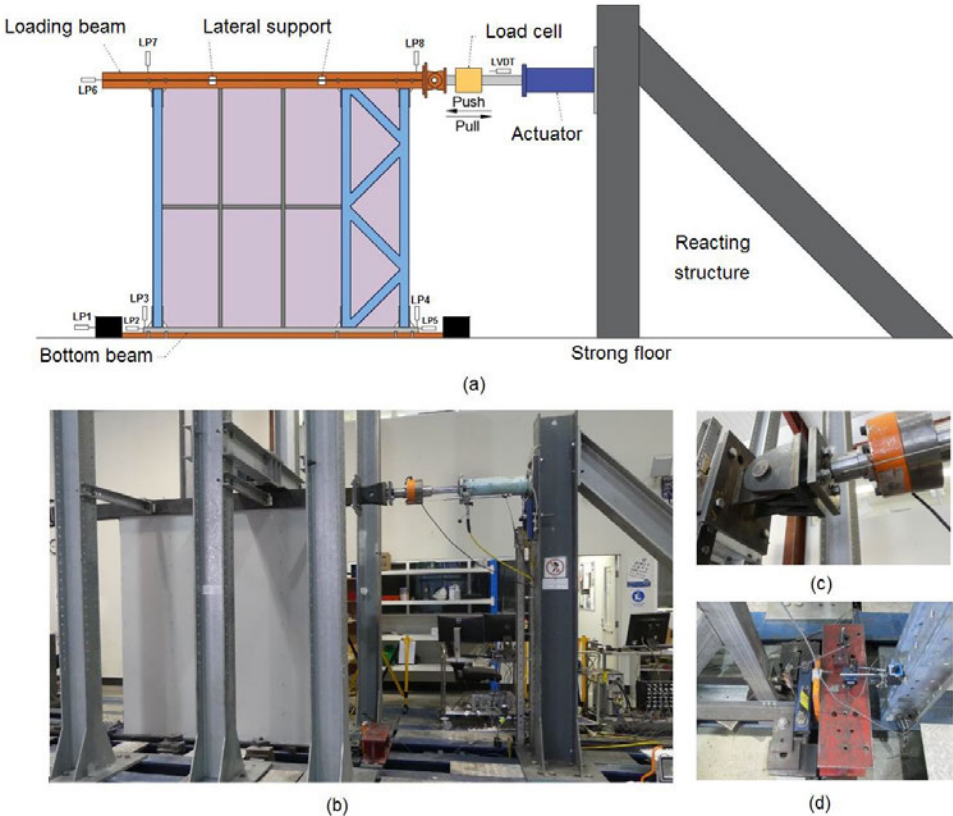
Figure 4.2. Test rig: a) schematic of the test rig, b) actual test rig, c) loadcell and hinge connection d) restrain and LPs

The method B (International Standards Organization protocol, ISO) and method C (CUREE protocol) of ASTM E2126 [115] standard have been extensively used for testing of lightweight CFS wall panels. Since method B of ASTM E2126 standard [115] is more frequently used for CFS walls with 2400 mm to 2400 mm dimension (same as hybrid walls in this study), this method was implemented for cyclic loading of the wall panels of this study. ASTM E2126 [115] specifies two loading patterns for this loading protocol: a) single cycles at 1.25%, 2.5%, 5%, 7.5% and 10% of the ultimate displacement (Δ_m); and b) three cycles at displacements of 20%, 40%, 60%, 80%, 100% and 120% of the ultimate displacement (Δ_m). Δ_m is defined as the ultimate displacement capacity specified from the monotonic tests. However, it was not possible to capture the Δ_m value based on the monotonic test results as the applied lateral load did not decline to 80% of the peak load because of the stroke limit of the hydraulic jack. The 2.5 % maximum allowable storey-drift limit (60 mm for a 2400 mm wall) was therefore considered as the value of Δ_m for cyclic tests. Table 4.3 and Figure 4.3 show the regime of cyclic loading in this study. The loading rate was 2 mm/s, which is within the displacement rage of 1–63 mm/s recommended by ASTM E2126 [115].

Table 4.3. Cyclic loading regime, Method B - ASTM E2126

Pattern	Step	Minimum Number of Cycles	Amplitude, % Δ_m (% 60 mm)	Actuator stroke (mm)
1	1	1	1.25	0.75
	2	1	2.5	1.5
	3	1	5	3
	4	1	7.5	4.5
	5	1	10	6
2	6	3	20	12
	7	3	40	24
	8	3	60	36
	9	3	80	48
	10	3	100	60
	11	3	120	72
	12	3	140	84
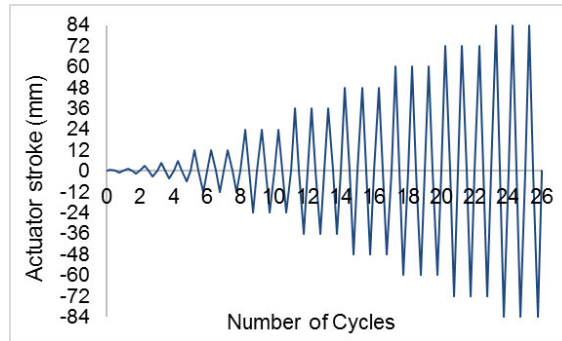
Figure 4.3. Cyclic load protocol

4.3 Experimental results

4.3.1 Observations and Failure Modes

According to the observations made during the tests, elastic deformation in SHS elements occurred for all specimens throughout the initial stages of loading. By increasing the displacement amplitudes, plastic deformations were formed at the hold-down locations of the specimens with the SHS truss element, HW-C1, HW-C2 and HW-C3.

In general, all unsheathed walls demonstrated similar failure mechanism. During the final stages of loading on HW-C1 and HW-C2, the SHS truss element on the tension side was lifted up from the reaction beam which was followed by the upward deformation of the bottom track and consequently local failure of the track at the location of the track to SHS connection. The reason for this type of failure can be attributed to the non-existence of the vertical load, which allows overturning of the wall and therefore causes undesirable deformations. Overturning of the wall panel in specimens HW-C1 and HW-C2 also resulted in hole elongation of SHS at the hold-down connection which was due to the bearing between the edge of the SHS hole, the bolt and the hold-down. Figure 4.4 shows the uplift movement on the tension side of the SHS truss and the plastic deformations at the location of hold-downs. As shown in this figure, the general failure mechanism of specimens HW-C1 and HW-C2 is nearly similar. In specimen HW-C3, utilising one single SHS chord at the other side of the wall panel could reasonably control the unfavourable overturning of the panel. Accordingly, the risk of failure at the connection location was completely mitigated. New investigation methods [116, 117] can be utilised for the optimum design of connections

64

in the hybrid systems to eliminate the unfavourable connection failure. The typical track failures in the unsheathed wall panels were also observed during the cyclic tests, as shown in Figure 4.5.
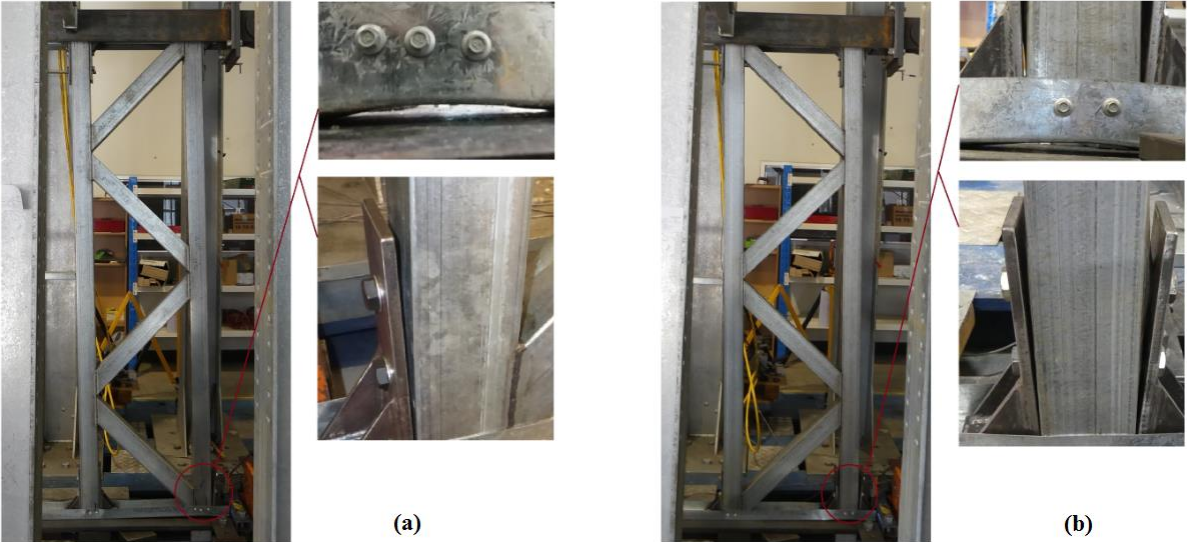
Figure 4.4. Deformation and failure in: a) HW-C1   b) HW- C2
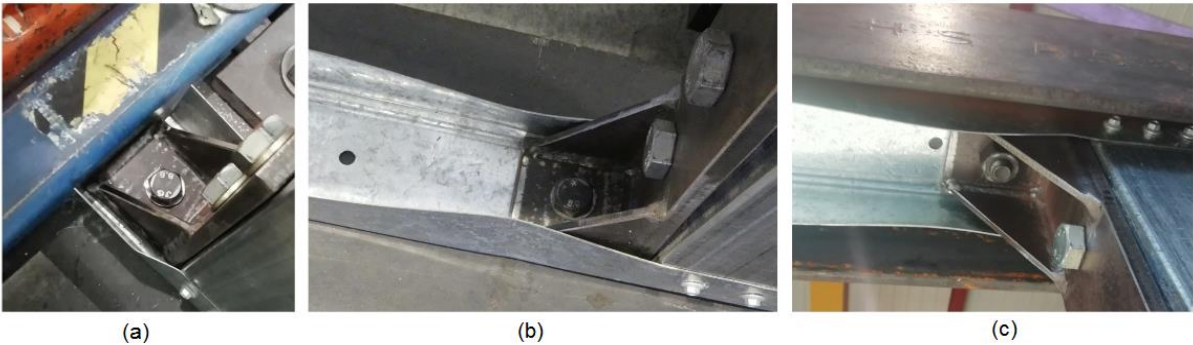
Figure 4.5. Track deformation at hold-down location: a) bottom- end hold-down, b) bottom-middle hold-down b) top-middle hold-down

The observations in test specimen HW-C4 with GWB showed that utilising sheathing board on the wall face can lead to superior force transmission between the wall components, including SHS elements and CFS members compared to when sheathing is not employed (specimen HW-C3). In this specimen, the localised failures observed in HW-C1, HW-C2 and HW-C3 were prevented or delayed due to the distribution of forces between the steel elements by GWB. Besides, the uplifting force in the tension side of SHS truss was restricted because of GWB, which prevented the undesirable failures such as the bottom track upward deformation and elongation of the hole at the hold-down connections. When lateral displacement was applied to the specimen HW-

C4, bearing and pull through damage in the GWB as well as screw tilting in the frame occurred primarily due to the non-uniform deformation between the GWB and the framing elements. Tilting of screws occurred first when loading was applied initially, and then the failure mechanism was followed by other types of failure modes such as bearing and pull through of screws. The screw failures around the perimeter elements were found to be more severe than the failure of screws near the interior studs. This is because the perimeter screws were under higher differential displacement compared to field screws. At higher load increments, the sheathing was gradually subjected to intensive damage around the location of screw connections which was followed by partial separation of the GWB from the framing elements (pull-through failure). This detachment resulted in the lack of rigid body movement of the wall panel and therefore decreased the lateral stiffness of the wall panel. Figure 4.6 shows different failures of the specimen HW-C4. For the specimen HW-C6, when the field stud was replaced by a single SHS, gypsum splitting at the field stud was much less than that in specimen HW-C5 due to the implementation of thicker elements which could control the tilting of screws.
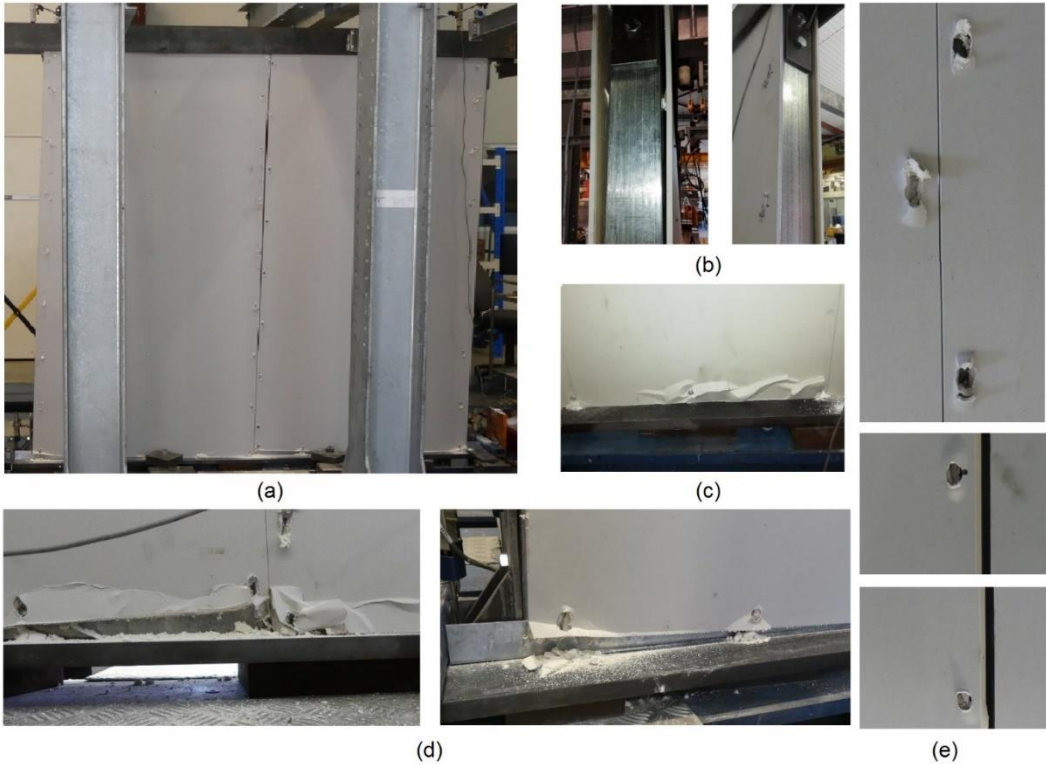
Figure 4.6. Failure modes of the specimen HW-C4: a) Overall deformation of GWB board, b) detachment of the GWB from the frame, c) bearing failure of GWB, d) Tear-out sheathing failure and GWB crashing, e) Pull-through of the screw

4.3.2 Hysteretic response and envelope curves

Figure 4.7 and Figure 4.8 display hysteresis and envelope curves of wall panels under cyclic loading, respectively. The net displacement was determined according to the method presented in Chapter 3, which considers wall sliding as well as deformations due to rigid body rotation of the panel. It is also notable that because of the limitation of the actuator stroke, the failure of wall panels could not be reached during the test, and therefore, the maximum shear resistance was recorded at a drift of 3.5%.

The hysteresis results of HW-C2, HW-C3 and HW-C4 indicate that the walls under pulling phase provide less shear resistance compared to walls under pushing phase. This difference is generally the result of two particular factors: The first reason is that the walls were originally subjected to pushing deformation and consequently, experienced inelastic deformations which directly affected the walls' ability to bear the lateral load in the reverse pulling direction. The second reason is attributed to the unsymmetrical structure of hybrid panels and particularly the SHS truss part. The SHS truss on tension side was restrained by two connectors when wall panel was under pushing phase, while only one hold-down was employed on the tension side of the truss when the pulling load was imposed to the panel. The difference between pushing and pulling phases of specimens HW-C5 and HW-C6 is relatively negligible owing to their symmetrical configuration.
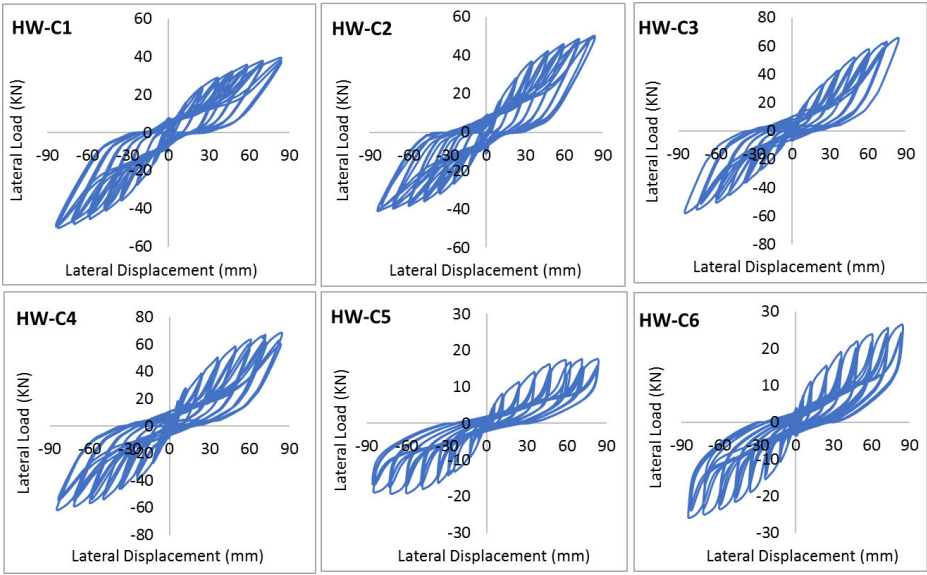
Figure 4.7. Load–lateral displacement hysteresis curves of the specimens
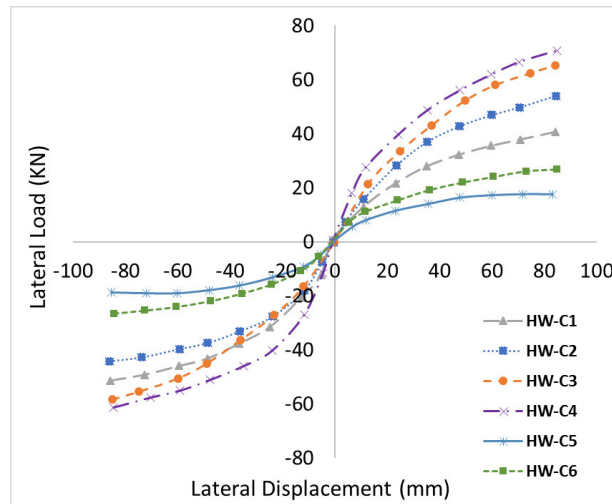
Figure 4.8. Envelope curves

Comparing the energy dissipation of the first and the third cycle of the specimens HW-C4 and HW-C5 indicates that the energy dissipation in consecutive cycles of identical displacement for a hybrid wall with truss brace is more than a hybrid panel in the absence of truss frame. It is also important to note that the energy dissipation trend in cycles with similar displacement amplitude for bare hybrid wall panel is different from wall panels with GWB sheathing. The variation in energy dissipation at identical displacement for wall panels with GWB sheathing is more evident than panels without GWB. This is mainly because GWB loses much of its load bearing ability in the first cycle and therefore, its energy absorption is significantly reduced in the second and third cycles of similar amplitude. Accordingly, in large lateral displacements, the strength and stiffness degradation between the first and second cycle is considerably higher than the second and the third cycles of the same displacement amplitude. Notably, the energy dissipation and ductility of the proposed hybrid system can also be increased by modifying the diagonal SHS elements to a fuse element according to the capacity-based design approach [118].

4.4 Analysis of the test results

The Equivalent Energy Elastic-Plastic (EEEP) model is employed for establishing design parameters of hybrid panels under cyclic load. The results include the test peak point, elastic point, yield point and ultimate point. The peak point (Δ_{max}, P_{max}) is defined as the maximum load and the corresponding displacement on the envelope curves. The elastic point (Δ_e, P_e) is positioned at 0.4Pmax, and the yield point (Δ_y, P_y) is achieved through EEEP method according to the method given in AISI-S400 [16]. The

68

ultimate point (Δ_u, P_u) is determined as the location of the 80% post-peak load; however, the ultimate point could not be achieved since the wall panel strength did not drop within the demand displacement range and therefore, the pick point is considered as the ultimate point of all hybrid panels.

Initial stiffness, ductility factor and absorbed energy are determined from the test results for each reversed cyclic test in pushing and pulling phases, and an average value is then obtained. Ductility factor is specified by the ratio of the ultimate to the yield displacement. Energy absorption is characterised as the area under the backbone curve, and the lateral stiffness is defined as the secant stiffness to a load of $0.4P_{max}$, as per AISI recommendation [16]. The design values captured from each wall panel under cyclic loading are presented in Table 4.4.

Table 4.4. Design values for hybrid walls

Specimen		Δ_e	P_e	Δ_y	P_y	$\Delta_{max}= \Delta_u$	$P_{max}= P_u$	K	μ	E
	(+)	15.0	16.3	30.9	33.5	84	40.7	1.09	2.7	2298
HW-C1	(-)	12.9	20.5	28.1	44.7	84	51.3	1.59	3.0	3128
	Ave.	14.0	18.4	29.5	39.1	84	46.0	1.34	2.8	2713
	(+)	16.0	21.6	33.3	45.1	84	54.1	1.35	2.5	3036
HW-C2	(-)	11.3	17.7	24.4	38.1	84	44.2	1.56	3.4	2738
	Ave.	13.7	19.7	28.8	41.6	84	49.2	1.46	2.9	2887
	(+)	16.5	26.1	34.0	53.8	84	65.2	1.58	2.5	3604
HW-C3	(-)	18.0	23.2	37.7	48.7	84	58.1	1.29	2.2	3172
	Ave.	17.3	24.7	35.9	51.3	84	61.7	1.44	2.3	3388
	(+)	12.0	28.3	24.3	57.5	84	70.8	2.36	3.5	4127
HW-C4	(-)	10.0	24.5	20.8	51.0	84	61.3	2.45	4.0	3753
	Ave.	11.0	26.4	22.6	54.2	84	66.1	2.41	3.7	3940
	(+)	9.5	7.1	26.0	19.3	71	17.6	0.74	2.7	1120
HW-C5	(-)	9.3	7.6	27.2	22.2	71	19.0	0.82	2.6	1275
	Ave.	9.4	7.3	26.6	20.8	71	18.3	0.78	2.7	1198
	(+)	11.0	10.7	22.7	22.1	84	26.7	0.97	3.7	1604
HW-C6	(-)	12.9	10.6	27.2	22.3	84	26.5	0.82	3.1	1573
	Ave.	12.0	10.6	25.0	22.2	84	26.6	0.90	3.4	1589

Figure 4.9 shows the comparison of energy absorption, stiffness and maximum shear capacity under pushing and pulling phases for hybrid wall panels in this study. As shown in this figure, the SHS truss skeleton in both HW-C1 and HW-C2 is able to provide sufficient resistance. In general, the overall average values of HW-C2 are higher than HW-C1, which indicates that the truss direction in the panel can slightly affect the performance of the hybrid wall. In specimen HW-C3, by using the single SHS

element at the other end of the wall, the wall panel provides superior performance in terms of maximum lateral resistance and energy absorption in comparison to HW-C2. The average increase in maximum strength, due to the replacing the CFS stud with SHS, in both positive and negative phases is about 20% and 31%, respectively. Using GWB in HW-C4 also leads to a significant increase in the peak load, initial stiffness, energy absorption and ductility than the wall without sheathing (HW-C3), which is attributed to the restrictive effect of GWB on the wall panel and screw connections. Specimens HW-C5 and HW-C6 were only tested to compare the impact of using a single SHS element as a field stud. The ductility ratio, stiffness and energy absorption of the specimen HW-C6 show that replacing CFS field stud with SHS stud leads to increase in the shear capacity of the sheathed shear wall.

The overall comparison of all wall panels shows that specimens HW-C5 and HW-C6 are not suitable for mid-rise structures as their strengths are relatively low compared to their weights. This indicates that the performance of the hybrid wall is mainly determined through the truss structure of SHS elements. It is notable that the obtained results of the hybrid wall panels when no vertical load is applied are conservative compared to when gravity load is applied on the wall panels. Applying gravity load on panels would increase the stiffness and shear strength of the system mainly due to two main reasons: a) the membrane action of the sheathing generated under vertical load would provide superior performance for the entire system, and b) applying vertical load would control the uplift and overturning of the walls which results in less undesirable failure modes such as hole elongation in the hold-down [119]. It should also be noted that the rotation and overturning of the wall panels in an actual building do not occur due to the assumption of rigid floor diaphragm.
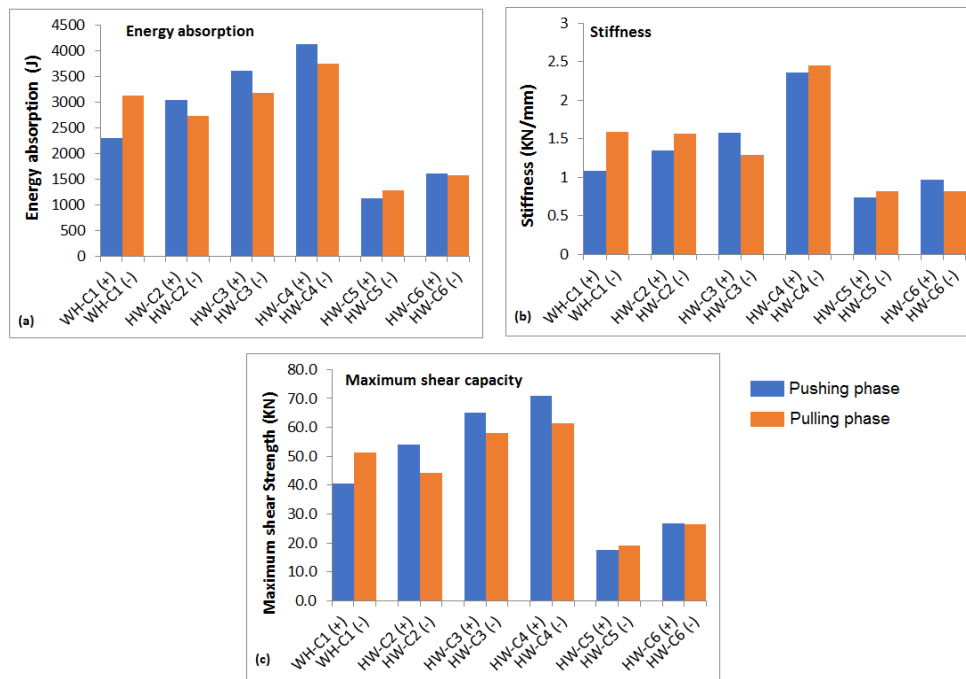
Figure 4.9. Comparison of different parameters in pushing and pulling phases: a) Energy absorption b) Stiffness c) Maximum shear capacity

It is notable that the lateral stiffness and load carrying capacity of the walls could possibly be increased under combined action of lateral and gravity load, since this has been shown in other previous studies. Discussion about the possible failure mode under combined action of lateral and gravity load is not a simple topic and requires experimental tests to be conducted.

4.4.1 Comparison between cyclic and monotonic results

Comparison of the cyclic test results of this chapter against the monotonic results obtained from the previous chapter is shown in Figure 4.10. The results are compared in terms of maximum strength at 2.5% and 3.5% inter-storey drifts as well as stiffness and ductility. The comparison is only provided for the pushing phase of the specimens HW-C2, HW-C3, HW-C4 and HW-C5 since no monotonic test was conducted for the specimens HW-1 and HW-6.

The overall response and trend of the hybrid walls under cyclic loading is similar to that obtained from monotonic loading, both with ascending behaviour. The comparison of maximum strength at different inter-storey drifts indicates that the unsheathed wall panels have captured about similar shear strength values for cyclic and monotonic tests. However, for sheathed panels (HW-C4 and HW-C5), the shear strength

71

achieved by the cyclic load is between 4%-12% lower than the monotonic results. This is mainly due to the strength degradation of GWB and its corresponding failures during the cyclic loading protocol. In terms of stiffness and ductility, the unsheathed walls can provide almost equal performance in cyclic and monotonic tests, while a considerable difference between monotonic and cyclic results (stiffness and ductility) is obtained for sheathed wall panels.
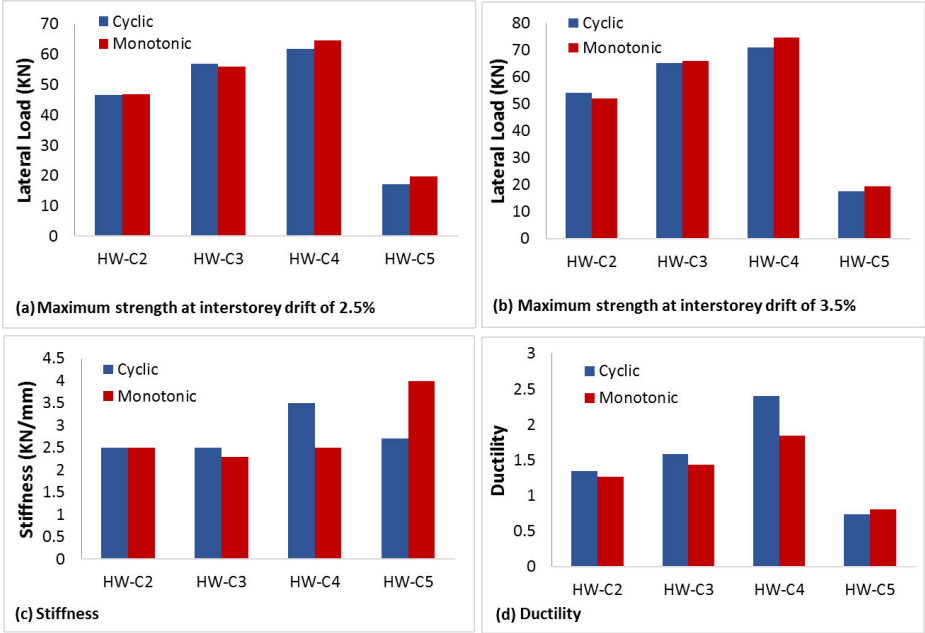
Figure 4.10. Comparison between cyclic and monotonic results: a) maximum strength at 2.5% drift, b) maximum strength at 3.5% drift, c) stiffness, d) ductility

4.4.2 Comparison with the test results from other researchers

Based only on the load-displacement characteristics of the CFS walls, it is challenging to identify whether a wall panel is sufficiently qualified for a lightweight or modular building in high seismic regions [120]. Strength to weight ratio (S/W) is recognised to be a critical parameter for evaluating the system in terms of strength and weight relationship and comparing the effectiveness of the structural components for modular or prefabricated lightweight steel buildings.

In order to investigate the S/W ratio of hybrid walls in this study, 87 tested CFS wall panels from 28 previous studies along with the hybrid walls presented in this study are compared. The parameters used for this comparison include the total frame weight, the maximum strength before or at 2.5% maximum allowable lateral drift, the

displacement at maximum strength, elastic stiffness and S/W ratio. The limitation of 2.5% maximum allowable drift is accounted for this comparison since the maximum shear resistance of some wall panels was reached after this maximum allowable drift.

In order to undertake a reasonable comparison between the lateral behaviour of hybrid shear wall panels in this study and the other CFS walls in the previous studies, the following assumptions are taken into account:

➢ The screws weight is ignored in measuring the total weight of the walls.

➢ The maximum strength is considered as the pick point of the load-displacement curve before or at 2.5% maximum allowable lateral drift. For walls with both monotonic and cyclic results, the maximum strength value of either cyclic or monotonic response is considered. The average amount of pushing and pulling phases is employed for this comparison.

➢ Only wall panels with 2400 mm width or longer are considered for this evaluation. The results found can be generalised to wider wall panels as those wider walls will provide higher shear resistance and thus using the values obtained from the 2400 mm walls is conservative though certainly acceptable approach.

➢ Wall panels with different sheathing materials are employed for this comparison. Although Plywood, Oriented Strand Board (OSB) and steel sheets are of greater shear stiffness than the GWB, the hybrid wall with GWP in this study (HW-C4) is placed on the conservative side of this comparison.

➢ The density of wall components (framing, sheathing and infilled materials) are extracted from either the original reference or reliable industry references.

4.4.2.1 Comparison of unsheathed walls (HW-C2, HW-C3)

Table 4.5 shows the characteristics of CFS walls which are relying only on bracing systems. Truss brace, strap brace, knee brace, k brace and hybrid systems tested by other researchers along with specimens HW-C2 and HW-C3 of this study are taken into consideration for this comparison. Figure 4.11 also shows the S/W ratio for the wall panels without sheathing board.

As shown in this figure, the S/W ratios of HW-C2 and HW-C3 are basically higher than other CFS braced wall panels tested in other studies (except WHE by Fiorino et al., [88]). This indicates that besides the superior load-bearing capacity of the hybrid walls

73

in this study, they can also offer the benefits of a lightweight system by keeping the weight and size of the walls reasonably low which fully satisfies the requirement of prefabricated and modular structures.

Only specimen WHE tested by Fiorino et al. [88] has provided higher S/W ratio than hybrid panels in this study; nevertheless, the total weight of this former wall is nearly four times greater than HW-C2 in this study (217 Kg for the WHE [88] and 54 Kg for the HW-C2 in this study). Although innovative wall panels such as specimen WHE [88] can offer remarkable seismic performance, the high mass of the entire wall intensifies the dead load of the wall panel and as a result the seismic base shear of the building during an earthquake. Besides, the higher weight of the wall panel would cause some difficulties during lifting and installation of panels and limits the prefabrication advantages.

It is also interesting to note that, unlike hybrid walls in this study, the maximum shear resistance of the majority of CFS walls has reached before the 2.5% maximum allowable drift demonstrating that the hybrid wall is characterised with high ability to absorb energy well beyond the design requirements. Considering that enhancing the shear wall length can accordingly increase the stiffness and lateral strength, specimens III [121], V [95] and HWPS [122] even those longer than hybrid walls cannot provide better performance compared to the hybrid panels in this study.

Table 4.5. Previously tested braced walls by different researchers

Au hor, Reference	Bracing system	Specimen ID	Span (m×m)	Frame weight (Kg)	Maximum strength (KN)	Maximum Displacement (mm)	Elastic stiffness (KN/m)
Tian et al., [102]	Truss brace	Configuration 4	2.4×3.0	139	47	31	1.29
Accorti et al., [123]		G6-XX2	2.4×3.0	79.2	13	75	0.50
		G9-XX2	2.4×3.0	89.8	36	75	2.61
Iuorio et al., [79]		WHD	2.4×2.7	208 2	121	67.5	5.53
		WLD	2.4×2.7	114 3	62	67.5	4.10
		WLE1	2.4×2.7	112.7	70	33	4.00
Fiorino et al., [88]		WHE	2.4×2.7	217.1	198	61.3	5.60
		WLE2	2.4×2.7	137 5	102	65.5	3.40
Al-Kharat and rogers,[89]	Strap brace	2C	2.44×2.44	56.4	35	60	1.40
		4C	2.44×2.44	95.3	60	44	2.10
		6C	2.44×2.44	125.7	85	40	3.60
Serrette et al., [92]		Type A	2.44×2.44	40.2	13	60	1.20
Dubina,[121]		III	3.6×2.44	107 0	53	18	2.70
Moghimi and Ronagh, [99]		DA2	2.4×2.4	16.0	4	60	0.10
		DA1	2.4×2.4	16.0	4	60	0.10
		DA4	2.4×2.4	21.0	9	60	0.18
		DB4	2.4×2.4	20.5	4	60	0.09
		DB1	2.4×2.4	15.7	5	60	0.08
Liu et al., [17]		F-XB	2.4×3.0	54.8	27	29	1.50
		F-KB	2.4×3.0	45.1	3	57	0.10
Zeynalian and Ronagh, [85]	Knee brace	N1	2.4×2.4	24.0	2	60	0.06
		N2	2.4×2.4	23.4	2	30	0.10
		N3	2.4×2.4	23.6	2	46	0.90
		N4	2.4×2.4	23.2	2	34	0.90
Pourabdollah et al. [82]	K brace	K1	2.4×2.4	34.3	3	47	0.16
		K2	2.4×2.4	34.3	4	59	0.14
		K3	2.4×2.4	40.0	21	59	0.58
		K4	2.4×2.4	46.7	18	60	0.52
Zeynalian et al.[83]		K1	2.4×2.4	19.0	3	59	0.09

		K2	2.4×2.4	19.0	3	60	0.07
		K3	2.4×2.4	19.0	3	53	0.07
		K4	2.4×2.4	23.2	3	28	0.22
		K5	2.4×2.4	19.0	2	37	0.10
		K6	2.4×2.4	26.5	3	60	0.07
		K7	2.4×2.4	26.5	3.2	60	0.08
		K8	2.4×2.4	22.7	3	55	0.09
		K9	2.4×2.4	28.7	5	35	0.21
		K10	2.4×2.4	22.7	3	39	0.08
		K11	2.4×2.4	31.4	3.3	12	0.64
		K12	2.4×2.4	30.6	5	35	0.24
Sharafi et al., [95]	Hybrid	V	3.6×3.0	99.7	8	75	0.15
Sharafi et al., [122]		HWPS	3.6×3.0	115.4	20	75	0.39
This Study	**Hybrid**	**HW-C2**	**2.4×2.4**	**54.3**	**43.5**	**60**	**1.46**
		HW-C3	**2.4×2.4**	**65.1**	**54.5**	**60**	**1.44**
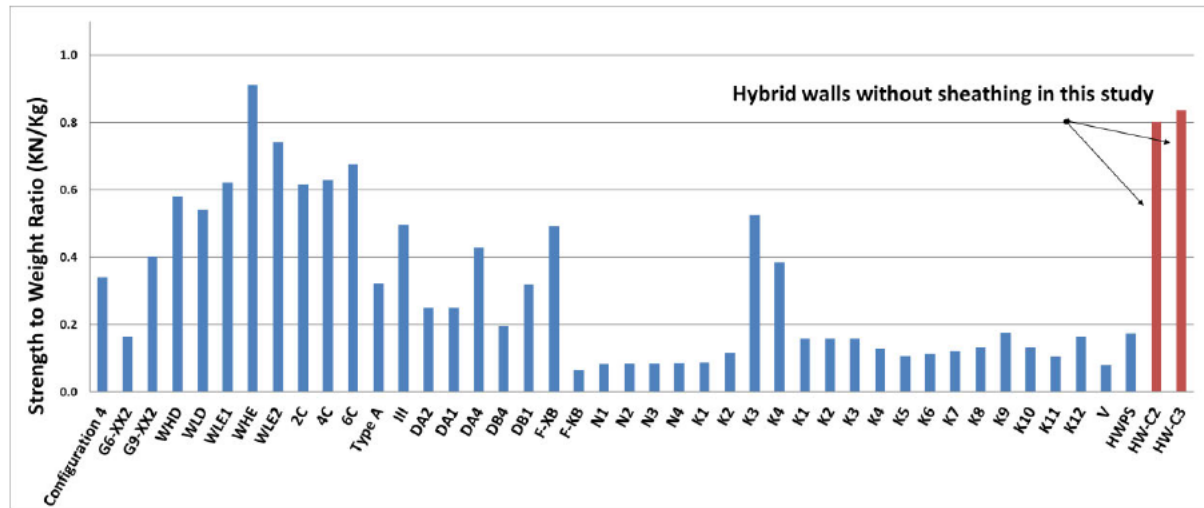
Figure 4.11. Comparison of strength to weight ratio for braced walls.

4.4.2.2 Comparison of sheathed walls (HW-C4)

The comparison of the wall panels with various sheathing materials along with specimen HW-C4 with GWB in this study is also provided in Table 4.6. In some specimens, infill material such as concrete or cement grout has been used to increase the shear resistance of the panel. Figure 4.12 illustrates the S/W ratio for the sheathed wall panels.

Comparison of the maximum displacement values in Table 4.6 indicates that the sheathed hybrid panel (HW-C4) is also described with high ability of energy absorption to be used for mid-rise buildings in high seismic regions. This again proves that the SHS elements in the form of truss structure can enhance the seismic performance as well as energy absorption through employing diagonal members. Except for wall panels WA1 [19], FFM-O09-FO [42], FFM-O12-FO [42], H3 [74] and D-C-3 [67]; the S/W ratio of the sheathed HW-C4 in this study is basically up to 860% higher than that

of the wall panels in Table 4.6. The lower S/W ratio of the HW-C4 compared to specimens WA1 [19], FFM-O09-FO [42], FFM-O12-FO [42], H3 [74] and D-C-3 [67] can be attributed to this point that GWB has been utilised for face sheathing of this wall which provides lower stiffness and lower resistance compared to ply bamboo, fibre cement and OSB sheathing materials. The separate comparison on wall panels only with GWB sheathing provided in Figure 4.12 demonstrates that the S/W ratio of the HW-C4 is more than 2 to 10 times greater than that of gypsum sheathed walls in the literature. Besides, specimens WA1 [19] has been filled with concrete material, which can significantly improve the strength and rigidity of the wall panel. The hybrid wall, on the other hands, is less dependent on the sheathing or infilling material resistance and is more relied on the steel frame components.

The results of Figure 4.12 and Table 4.6 also reveal that in terms of structural performance, the proposed hybrid CFS system in this study gives the same design and construction flexibility as many new CFS wall panels, while it offers the advantage of lightweight prefabrication, manufacturing, transportation and installation. In addition, the hybrid CFS method is relatively more cost-effective, which is mainly due to less material used. The shorter time of providing a dry all-steel wall such as the hybrid wall in this study compared to wall panels filled with concrete, foam and mortar can also have a positive effect on reducing costs and earlier return on investment.

Table 4.6. Tested sheathed walls by different researchers

Author, Reference	Sheathing type	Specimen ID	Span (m×m)	Frame weight (Kg)	Other material weight (Kg)	Total weight (Kg)	Maximum strength (KN)	Maximum displacement (mm)	Elastic Stiffness (KN/mm)
Balh et al, [124, 125]	Steel	Specimen 11	2.44×2.44	36.3	71	107 2	39	27	3.2
Tone et al,[125, 126]		Specimen 16	2.44×2.44	34.7	53	87.7	24	31	3
Gao and xiao,[67]	Ply bamboo	D-C-3	2.44×2.44	36.3	38.7	75	33	56	1.1
Zeynalian and Ronagh, [74]	FCB[a]	H1	2.4×2.4	14.9	86.4	101 3	29	40	1.2
		H3	2.4×2.4	20.1	43.2	63.3	29	41	1.1
Moghimi and Ronagh, [99]		AB1	2.4×2.4	15.8	32	47.8	6.5	44	0.6
		CB1	2.4×2.4	16.7	32	48.7	9	60	0.9
Peck et al. [30]	GWB[b]	GWB.4-12	2.44×2.44	31.4	51	82.4	11.7	23	1.5
		GWB.4-6	2.44×2.44	31.4	51	82.4	12.4	20	1.5
		GWB.4-4	2.44×2.44	31.4	51	82.4	11.2	44	1.5
		GWB.6-12	2.44×2.44	31.4	51	82.4	7.3	20	1.3
Morgan et al. [127]		12	2.44×2.44	23.8	51	74.8	6.1	32	1.5
		14	2.44×2.44	23.8	51	74.8	4.2	58	2
		16	2.44×2.44	23.8	51	74.8	3.5	45	1.5
		18	2.44×2.44	25.8	51	76.8	10.6	27	2
		20	2.44×2.44	23.8	51	78.8	3.6	47	1
Serrette and Ogunfunmi, [92]		Type B	2.44×2.44	33.4	77	110.4	25.3	38	3
		Type C	2.44×2.44	37.9	77	114 9	28.9	38	2.5
Pan and Shan, [42]		FFM-G09-FO	2.4×2.4	63	27.7	90.7	16.7	53	1.2
		FFM-G09-FT	2.4×2.4	63	54	117	28.8	50	1.7
		FFM-G12-FO	2.4×2.4	63	36	99	18	55	1.1
	OSB[c]	FFM-O09-FO	2.4×2.4	63	35	98	44	59	1.7
		FFM-O12-FO	2.4×2.4	63	42	105	49	60	1.6

Reference	Material	Specimen	Dimension						
Dubina, [121]		OSB I	3.6×2.44	120	51	171.1	51	19	4.2
Liu et al., [128]		12	2.44×2.74	63	44.1	107.1	41	50	2
		14	2.44×2.74	63	44.1	107.1	36	49	2.2
		15	2.44×2.74	63	44.1	107.1	31	42	1.6
	OSB, GWB	13	2.44×2.74	63	89.5	152 5	44	50	1.8
	GWB	16	2.44×2.74	63	45.4	108.4	8	37	0.9
Wang, and Ye, [19]	GWB,CON[d]	WA1	3.6×3	50.7	107.3	158	96	29	15
	GWB,BMB[e]	WA2	3.6×3	50.7	236.3	314	96	25	10.9
	,CON	WA3	3.6×3	73.5	236.3	336 8	98	34	11
	GWB,BMB,	WB1	3.6×3	134.7	498	632	76	43	19
	CON, ALC[f]	WB2	3.6×3	97.1	498	595.1	123	47	23
YE et al,[59]	GWB, CSB[g]	Specimen 1	3.6×3	50.7	470	520.7	93	38	10.7
		Specimen 2	3.6×3	54.7	470	524.7	79	30	10.7
	GWB, BMB	Specimen 4	3.6×3	63.8	384	447 8	73	28	10.3
		Specimen 5	3.6×3	97.1	384	481.1	101	75	10.7
		Specimen 6	3.6×3	119.7	384	503.7	94	36	10.7
Xu et al., [18]	SB[h]	WA-1	2.4×3	43.5	288	331 5	37	33	4.1
	SB, LFC[i]	WB-1	2.4×3	43.5	623	666 5	88	60	10
		WB-2	2.4×3	43.5	748	791 5	106	44	11.8
		WB-3	2.4×3	65.3	622	687 3	96	57	15
		WC-1	2.4×3	62.1	810	872.1	107	50	13.5
		WC-2	2.4×3	62.1	810	872.1	110	48	14
This study	GWB	HW-C4	2.4×2.4	65.1	66.4	131.5	59	60	2.4

[a]Fibre cement board, [b]Gypsum wall board, [c]Oriented strand board, [d]Fine aggregate concrete (infilled material), [e]Bolivian magnesium board, [f]Autoclaved lightweight concrete slab, [g]Calcium silicate board, [h]Straw board, [i]Lightweight foamed concrete (infilled material)
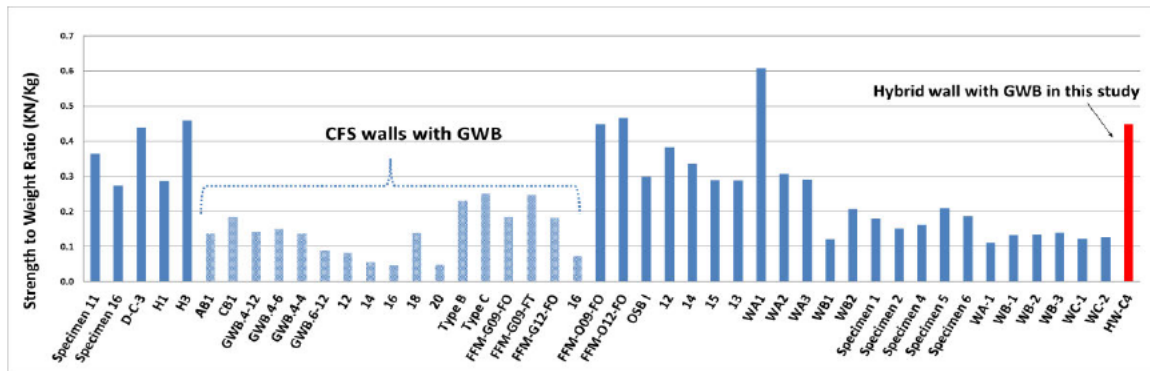
Figure 4.12. Comparison of strength to weight ratio for sheathed walls.

4.5 Response modification factor (R factor)

4.5.1 R factor in CFS regulations

R factor is an important parameter that is required to investigate the induced seismic force and to determine the reduced lateral loads for design of a building. The values of R factor for CFS buildings are proposed by several codes including Uniform Building Code (UBC) [129], International Building Code (IBC) [130], FEMA P-1050 [113], American Society of Civil Engineers (ASCE) ASCE07 [131] and National Building Code of Canada (NBCC) [132]. However, these codes do not necessarily provide similar R factor values for similar CFS buildings. The disagreement between R factor values of the mentioned regulations is mainly due to the different approach of calculating R factor

as well as the different employed bilinear curve. In some provisions such as the European code for seismic design [133], the design of CFS walls is based on hot-rolled steel formulations and also the design of sheathed CFS walls is not possible if the sheathing material is different from steel.

Table 4.7 shows the values of the R factor identified by different CFS codes. As shown in this table, there is no consensus on the R factor value for CFS solutions, and especially, there is no R factor value in these regulations for systems braced with CFS truss elements. Therefore, this study also aims to estimate the R factor for an SHS truss-braced CFS hybrid wall through FEMA 356 [112] and FEMA P-1050 [113] procedures and based on the experimental results.

Table 4.7. R factor values according to different CFS codes

Code	R factor value	Detail
ASCE7 [131]	6.5	Light frame wall sheathed with wood structural panels rated for shear resistance or steel sheets
	4	Light frame wall systems using flat strap bracing
	2	Light frame wall with shear panels of all other materials
FEMA P-1050 [113]	6.5	Light frame wall with shear panel
	4	Light frame wall with diagonal braces (special requirements)
	3	Light frame wall with diagonal braces or other systems such as K brace
UBC [129]	2.8	Light frame wall systems using flat strap bracing
	5.5	Walls sheathed with wood-based panels
	4.5	Other types of lightweight walls
AS/NZS 4600 [134]	2	When CFS members are used as the primary seismic lateral load-bearing system,
AISI-S400 [16]	2<R<3	Walls with no special requirements
	3<R<7	Walls with implementation of detailing
NBCC [132]	2.55	Gypsum wall with wood base panel
	2.6	Walls with strap brace and limited ductility
	1.6	Conventional structures with strap
IBC [130]	6.5	Shear walls sheathed with wood panels or steel sheets
	2	Walls with other types of sheathings
	4	Walls with strap brace

4.5.2 R factor in this study

In this chapter, the proposed method by FEMA 365 [112] and FEMA P-1050 [113] is employed to estimate the R factor for hybrid CFS walls. The hybrid wall envelope curve results are utilised to determine the lateral characteristics of the hybrid system through preliminary analysis of the R factor. As stated in FEMA P-1050 [113], the R factor can be obtained by two main parameters: ductility reduction factor (R_d) and structural over-

strength factor (Ω_0). R_d demonstrates the ability of a structure to dissipate energy through inelastic response. Ω_0 considers the possible sources that may provide additional strength beyond its nominal value. Then, the R factor can be defined as:

$$R = R_d \times \Omega_0 \tag{4-1}$$

$$R_d = \frac{V_e}{V_y}, \quad \Omega_0 = \frac{V_y}{V_s} \tag{4-2}$$

Where V_e is the maximum base shear that is induced in the system if it is to remain in the elastic range and is calculated based on the equal energy concept as prescribed by FEMA [113], V_y is determined as the idealised yield strength and V_s corresponds to the first significant yield strength, which is defined as a node on the envelope curve where the structural response begins to considerably deviate from the initial elastic response. As shown in Figure 4.13, the key components of the R factor are identified through the concept of equal energy which indicates the energy under elastic response of a system is equal to the energy of the idealised bilinear force-displacement curve.
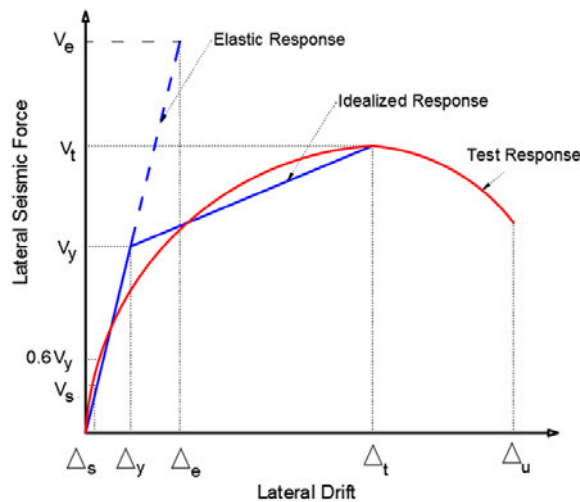
Figure 4.13. Idealized bilinear curve for calculation of R factor

Table 4.8 shows the test-based values of R factor components captured by the experimental results. The table shows that the R factors for hybrid walls without sheathing (HW-C1, HW-C2 and HW-C3) range between 5.4 and 7.1; with average of 6.1. For the hybrid walls with SHS truss frame (HW-C1 to HW-C4), the R factor is mainly affected by the overstrength factor ranging from 3.5 to 4.7. The ductility factor of the braced hybrid walls is also between 1.5 to 1.9. For the unbraced walls, on the other hands, the R factor mostly relies on the value of the ductility factor. Analysing the R factor values also indicates that there is a considerable difference between the

R factor of specimens with and without GWB. Taking into account that the shear strength of the wall panel with GWB material (HW-C4) is about 1.16 times than the capacity of the bare panel (HW-C3), the R factor value is 1.3 times higher when GWB is utilised on a braced hybrid wall. This again demonstrates the favourable impact of utilising GWB for the hybrid panels.

Comparing the R factors of this study with the prescribed values of the R factor in CFS regulations presented in Table 4.7 shows that the hybrid wall panels meet the current provisions in terms of response modification factor.

Table 4.8. Test-based R factor values determined based on FEMA

Specimen	Overstrength factor (Ω_0)			Ductility factor (R_u)			Response modification factor (R)		
	Push	Pull	Average	Push	Pull	Average	Push	Pull	Average
HW-C1	3.1	4.5	3.8	2.3	1.5	1.9	7.2	6.9	7.1
HW-C2	4.4	2.6	3.5	1.5	1.9	1.7	6.9	5.1	6.0
HW-C3	3.2	3.8	3.5	1.6	1.5	1.6	5.1	5.7	5.4
HW-C4	5.3	4.1	4.7	1.4	1.6	1.5	7.5	6.5	7.0
HW-C5	1.2	1.6	1.4	3.8	3.4	3.6	4.6	5.3	4.9
HW-C6	1.4	1.5	1.5	3.3	3.5	3.4	4.8	5.4	5.1

It is notable that the test-based R factor is affected by different structural parameters and is not merely relied on the maximum strength and displacement of the frame. Hence, a lower R factor value might be obtained for a CFS wall with higher shear strength and lateral drift compared to another wall specimen. For example, the results reveal that while the maximum shear capacity of HW-C3 is higher than HW-C1 and HW-C2, the R factor of the latter walls is more than the former. This concern has also been reported by other researchers when they compared the R factor with the corresponding strength [79, 83, 85].

Accurately comparing the results of Table 4.8 and Table 4.4 indicates that the higher shear capacity of specimen HW-C3, compared to the HW-C1 an HW-C2, is not reflected by the test-based R factor values. Since the seismic design and base shear of a building directly depend on the R factor, the unreliable test-based R factor of a specimen like HW-C3 can lead to a building with overdesigned sections. In other words, the unique capability of a wall with high lateral capacity and ductility is not necessarily included in the test-based overstrength and ductility reduction factors, respectively. Since the test-based R factor of specimen HW-C3 limits the potential

benefits of this system in design, the R factor values need to be determined using more sophisticated methods such as FEMA P-695 [135] methodology which determines the R factor through nonlinear response history analyses.

4.6 Conclusion

This chapter provided the test results of six full-scale hybrid CFS walls under cyclic lateral loading that were performed to investigate the seismic characteristics of the system, such as response modification factor. Based on the cyclic test results, the following conclusions can be drawn:

- The test results indicated that the direction of SHS truss frame in the panel would not markedly affect the performance of the walls. In contrast, implementation of a single upright SHS at the other end of the panel led to reasonably better ductility and energy-absorbing capabilities than those without single SHS.

- Comparing seismic behaviour of hybrid specimen with sheathing (HW-C4) against the bare hybrid panel (HW-C3) also showed that strength and ductility of the wall were increased when GWB was used as a finishing material.

- It was also observed that shear strength and stiffness of specimens without truss brace configuration was not reasonable and therefore not recommended to be used for mid-rise structures.

- The R factor evaluation was performed through data analysis, and the average values of 6.1 and 7 were obtained for sheathed and unsheathed braced walls, respectively. Besides, specimen HW-C4 with GWB provided a higher R factor value than those CFS walls with sheathing material listed in the CFS regulations.

- Comparison of S/W ratio of CFS walls showed that the innovative solution of using SHS truss-braced design is deemed satisfactory for high seismic regions. It was also demonstrated that specimen HW-C3 as a braced wall and HW-C4 as a sheathed wall were adequately competent as a lateral-resistant system in modular mid-rise buildings, considering their lower weight compared to several massive walls.

Chapter 5   Numerical method: classification of numerical models for CFS structures

This chapter has been published in:

Nima Usefi, Pezhman Sharafi, and Hamid Ronagh. "Numerical models for lateral behaviour analysis of cold-formed steel framed walls: State of the art, evaluation and challenges." Thin-Walled Structures, 138 (2019): 252-285.

5.1 Introduction

In recent years, published papers on the development of numerical models for the study of CFS framed shear wall structures has been significantly exhibiting a growing interest towards research in this area. In fact, a large number of numerical models have been developed for simulating the behaviour of CFS shear walls in the literature; each naturally possessing their own strengths, weaknesses and limitations. This chapter classifies the numerical methods used for modelling the lateral performance of CFS framed wall structures available in the open literature, and discusses their pros and cons, limitations, their applicable software, and challenges for simulation of different scenarios. To that end, the existing models are classified into macro modelling and micro modelling methods, and each is discussed within their own context. Then a comparative discussion on both macro and micro categories is carried out in order to evaluate their effectiveness, positive and negative aspects, and their accuracy. The study only focuses on numerical models for CFS framed shear wall structures acting as lateral resistance systems for buildings. Therefore, purely theoretical and mathematical studies as well as studies on individual, independent and stand-alone CFS members are not discussed as they are not within the scope of this study.

5.2 Classification of numerical methods

Many structures are too complex to be analysed by analytical or classical techniques and, therefore, numerical analysis is generally utilised. The FE method is the most

widely used numerical technique for structural analyses [136-140]. For the analysis and design of complex CFS structures with relatively large deformations and instability issues, selecting an appropriate computational technique plays a substantial role. In the structural analysis, the finer FE methods provide more accurate results at the cost of higher computational effort. When dealing with large structural dynamic problems such as studying the effects of earthquake loads on tall buildings, a large amount of simulation is required during the design and analysis stage, which results in extremely large number of describing equations and consequently very slow convergence. An effective approach for reducing the computational complexity of these models in numerical simulations is Model Order Reduction (MOR) techniques. MOR techniques lower the computational complexity of large-scale and/or dynamical systems, by a reduction of the model's associated state space dimension or degrees of freedom through computing an approximation to the original model. MOR techniques are useful for studying large-scale complex systems whose behaviour can be described by interactions of a number of interconnected subsystems. In structural analysis, the topology of the reduction would have some sparse structure to preserve the original structures topology through appropriate clustering method. Figure 5.1 shows how a large structure's topology model, made of a large number of nodes and members, can be simplified trough model reduction and clusterisation [141].
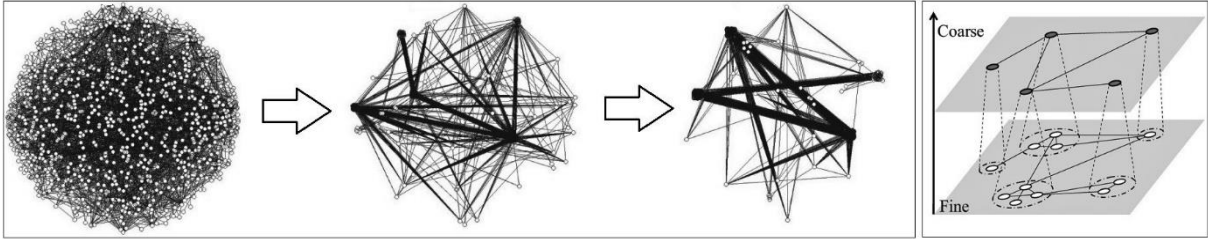
Figure 5.1. Model order reduction through structure's topology clusterisation

The existing MOR methods are classified into different categories. If the reduced model is obtained by removing parts of the physical coordinates of the full model, the MOR technique is called physical coordinate model reduction, which is the most straightforward method and commonly used in structural analysis. All other non-physical coordinates such as modal coordinate and the Ritz coordinate are generally referred to as generalized coordinates. In the structural dynamics community, MOD techniques have been widely employed in complex global-local analysis, optimization and structural vibration and buckling [142].

Although FE methods themselves could be assumed as a class of MOR techniques [142], in the literature MOR methods are mostly referred to techniques replacing the large scale original model by a significantly smaller one, while maintaining characteristic properties of the former and approximate its transfer behaviour as much accurate as possible. MOR techniques are mostly employed in conjunction with FE methods to facilitate solving complex problems. In fact, in computational mechanics, the numerical modelling of structures can be classified into two major groups: (1) the models simulating fine-scale details, known as micro models; and (2) those amalgamating details into select categories being used to quickly capture the essential features of a structure; known as macro models. These two strategies refer to different fields of applications: micro models are applicable when the scope of the study is the local behaviour of the structures and elements, while macro models are used when the global behaviour of the structure is required. Micro and macro models can be used together to study different aspects of a problem [143].

Due to the thin-walled nature of the structural elements used for building CFS structures, accurate analysis of such systems is mainly performed using detailed micro modelling. Yet, micro modelling of buildings made of a relatively large number of CFS elements takes a lot of time and effort. Therefore, the development of a strong macro analysis method for CFS structures has attracted considerable attention in the past few years.

In the study of CFS systems, micro modelling methods, also called as detailed models, are those modelling the structures while considering all the components and interactions, including CFS framing members, sheathings, the connection between the framing members and the sheathing, as well as attachments. In this approach, the nonlinear behaviour of structure is usually interrelated with the nonlinear behaviour of the boundary conditions, elements and connections; therefore, an appropriate basic behavioural model of the elements, usually obtained from experimental data, is required. The accuracy of micro modelling primarily depends on the type, size, and number of elements used to model a CFS structure. Micro modelling approach is usually used for smaller CFS structural elements, with strongly heterogeneous states of stress and strain. This approach provides possibility of real simulation of the CFS frames, with local effects in each material and element as well as at contact.

As CFS structure becomes more complex with larger number of elements, the required

order of the model becomes higher which markedly influences the computational efficiency of analyses. In those cases, reducing the order of model is a useful and practical solution. In macro modelling, also known as simplified methods, the complex building components are simulated as equivalent structural elements, in which the adopted properties of equivalent element are corresponding representatives of the real structure. Macro models remarkably simplify the analysis of complex structures; thus, can be effectively used for the evaluation of the dynamic response of larger CFS structures and those with sub-system consisting of wall panels and their connection to other adjacent sub-systems, such as panelised buildings [1, 144, 145]. Macro models are particularly appropriate when the structure is composed of elements with adequately large dimensions, so that the stresses across or along a macro element is essentially uniform, negligible and/or of not much importance. Macro models are most applicable when a certain level of both accuracy and efficiency is needed.

A reasonably great number of macro and micro models have been developed for simulation of CFS framed wall structures under lateral loading. These models offer different levels of complexity, precision, efficiency, strength and applicability. A comprehensive database comparing different modelling approaches seems to be essential for the future development of more effective and comprehensive modelling methods for CFS wall structures under lateral loads. This chapter first classifies the existing numerical methods in the literature, evaluates their performance, and then compares their characteristics. Figure 5.2 outlines the overall classification of numerical methods for CFS shear walls under lateral loads, in this chapter.
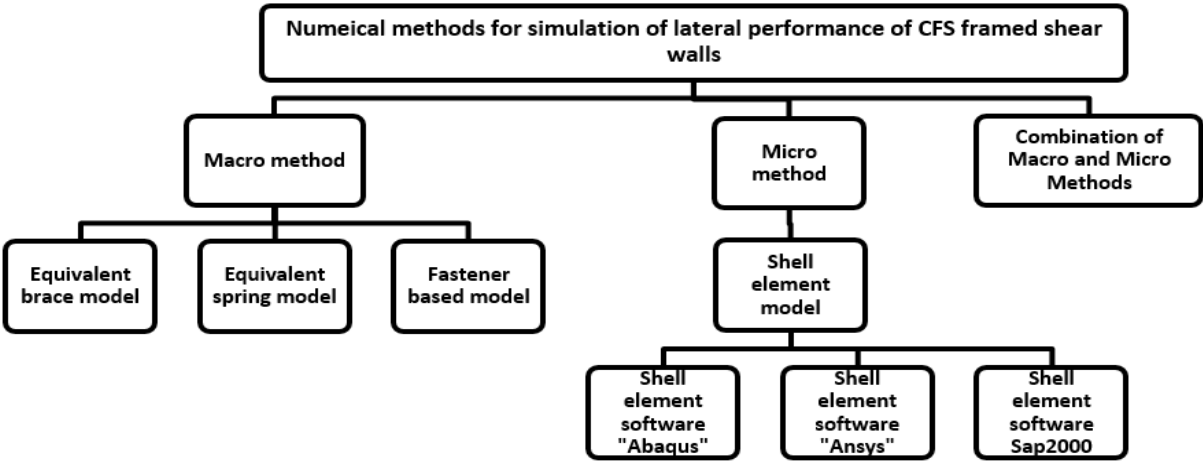
Figure 5.2. Classification of numerical methods for CFS framed shear walls

5.2.1 Macro models for simulation of CFS framed walls

The computational effort, i.e. time and cost, is a key issue in the modelling of large CFS structures, because of their nonlinear behaviour, various instabilities, and relatively large deformations. The computational effort of an FE analysis is considered to be relative to the cubic of the size of a problem [142]. Therefore, the development of efficient macro models for accurate model reduction has recently become a major objective of simulation and modelling. Such models are developed to keep the balance between the required accuracy and efficiency.

For simulation of steel structures, in order to represent the real pre- and post-buckling behaviour, different macro modelling techniques have been developed by researchers. Line element models, with beam or truss elements, are the most widely adopted approaches in analyses of steel shear wall structures (hot-rolled steel shear walls by bracing or steel sheathing) [146]. To simulate the behaviour of steel shear walls, these approaches employ line type element methods such as multi-angle strip model [147], cross-strip model [148], multi strip model [149], modified strip model [150], combined strip model [151], and equivalent brace model [149] for as macro models. While equivalent brace method can be used for both shear walls by bracing and steel sheathing, other methods are only applicable for shear walls with steel sheets. Figure 5.3 schematically depicts these six macro modelling strategies graphs, which are mainly used for simulations of various types of conventional hot rolled shear wall structures.

| Multi-angle strip[*] | Cross-strip model[*] | Multi strip[*] |
| Modified strip model[*] | Equivalent brace[#] | Combined strip model[*] |

[*] Is used for modelling of hot-rolled steel shear walls with steel sheets
[#] Is used for modelling of hot-rolled steel shear walls with steel sheets or bracing system
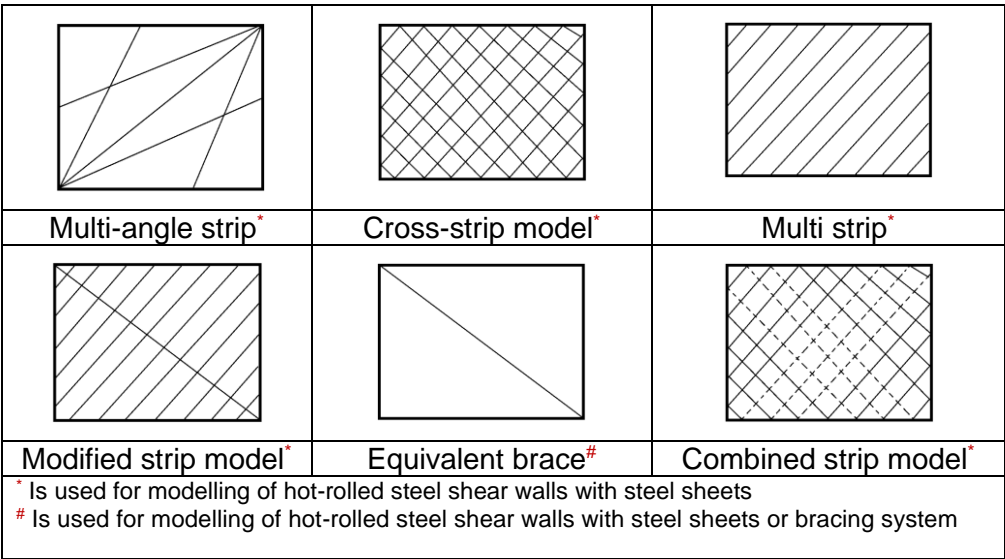
Figure 5.3. Some of the available macro models for simulation of steel shear wall structures

With regard to CFS framed walls, four classes of macro models have been proposed in the literature to simulate the existing design and construction considerations. These four methods, which are generally developed for numerical modelling of CFS framed walls under lateral loading, are (1) equivalent brace method, (2) equivalent spring method, (3) fastener based method, and (4) effective strip method. Figure 5.4 schematically depicts these four macro modelling methods' graphs. The following sections discuss the methods and applications in the literature.

Equivalent brace method	Equivalent spring method	Fastener based method	Effective strip method
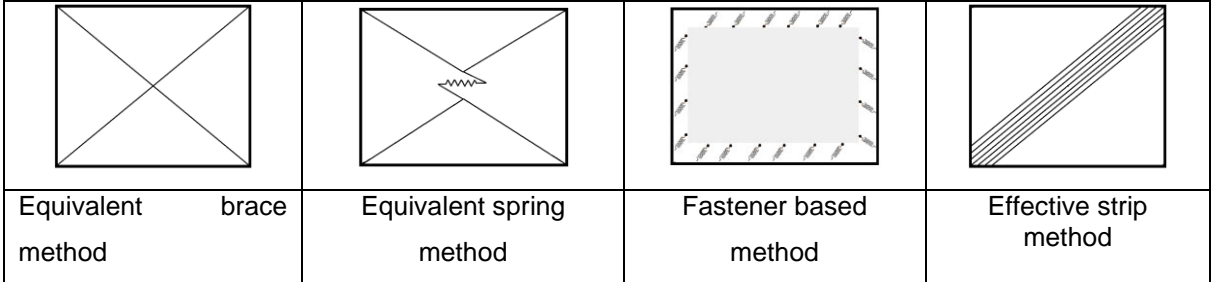
Figure 5.4. Macro methods techniques used for modelling of CFS framed walls under lateral loads

5.2.1.1 Equivalent Brace Method

In this method, the sheathing plate/braces as well as the screws are represented by a single equivalent diagonal brace, whose stiffness is equal to the stiffness of the infill sheathing/brace and screws. This stiffness is derived from experiments. The main advantage of the equivalent brace model lies in the reduced modelling effort and computation time. However, this method is unable to characterize the distributed forces applied by the sheathing on the boundary studs.

One of the first macro modelling of CFS structures using equivalent brace method was carried out by Gad [152], in which a simplified model of a house was developed and verified against experimental results. The nonlinear time-history dynamic analysis program Ruaumoko [153] and the Stewart [154] degrading hysteresis model were selected for this modelling and dynamic analyses. They assessed the interaction between out of plane veneer walls and frame and verified their model by a modal analysis where the mode shapes and the natural frequencies matched the experimental results. Figure 5.5 shows the macro model and the comparison between experimental and numerical results.
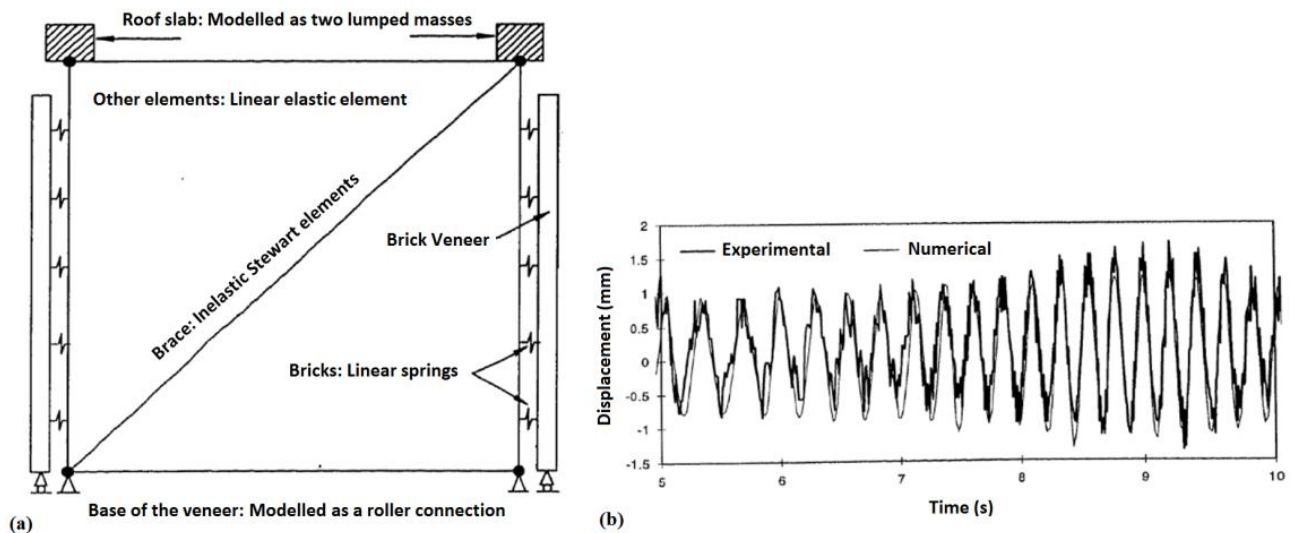
Figure 5.5. (a) Equivalent brace model of the tested house, (b) experimental and numerical top of the frame displacement at resonance for SSW input [152]

Using Ruaumoko program, the seismic force resisting system of two representative buildings was analysed by Boudreault et al. [155, 156] in order to assess the performance of the shear wall panels under earthquake loading. In these studies, the Stewart hysteresis model based on the experimental results (Figure 5.6) was verified, then two and three storey strap braced structural models were established in order to simulate the oriented strand board (OSB) sheathed shear wall. The gap between the upper and lower walls was created to represent a floor of the two storey model, which is shown in Figure 5.6.
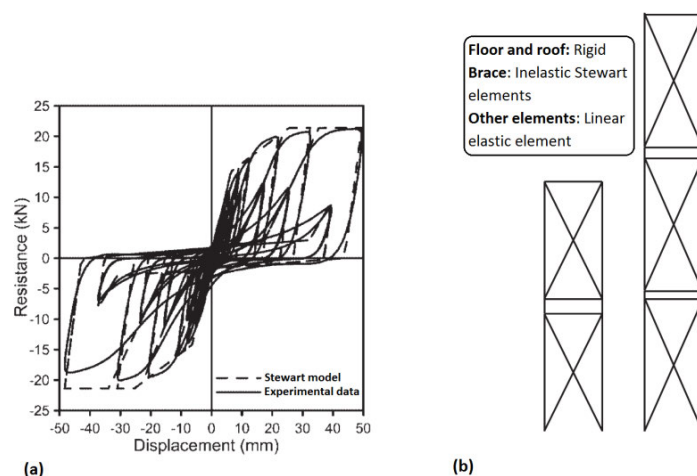
Figure 5.6. (a) Resistance versus displacement curve for Stewart model and test data, (b) two and three storey shear wall models [155, 156]

Based on the experimental tests on shear walls, a numerical equivalent brace model

88

for hysteretic behaviour of wall panels was created and employed in 3D dynamic nonlinear analysis of CFS framed buildings by Fulop and Dubina [48, 121, 157]. A tri-linear model, based on Drain -3DX [158] computer code, was utilised with the full nonlinear model. They hinged all column ends in the model, and assumed that the frame itself is a mechanism not contributing to load bearing capacity (Figure 5.7). Their model can consider most of the important features of the hysteretic behaviour and can be implemented in more complex structural systems.
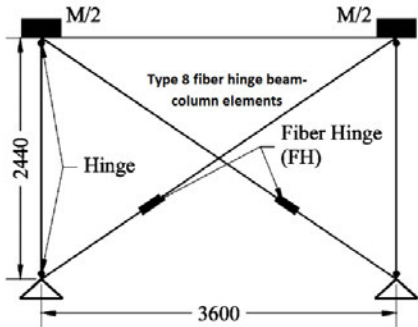
Figure 5.7. Wall-panel simulation with equivalent bracing [48]

Foutch and Lee [159] simulated two, four and six-storey prototype CFS buildings with gypsum wall under seismic loading. The Drain-2DX [160] program was used for nonlinear time history analyses. They indicated that the inelastic behaviour of the numerical model comes from the truss elements with gap properties for braces and at the column ends. Each modelling elements of Drain-2DX and lumped mass position for building are shown in Table 5.1 and Figure 5.8a. The authors had to choose the strength degradation rate of the wall conservatively for the modelling of the gypsum wall, because test results at large drifts were not available. Figure 5.8b also demonstrates that the macro model can successfully represent the hysteresis result of the test.

Table 5.1. Element used in numerical modelling by Foutch and Lee [159]

Element	Element assigned in Drain-2DX	Detail
Stud	Elastic beam element using Plastic Hinge Beam-Column	-
Track	Plastic Hinge Beam-Column Element (type 02)	To represent a rigid element with high stiffness and moment resistance
Brace	Inelastic Truss Bar Element (Type 01) in conjunction with truss element with gap property	To consider pinched model in the truss element
Sheathing	Horizontal spring Element (Type 10, Elasticity Code 4)	-
End of studs	Inelastic rotational spring elements Element (Type 04)	Plastic hinges was expressed to express the moment capacity of the column
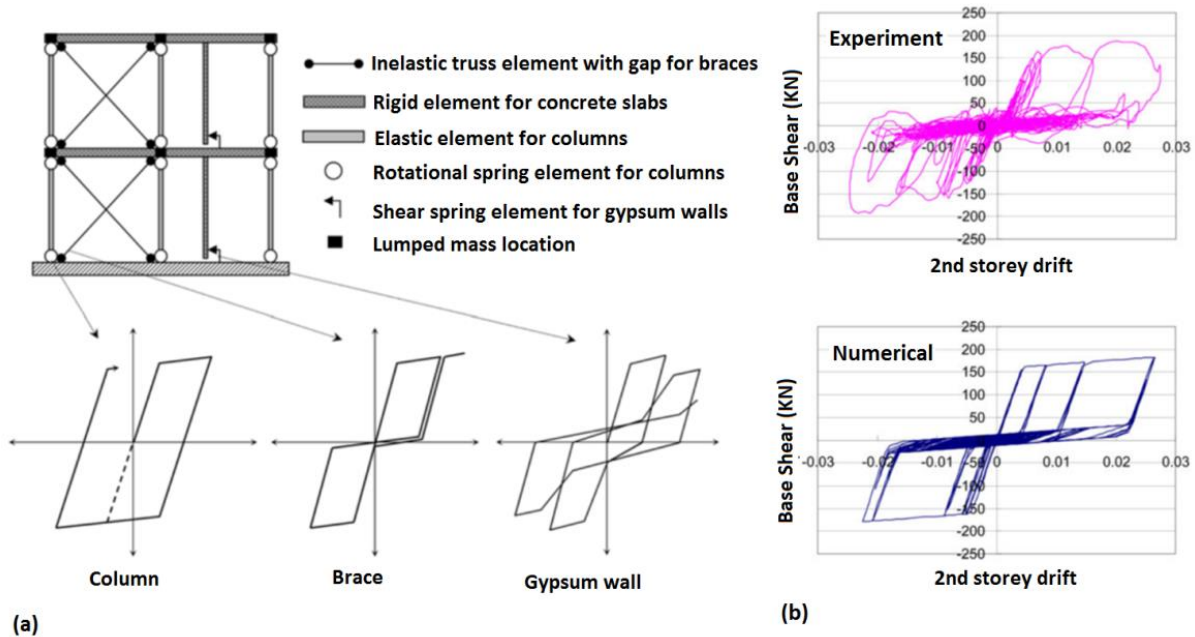
Figure 5.8.(a) Macro model for 2-storey CFS Building, (b) comparison of numerical and experimental results [159]

Foutch et al. [64] studied the dynamic behaviour of a two storey, one bay frame under large seismic motions to assess if commonly used numerical models are capable of predicting the measured motion of the structure with an adequate accuracy. In that study, a macro model similar to method of Foutch and Lee [159] was introduced in Drain-2DX for dynamic analysis of the specimen, and the results were compared with the results of the shake-table test.

An extensive numerical study by equivalent brace method was developed and then modified by Shamim et al. [50, 51, 161-163] based on the response captured from single and double storey steel sheathed CFS framed shear wall tests. They proposed the macro method using OpenSees [164] software for modelling steel sheathed CFS framed shear wall specimens under dynamic loading. The modelling was carried out before and after dynamic testing of shear walls [50]. Table 5.2 and Figure 5.9a show the elements used for the model. Their findings indicated that the final lateral displacement of the walls calculated with the model could be affected by three main factors, namely shear force flexural displacement, and uplift displacement of each wall section's rigid rotation due to elongation in anchor rod. Figure 5.9 also displays a comparison of the test and numerical results in that study.

Table 5.2. Element used in numerical modelling by Shamim et al. [50, 51, 161-163]

Element	Element assigned in OpenSees	Detail
Stud	Elastic beam-column elements	-
Track	Rigid beam-column elements	-
Strap and Sheathing	Inelastic Pinching04 truss members	-
Hold-down	Linear elastic uplift spring elements	To determine the lateral displacement of the wall associated with elongation of anchor rod
Stud-track connection	Elastic rotational spring elements for corners	Represents the in-plane flexural stiffness of the bare frame without sheathing
Floor	Elastic truss elements	-
P-delta effect (fictitious column)	Rigid beam-column element with co-rotational coordinate transformation capability	-
P-delta effect (linking the fictitious column to the CFS frame)	Rigid truss element linking	-
Seismic mass	Lumped at each storey level	Representing the supporting columns and seismic weight
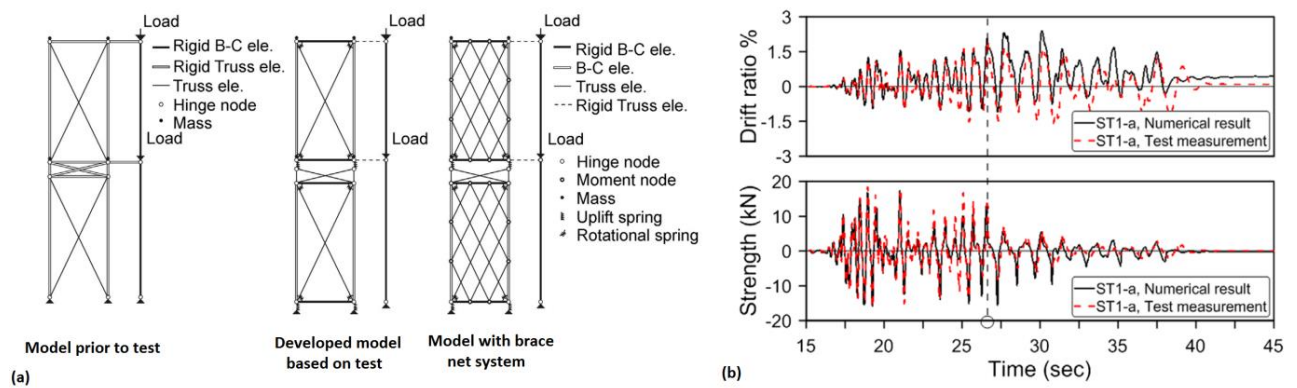
Figure 5.9. (a) Numerical models in OpenSees, (b) comparison of numerical and experimental results [51]

In another study by Shamim et al. [52], an archetype building developed and calibrated based on the findings of their previous work. Figure 5.10 illustrates the components of the macro model utilised for the CFS wall of a double storey archetype building used in that study.
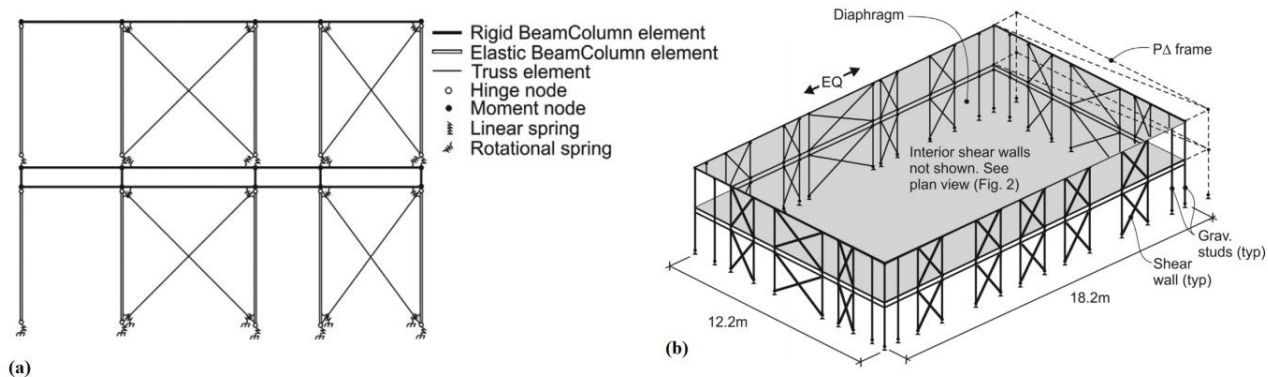
Figure 5.10. Schematic representation: (a) office building model used without P–Δ framing, (b) residential building [52]

Lu et al. [165] proposed a numerical model for sheathed walls that can be used to evaluate the effect of gypsum on behaviour of a strap braced building. The modelling strategy as well as experimental test data for verifying their model were based on Shamim [161]. The OpenSees macro model with its components, as well as a comparison between the numerical model and the results of the corresponding cyclic test for the strap-braced wall frame are presented in Figure 5.11.
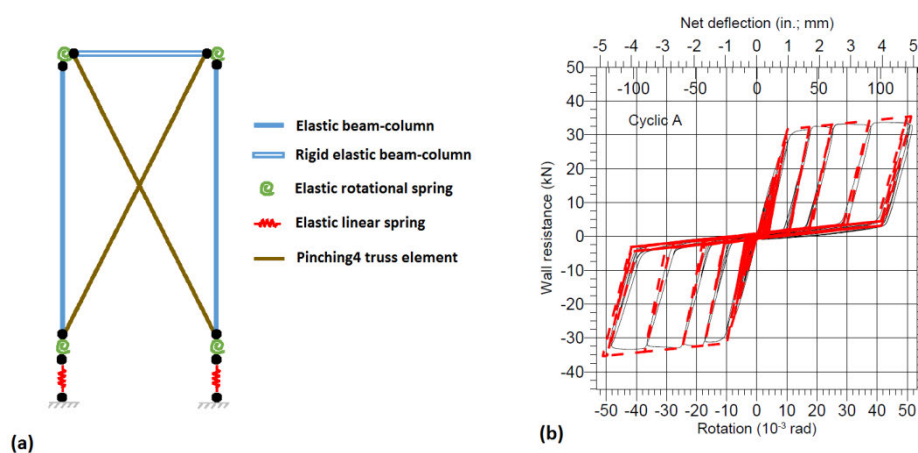
Figure 5.11. (a) Macro model of the shear walls in OpenSees, (b) comparison between the numerical model and cyclic test [165]

An improved equivalent bracing model of CFS shear walls with concrete-filled rectangular steel tube column (as reinforced end studs) was proposed by Wang et al. [166] in order to evaluate the seismic behaviour of mid-rise CFS structures. Two different types of modelling, and the elements used in their model are shown in Figure 5.12 and Table 5.3 respectively. They concluded that by taking end stud's compression buckling and beam-column joint's behaviour into account, the results for model 1 are

much closer to the experimental results (the error is below 9%) than model 2 with the maximum relative error up to 24%.

Table 5.3. Element used in numerical modelling by Wang et al. [166]

Element	Element assigned in OpenSees	Detail
Stud	Elastic beam-column elements	-
Track	Elastic beam-column elements and truss element rigid bar	Based on the rigid diaphragm assumption
Strap and Sheathing	Nonlinear spring elements with Pinching4	-
Hold-down	Axial spring elements	-
Stud-track connection	Rotational spring elements for chord stud	Due to the effective connection between end studs and foundation by hold-downs
End studs	Axial spring along Y-direction	To account the possible buckling at the bottom of columns
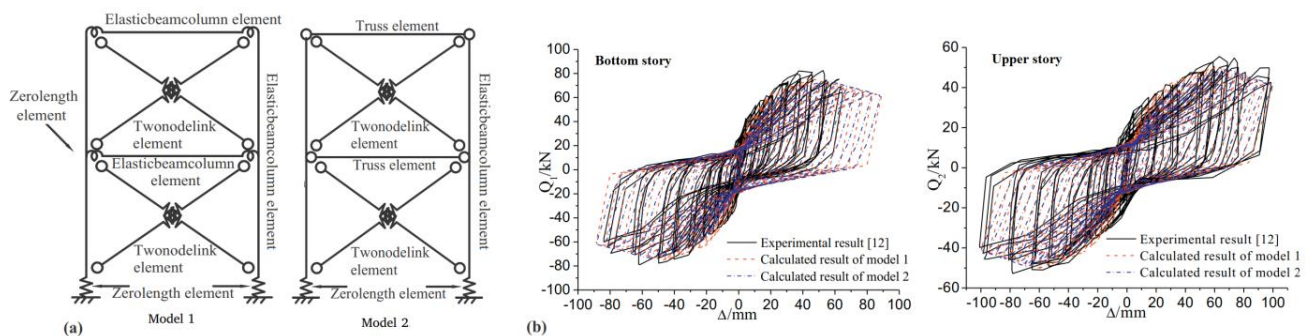
Figure 5.12. (a) Macro models of mid-rise CFS shear wall, (b) load-displacement curves of the double-storey specimen [166]

A number of comprehensive numerical studies on seismic response of a two-storey CFS framed building with OSB sheathed shear walls (formally a part of the Network for Earthquake Engineering Simulation research program), or in short CFS-NEES) were performed by Leng et al. [167-171]. The authors' earlier works on modelling the seismic response of CFS-framed buildings normally relied on simplifications to minimise computational cost [169, 170]; however, significant differences were reported between numerical and experimental results. Therefore, they developed higher fidelity models that offered dependable prediction of CFS-framed building response under seismic loads [167, 171]. A remarkable feature of their simulated shear walls was the subdivision of the sheathing board into subpanels. It was mentioned that in actual framed system, a number of intermediate members were connected to the shear wall, including the ledger, window and door headers. Hence, the secondary load paths were allowed in the model by subdividing the shear. Figure 5.13 shows the models with and

without subpanels, and the simulated CFS-NEES building. The method given in that study provides comprehensive details of how the building attains its beneficial performance.
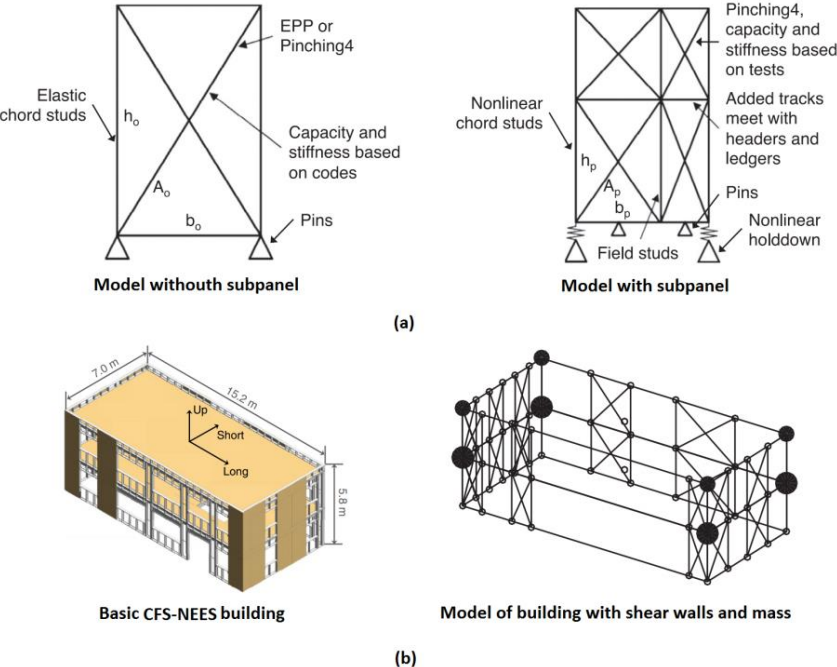
Figure 5.13. (a) Comparison of modelling strategies, (b) CFS-NEES building and macro model [167, 171]

The CFS-NEES building was redesigned by Yu et al. [65, 66, 172, 173] to include the new corrugated steel sheathing shear walls to the system. A numerical model was developed and seismic performance was evaluated through incremental dynamic analysis using a methodology proposed by FEMA [174]. They employed rigid connection method for their macro modelling, because their linear static analysis results showed that the diagonal bracing stiffness is much greater than the small moment stiffness of the stud to-track connection. In addition, they indicated that using two spring for hold-downs (one spring uses a Pinching4 and other spring uses an elastic-perfectly plastic gap material, with the gap close to zero and a very large stiffness in compression) is more reliable in simulations. Figure 5.14 shows the macro model of shear wall and the comparison between experimental and numerical results.
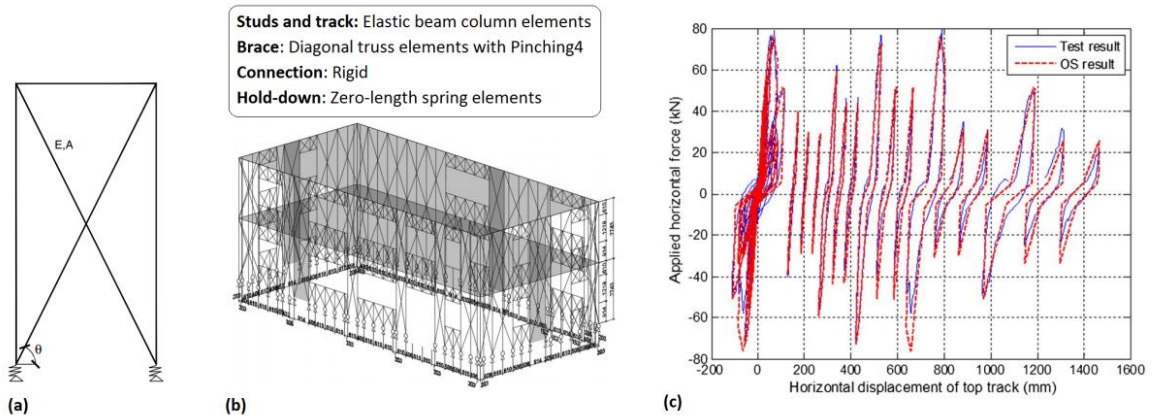
Figure 5.14. (a) Macro model of shear wall, (b) developed model for a two storey building, c) comparison between the experimental and numerical results [65]

In recent years, a European research project named ELISSA [175] was conducted in order to study the seismic performance of CFS shear walls sheathed with nailed gypsum based panels. In this project, Fiorino et al. [176] developed a macro model for shear wall panels with an ability to model their nonlinear hysteretic characteristic and possessing the capability of being employed in the collapse simulations of whole building. The elements implemented in their numerical study are described in Table 5.4. Figure 5.15 also shows the model developed in the study, as well as the force vs displacement response curves of both numerical simulations and experimental results for a long and short shear wall. They reported that numerical models were able to capture the experimental hysteretic response in terms of final shape and peak locations as well as dissipating energy similar to the experimental tests.

Table 5.4. Element used in numerical modelling by Fiorino et al. [176]

Element	Element assigned in OpenSees	Detail
Stud	Elastic beam-column elements with MinMax material in conjunction with uniaxial elastic material	To model the failure of chord stud due to tension or global buckling
Track	Rigid horizontal displacement constraint	The effect of rigid diaphragm was combined by constraining the horizontal displacements
Brace	Truss element with Pinchinng4 material	-
Hold-down	Zerolength elements with ElasticMultiLinear material in conjunction with MinMax material	In order to consider tensile failure of anchors

95
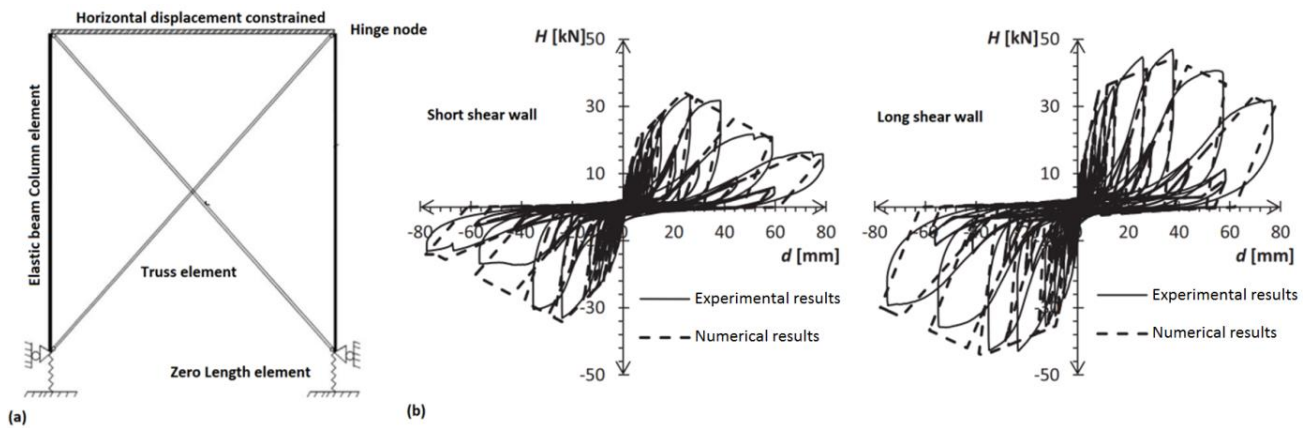
Figure 5.15. (a) Macro model for CFS sheathed-braced shear walls, (b) comparison of load-displacement curves between numerical model and test [176]

After modelling and verifying the single CFS walls, complete 3D models of archetypes, with application of strap brace walls, were created in another study by Fiorino et al. [177]. In this modelling strategy, floor elements (composite floor, joist and racks) are assumed to be rigid elements, due to their large stiffness. Moment releases in this model were established between studs and rigid floors in order to avoid the transfer of moments from floor. The gravity load was applied on the chord studs of walls based on their tributary areas. In addition, seismic mass was utilised at the four corners of building. Figure 5.16 schematically illustrates a 2D illustration of a braced bay in two storey residential building designed for low intensity seismic loads.
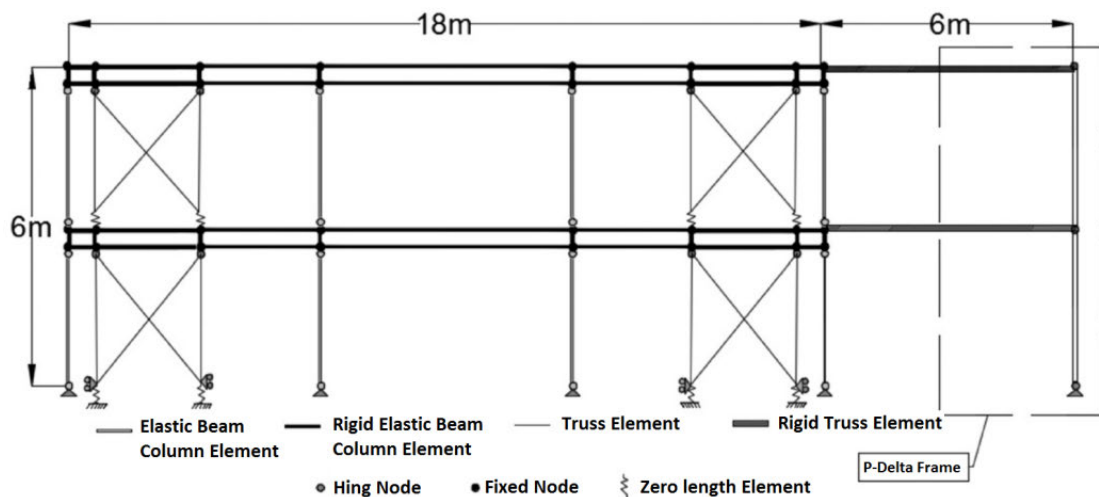
Figure 5.16. 2D Schematic of a braced bay in residential building [177]

A numerical macro model was developed in OpenSees by Macillo et al. [178, 179], which is able to simulate the dynamic response of the entire building, while considering the effects of non-structural elements. The authors indicated that their model is able to

96

predict the response of the first floor with good accuracy, whilst the prediction of the behaviour of the second storey is not so precise. In another similar macro model, by Scotta et al. [180], the dynamic non-linear behaviour of buildings was evaluated. The numerical results were then used to assess the proper behaviour factor value, according to the European seismic codes. Figure 5.17 shows the macro model of the one storey wall system in their study with its elements, and also a comparison between the numerical and experimental results.
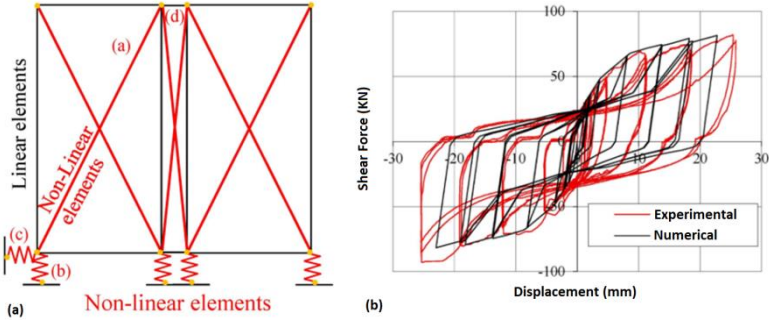
Figure 5.17. (a) macro model of a one storey frame, (b) comparison of numerical and experimental results [180]

Table 5.5 briefly summarises some basic information about the numerical research works on lateral behaviour of CFS framed shear wall structures by equivalent brace method, presented in this section.

Table 5.5. Summary of the macro model studies by equivalent brace method

Author, reference	Year	Software	Employed hysteresis model	Specimen modelled	Brace or sheathing system
Gad, [152]	1997	Ruaumoko	Stewart	1 storey domestic house	Brick veneer
Boudreault et al., [155, 156]	2005 2007			2 and 3 storey frame	OSB sheathing
Fulop and Dubina, [48, 121, 157]	2002 2004 2008	Drain-3DX	Trilinear	Single wall panel	OSB, gypsum and corrugated steel sheathing
Foutch and Lee, [159]	2010	Drain-2DX	Bilinear with gap property and trilinear	2, 4 and 6 storey building	Brace and gypsum sheathing
Foutch et al., [64]	2007		Bilinear with gap property	2 storey building	Strap brace
Shamim, [161]	2013	OpenSees	Pinching4	1 and 2 storey wall panel and 2,4,5 storey office and residential building	Steel sheathing
Shamim et al., [50, 162, 163]	2011, 2012, 2013			1 and 2 storey wall panel	
Shamim et al., [51]	2013			1 and 2 storey wall panel and 2 storey office building	
Shamim et al., [52]	2015			2,4,5 storey office and residential building	

Lu et al., [165]	2015		Single wall panel	Gypsum sheathing
Wang et al., [166]	2017		1 and 2 storey wall panel	concrete-filled rectangular steel tube column as reinforced end studs, and double layer wallboard
Leng et al., [167-171]	2012, 2013, 2015, 2016, 2017		2 storey building (CFS-NEES building)	Gypsum and OSB sheathing
Yu et al., [65, 172]	2014, 2017		2 storey building	Corrugated steel sheathing
Yu et al., [66]	2017		2,3,4, 5-storey hotel and office building	
Yu et al., [173]	2018		Single wall panel and 2 storey building	Non-perforated corrugated steel sheathing and corrugated steel sheathing with vertical slits.
Fiorino et al., [176]	2018		Single wall panel	Nailed gypsum sheathing
Fiorino et al., [177]	2017		1,2 3,4 residential and office building	Strap brace
Macillo et al., [178]	2018		2 storey residential building	Gypsum-based panels
Macillo et al., [179]	2018		Single wall panel	Strap brace
Scotta et al., [180]	2015		Single wall panel and 3 storey building	OSB sheathing and external techno-prene plaster-infilled slab

5.2.1.2 Equivalent spring method

Equivalent spring method is another macro modelling strategy for the simulation of CFS framed shear wall structures under lateral loads. Similar to the equivalent brace method, in this approach the sheathing plate/braces as well as the screws are simulated by a single equivalent spring, in which the overall stiffness and strength of the sheathing/brace and screws are equal to the stiffness and strength of the spring. The lateral stiffness and strength are derived directly from the spring element implemented in the shear wall.

For a successful macro model, it is required to verify the design procedure and the R values using dynamic analyses or dynamic tests. To address this need, fourteen structures (4, 6 & 7 storeys) were designed and modelled By Morello [181] employing two different software packages: Ruaumoko and SapWood [182]. With SapWood, they employed a multi-dimensional model of a structure, in which a number of walls were placed throughout the multi-storey building. This technique offers a considerably less complicated model, while still describing the behaviour of a single shear wall under dynamic loading. Figure 5.18 and Table 5.6 show the elements used in both software and schematically depict the models. They reported that the structures modelled in

SapWood fails at lower scaling factors compared to the structures modelled in Ruaumoko, because SapWood considers strength degradation. Generally, a more conservative result was provided with the SapWood models in their study.

Table 5.6. Element used in numerical modelling by Morello [181]

Element	Element assigned in software	Detail
Connection between floors	Spring element with Stewart hysteresis model	To dissipate the seismic energy
Lumped mass	-	Assigned to the node at each floor
P-delta effect	Infinitely stiff column	Its lateral displacement was set to be the same as the corresponding nodes on the shear wall
Walls in SapWood	Spring elements	EPHM hysteresis parameters was used
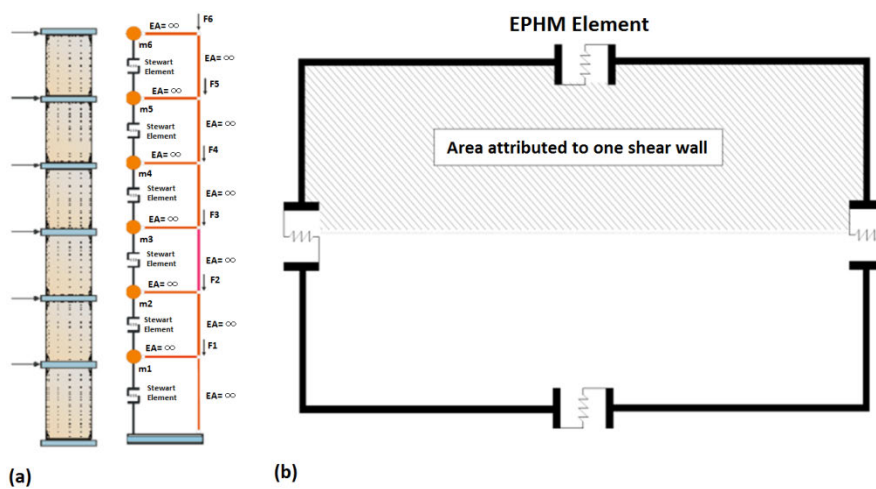
Figure 5.18. (a) Shear wall in Ruaumoko for 6 storey building (b) plan of shear building model in SapWood [181]

Similar to the modelling technique of Morello [181], dynamic analysis of multi-storey structures was carried out by Balh [183] in order to validate the recommended R-values and to determine height limits provided in building regulations. The building was simulated as a stick model in Ruaumoko without considering the exact location of each shear wall. Non-linear dynamic analysis of a multi-storey structure, designed using the AISI S-213 [184] provisions and the NBCC [185], was performed by Comeau et al. [186] and Velchev [187]. The aim was to verify their capacity-based design approach, the R_d and R_o values and the building height limit. They compared the six-storey stick model and full brace/chord stud model, in order to confirm the application of the stick models for the analyses. They indicated that the simpler (stick) model significantly reduces the needed computational time. Figure 5.19 displays both simple and complex models.
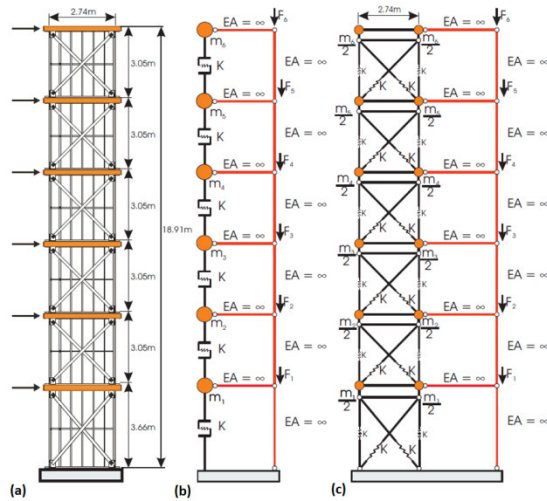
Figure 5.19. (a) Six-storey shear wall, (b) macro model, (c) full brace-chord stud model (complex) [187]

Another macro FE modelling technique for CFS shear wall panels was proposed by Bourahla et al. [188]. The strategy was based on substituting the entire panel by a nonlinear spring element connected to rigid body elements transmitting the forces to the end studs resisting tension and the compression. A number of vibrations testing on a recently constructed five storey building were used in their study to validate the initial elastic stiffness of the wall panels. Figure 5.20 displays the macro model proposed in their study as well as the real building used for verification of the numerical method.
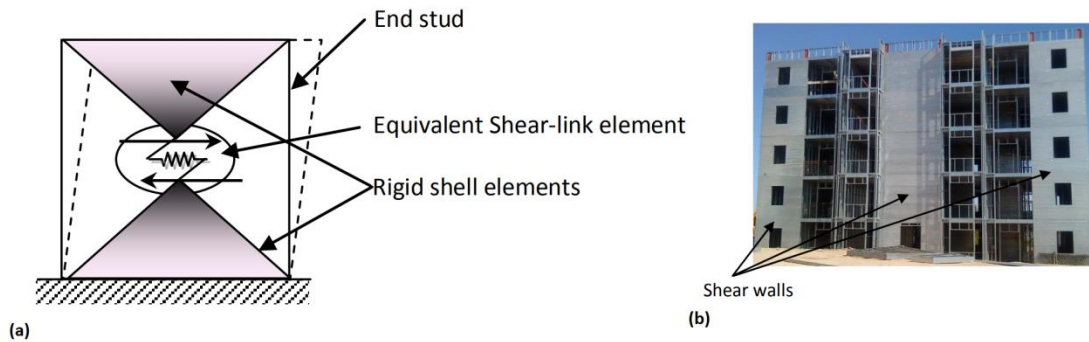
Figure 5.20. (a) Macro model of frame (b) real 5 storey building for verification [188]

A numerical study of the seismic behaviour of an innovative light-gauge CFS mid-rise building, designed using direct displacement design method, was presented by Dao and Lindt [189, 190]. This advanced system comprised open panel, floor trusses, V-braced panels, columns and connections between components. First the numerical method by experimental data of a wall panel was verified and then a five-storey example building was examined. The panels in the building were modelled by a

100

hysteresis spring (Folz and Filiatrault hysteresis model [191]), and the columns were modelled by beam elements. The second-order effects, i.e., the P-Delta effect, as well as stiffness and strength degradation were also involved in the analysis. Figure 5.21 shows a comparison between experimental and numerical results of a wall panel, as well as the developed model for a mid-rise CFS building.
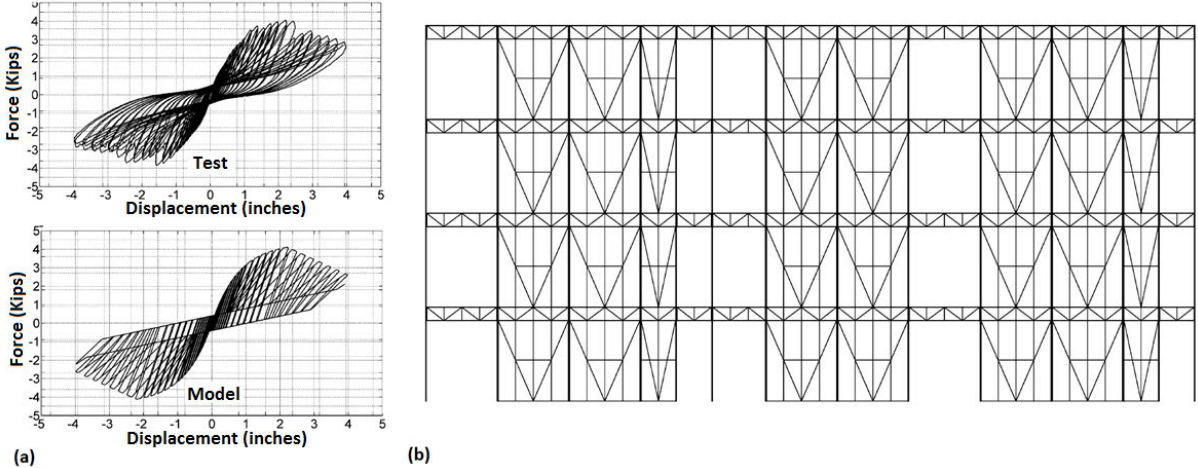
Figure 5.21. (a) Comparison of numerical model and experimental data, (b) developed mid-rise building [190]

Shahi et al. [192, 193] presented an incremental dynamic analysis on CFS fibre cement board (FCB) shear walls, which comprised a systematic application of non-linear time-history analysis to implement correlations between the damage state of the structure with the severity of earthquake ground shaking. To that end, SapWood computer program was employed for the analysis of equivalent single degree-of-freedom (SDOF) systems.

Kechidi and Bourahla [194] proposed a smooth hysteresis model for lateral behaviour of CFS framed structures that considers stiffness and strength degradation as well as pinching effects. They implemented that model in OpenSees software, as user-defined uniaxial materials named CFSWSWP and CFSSSWP for CFS-wood and CFS-steel sheathed shear wall panels, respectively. The elements used for this macro modelling approach and a comparison between experimental data by Balh [183] and numerical results for both walls with wood and steel sheathing are shown in Figure 5.22.
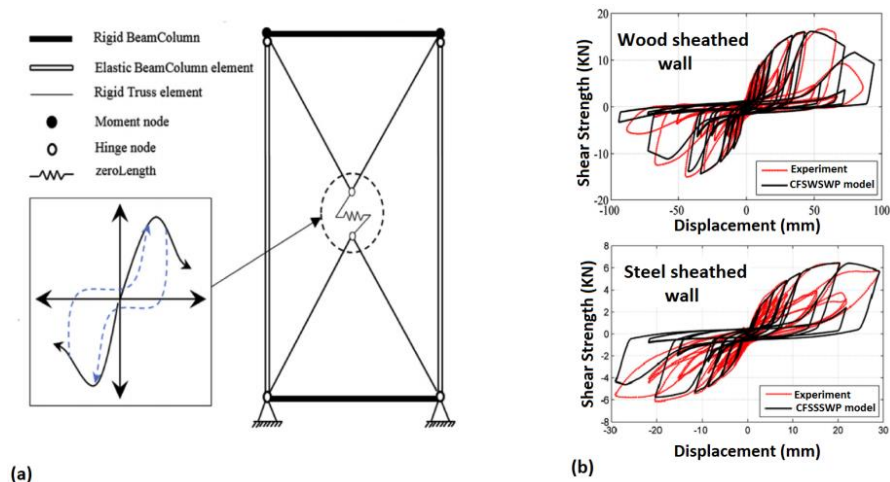
Figure 5.22. (a) Macro model of a one storey frame; (b) comparison between model and experiment [194]

In another study by the same authors [195], a probabilistic seismic behaviour and risk assessment of CFS sheathed shear wall panel structures was carried out, where a series of 12 building structures, were designed for two seismic intensity levels. To model their nonlinear behaviour, the structures were simulated adopting the abovementioned model. In addition, a seismic design strategy for CFS structures utilising sheathed shear wall panels was proposed by Kechidi et al. [196] in accordance with the framework of the Eurocodes and then nonlinear static and incremental dynamic analyses were carried out on 54 CFS frames. First, they verified their model by experimental data (Figure 5.23a) obtained from a single frame, and then used the data to develop a macro model of a higher storey frames. The schematic model of a two storey frame and the elements employed for modelling in the study, are given in Figure 5.23b and Table 5.7. It can be seen that the continuity of chord studs along the height of the structure is not taken into account in their macro models. In their model, it is also noted that the gravity load resisting system had to be prevented from contributing to the lateral stiffness, while considering P-delta effects.
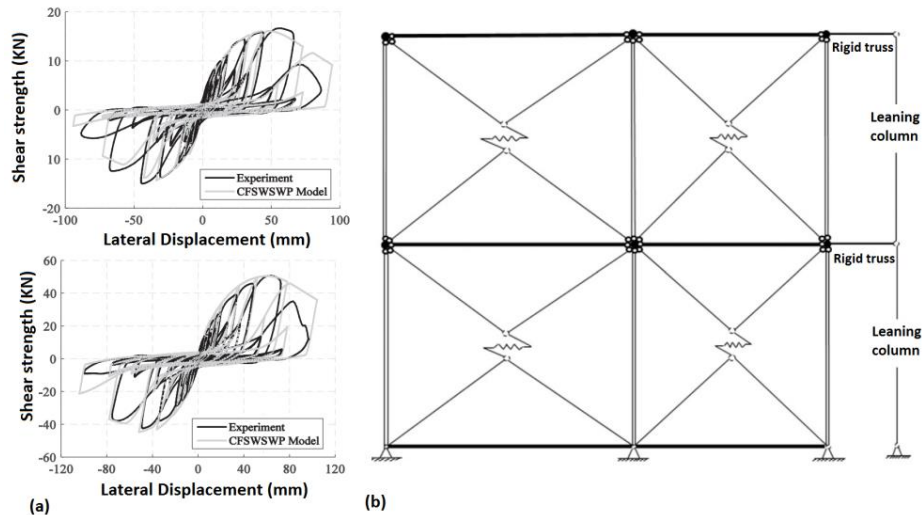
Figure 5.23. (a) Verification of the single wall by experimental data (b) Macro model of a two storey frame [196]

Table 5.7. Element used in numerical modelling by Kechidi et al. [196]

Element	Element assigned in OpenSees	Detail
Stud	Elastic beam-column elements	-
Track	Rigid beam column element	A multipoint constraint is employed to slave the horizontal DOF at each floor level to model a rigid diaphragm
Framing end	Modelling as pin (hinge node)	To prevent any resistance to lateral loads
Connection of leaning column and the wall	Rigid truss elements	Are hinged around the wall
Seismic mass	-	Is uniformly distributed at the top corners of each wall
Bearing and partition walls	Rigid truss element	Leaning column to the CFS frame
Connection to springs	Rigid truss element	-
Sheathing	Zerolength element	-

Zeynalian et al. [197] evaluated the seismic behaviour of CFS-FCB shear walls by nonlinear incremental dynamic analyses of multi-storey CFS structures. A modelling approach similar to Morello's method [181] was utilized in OpenSees software using pinching04 element for nonlinear dynamic time history analysis of a FCB wall. In another study, macro models for four 2-storey steel-sheathed CFS framed buildings were provided by Jiang and Ye [198] based on shaking table tests on steel-sheathed CFS walls using OpenSees software. The elements utilized for their macro modelling are presented in Figure 5.24a and Table 5.8. They established a group of fragility curves for CFS buildings after validation of their proposed model, as shown in Figure

5.24b.
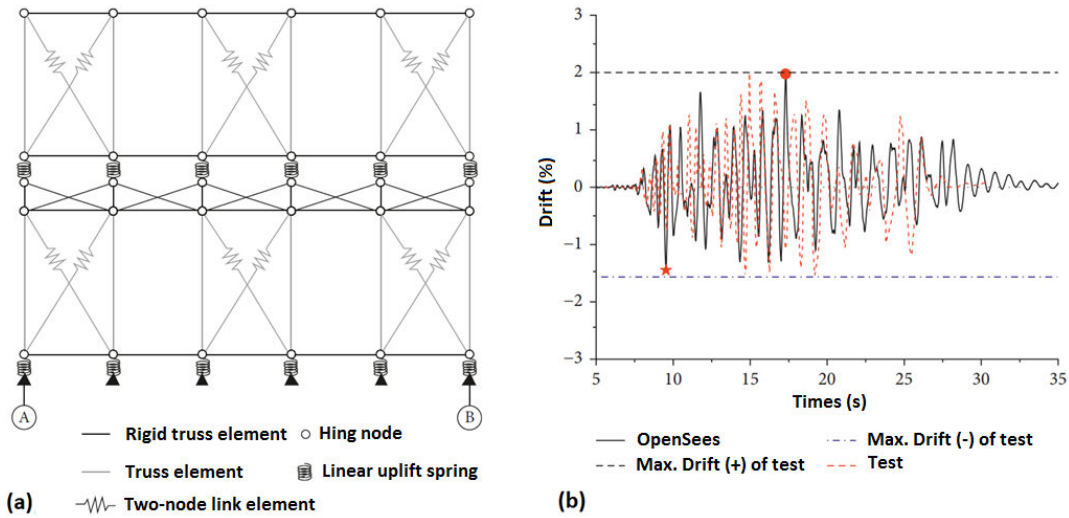
Figure 5.24. (a) Macro model of the frame, (b) comparison of model results and test data for specimen ST1 [198]

Table 5.8. Element used in numerical modelling by Jiang and Ye [198]

Element	Element assigned in OpenSees	Detail
Stud	Elastic truss	-
Track	Rigid truss	-
Framing end	Simplified hinge nodes	Because there is no bending moment transmitted in these connections
Floor and roof	Rigid planes	Planes are connected with the hinge nodes
Hold-down	Linear springs	To consider uplift behaviours of the anchor rods and hold downs
Sheathing	Two-node link elements with Pinching04 material	-

They also numerically developed a CFS building model from low-rise to mid-rise, made by a new type of CFS composite shear wall system [199]. The simplified model utilised in that study is shown in Figure 5.25a. The rigid diaphragm approach was employed to simulate the composite floor system in order to improve the computational efficiency of the macro model. They compared the numerical results with the experimental data of a five-story CFS 1:2 scaled composite shear wall, and reported a reasonable agreement between results. The comparison of numerical and experimental results is illustrated in Figure 5.25b.
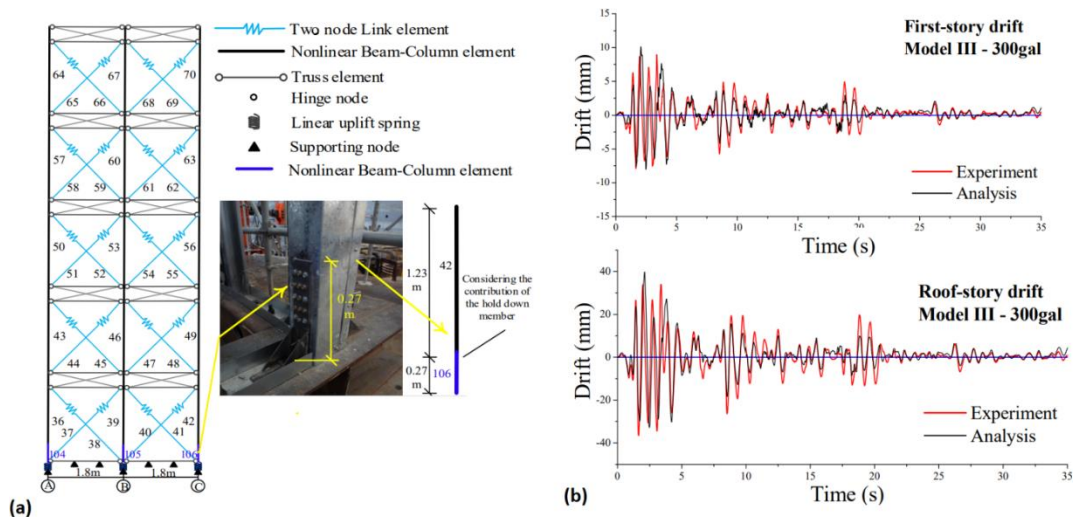
Figure 5.25. (a) Macro model for the shaking table test specimen, (b) comparison of numerical and experimental data [199]

A summary of basic information obtained from the numerical studies on the lateral behaviour of CFS framed shear wall structures, which were presented in this section and employed equivalent spring method is provided in Table 5.9.

Table 5.9. Summary of the macro model studies by equivalent spring method

Author, reference	Year	Software	Employed hysteresis model	Specimen modelled	Brace or sheathing system
Velchev, [187]	2008	Ruaumoko	Bi-linear with slackness hysteresis	2,4 and 5-storey building	Strap brace
Morello, [181]	2009	SapWood Ruaumoko	Stewart and EPHM	4, 6 and 7-storey building	Wood and gypsum sheathing
Comeau, [186]	2010	Ruaumoko	Bi-linear with slackness hysteresis	2,4,6 and 7-storey building	Strap brace
Balh, [183]	2010		Stewart	4-storey building	Steel sheathing
Bourahla et al., [188]	2012	Sap2000	Pivot	5 storey building	Gypsum or wood sheathing
Dao and Lindt, [189, 190]	2012, 2013	NG		4 and 5 storey building	V-braced panels
Shahi, [192]	2015	SapWood	Folz and Filiatrault	Single wall panel	Fibre cement boards
Shahi et al., [193]	2017			Single wall panel and Typical domestic houses	
Kechidi et al., [194]	2016	OpenSees	Pinching04	Single wall panel	Steel and wood sheathing
Kechidi et al., [195, 196]	2017a,b			2,4,5 storey building	Wood sheathing
Zeynalian et al., [197]	2018			1,2 and 3 storey building	Fibre cement board
Jiang and Ye, [198]	2018			Two storey building	Steel sheathing
Jiang and Ye, [199]	2018			Five storey building	Gypsum wall board

5.2.1.3 Fastener based method

In the fastener-based modelling approach, each fastener (mainly screw) is characterised by a non-linear, radially-symmetric spring element. The material properties of the fastener element are specified from experimental tests of sheathing-to-stud connections. The softening backbone curve, pinching, and loading and unloading parameters are included in the fastener material model. The CFS-sheathing connections highly affect the load-deformation curves of the CFS shear walls. In fact, combined behaviour of connections, frame and sheathing are responsible for the total shear resistance. The interaction between fasteners and sheathing is especially important because first, sheathing-to-steel fastener response is the main reason of shear wall nonlinearity, and second, there is high variation in this fastener response. Buonopane et al. and Bian et al. [41, 200-205] comprehensively employed this macro modelling technique in order to evaluate CFS framed structures under lateral loading. They simulated full-scale shear walls of several widths with various construction details relevant to the ledger track, gypsum board, vertical and horizontal seams, and number and thickness of field studs. The numerical results were compared to the full-scale shear wall tests in terms of load–displacement behaviour, initial stiffness, lateral strength, drift at failure, and energy dissipation. The results were then compared to specification-based strengths and displacements. The modelling elements and configuration of fastener based model, employed in most of their studies, are presented in Table 5.10 and Figure 5.26a. In these studies, each OSB or gypsum board panel was modelled as a separate rigid body. The rigid panel assumption seems not to be appropriate for steel sheathing material, which withstands considerable deformation within the panel and smaller deformations surrounding the fasteners. Figure 5.26(b) depicts the comparison of numerical and experimental results for two models with OSB and gypsum sheathing. The results obtained from the fastener based method were consistent with the test result, but failed at a slightly reduced strength.

Table 5.10. Element used in numerical modelling by Buonopane et al. and Bian et al. [41, 200-205]

Element	Element assigned in OpenSees	Detail
Stud	Linear elastic, displacement-based beam elements	-
Track		
Ledger track	Linear elastic beam–column elements along its centreline	Connected to the chord studs using a rigid link that transfers only vertical forces
Hold-down	Uniaxial spring elements	Active in the vertical direction only,

		horizontal degree-of-freedom is restrained.
Sheathing	Rigid body (RigidDiaphragm in OpenSees)	To assume that deformation in the sheathing occurs locally around the fasteners. It does not include global shear deformation of the sheathing.
Stud to track connection	Semi-rigid rotational springs	Allow for semi-rigid connections
Fastener	Zero-length element (CoupledZeroLength in OpenSees) with uniaxial force-deformation behaviour and Pinching4 material	Symmetric in the plane of the sheathing
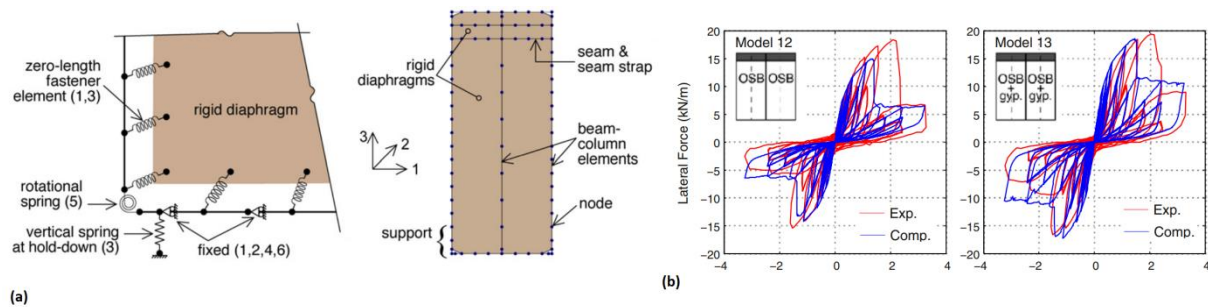
Figure 5.26. (a) Macro model of a one storey frame (b) load–displacement response for shear walls [204]

In addition, a model was proposed by Padilla-Llano [206] to indicate failure mechanism due to the development of local buckling on the chord studs. To study the effects of the vertical member slenderness on the response of a shear wall, they assigned a specific value to the slenderness of vertical framing members and employed asymPinching model for studs to consider local buckling effects. Table 5.11 summarises the elements implemented in their study. The macro models of a wall, as well as the comparison between experimental and numerical results are illustrated in Figure 5.27.

Table 5.11. Element used in numerical modelling by Padilla-Llano [206]

Element	Element assigned in OpenSees	Detail
Stud	Nonlinear beam-column using asympiching behaviour	-
Track		
Shear anchors	-	Fixing the horizontal degree of freedom at two of the track nodes next to the hold-downs
Hold-down	Elastic zeroLength springs	Low stiffness for tension and high stiffness in compression to simulated the contact with the foundation.
Sheathing	ShellMITC4 element	To accommodate any deformations the sheathing can experience

Contact with foundation	Springs with large stiffness in compression and close to zero stiffness in tension	Allowing uplift of the track nodes
Fastener	Nonlinear CoupledZeroLength element with pinching4	Can provide the flexibility needed for this type of connection and eases the formulation of a model
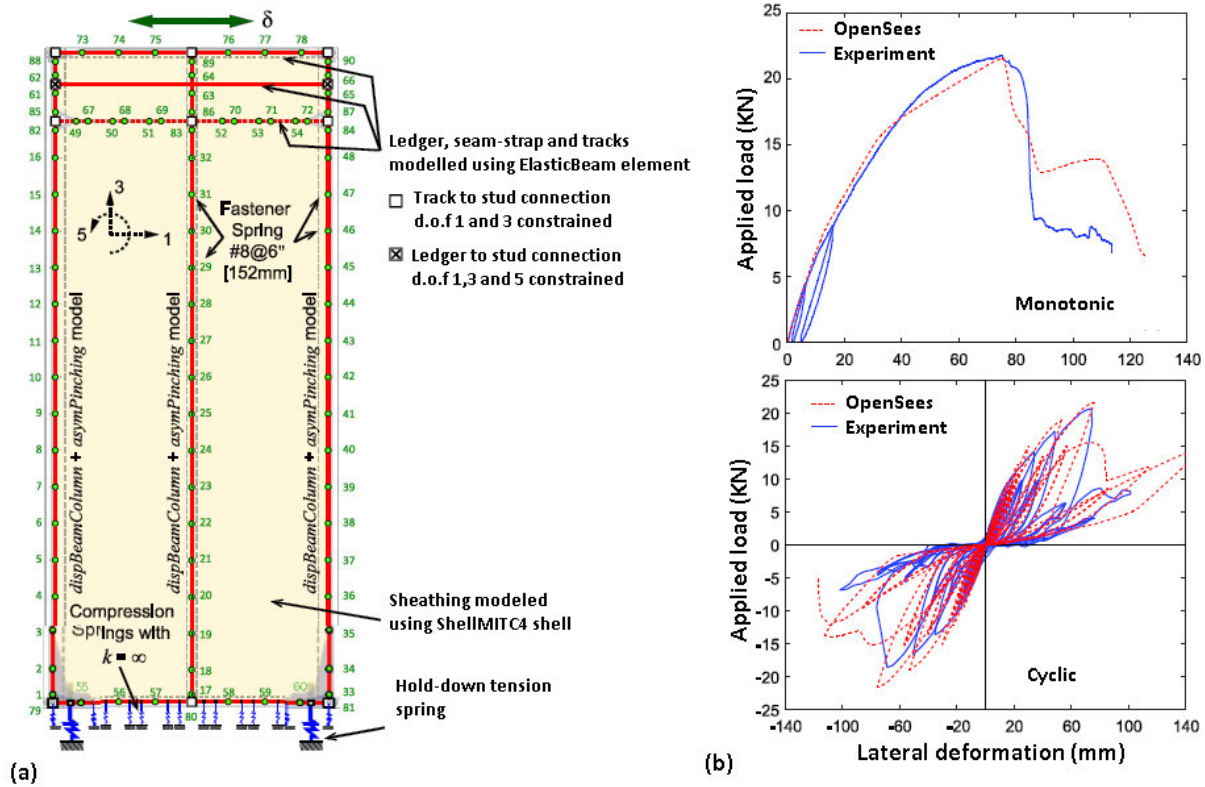
Figure 5.27. (a) Macro model of shear wall, (b) comparison of numerical and experimental results [206]

A summary of numerical studies using fastener-based method on the lateral behaviour of CFS framed shear wall structures is given in Table 5.12.

Table 5.12. Summary of the macro model studies by fastener-based method

Author, reference	Year	Software	Employed hysteresis model	Specimen modelled	Brace or sheathing system
Bian et al., [41, 200, 201, 205]	2014, 2015, 2017a,b	OpenSees	Pinching4	Single wall panel	Gypsum and OSB sheathing
Bian et al., [202]	2015				OSB sheathing
Buonopane et al., [203, 204]	2014, 2015				Gypsum and OSB sheathing
Padilla-Llano et al., [206]	2015				OSB sheathing

5.2.1.4 Effective strip method:

The effective strip method was theoretically developed by Yanagi and Yu [207], and is

generally employed for CFS shear walls with steel sheathing. In this model, it is assumed that a partial width of the steel sheet in the diagonal direction (the effective strip) is engaged in the tension field action to undergo the lateral force applied to the top of the wall. Therefore, the tension force created in the effective strip of the steel sheathing is directly related to the lateral capacity of the wall.

Employing the effective strip method, Santos [208] and Briere et al. [209, 210] developed an innovative configuration for CFS walls to address the need for a ductile lateral framing system for mid-rise buildings. In the numerical models, the effective strip method was implemented in Sap2000 program in order to find the ultimate shear capacity of CFS shear walls with steel sheets. The strips were simulated by equivalent strip elements pin-connected to the studs and tracks at the appropriate fastener spacing. In addition, the bottom corners were simply supported, and the framing elements were all pin connected to each other in order to indicate the screw connections between the different framing members. The number of strips used depended on the number of sheathing connections on the chord stud, located within the tension field. Figure 5.28 shows the transient development of CFS shear wall from experimental specimen to simplified numerical model in that study. They also calculated the ultimate shear capacity of walls and reported a good agreement between test data and numerical results.
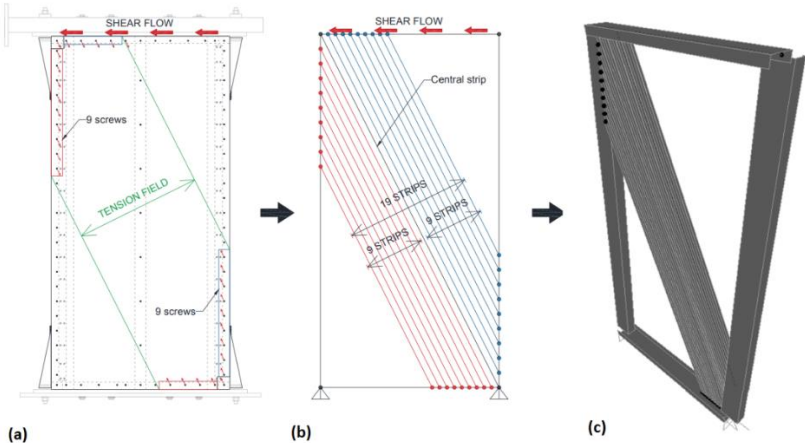
Figure 5.28. From experimental specimen to numerical model: a) screws located within the tension field b) equivalent frame elements for the numerical model c) numerical model in Sap2000 [208-210]

A summary of numerical studies using effective strip method on the lateral behaviour of CFS framed shear wall structures is presented in Table 5.13.

Table 5.13. Summary of the macro model studies by effective strip method

Author, reference	Year	Software	Employed hysteresis model	Specimen modelled	Brace or sheathing system
Santos, [208]	2018	Sap2000	Not applicable (just ultimate capacity is captured)	Single wall panel	Steel sheathing
Briere et al., [209, 210]	2017, 2018				

5.2.1.5 A comparison of hysteresis models used in macro modelling methods

Generally speaking, an appropriately designed CFS framed structure dissipates energy mostly through the inelastic performance of its connections. When a CFS framed structure is subjected to frequent cyclic loading, the generated hysteresis loops are characterised by strength and stiffness deteriorations as well as a pinching effect. Such characteristics, which significantly contribute to the post-elastic behaviour of the system, must be taken into consideration in the dynamic nonlinear analyses. The essential demand to implement such analyses is the availability of a basic model able to simulate as precisely as possible the structure response when exposed to a quasistatic or dynamic loading. Due to the complicated nature of the behaviour, and the difficulties occurred in simulation, many hysteresis models proposed in the literature ignore some (or even a majority) of the key aspects observed in experimental test. Researchers on the other hand, have developed a variety of complex hysteresis models attempting to represent hysteresis behaviour of shear walls as accurately as possible. These models have been mainly used for research purposes and are not commonly utilised for seismic analysis of real structures. Eight hysteresis models employed by researchers in the numerical models for the study of CFS framed structures under lateral cyclic loading, are briefly reviewed here in this section, and the characteristics of each model are discussed. Some theoretical research studies have been also carried out in order to calculate the hysteretic behaviour of CFS wall panels [36, 43, 81, 211], which are beyond the scope of this study.

The evolutionary parameter hysteresis model (EPHM):

This model was developed by Pang et al. [212] and can be used for many engineering

fields. The EPHM employs a total of seventeen parameters to capture the nonlinear hysteretic behaviour of shear walls. The EPHM is a relatively good choice for peak displacement analyses, when validity in the displacement calculations is needed over the whole range of design hazard levels. The model is able to precisely account for the degradation of a CFS wood sheathed shear wall by modifying its loading and unloading paths with evolutionary parameters. The ability of the EPHM to obtain energy dissipation at large displacements also makes it a good option for performance-based design applications, which may consider the performance requirements associated with significant deformation demand.

Stewart model:

The Stewart hysteresis model was proposed by Stewart [154] and found to best represent the strength and stiffness characteristics of a steel frame with wood panel shear wall components. The model is a SDOF model and can only examine the overall wall response. Stewart model is commonly in use for CFS wood sheathed shear walls studies and is included in the Ruaumoko [153] inelastic dynamic analysis software package. A series of rules are employed to develop this model, which offers pinching and stiffness degradation but not strength degradation. As reported by some authors [152, 155, 156, 181, 183], the main issue with modelling CFS framed structures under lateral load by this model is the lack of strength degradation considerations.

Folz and Filiatrault model:

This hysteresis model, which is also used for CFS wood sheathed shear walls, was developed by Folz and Filiatrault [191]. A key characteristic of this model is the lack of a linear part of the load-deformation curve, even at a low displacement level. A total of ten parameters are required to validate this model; parameters that can be captured either from experimental test of shear wall or from the results of a numerical analysis with the CASHEW computer program [213]. The model is added to the dynamic analysis software SAWS (Seismic Analysis of Woodframe Structures) [214] to be used for lateral assessment of CFS wood sheathed framed structures.

Pinching4 model:

One of the currently in-use and widely applicable hysteresis models for lateral evaluation of CFS structures with different sheathing materials is Pinching4 model,

which was developed by Lowes et al. [215] and is being implemented in OpenSees software. Pinching4 parameters comprise the backbone points in addition to parameters defining the pinched and unloading/re-loading behaviour of the model. The model is able to capture pinching, stiffness and strength degradation depending on damage level, such as unloading stiffness degradation, reloading stiffness degradation, and strength degradation.

Pivot model:
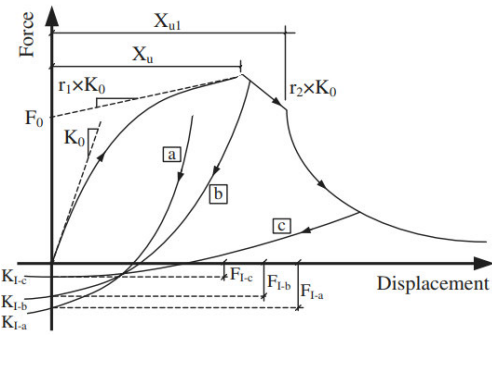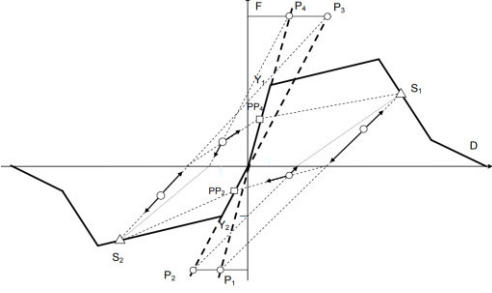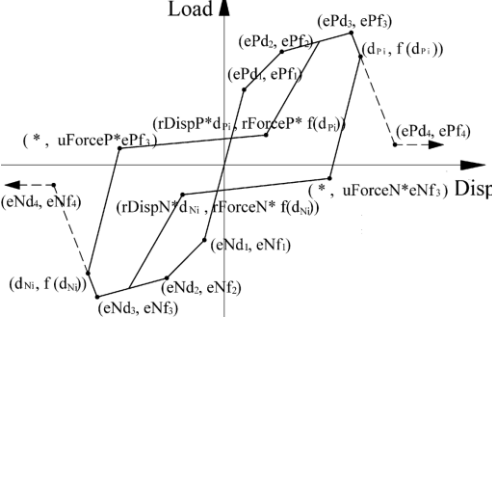
This model is developed by Dowell et al. [216] and is generally used for reinforced concrete members; however, it was also used by Bourahla et al. [188] for lateral evaluation of CFS shear walls. Pivot model is able to take into account the strength degradation, effect of axial load and lack of section symmetry and is also implemented in Sap2000 software.

Bi-linear with slackness hysteresis model, Tri-linear model and Bilinear inelastic with gap hysteresis models:

The bi-linear with slackness model can be utilised to represent diagonal braced systems where yield in one direction may stretch the elements leading to slackness in the bracing system [158, 160]. The bilinear inelastic and bi-linear with slackness models, employed in the literature, are unable of considering strength deterioration, due to repeated loading [158, 160]. In order to cover this inadequacy, they have been defined based according to the stabilised envelope of the cyclic curve.

Table 5.14 shows a summary of the abovementioned hysteresis models, in which the strength degradation is captured; and Table 5.15 shows those, in which the strength degradation is not taken in to account.
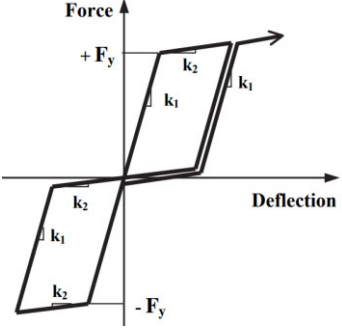
Table 5.14. Hysteresis models used for lateral performance of CFS framed structures (with strength degradation)

Model Name	Model shape	Description	Used by
EPHM		**K0:** Initial stiffness, **F0:** Resistance force parameter of the backbone **r1:** Stiffness ratio parameter of the backbone **Xu:** Displacement corresponding to max. restoring force of the backbone **r2:** Ratio of the degrading backbone stiffness to K0 **Xu1:** Displacement corresponding to the end of linear portion degrading backbone **P1:** Exponential degrading rate parameter of he backbone **Flm and Fir:** Max and min value of residual pinching force **DFla and DFlb:** Damage index corresponding to he starting/End point of the plateau portion of the FI **PFI and Pr4:** Exponential degrading rate parameter of the FI and KI degrading function **r4r:** Ra io of the residual KI to initial stiffness **β:** Strength degradation parameter	[181]
Pivot		**P1 :** P1 through P4 on the elastic loading lines control the amount of softening in each quadrant **P2:** Pinching Pivot points PP2 and PP4 fix the degree of pinching following load reversal in each quadrant **Fy, D:** yield resistance, degradation point **αFy :** resistance of primary pivot points **PP:** resistance of pinching pivot point **α1 and α2 :** locates the pivot point for unloading to zero from positive and negative force **β1 and β2 :** locates the pivot point for reverse loading from zero toward positive and negative force	[188]
Pinching 4		**ePf1,ePf2,ePf3,ePf4 and ePd1,ePd2,ePd3,ePd4:** Defining force and deformation points on the positive response envelope **eNf1,eNf2,eNf3,eNf4 and eNd1,eNd2,eNd3,eNd4 :** Defining force and deformation points on he negative response envelope **rDispP and rDispN:** Defining the ra io of he deformation at which reloading occurs to he maximum and minimum historic deformation demand **fFoceP and fFoceN:** Defining the ratio of the force at which reloading begins to force corresponding to the maximum and minimum historic deformation demand **uForceP and uForceN:** Defining the ra io of strength developed upon unloading from negative load to he maximum strength developed under monotonic loading **gK1,gK2,gK3,gK4,gKLim** and **gD1,gD2,gD3,gD4,gDLim:** Controlling cyclic degradation model for unloading and reloading stiffness degradation **gF1,gF2,gF3,gF4,gFLim:** Controlling cyclic degradation model for strength degradation	[41, 50-52, 65, 66, 161-163, 165-173, 176-180, 194-206]

113

| Folzand Filiatrault | | S0: Initial stiffness of shear wall spring element
F0: Resistance force parameter of the backbone
F1: Pinching residual resistance force
R1: Stiffness ratio parameter of the backbone,
R2: Ratio of the degrading backbone stiffness to K0
R3: Ratio of the unloading path stiffness to K0
R4: Ratio of the Pinching load path stiffness to K0
Du: Drift corresponding to the maximum restoring force
B (Beta): Strength degradation parameter for shear wall spring
A (Alpha): Stiffness degradation parameter for spring element | [189, 190, 192, 193] |
| | | K0: Initial wall stiffness

Mc: moment at first linear behaviour

My: Yield moment | [48, 121, 157, 159] |

Table 5.15. Hysteresis models used for lateral performance of CFS framed structures (without strength degradation)

Model Name	Parameter	Description	Used by
Steware		K0: Initial wall stiffness Fu: Ultimate force Fy: Yield force R: Bi-linear factor beyond yield force Fi: Intercept force PTri: Tri-linear factor beyond ultimate force PUNL: Unloading Stiffness factor Gap+: Initial slackness. Positive axis Gap-: Initial slackness, negative axis B (Beta): Softening factor A (Alpha): Reloading or pinch power factor	[152, 155, 156, 181, 183]
Bi-linear with slackness		K0: Initial wall stiffness R: Bi-linear factor beyond yield force Fy: Yield force Δ: Ini ial slackness	[186, 187]

| Bilinear inelastic with gap | | **K0:** Initial wall stiffness **Fy:** Yield force | [64, 159] |

5.2.2 Micro method for simulation of CFS framed walls

Micro models are the most accurate and widely-used tools available for in-depth analysis of the CFS framed structures' behaviour. The main advantage of using micro modelling methods is that all possible failure mechanisms can be captured. Although micro method is a numerical approach, whose results may not be considered as exact answers, it can provide adequately accurate results for most engineering problems. A precise micro model for CFS structures must comprise the basic types of boundary conditions and local failures mechanisms. The accuracy of micro method modelling of CFS framed shear walls under lateral load depends on many parameters such as the geometry, material properties, boundary condition and interactions between components, connections, solver systems and elements. Figure 5.29 categorises the parameters that affect the numerical results of CFS framed shear wall structures under lateral loading, discussed in the literature. Different numerical models have focused on one or some of these parameters to study their role in the CFS walls performance.
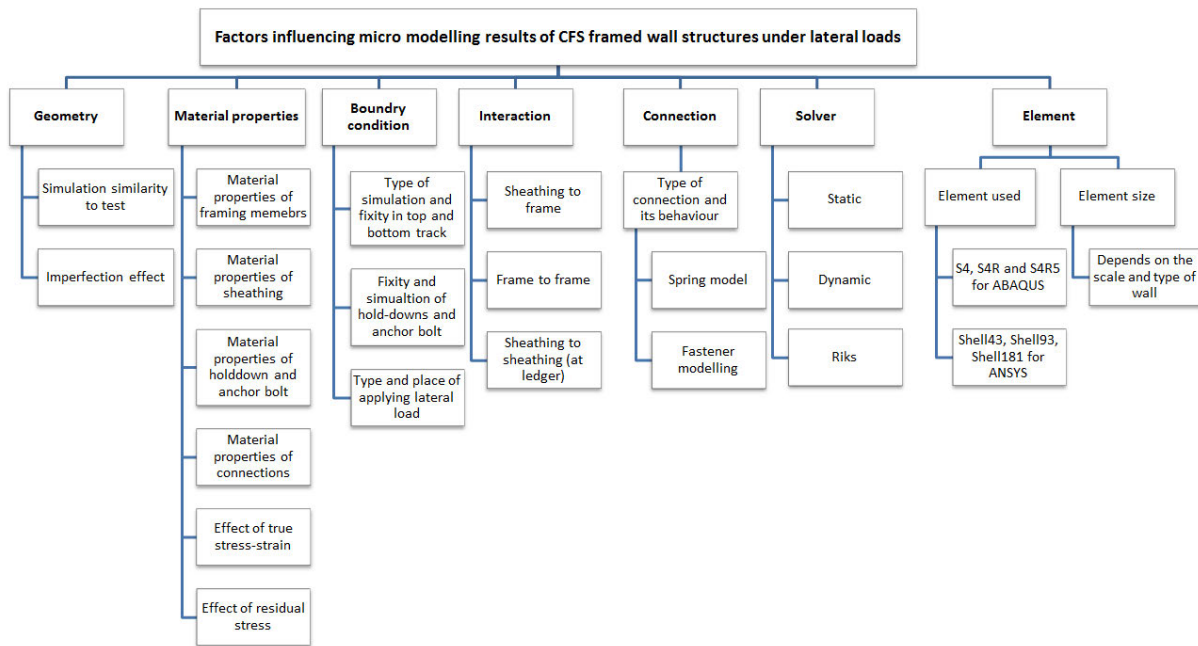
Figure 5.29. Factors affecting numerical results of CFS framed shear wall structures under lateral loading

In recent years, there has been an extensive growth in application of computer programs, corresponding to micro modelling of different CFS structures under various loading conditions [217-220]. In this section, the micro modelling methods in the literature for simulating the behaviour of CFS framed shear walls are classified based on the computer programs they have employed for modelling. In general, three FE computer programs are being widely used for micro modelling of CFS shear walls in the literature: Abaqus [221], Ansys [222] and Sap2000 [223]. An absolute majority of micro modelling of CFS shear walls under lateral loads in the literature are carried out using one of these three software packages. For the analysis of CFS shear walls, each package possesses its own capabilities and limitations, employs different behavioural models, is affected by different factors, and characterised by different parameters and functions, which will be discussed in this section.

5.2.2.1 Micro modelling studies by Abaqus

Abaqus [221] is an advanced and valuable general FE software, which has been used extensively for micro modelling of CFS components in recent years. It is also being employed as a powerful tool for micro modelling of CFS framed shear wall structures under lateral loading through implementing appropriate criterion and parameters to ensure the accuracy of the results.

116

Using Abaqus computer package, a FE model was developed by Telue and Mahendran [69] to understand the performance of steel wall frames with plaster boards on both sides. They utilised two load steps in the non-linear analyses, one for residual stress and the other for applying lateral load. Parametric studies on the effect of the first screw connection's variations, the effect of plasterboard fastener spacing and thickness was also conducted in that study. Attari et al. [54] simulated CFS shear walls with single and double sided steel sheathing under monotonic loading. The details of the specimens, boundary conditions and materials are precisely modelled based on the experiments. For creating an imperfection to the numerical models, the middle point of the steel sheathing is pushed 10 mm out of plane, prior to lateral pushover analysis. They indicated that their micro model is in good agreement with test results with respect to post buckling response, the peak strength estimation and initial stiffness. Figure 5.30 shows the micro model and comparison of numerical and experimental results.
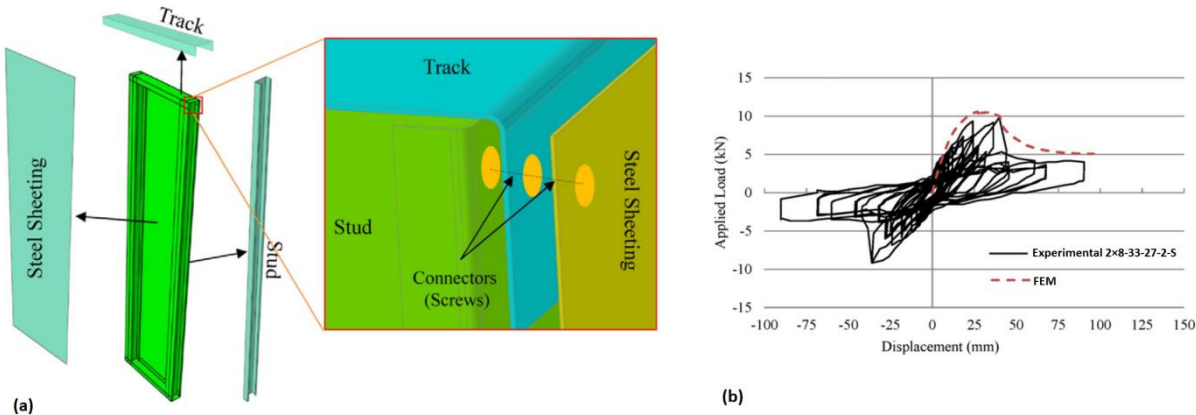
Figure 5.30. (a) Simulated model, (b) lateral load displacement response of numerical and experimental [54]

In another study, non-linear FE analyses were employed by Niari et al. [56] in order to examine the seismic performance of steel sheathed CFS shear wall panels. Geometric and material non-linearity were also included in their FE models. They noted that the displacements corresponding to the maximum loading, obtained by FE method, are smaller than experimental data and therefore, the elastic stiffness of numerical models are greater than corresponding experimental specimens. Their numerical method was able of capturing the seismic behaviour of actual CFS shear wall, when compared numerical and experimental results in terms of shear resistance, stiffness and failure modes. Figure 5.31 shows the numerical results compared to experimental data.
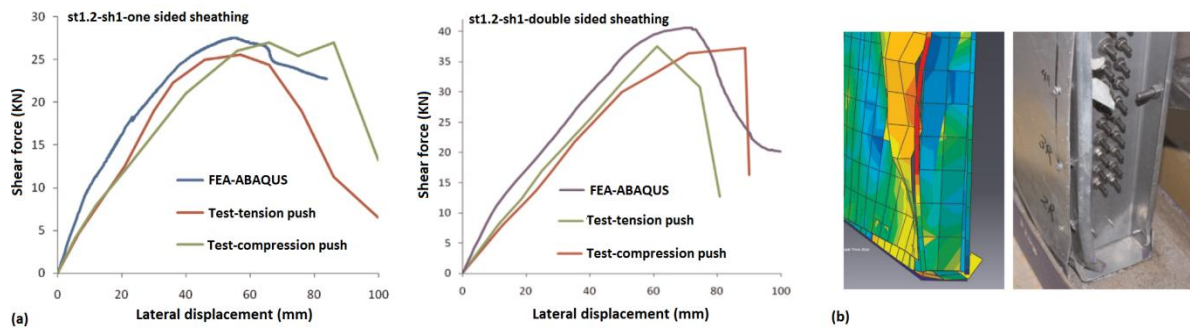
Figure 5.31. (a) Comparison of numerical and experimental results, (b) failure mode of CFS shear wall panel [56]

A numerical micro modelling study was developed and validated by Borzoo et al [224], on the CFS shear panels with steel sheathing, in order to evaluate the stiffness, strength and failure mode of walls. In a recent study by Hatami et al. [225], the behaviour of CFS steel sheathed shear walls and their response modification factors were investigated and the accuracy of the numerical method was assessed. A parametric study containing various ranges of wall parameters such as wall height, steel sheet thickness, spacing of screws, and thickness of the frame members was also implemented in that study.

Although it is possible to model the corrugated geometry of steel sheeting in many advanced commercial software packages, the process is time consuming and fairly complex. Dai [226, 227] developed a numerical micro method for the structural behaviour of typical CFS walls sheathed by corrugated steel sheets, in which they simplified the corrugated sheet into an equivalent orthotropic flat sheathing board with two elastic moduli for simplifying calculation and analysis. After validation of the numerical method, they adopted different parameters for the equivalent sheet in order to understand their effects on the structural behaviour of a wall panels. In a similar study, Yu et al. [173] performed a series of numerical analyses in order to capture nominal shear strengths for corrugated steel sheathed shear walls. They utilised tie constraints for stud-to-stud and stud-to-track connections as no framing connection failure occurred in the tests. The sheathing-to-frame and sheathing-to-sheathing screws were also modelled by Spring2 elements in their study. Modelling strategy and comparison of the load-deformation responses are illustrated in Figure 5.32. Although their model was able to match the shear wall behaviour prior to the peak load and the initial stiffness, it was noted that the displacement at the peak load, obtained from the

118

test, varies slightly from those captured by numerical method.
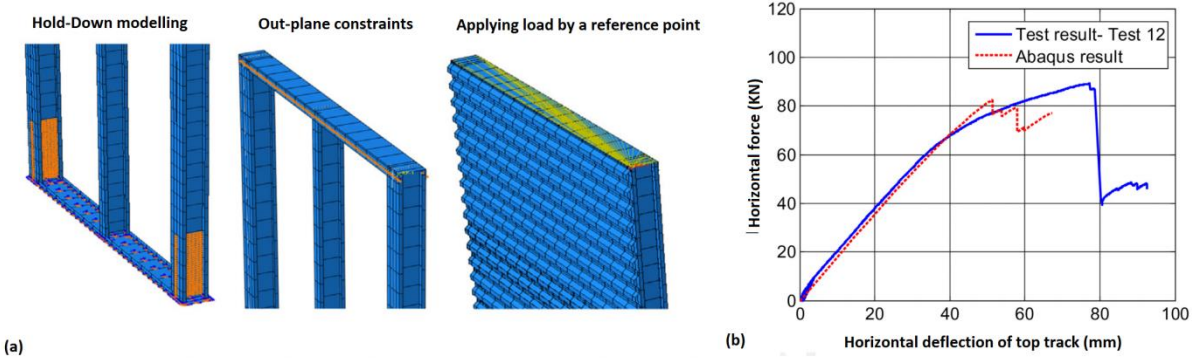
Figure 5.32. (a) Modelling strategy, (b) comparison of numerical and experimental results [173]

A reliable and detailed micro modelling strategy that can be used for accurate simulation of wood-sheathed CFS shear wall was proposed by Ngo [228]. Their numerical model provided a conservative prediction of the peak load for the specimens only sheathed by OSB, and provided an optimistic prediction for the specimens, in which gypsum board was also included. Figure 5.33 shows the micro model of their shear wall as well as a comparison of experimental and numerical results, which shows that the developed numerical models can precisely capture the initial stiffness, but become overly stiffer afterwards. Similar to Ngo's [228] modelling strategies a micro model of CFS shear wall was developed in Abaqus by Bian et al. [202]. The final result was a model, which was similar to OpenSees models in many ways, but included a full and accurate 3D treatment of the framing. They concluded that the OpenSees and Abaqus results agreed well with one another.
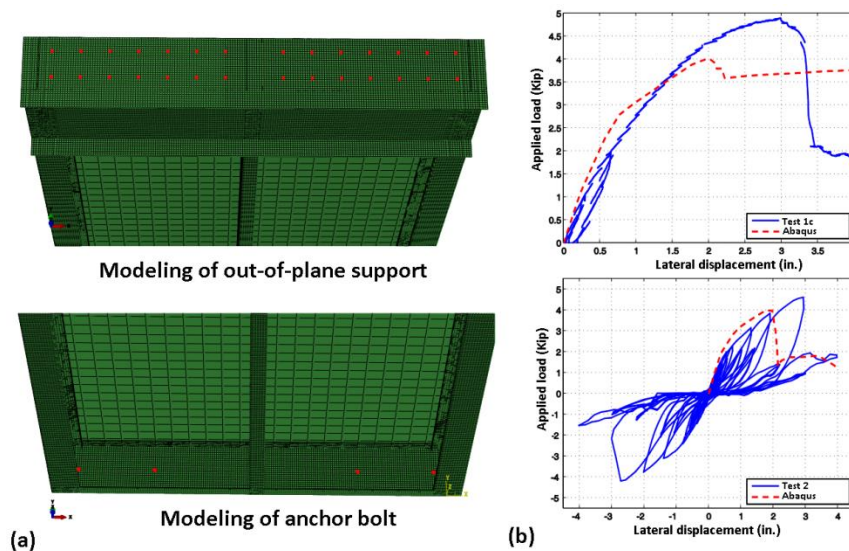
Figure 5.33. (a) FE model, (b) nonlinear response of micro models compared with experimental results [228]

Due to some commercial FE software limitations, it is not simple to capture the complete hysteretic behaviour of CFS-sheathing's connections. To achieve a widely applicable modelling protocol for both monotonic and cyclic analysis, Abaqus requires an extension that incorporates complete CFS-sheathing connection hysteresis behaviour. To that end, a comprehensive study was performed by Ding [229] on the modelling of both monotonic and cyclic response of CFS framing screw-fastened connections. An Abaqus user element (UEL) was developed and validated for a nonlinear hysteresis model that can simulate pinching and strength and stiffness degradation for CFS screw-fastened connections. In that study, the OpenSees Pinching4 model parameters were implemented in Abaqus and the method was verified by comparing to OpenSees connection simulation results. In addition, unlike Ngo's study [228], which assumed the OSB sheathing as a rigid diagram, Ding [229] accounted the real OSB material strength in order to consider flexural and shear deformation of OSB sheathing boards. Configuration of micro model in that study, comparisons of numerical and experimental results, as well as pinching behaviour captured by Abaqus are shown in Figure 5.34.
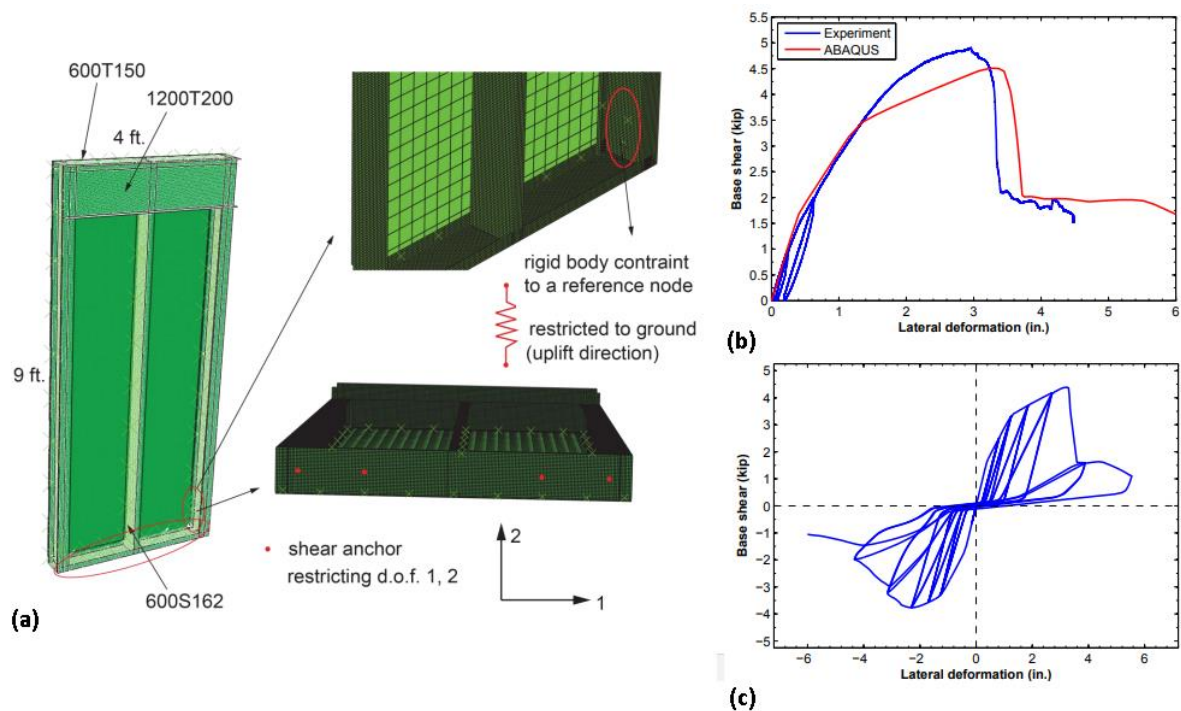
Figure 5.34. (a) Micro model of shear wall, (b) comparison of numerical result to experiment, (c) pinching in numerical cyclic response of shear wall model [229]

For further evaluation of the contribution of OSB boards on CFS shear walls, in comparison with a steel-braced and non-braced panel, a series of numerical simulations were conducted by Henriques et al. [230]. They also used the numerical method to assess the impact of additional bracing systems, such as standard diagonal steel strips bracings. In that study, it was assumed that all screw connections and anchorage were fully rigid. They reported that (i) the numerical model is not able to capture the complete behaviour of the panel under lateral loading, when the behaviour is governed by the connections; and (ii) accurate results is obtained, when the connections remain in the elastic range. Mojtabaei et al. [98] also tried to numerically evaluate the seismic behaviour of an innovative CFS moment resisting frame. A micro model was developed by considering the material non-linearity and geometrical imperfections. The ultimate strength, lateral load-displacement behaviour and failure modes estimated by the model were in very good agreement with the test data in that study. The validated model was then employed to evaluate the effects of key design parameters on the lateral load capacity, ultimate displacement, energy dissipation, ductility, and ductility reduction factor of the frame. Figure 5.35 shows the model and

the numerical results of their study.
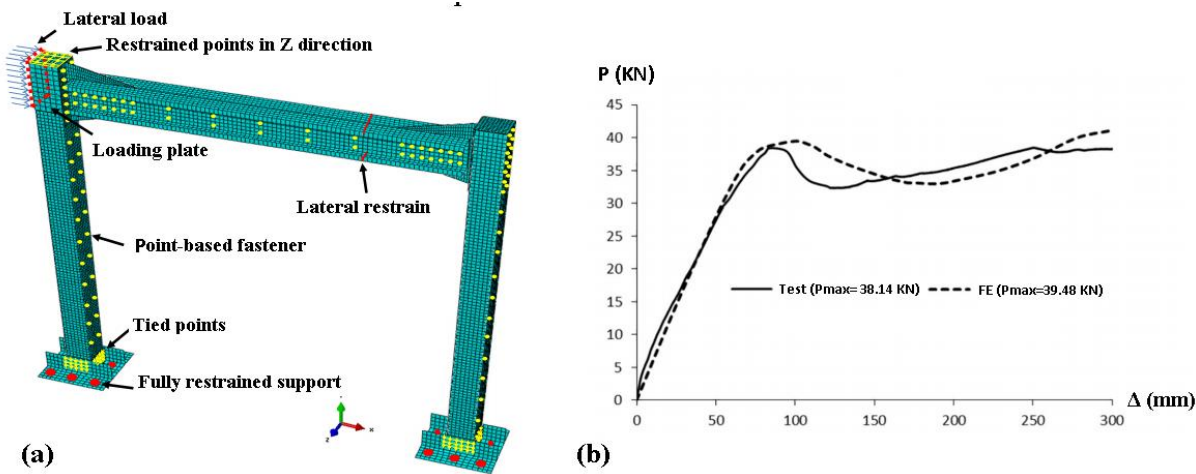
Figure 5.35. (a) Typical FE model of the tested CFS moment-resisting frame, (b) lateral load versus lateral displacement [98]

The micro modelling studies on the lateral behaviour of CFS framed shear wall structures using Abaqus computer package, in the literature, was reviewed in this section. A summary of the modelling techniques classified based on the "boundary condition", "interaction and connection" and "material details, imperfection and element type" is provided in

Table 5.16, Table 5.17 and Table 5.18, respectively. Some modelling details that are not provided by the authors are marked as Not Given (NG) in tables.

Table 5.16. A summary of the micro modelling studies by Abaqus, based on boundary conditions

Author, Year, Reference	Fixity and loading
Telue and Mahendran, 2004, [69]	Rigid plate for modelling of top track (the track was free to rotate about the global X, Y and Z)
Attari et al., 2016, [54]	Three selected regions on top track for applying load Two selected regions at two sides of the bottom track for modelling of hold-down bolts
Niari et al., 2015, [56]	The hole top track nodes were used for applying load Displacements of bottom track nodes in position of bolts were restrained
Borzoo et al., 2016, [224]	Rigid plate for modelling of top track All parts of the bottom plate in the six degree of freedom were constrained
Hatami et al., 2017, [225]	MPC constraint for top track modelling and for bolts connected to the ground Tie constraint at the point where hold downs are screwed to the stud
Dai, 2012, 2013, [226, 227]	Load was applied to the top track via seven points The bottom track was pinned to the ground through 27 points to model the hold-down blots
Yu et al., 2018, [173]	All nodes on web of the bottom track as well as the bottom edges of the studs were constrained in all three directions. For simulation of lateral supports, two lines of nodes on the web of top track were restricted against out-of-plane movements The vertical displacement of all the nodes at the hold-down area of each chord stud was restrained For applying load, all nodes on web of top track were coupled to a reference point located on the edge of the top track
Ngo, 2014, [228] Bian et al., 2015, [202] Ding, 2015, [229]	Rigid plate for modelling of top track Fixing the nodes at the bolt locations (anchor bolts) Hold down is connected to the ground via a bi-linear spring
Henriques et al., 2017, [230]	Panel anchorage is assumed as rigid Load was applied at the top of the frame (with no rigid assumption)
Mojtabaei et al., 2018, [98]	Rigid plate for modelling of top track The base angles at the place of the bolts were fully constrained by using "Tie" constraint

Table 5.17. A summary of the micro modelling studies by Abaqus, based on connections and interactions

Author, Year, Reference	Connection (Sheathing to frame and frame to frame)	Interaction (Sheathing to frame Frame to frame)
Telue and Mahendran, 2004, [69]	Beam elements with two nodes and six active degrees of freedom for screw connection (is not a perfect pin and is partially restrained)	Smooth interaction with zero friction for sheathing and frame interaction
Attari et al., 2016, [54]	Fastener with Cartesian type and elastic behaviour for screw connection	Surface to surface contact-separation is allowed (for Sheathing to frame interaction)

Niari et al., 2015, [56]	Fastener with Cartesian type with elastic-plastic behaviour for screw connection	Surface to surface contact- for both sheathing and frame interactions
Borzoo et al., 2016, [224]	Nonlinear fasteners with Cartesian type for screw connection	Surface-to-surface contact with a friction factor of 0.2 for all interactions
Hatami et al., 2017, [225]	Elastic spring elements with Cartesian type (translational and rotational links) for screw connection	Surface-to-surface contact with a friction factor of 0.3 for all interactions
Dai, 2012, 2013, [226, 227]	3 non-linear spring element for screw connection (one for tension action and the other two for the shear actions)	Surface-to-surface contact with a finite sliding option- friction factor of 0.4 for all interactions
Yu et al., 2018, [173]	Spring2 element was used for modelling sheathing-to-frame and sheathing-to-sheathing screws (3 spring elements for each screw, one withdrawal spring and two shear springs) Tie constraints were used for stud-to-stud and stud-to-track connection	Surface-to-surface contact was sued between the frame and the sheathing (frictionless tangent behaviour and hard-contact normal behaviour were used)
Ngo, 2014, [228] Bian et al., 2015, [202] Ding, 2015, [229]	MPC type PIN for steel-to-steel connections Nonlinear springs for sheathing to frame connection	
Henriques et al., 2017, [230]	Fully rigid (only in the screw position) for screw connections	NG
Mojtabaei et al., 2018, [98]	Point-based fastener with beam connector for screw connection	

Table 5.18. A summary of the micro modelling studies by Abaqus, based on material detail, imperfection and elements

Author, Year, Reference	True stress strain	Residual stress	Imperfection	Abaqus element		
				S4R	S4R5	S4
Telue and Mahendran, 2004, [69]	✓		✓		✓	
Attari et al., 2016, [54]			✓	✓		
Niari et al., 2015, [56]	✓		✓	✓		
Borzoo et al., 2016, [224]	✓					
Hatami et al., 2017, [225]			✓	✓		
Dai, 2012, 2013, [226, 227]						✓
Yu et al., 2018, [173]				✓		
Ngo, 2014, [228]				✓		
Bian et al., 2015, [202]				✓		
Ding, 2015, [229]				✓		
Henriques et al., 2017, [230]				✓		
Mojtabaei et al., 2018, [98]	✓		✓	✓		

5.2.2.2 Micro modelling studies by Ansys

Another general purpose FE computer program, being widely used for micro modelling of CFS framed shear wall structures is Ansys [222] software package. The software comprises many special characteristics, which allow non-linearity or secondary effects to be included in the lateral analysis of CFS framed shear walls.

Some of the first numerical analyses by Ansys on CFS framed shear walls were carried out by Gad et al. [76, 152, 231]. They conducted a detailed investigation into the contribution of plasterboard to the lateral performance of CFS framed residential

structures. They implemented both isolated wall panels (with strap and without strap bracing) and walls with full boundary conditions for their purposes. In their experiment and numerical models, the racking load was applied at the bottom, while the top of the house was restrained horizontally only. The equivalent models for strap bracing system as well as the numerical and experimental load-deflection curves for both walls with and without bracing system are shown in Figure 5.36. They concluded that the numerical model was able to accurately predict the ultimate load capacity and the deflected shape of frame.
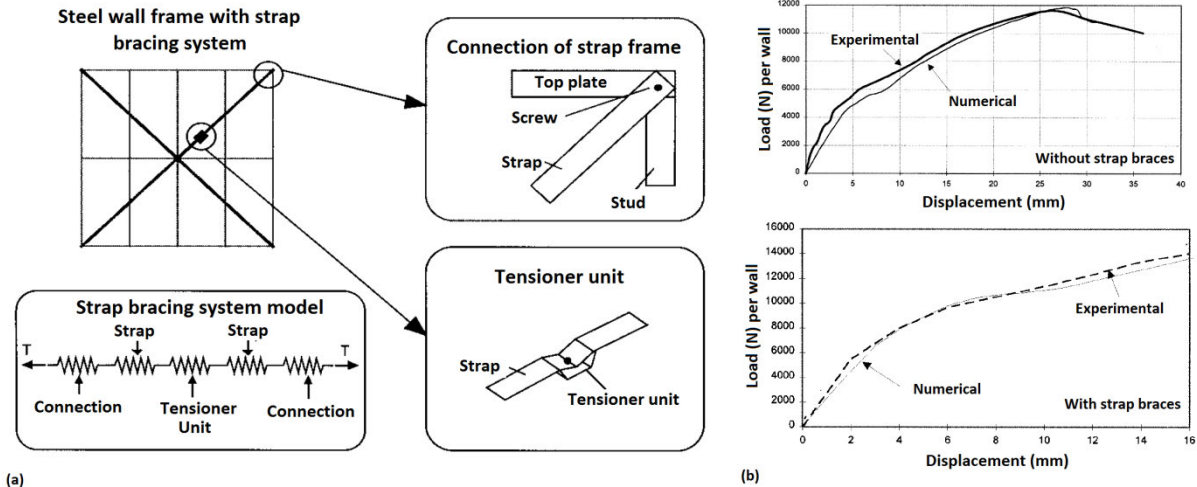
Figure 5.36. (a) Equivalent model for strap bracing system, (b) comparison between experimental and numerical results [76]

In a micro modelling attempt by Fulop and Dubina [232] to capture the behaviour of shear wall panel with corrugated steel sheets, the corrugated sheet was simulated as an equivalent orthotropic plate (SHELL43). The aim was to consider the basic different mechanical characteristics of the corrugated sheet in two principal directions and the distortion of the corrugated sheet when loaded in shear. As it is depicted in Figure 5.37 and Figure 5.38, a good agreement with experiment in terms of deformation pattern and nonlinear behaviour for large displacements is observed, respectively.
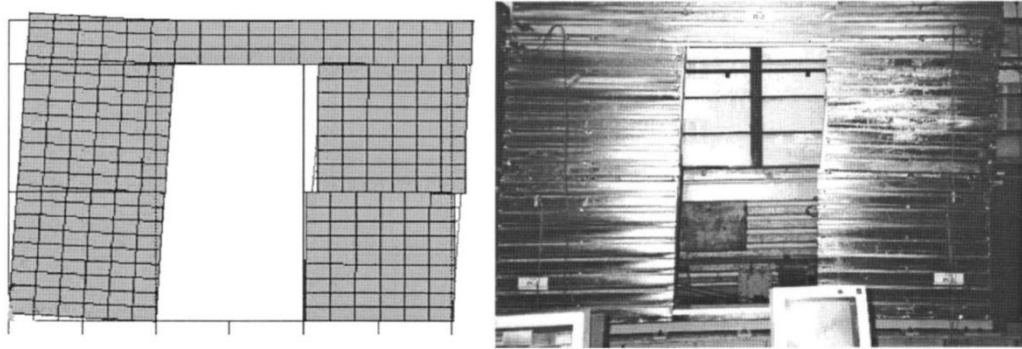
Figure 5.37. Comparison of deformation pattern in micro model and experiment [232]
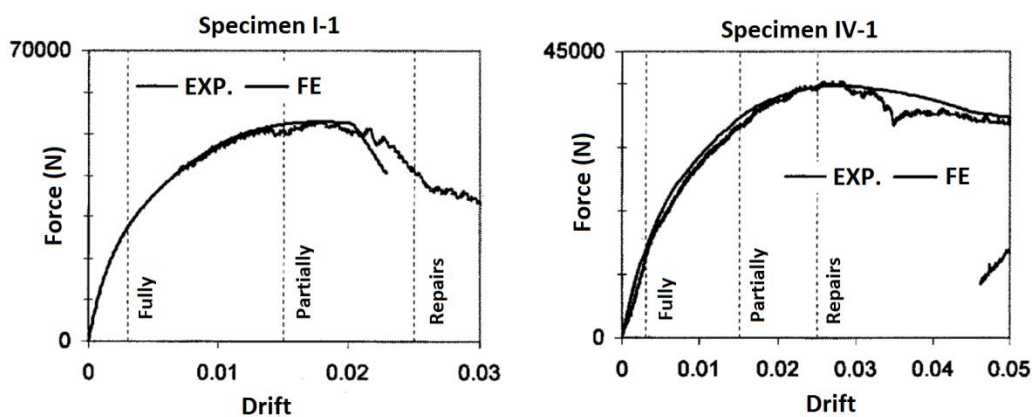
Figure 5.38. Comparison of experimental and numerical results [232]

Xuhong et al. [233] employed Ansys to study the shear resistance of CFS stud walls in low-rise residential structures. Based on the verified numerical analyses on Gypsum and OSB sheathed walls, a set of parameter analyses were conducted to study the influence of the steel strength, stud spacing, stud height, and screw spacing on the shear resistance of walls. A numerical study on the lateral performance of shear wall panels sheathed with different materials such as OSB, Canadian softwood plywood, Douglas-fir plywood and gypsum wall board was conducted by Hatami et al. [234]. Using the validated model, they built up a parametric study to examine strength, drift and seismic performance of the shear wall panels. A series of comprehensive non-linear numerical analyses by Ansys package were carried out by Zeynalian and Ronagh [84, 86] to evaluate and optimise the seismic characteristics of knee-braced and strap-braced CFS shear wall panels. Different structural features including: material nonlinearity, geometric imperfection, residual stresses and perforations were

taken into consideration in that study. Good agreement between numerical results and experimental data was achieved in their numerical simulations, where the numerical method can be used to predict the ultimate capacity of knee-braced and strap brace CFS shear panels. After validation of the numerical method, they analysed various CFS walls and provided the response modification factor for each panel. Numerical results of knee-braced and strap-braced walls are presented in Figure 5.39 and Figure 5.40 respectively.
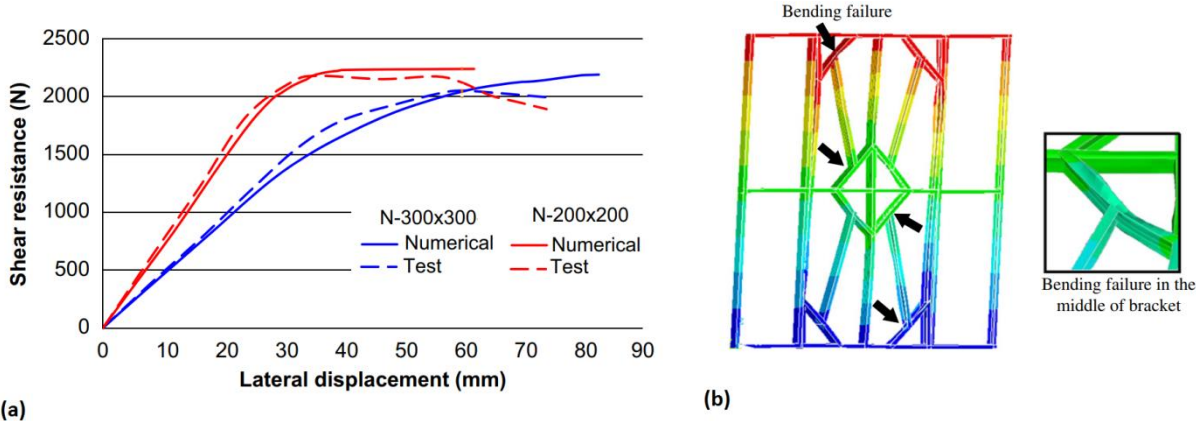
Figure 5.39. (a) Experimental and numerical load-displacement curves, (b) failure mode for specimen N-400 [84]
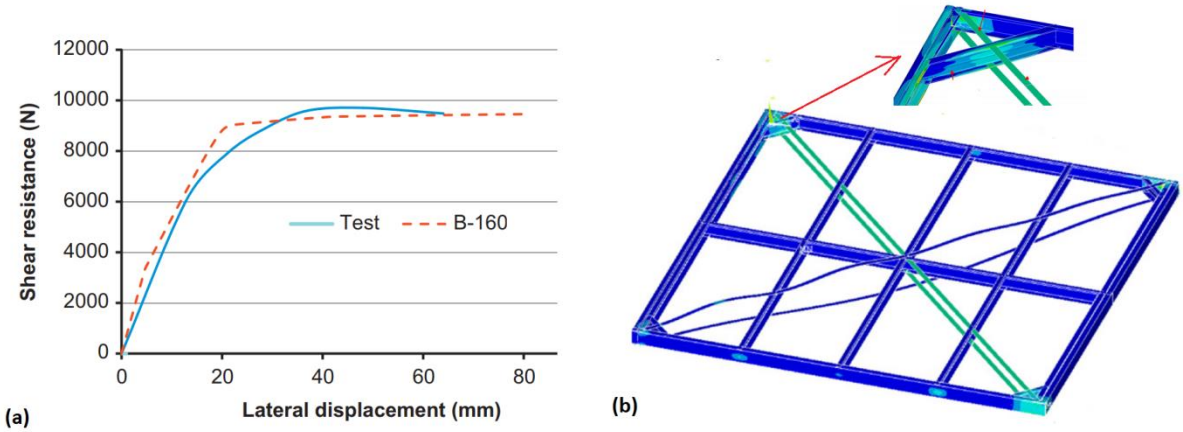
Figure 5.40. (a) Experimental and numerical load-displacement curves, (b) deformed X-braced frame [86]

In another study, Zeynalian [235, 236] carried out a non-linear numerical analysis in order to evaluate the seismic behaviour of steel sheathed CFS walls. To take the fasteners' failure modes into account, Zeynalian modelled the screws connections using COMBIN39 element, which are nonlinear spring elements available in the Ansys

package [222]. This element is a unidirectional element with nonlinear generalized force-deflection capability that can be used in a variety of analyses. They concluded that the effects of residual stresses and section perforations are negligible. In another study, Abu-Hamd et al. [237] performed nonlinear verification analysis for CFS-braced shear walls and implemented parametric study using the nonlinear FE model. They also verified and thus investigated the response reduction factor R.

The micro modelling studies on the lateral behaviour of CFS framed shear wall structures using Ansys computer package, in the literature, was reviewed in this section. A summary of the modelling techniques classified based on the "boundary condition", "interaction and connection" and "material details, imperfection and element type" is represented in Table 5.19, Table 5.20 and Table 5.21, respectively. Some modelling details that are not provided by the authors are marked as Not Given (NG) in tables.

Table 5.19. A summary of the micro modelling studies by Ansys, based on boundary conditions

Author, Year, Reference	Fixity and loading
Gad 1997a,b, 1999, [76, 152, 231]	Pin connections were used for hold down modelling
Fulop and Dubina, 2006, [232]	Bars of the skeleton were modelled as elastic beam elements (BEAM4) (it is assumed that elements were not highly deformed in the post elastic range)
Xuhong et al., 2006, [233]	The nodes of top track were coupled for applying load Displacements along the X, Y and Z-directions and rotations along Y and Z-directions of bottom track were restrained
Hatami et al., 2014, [234]	The nodes of top track were coupled to one node for applying load
Zeynalian and Ronagh, 2012, 2011, [84, 86]	NG
Zeynalian, 2015, 2017, [235, 236]	Coupling command for relevant nodes at bottom track
Abu-Hamd et al., 2018, [237]	Reference nodes defining the hold-down elements are connected to nodes on the ground in the vertical direction via a bilinear spring element type COMBIN39

Table 5.20. A summary of the micro modelling studies by Ansys, based on connections and interactions

Author, Year, Reference	Connections (Sheathing to frame and frame to frame)	Interactions (Sheathing to frame Frame to frame)
Gad 1997a,b, 1999, [76, 152, 231]	Pinned connection was used for tab-in-slot connection of the frame Four springs with Non-linear behaviour for modelling of screw connection	NG
Fulop and Dubina, 2006, [232]	Connections, both between the skeleton and the sheathing and the seam connections, were modelled using COMBIN39 elements	NG
Xuhong et al., 2006, [233]	Coupling method for modelling of screw	Without considering the slip

	connections (with free rotations but no displacement)	between sheathing and steel members
Hatami et al., 2014, [234]	Coupling for modelling of screw connections (sheathing to frame)	
Zeynalian and Ronagh, 2012, 2011, [84, 86]	Coupling technique for modelling of rivet connections	NG
Zeynalian, 2015, 2017, [235, 236]	Coupling technique for modelling of rivet connections Screws connections were modelled using COMBIN39 (Consider the fasteners failure)	
Abu-Hamd et al., 2018, [237]	Coupling set for shear nonlinear failure in-plane mode of the screws using two nonlinear spring elements COMBIN39	Contact elements surface to surface (TARGE170 and CONTA174) for connections between the bracing and the gusset plate

Table 5.21. A summary of the micro modelling studies by Ansys, based on materials, imperfections and elements

Author, Year, Reference	True stress strain	Residual stress	Imperfection	Ansys element		
				shell181	Shell43	Shell93
Gad 1997a,b, 1999, [76, 152, 231]						✓
Fulop and Dubina, 2006, [232]					✓	
Xuhong et al., 2006, [233]				✓		
Hatami et al., 2014, [234]			✓	✓		
Zeynalian and Ronagh, 2012, 2011, [84, 86]	✓	✓	✓	✓		
Zeynalian, 2015, 2017, [235, 236]	✓	✓	✓	✓		
Abu-Hamd et al., 2018, [237]			✓	✓		

5.2.2.3 Micro modelling studies by Sap2000

One of the widely used engineering software is Sap2000 [223], which is ideal for both micro and macro modelling of CFS components. Although micro modelling by this software is not as accurate as Abaqus and Ansys, it is broadly used in practice and research for the FE modelling and simulation of framed structures. Yet quite few research studies have employed this software for the micro analysis of CFS shear walls.

Some simplifications need to be implemented in micro modelling strategy when analysis of a mid-rise CFS building by micro methods. In this context, Martinez and Xub [238, 239] simplified the conventional micro method by suggesting that the individual modelling of the studs and sheathing plates in a building is not necessary. Instead, the walls were transformed into a sixteen-node shell element with equivalent properties for modelling complete panels. Figure 5.41 displays both conventional and simplified micro modelling of a CFS shear wall, as well as the developed model for a three-storey building by the proposed simplified micro method in that study. Results of the simplified micro method, compared with the experimental data, are shown in Figure

5.42. In linear analysis of the single shear wall, it was explained that the results obtained from simplified micro method for isolated wall of various lengths are in good agreement with those captured from conventional micro method. In the building model, the lateral displacements obtained by the conventional micro method were also in good agreement with those captured by simplified micro method. The internal forces were overestimated in simplified micro method though. They suggested that the proposed simplified micro method can be used to provide global performance of the structure such as lateral deformation of the building and lateral forces in walls. Due to the differences in the axial forces of the studs between the results from simplified and conventional micro method, they recommended not to use the axial forces obtained from simplified micro method for design of the steel stud of wall.
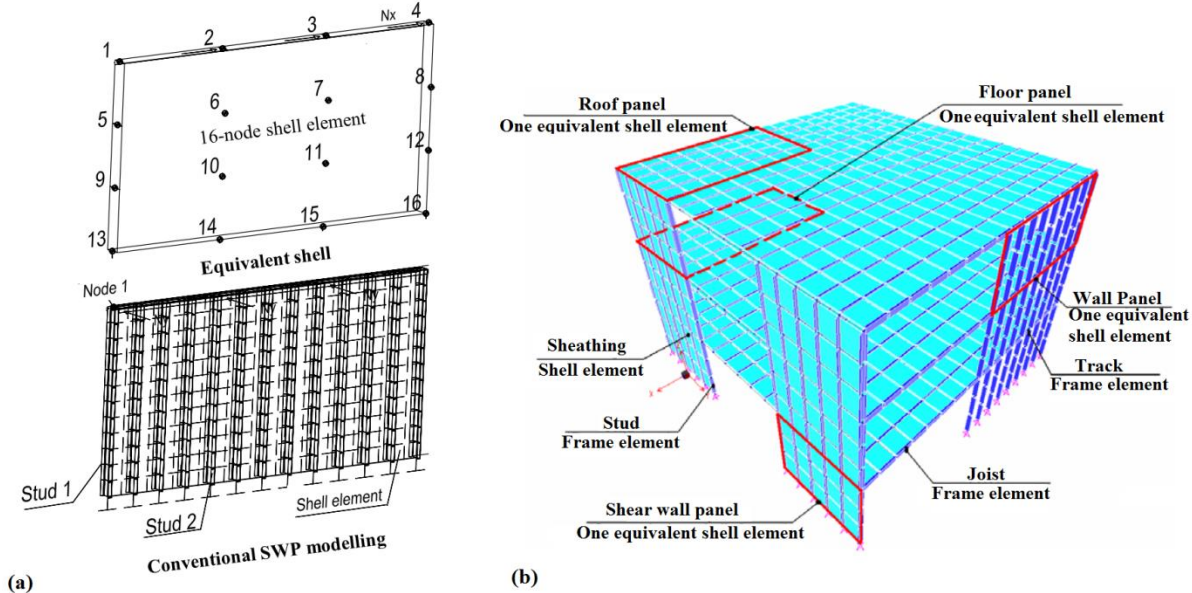
Figure 5.41. (a) Conventional and simplified micro modelling of CFS wall, (b) modelling of a CFS building using simplified micro method [238]
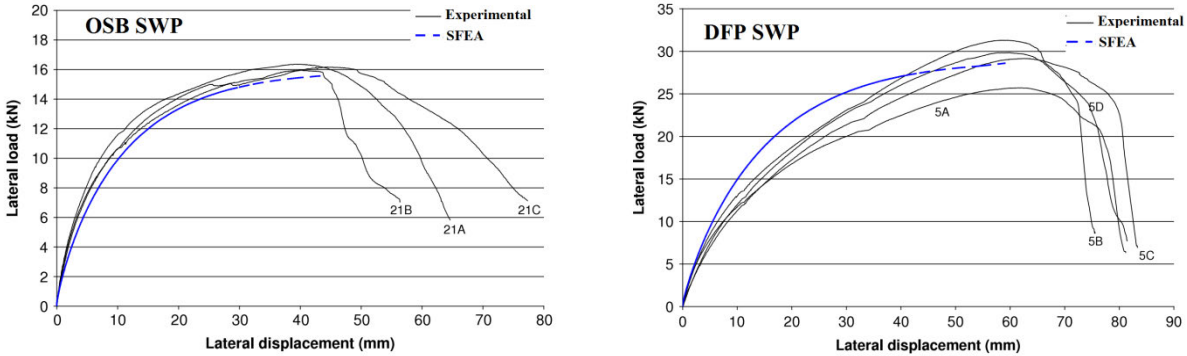
Figure 5.42. Numerical vs. experimental curves of CFS walls [238]

Li et al. [234] performed a refined numerical simulation of CFS shear walls based on modified exponential Foschi skeleton [240] to simulate the behaviour of stud-sheathing screw connections in shear loading. The modelling was carried out on walls sheathed with OSB and gypsum boards. Studs and sheathings' connections were modelled using two-freedom spring elements in order to capture deformation along and perpendicular to the loading directions. Figure 5.43 illustrates how the numerical results, including deformed shape as well as load vs. deformation curves agree with the tests. It indicates that the behaviour of shear walls can be precisely assessed through the numerical simulation technique proposed in that study.
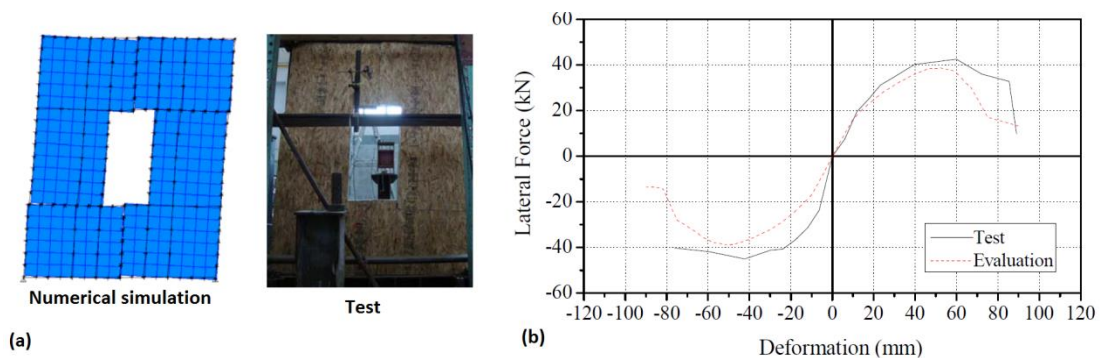
Figure 5.43. (a) Deformation comparison of specimen SW6, (b) load vs. deformation curve comparison of specimen SW11 [234]

Karabulut and Soyoz [25] provided numerical models by Sap2000 for the study of CFS shear panels to be used for 3D structural analysis and seismic performance investigation. They verified the modelling approach by simulating a CFS bare frame with sheathing board. Their geometry model of single wall and comparison of FE and experimental results are shown in Figure 5.44a and Figure 5.44b respectively. Since a relatively good agreement between the numerical and experimental results was captured, they developed the numerical model to be implemented in a one-story residential building. The building's model is presented in Figure 5.44c. Their study tried to assure the capability of CFS structures to possess a sufficient performance in seismic prone regions such as Turkey.
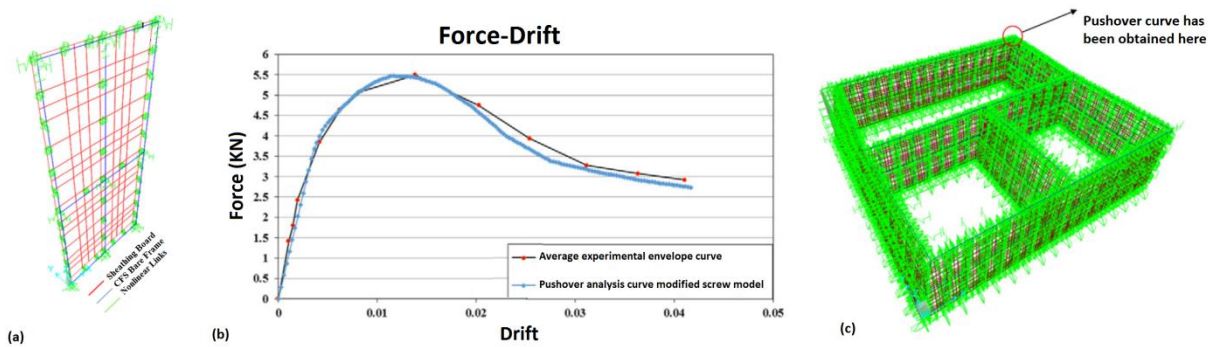
Figure 5.44. (a) Numerical model of the CFS shear panel, (b) comparison between numerical and experimental results of type 6 CFS shear panel, (c) one-storey residential building [25]

Recently a new numerical model was proposed in Sap2000 by Fiorino et al. [176] for CFS shear walls with capability of capturing their nonlinear behaviour. It was indicated that the numerical models are in good agreement with experimental observations in terms of deformation mechanism. They implied that the models developed in their study can be useful for a practicing engineer to calculate strength and stiffness of single shear wall. Figure 5.45 shows schematisation of their numerical model developed in Sap2000 for CFS sheathed braced shear walls as well as comparison of the short wall numerical models (WS_2400_M) with its monotonic test response.
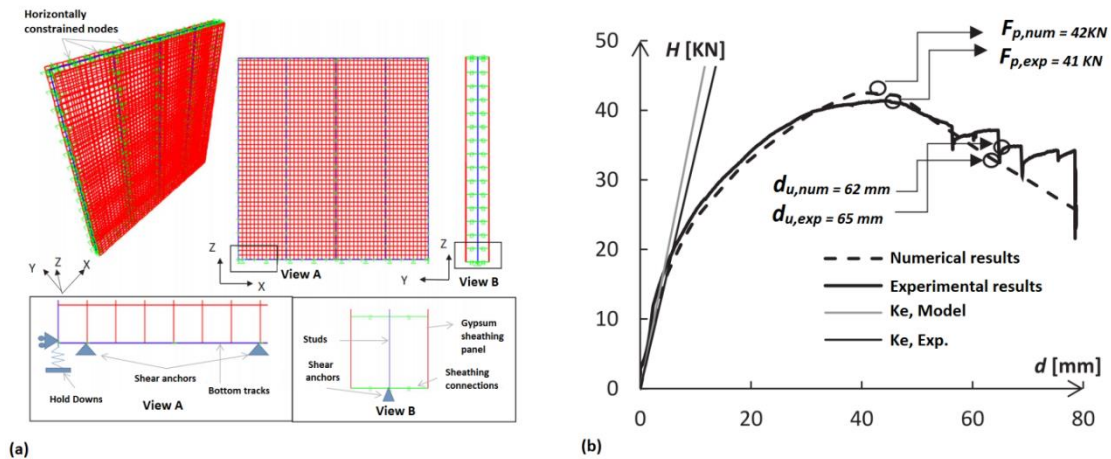
Figure 5.45. (a) Schematisation of micro model developed for CFS sheathed braced shear walls, (b)comparison of experimental and numerical results [176]

In another study, Pourabdollaha et al. [82] conducted a brief numerical simulation to predict the shear strength of K-braced CFS shear panels for practical simple engineering design. Having defined the plastic hinges at the mid-length of the brace

elements, nonlinear static analysis was performed for a target displacement. As Figure 5.46 depicts, the first plastic hinge occurred at the brace element under compression around a drift of 2.5%.
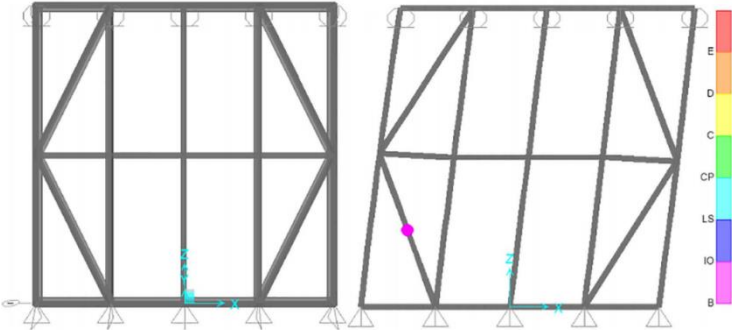
Figure 5.46. Nonlinear static analysis of the K3 model before and after formation of the first hinge in the brace element [82]

As stated above, because micro modelling simulation of CFS framed structures in Sap2000 is not as accurate as modelling by Abaqus and Ansys, a lower number of micro modelling studies by this software exists in the literature. In addition, there is not clear detailed information about the modelling strategies in Sap2000, with regard to CFS framed walls under lateral loads. A brief summary of the modelling techniques in terms of "boundary condition" and "interaction and connection" using Sap2000 is given in Table 5.22 and

Table 5.23, respectively.

Table 5.22. A summary of the micro modelling studies by Sap2000, based on boundary condition

Author, Year, Reference	Fixity and loading
Martinez and Xub, 2007, 2011, [238, 239]	Bottom track was not included in the model because the bottom nodes are fixed sheathing is modelled using square four-node shell elements Load was applied at the top four nodes in the x and y directions
Li et al., 2014, [234]	Top and bottom girders were considered as the rigid members by means of increasing their elastic modulus.
Karabulut and Soyoz, 2017, [25]	NG
Fiorino et al., 2018, [176]	Rigid plate for top track modelling A simple support, and a vertical linear springs for modelling of hold-downs Pinned restraints for modelling of shear anchors
Pourabdollah et al., 2017, [82]	Fixity is applied under each stud location

Table 5.23. A summary of the micro modelling studies by Sap2000, based on connection and interaction

Author, Year, Reference	Connection (Sheathing to frame and frame to frame)
Martinez and Xub, 2007, 2011, [238, 239]	NG
Li et al., 2014, [234]	Connections among the framing members were modelled as hinges

	Connections between the studs and sheathings were modelled using two-freedom spring elements
Karabulut and Soyoz, 2017, [25]	Nonlinear link elements for screws (moment is released for the connections)
Fiorino et al., 2018, [176]	Hinge technique for modelling of frame connection Two nonlinear link element with a multi-linear backbone curve for modelling of sheathing connection
Pourabdollah et al., 2017, [82]	Plastic hinges were used at the mid-length of the brace elements

5.3 Comparison and Discussion

Based on the research studies reviewed in Sections 3 and 4, it can be concluded that the analysis with well-developed macro-models can provide the same accurate results as micro-models. Yet, the findings indicate that the accurate representation of all structural elements by micro method can be relatively too complicated, and result in disproportionate computational cost, when modelling the entire structure. A micro model of a CFS frame that includes all aspects of the problem requires consideration of many geometric details and contact relations between several parts of the frame, as indicated in Figure 5.29. Knowing that, even for a simple CFS panel containing a great number of fasteners, analysing the entire structure with all its complexity can lead to unreasonably long computational time. This was the motivation for many of the proposed macro models.

The aim of many research studies of developing strong macro models for the analysis of CFS frames has been to reduce the difficulty of the geometry and the number of contact relations, so that the analysis can be finalized in a reasonable time, without significantly compromising the accuracy. This is even more evident, when it comes to large scale structures, such as multi-storey buildings made of CFS elements [50-52, 64-66, 155, 156, 159, 161-163, 166-173, 177, 178, 180, 181, 183, 186-190, 195-199].

Furthermore, micro-models have been mainly used only for detailed analysis of local responses of small CFS framed structures such as wall panels [25, 54, 56, 69, 76, 82, 84, 86, 98, 152, 173, 176, 202, 224-239]. Some micro models however, have been used as the input to determine individual element and node responses. Conversely, in some cases the output from a macro model has been used to determine the properties of a simple global model, and then has been employed to derive global responses (e.g. storey drift), through repeated analyses.

The proposed macro methods, on the other hand, are not able to account for the local failures (detachment of sheathing to frame, screw pull out and failure of stud, track and

sheathing) and the effect of different buckling modes on the entire structures behaviour; thus, not applicable for problems in which local buckling may occur. In most macro models, it has been also assumed that the hold-down anchors and screw connections have been properly designed to resist the entire forces in the wall panels. Therefore, hold-down anchor and screw failures are not accounted for in the determination of the walls' lateral strength. Quite the contrary, the local failures and buckling modes, as well as hold-down and screw failure mechanisms can be captured from the micro methods.

In both micro and macro methods, it is mainly suggested that the rigid panel assumption may not be appropriate for shear walls sheathed with steel sheathing, which undergo substantial deformation within the panel and smaller deformations around the fasteners. In macro modelling methods, the CFS framing members (stud, ledger or track) are mostly modelled by elements assumed to be rigid cross-sections and do not allow for localized plate flexibility in the CFS framing. In most proposed macro modelling methods, extracting the graphical results, such as stress and strain distribution and deformation, is not also possible.

In dynamic and cyclic analysis of CFS shear walls by micro method, some issues may occur due to unknown problems of numerical algorithms for time integration. Dynamic analysis needs a large number of relatively small finite and contact elements, i.e. a greater number of uncertainties in the system. In addition, pinching phenomenon usually occurs in real CFS structures, which need to be accounted in numerical modelling. Technically, micro modelling methods have some limitations in capturing pinching behaviour of fasteners. This phenomenon therefore, can be modelled by defining a subroutine to incorporate a physical gap between screws and holes' bearing faces in the software that may need considerable effort. Hence, due to the lack of a proper models for simulation of pinching behaviour in screws and walls, almost all micro modelling studies (except Ding [229]) have been carried out under monotonic loading and static analysis. The proposed macro modelling methods on contrary can simply capture the pinching behaviour by defining the hysteresis models during simulation, so that all monotonic, cyclic and seismic actions and responses can be conveniently simulated.

There have been some discrepancies between numerical results and experimental

data reported for both micro and macro methods. The reasons for such discrepancies are summarised in Table 5.24 and Table 5.25 respectively

Table 5.24. Reason for discrepancy of numerical and experimental results for macro modelling method

	Method	Author, Year, Reference	Reason for discrepancy of numerical and experimental results
Macro modelling	Equivalent brace	Shamim and Rogers, 2012, [51, 161]	- Sheathing can be detached in walls during experiment; however, this is not happening in numerical method. - Employing smaller damping value in numerical method can be resulted in an increase in the differences between numerical and experimental results.
		Leng et al., 2017, [167]	- Damping value in numerical method is held constant at 5%, while in the tests the damping is increased with construction phase. - Simpler simulation of vertical load path at the floors in the simulation compared to the actual building. - Other parameters such as: the conservative estimation of connection stiffness as fixed, the accuracy of stiffness estimate of gravity and interior wall sheathing and semi-rigid diaphragms as subpanels and the approximation of built-up members as isolated ones.
		Leng et al., 2016, [168]	- Modelling of the wall-ledger-diaphragm interactions (line elements may fail to fully capture the stiffening effect of thick ledgers and joists in boxing and stiffening this top of the shear and gravity walls). - Inter-story stiffness of the chord studs are is not accurate. - Conservative assumption of zero tensile strength of shear anchors along the gravity walls limiting lateral strength and coupling ability
		Fiorino et al., 2017, [176]	- Underestimation of post-peak response is due to post-peak shape of sheathing connections backbone envelope, which is characterized by a higher slope respect to those showed by walls
		Macillo et al., 2018, [179]	- Strain hardening of the material is not taken into account for the theoretical backbone curve utilized in numerical method resulting in the under-prediction of strength and energy dissipation
		Boudreault, 2005, [155]	- The Stewart Model is unable to capture failure of the wall and doesn't offer strength degradation
		Foutch and Lee, 2010, [159]	- Straps in the numerical method are simulated to be tightly attached to the columns, while attachment of the straps in test is loose - Base of the shake-table is flexible in test due to the oil columns and vertical actuators, but the base is assumed to be fixed in the numerical model
		Foutch et al., 2007, [64]	- Complete control of the shake-table during experiment was not possible - Since the effective lengths of the straps are not identical (as welded in place), little slack of some straps occurs which is not happening in numerical method - Deformation and separation of some anchors from the slab during the test which is not happening in numerical method
	Equivalent spring	Kechidi and Bourahla, 2016, [194]	- Sheathing can be detached in walls during experiment, while this is not happening in numerical method - The model does not dissipate energy below predicted value, but energy dissipation is exhibited in experimental test at displacement level below the predicted value.
		Jiang and Ye, 2018, [199]	- Overestimation in lateral stiffness is due to rigid connection assumption at column base in numerical method - The natural frequency of the numerical model is higher than the test - Underestimation in energy dissipation of the structure is due to the Pingching04 hysteretic model. Because the unloading stiffness is lower than the loading stiffness, but the unloading stiffness of the test shear wall is larger than the loading stiffness. - Pin connection simulation for connections between the CFS beams and CFRST in numerical model prevents to capture the energy dissipation of these connections
	Fastener based	Bian et al., 2014, [200]	- Additional flexibility and redistribution in real wall which is not included in the numerical model. - Degrading branch in the Pinching04 "fastener" model is possibly too severe - Rigid sheathing assumption doesn't create a favourable load distribution to the fasteners
		Buonopane et al., 2014, [204]	- Fully pinned modelling of shear anchors which is not similar to test - The per cycle error between energy dissipated in the numerical model and tested specimens - Numerical models may fail is a smaller magnitude peak displacement cycle than the physical tests
		Padilla-Llano et al., 2015, [206]	- Discrepancies in post-peak monotonic response is due to the use of the contact springs along the bottom track

Table 5.25. Reason for discrepancy of numerical and experimental results for micro
modelling method

Method		Author, Year, Reference	Reason for discrepancy of numerical and experimental results
Micro modelling	Shell element computer programs	Attari et al., 2016, [54]	- Screw pull out phenomenon and imperfections of tested specimens are not modelled in numerical method which cause some discrepancies
		Mojtabaei et al., 2018, [98]	- Small friction in the lubricated interface of the beam and bracing elements in test which is not happening in numerical model - Fixed bearing connections in the FE models can provide additional strength, while no additional strength is observed in test.
		Esmaeili et al., 2015, [56]	- It is the nature of the numerical method to have higher stiffness than the real experimental specimen.
		Telue and Mahendran, 2004, [69]	- Ultimate strength of studs in numerical method may be lower than experimental test which may be due to considering geometric imperfections and residual stresses in numerical model
		Ngo, 2014, [228]	- Assumption of rigid or semi-rigid diaphragm for sheathing which is not same as experimental test - The error in test results itself when only one specimen is tested for each shear wall configuration Modelling hold-downs as springs does not capture moment of the couple consisting of axial force in chord studs and reaction force on the hold-down rod from the foundation. However, in the tests, the anchor rod connecting hold-down to the foundation is slightly offset from the line along chord studs web.
		Ding, 2015, [229]	- The stiffness of the members is underestimated
		Hatami et al., 2017, [225]	- The tested walls also have some differences in results (experimental errors) - Although the failure of any screw connection has a major impact on convergence phenomenon, it has no significant impact on displacement. But, this is different in experiment.
		Hatami et al., 2014, [234]	- Some factors such as accuracy of measuring tools and experimental errors including, imperfection of shear wall panels, cracking of wood and gypsum panels, etc. - It seems difficult to construct a model which is completely compatible with several experimental results.
		Martinez and Xu, 2011, [238]	- Even though the sheathing is attached to the studs in test, numerical model considers the shell and frame elements in the same plane, so that the offset of the sheathing from the centerline of the studs is not considered. - The type, size, and number of elements employed to simulate a structure can affect the accuracy of results.
		Bian et al., 2014, [200]	- Application of two separate translational in-plane springs for modelling of steel to sheathing connections in the board plane which is not exactly the same in the test
		Fiorino et al., 2018, [176]	- Higher slope of sheathing connections backbone envelope, in comparison to those showed by tested walls.
		Emad Gad, 1997, [152]	- Using higher shear modulus for plasterboard modelling than real experimental shear modulus
		Yu et al., 2018, [173]	- Small sliding during experiment, which is not considered in numerical method
		Henriques et al., 2017, [230]	- Screw connection modelling which is assumed more rigid in the numerical model than in the experimental test

Considering the findings of research studies reviewed in this study, the reflections on the present and future of the CFS shear walls modelling are as follows:

For micro models:

- In micro models, the lack of simulating the small friction between CFS elements has been reported as one of the reasons for discrepancy between experimental and numerical results (Table 5.25), while there is also no generic measure proposed for

estimating the friction coefficient between CFS structures elements. In addition, some researchers have also employed different friction coefficients in their simulation (Table 5.17 and Table 5.20), which needs further discussions on how the coefficient is calculated.

- Static analysis is an effective and accurate solver for capturing the behaviour of CFS shear walls under monotonic loading. Nevertheless, static analysis sometimes fails to converge due to unstable collapse or post-buckling. To avoid these issues, other analysis options such as dynamic and riks method can be also used for such simulation. While the type of solver is rarely mentioned in the previous research studies, the effects of using alternative and applicable solver options (dynamic and riks) should be also evaluated.

- Although some good numerical results have been captured by different models, there is not yet a general modelling approach for simulation of CFS shear walls. As an example, considering initial imperfection, residual stress and true material properties (e.g. stress-strain relation), as well as the type of elements used in modelling may or may not influence the numerical results. The effects of these parameters on numerical results need to be exactly evaluated in the future research.

- A major drawback of micro modelling method is the problem with simulating cyclic behaviour of screws with the ability of capturing pinching behaviour. Although Ding [229] provided a UEL code in Abaqus for capturing the hysteresis behaviour of CFS shear walls, this issue is still a big concern for micro modelling of these systems.

- Consideration of a rigid body motion for simulation of sheathing can decrease the computation time and convergence problems. Yet, the accuracy of results can be significantly affected. In addition, despite some researches having utilized rigid body mechanism for their simulation, there is not detailed information available on their assumptions for modelling. Numerical modelling with both rigid body and semi-rigid body assumptions and a comparison can help better understand this matter.

- Combining micro modelling method by some macro modelling assumptions can decrease the analysis time, while maintain the accuracy of capturing good results; nonetheless, it requires substantial research and model development. Implementation of both micro- and macro modelling methods in one numerical simulation, as it was performed by Martinez and Xu [238], can also provide a valuable comparison.

- Modelling of connections, as well as the interaction and fixity between members in shear walls have been modelled in some studies with different techniques.

- A comparison between these modelling techniques in terms of computational time and the accuracy of results can better help understand the strength and weaknesses.

- Although capturing the general failure mode of the CFS walls (such as cracking, braking and tearing of sheathing, deformation of studs or tracks, wedge failure and failure of strap [77, 92, 241]) is feasible and easy in micro modelling approach, modelling the failure of the screw connections such as pull-through failure, screw rotation, tearing of screw, etc still requires more attention [49, 242]. Some attempts have been made by Selvaraj and Madhavan [242] and Zeynalian [235, 236] in order to capture the correct screw failure mode which can be used for future studies.

For macro models:

- While different macro modelling programs have been developed in the literature, there is no specific section or toolbox for CFS modelling. An attempt has been made by Kechidi and Bourahla [194] in order to incorporate cyclic behaviour of CFS shear walls in OpenSees software by developing and implementing CFSWSWP and CFSSSWP materials in this program.

- Pinching4 hysteresis curve is mostly used for modelling of CFS shear walls under cyclic loading [41, 50-52, 65, 66, 161-163, 165-173, 176-180, 194-206]. A general data-base for Pinching4 parameters based on the previous experiments with different sheathing materials can significantly facilitate the future modelling methods.

- Most of the macro modelling software programs do not provide graphical user interface neither for modelling nor results. Computer program such as OpenSees, which is used by a large number of researchers in this area, requires less complex modelling strategies, better graphical user interfaces and a mechanism to identify the possible errors.

For the behaviour analysis of CFS shear walls, various model reduction techniques have been developed and used. Generally speaking, the implementation of a technique for analysing a system is quite case sensitive, and their performance is quite dependent upon the appropriate choice of an effective micro- or macro-model that

most suits the case. Although they work well in each of their purpose, there still remain hurdles such as comprehensive parametric methods that can be used for a variety of cases. In fact, with most proposed method, when parameters of a system change, the entire system is changed; the model is no longer valid; and consequently modelling, reduction, and analysis should be repeated for each case. Future research on the parametric model reduction techniques for CFS walls and panelised systems can pave the way for more efficient applications of these systems in the construction industry.

5.4 Conclusion

The advancement in CFS structures has been the results of a combination of developments in applications and improvements in simulation. The increased attention to these systems in more complex structures worldwide has placed engineers and researchers under pressure to find adequate modelling techniques for simulation of these structures under lateral loads. The emphasis of this study was to summarise and review the major research developments of numerical research related to lateral performance of CFS framed shear wall structures, and study their strengths, limitations and contributing factors, and parameters to their performance. The existing models were categorised under micro- and macro- modelling methods, and a summary of the modelling techniques, hysteresis models and the reason for discrepancy between experimental and numerical results were provided. The work is limited by the scopes of study, as well as the length of the publication, as there are more details that are worth to be further discussed.

Chapter 6   Numerical method: Micro and Macro modelling of CFS structures

6.1 Introduction

As indicated in Chapter 5, ABAQUS and OpenSees have been of particular interest for the simulation of CFS structures. This chapter aims at comparing ABAQUS and OpenSees as tools for Micro-element and Macro-element modelling of CFS shear walls, respectively, and discussing pros and cons of using different methods/software. In the first step, the micro-element modelling approach with ABAQUS is presented and details of different simulations are discussed. In the second step, the macro modelling with OpenSees is illustrated and different procedures for modelling are presented. In the third step, the results of both methods are compared with experimental data for validation and with each other. In the final step, a discussion on the differences of the modelling and results is presented for better understanding of the benefits and drawbacks of each numerical method.

6.2 Numerical modelling framework

Modelling approach of CFS walls in ABAQUS and OpenSees is presented in this section. Six CFS walls, sheathed with steel and wood previously tested by other researchers are considered for simulation in this study. Details of the specimens and material properties are presented in Table 6.1 and, Table 6.2 respectively. The elastic modulus of elasticity and Poisson's ratio was assumed as E=203.4GPa and =0.3, respectively.

Table 6.1. Details of the specimens

Specimen	Reference	Sheathing	Wall dimensions (mm)	Sheathing thickness (mm)	Frame thickness (mm)	Fastener spacing (mm)
C1		steel	2440×1220	0.46	1.09	150/300
C2	[124]	steel	2440×1220	0.46	1.09	50/300
C3		steel	2440×1220	0.46	0.84	150/300
C17		steel	2440×1220	0.46	1.09	-/300
P2	[243]	steel	2400×1200	0.7	0.75	150/300
T4	[128]	OSB	2740×1220	11	1.37	150/300

Table 6.2. Material properties of walls

Specimen	Stud		Track		Sheathing	
	F_y (Mpa)	F_u (Mpa)	F_y (Mpa)	F_u (Mpa)	F_y (Mpa)	F_u (Mpa)
C1	346	496	346	496	300	395
C2	346	496	346	496	300	395
C3	342	391	342	391	300	395
C17	346	496	346	496	300	395
P2	592	617	592	617	290	348
T4	387	543	443	500	-	-

6.2.1 ABAQUS modelling

ABAQUS is general purpose software based on FEM that can be used for micro-element modelling of CFS members. However, ABAQUS can also be used for macro-element modelling when simplification assumptions are made, which is out of the scope of this research. In the following, the micro modelling approach for CFS walls is presented.

Material properties: Material nonlinearity in all elements is modelled with elastic-plastic behaviour and von Mises yield criterion to define isotropic yielding. True stress and strains introduced to ABAQUS software can be obtained by converting nominal stress-strain to real. Some researchers have considered sheathing material as a rigid diaphragm by assuming very large modulus of elasticity. However, to incorporate flexural and shear deformation, the sheathing material can be assigned with flexure and shear modulus. Orthotropic material definition of different stiffnesses in different directions is required for such kind of modelling. For orthotropic elastic material definition in ABAQUS, modulus of elasticity parameters and Poisson's ratio in all three dimensions are required. In this study, both sheathing and CFS members are assigned with the same material behaviour; as a result, flexural and shear plastic deformations

can take place.

Boundary conditions and loading: A fix restraint was used to simulate the fixity conditions such as the location of hold downs. This is a simplified method of modelling the hold-downs. In this method the hold-down device is not modelled and therefore the overturning of the wall is allowed. This assumption can somehow affect the stiffness and obtained from FE simulations. A more sophisticated model for simulating hold-down connection is presented in chapter 7. The top track was assumed to have no displacement and rotation out of the wall plane. Both cyclic and monotonic loading can be simulated in ABAQUS. However, majority of researchers have performed ABAQUS modelling under monotonic loading protocol. Knowing that screws tend to move and rotate, therefore; pinching phenomenon can occur in reality. Technically, this phenomenon can be modelled by defining a subroutine to incorporate a physical gap between screws and holes' bearing faces. In this study, the monotonic loading was just considered for ABAQUS simulation. The displacement-controlled loading process was used and the lateral displacement was applied on the top track.

Mesh details and connections: Link constraints such as multi-point constraint (MPC), tie, coupling, wire or fastener can be used for connection modelling. Mesh-independent fasteners such as spot weld, rivet, screw, bolts are a convenient form of connections between two or more surfaces. Mesh-independent wire with Cartesian and Cardan criteria was utilised for the modelling of screw connections.

The most important point for the FEM is to define mesh size. Finer mesh size was used for CFS members while sheathing panel was coarsely meshed. Based on the mesh convergence study for identifying an appropriate mesh density, the 25 mm and 30 mm mesh size was chosen for modelling the CFS member and the sheathing, respectively. Figure 6.1 shows the mesh size for sheathing and members and also the location of screws. The results of mesh sensitivity analysis are also presented in this figure.

Element type: Several element types such as solid two and three dimensional (2D & 3D) elements, membrane and truss elements, beam elements, and shell elements are used for simulation in ABAQUS. Beam, membrane and truss elements might not be suitable for the buckling problems. Solid 3D elements can be used; however, it needs a fine mesh for modelling of high curvature zones. A finer mesh can increase the time of analysis and also does not necessarily take more degrees of freedom into account.

For bucking analysis, the suitable element is identified as shell elements herein. S9R5, S4, and S4R elements are three well-known finite elements in ABAQUS which are used for elastic buckling analysis of thin-walled structures. The S4 and the S4R finite elements employ linear functions for inserting deformation between nodes. These elements are four-node shell elements which can be used for thin and thick members. The S9R5 element is a nine-node doubly-curved thin shell element which uses shear flexible strain definitions and Kirchoff constraints enforced as penalty functions. By increasing the number of nodes from 4 to 9 it uses quadratic shape functions that engages higher order shape functions. This element has the ability to define initially curved geometries and to simulate a half sine wave with one element reasonably accurate. The 5 in S9R5 shows this element has five degrees of freedom in which rotation of the node about the axis normal to the element mid-surface is omitted from the element formulation for having better computational efficiency. The suffix "R" also shows that reduced integration is used for calculation of element stiffness which needs sensitivity analysis to be used. In this research, S4R was considered for spatial discretisation.
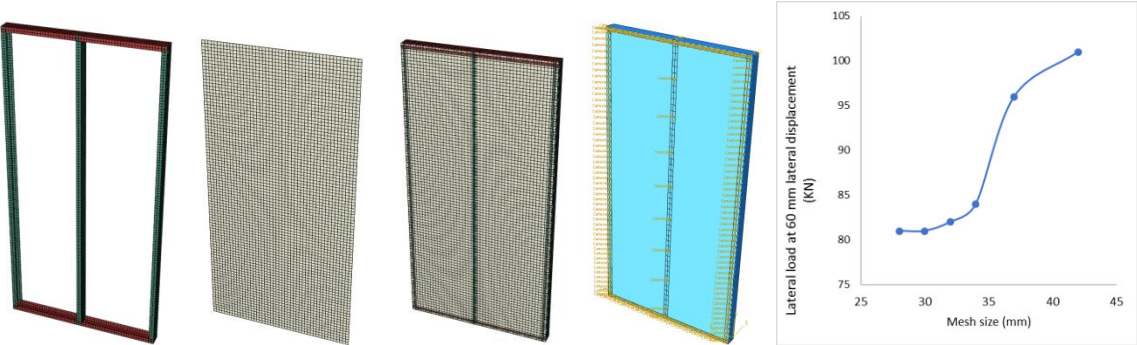
Figure 6.1. a) Mesh details for the specimens and location of screws, b) Mesh sensitivity analysis for sheathing mesh

6.2.2 OpenSees modelling

OpenSees platform is capable of simulating the response of structural systems subjected to earthquakes through FEM. In OpenSees, structural components can be defined at the element level, sectional level, and fibre level by introducing force-deformation/moment-rotation relations, force-axial strain/moment-curvature relations, and stress-strain curves, respectively.

Equivalent spring element method was used in this study to simulate the wall panels in the macro modelling approach. In this model, a simple non-linear zero-length element located at the centre of the wall panel is employed to simulate the performance of the wall. This element simulates the sheathing panel with all of its fasteners and incorporates several parameters in the simulation. This element is connected to rigid truss elements that transmit the force to studs. Zero-Length element is used to construct a zero Length element object, which is defined by two nodes at the same location. One benefit of this approach is the reduction of element numbers that causes a reduced number of degrees of freedom without adverse effects on the accuracy. CFSWSWP and CFSSSWP uniaxial materials, which are previously defined in OpenSees, are assigned to this element. The former is used for wood sheathing panels and the latter for steel sheathing panels. Elastic beam-column elements and rigid beam-column elements are also used for studs and tracks respectively for simulating their behaviour.

6.3 RESULTS

Figure 6.2 shows the results of micro and macro modelling in comparison with the experimental data. The results of specimens C1, C2, C3, and C17 under monotonic loading are extracted separately in this figure. Both micro and macro modelling results show reasonably good agreement with the experimental data; however, the ABAQUS results are slightly more accurate than the OpenSees results. In terms of initial stiffness, micro modelling results have an approximately similar stiffness to the experimental data; while, for macro modelling, the initial stiffness represents a slight deviation from the experimental results. One primary reason for the difference between the results of micro model and experimental data is that the effect of imperfection, which significantly changes the possible dominant buckling modes, was not considered in this study.
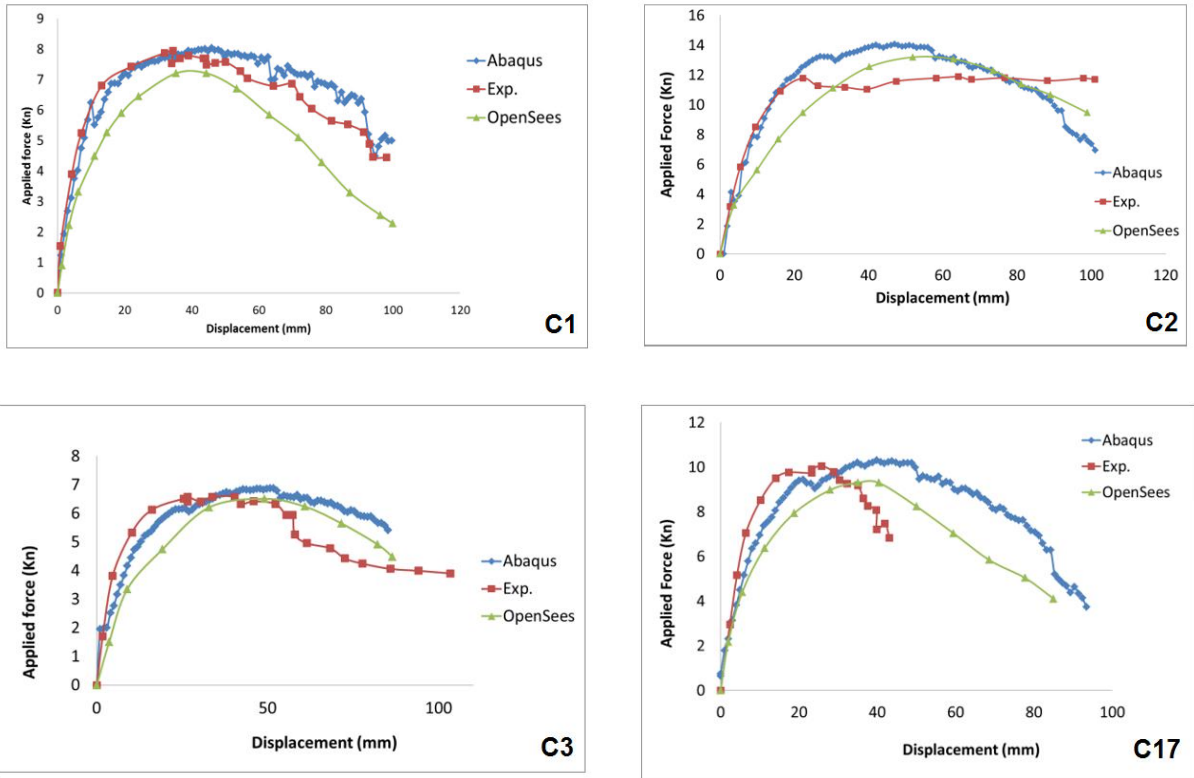
Figure 6.2 Comparison of the Macro and micro modelling results for specimens C1, C2, C3, C17

Hysteretic curves for specimens T4, P2, and C2 are presented in Figure 6.3. As mentioned previously, obtaining appropriate cyclic behaviour with pinching from ABAQUS software needs subroutine coding. Hence the hysteretic behaviour of these specimens was just obtained by OpenSees. As can be seen in Figure 6.3 , macro modelling results are in good agreement with experimental data. With a very simplified method in OpenSees and short time of modelling and analysis, seismic behaviour of a CFS wall can be gained, which is recommended for initial estimations.
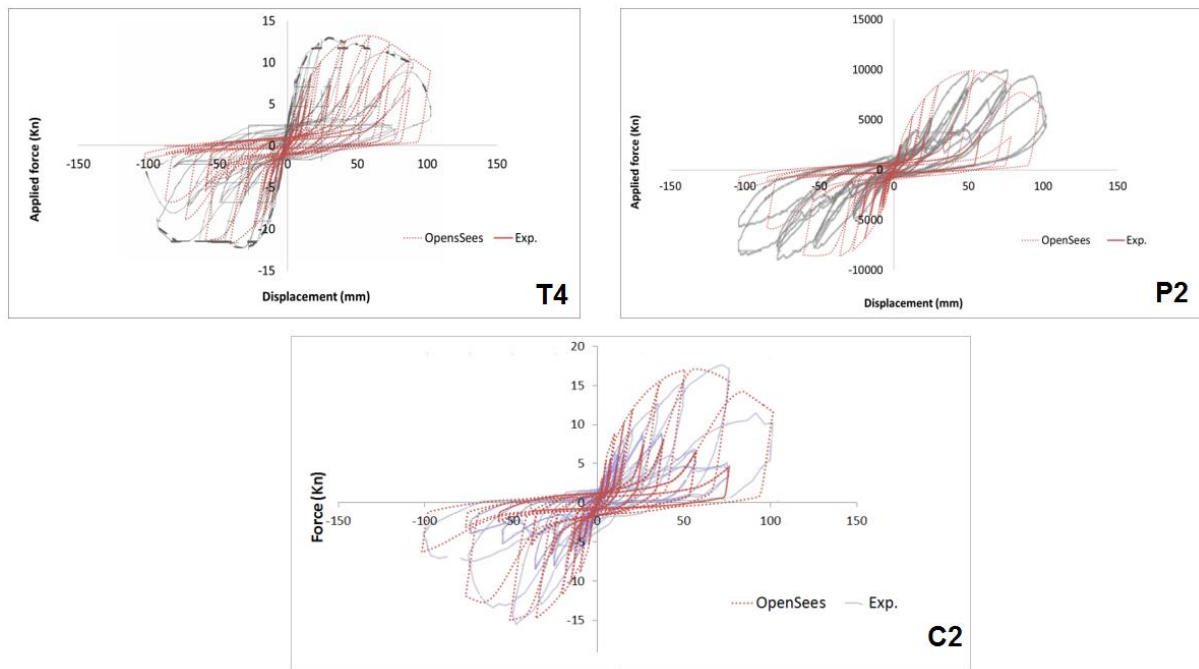
Figure 6.3. Hysteresis behaviour of the specimens T4, P2, and C2

Due to the simulation of details such as screws location and their behaviours, micro modelling in ABAQUS takes more time rather than macro modelling in OpenSees software. The time of analysis in ABAQUS is also much more than the time of analysis in OpenSees.

As ABAQUS does not have a suitable material or element for modelling CFS-sheathing connections that allow for the pinching behaviour, appropriate cyclic results are not obtained with common simulation approaches that are available in the literature for CFS shear wall. However, ABAQUS can also consider the pinching behaviour of the shear wall under cyclic loading, as long as pinching4 behaviour is introduced to the software via subroutine coding, which is very complicated. In OpenSees, the CFS members such as stud, ledger or track are modelled using displacement-based beam-column elements. Such elements assume rigid cross-sections and do not allow for localized plate flexibility in the CFS framing. In addition, in the benchmark shear wall testing, the OSB sheathing is attached to one face of the studs and the ledger track to the opposite face. These eccentricities are not included in the OpenSees model.

Figure 6.4 shows some graphical results which were obtained from ABAQUS. Different regions in CFS wall are compared to see the differences between the experimental test and the FE model. The blue region that shows lower stress distribution is the same

in real CFS wall. Figure 6.4a clearly shows this comparison. Von Mises stresses at the beginning of the loading and buckling of the studs are also shown in Figure 6.4b and Figure 6.5, respectively. In Figure 6.5, the buckling of the stud in the experiment is also shown alongside the buckling in ABAQUS, which shows one advantage of Micro modelling with ABAQUS. In a macro model, due to many simplifications, stress and strain distributions and some failures such as stud buckling, screw failure, etc. cannot be detected. In general, macro modelling with OpenSees can extract the behaviour of the whole wall after applying the load, while for the behaviour of screws during loading, ABAQUS should be used which is another advantage of this software.
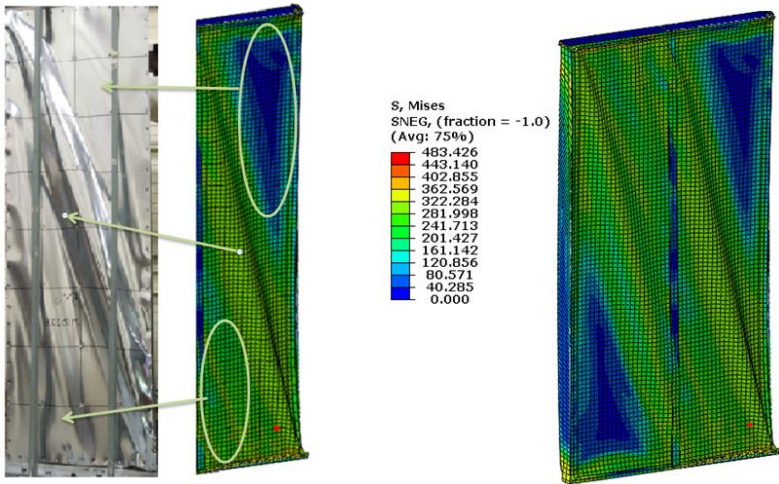
Figure 6.4. A) Sheathing deformation   b) von mises stress in sheathing
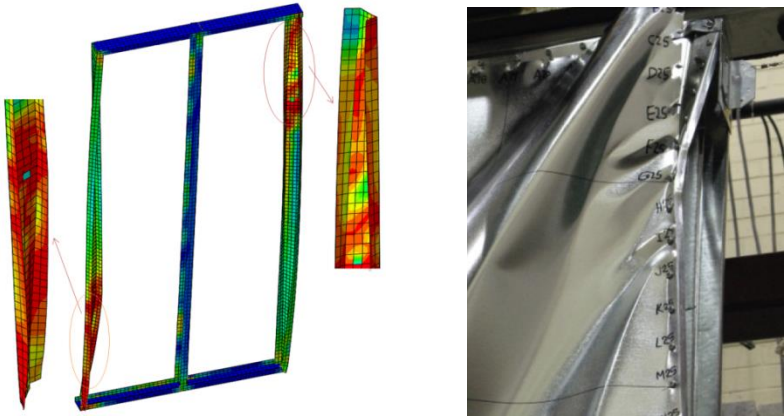
Figure 6.5. Buckling of the stud in   a) FE method   b) Experiment

Table 6.3 also shows a summary of differences in using micro modelling (ABAQUS modelling) and macro modelling (OpenSees Modelling) of CFS walls.

Table 6.3. Differences of micro-element and macro-element modelling of CFS walls.

Parameter	Time of modelling	Time of analysis	Local failure (buckling, screw failure, etc)	Graphical results	Cyclic behaviour with pinching	Initial stiffness	General behaviour
Macro modelling (OpenSees)	Short time	Short time	Cannot be gained	No graphical results	Able to consider	Slightly different with Exp. data	Good agreement with Exp. data
Micro modelling (ABAQUS)	Long time	Long time	Can be gained	Has graphical results	Unable to consider (except using subroutine)	Good agreement with Exp. data	Good agreement with Exp. data

6.4 Conclusion

Each of micro and micro modelling investigated have their own pros and cons and none is superior to others. OpenSees, which is used for macro modelling is very simple and time of modelling and analysing is much shorter compared to micro modelling in ABAQUS. In addition, due to the availability of Pinching4 material in OpenSees, the behaviour of walls under cyclic loading in OpenSees is well simulated. As mentioned previously, ABAQUS can also consider this Pinching4 material, but provision of a subroutine script is required, which is complex and time-consuming. ABAQUS results in comparison to the OpenSees results were in better agreement to the experimental data which shows that micro modelling is slightly more accurate than macro modelling.

Chapter 7   Numerical method: Modelling and design of hybrid wall panels

7.1 Introduction

This chapter presents non-linear finite element (FE) modelling of hybrid wall panels, calibrated through experimental tests, and their applications to different designs. The chapter involves the lateral behaviour of the proposed hybrid walls in terms of load-displacement curve, failure mode, stiffness, ductility ratio, energy absorption, and strength to weight ratio. First, a numerical model, verified and calibrated based on the experimental tests of Chapter 3, is presented. Thereafter, using the validated numerical model, twenty new hybrid wall panel designs are proposed in order to investigate the effect of different SHS brace configurations on the hybrid panels' performance.

In order to facilitate the analysis and design of hybrid systems, a detailed numerical model using ABAQUS package is developed to investigate the lateral performance of the hybrid CFS wall with different truss-bracing configurations. The accuracy of the numerical model for simulation of the hybrid wall depends on many parameters such as the geometry, material properties, boundary condition and interactions between components, connections, solver systems and elements, which are discussed in this chapter.

7.2 Numerical modelling

7.2.1 Material properties

To accurately capture the response of a hybrid wall, the material characteristics of the components need to be precisely determined and incorporated into the numerical

simulation.

Elastic-plastic behaviour: Material nonlinearity in all elements including CFS stud, tracks noggins and SHS bracing is modelled with elastic-plastic behaviour and von Mises yield criterion to define isotropic yielding. The elastic modulus, yield and ultimate stresses of the steel are those obtained from tensile coupon tests. The Poisson ratio of υ=0.3 is used in the FE models.

True stress-strain: Although the standardized coupon tests can provide stress-strain curves, it is not easy to measure the effect of post-necking strain (necking of the specimens) from the coupon test results [244, 245]. Therefore, the true stress (σ_{true}) and true strain (ϵ_{true}) are converted from the engineering stresses (σ) and engineering strains (ϵ) using the following equation [246]:

$$\sigma_{true} = \sigma(1 + \varepsilon) \tag{7-1}$$
$$\varepsilon_{true} = \ln(1 + \varepsilon) \tag{7-2}$$

where the engineering stresses (σ) and engineering strains (ε) are obtained from the coupon tests. It should be noted that the true stress and strain defined are based on assumption of constant material volume.

Residual stress and cold working effect: The residual stress and cold-working effect should not be simulated independently of one another because they are obtained from the same procedure [247]. Residual stresses can be idealised as a combination of flexural and membrane stresses [248]. The membrane residual stress can be ignored if the increase of the yield stress owing to the cold forming process is not included [248]. On the other hands, the flexural residual stress in elements with high values of yield strength and/or low thickness is insignificant and can also be ignored in the modelling [249, 250]. Due to this reason, the residual stress in CFS members is not generally considered in the numerical modelling [249]. Given that, residual stress and cold-work of forming are ignored in this study, and the mechanical properties of steel are assumed to be uniform across the cross-section, like other research in this field [247, 248, 251-253].

7.2.2 Contact modelling

Contact of the hybrid wall members is designated to model the interaction of frame elements, considering this assumption that two surfaces are not penetrated in each

other, and they may detach after the loading. Therefore, the surfaces are not interlocked and will be able to slide on each other.

The surface-to-surface contact using the finite sliding tracking method, which allows any arbitrary motion of the surfaces [254, 255], is used in this study to simulate the contact between hold-down and track, hold-down and SHS parts, as well as studs and tracks. This contact technique provides a reasonable convergence rate and is much less sensitive to the selection of master and slave surfaces [247]. Finite sliding also accounts for large displacements between contact pairs compared to their element sizes. Therefore, it is appropriate in this study with to develop models with large deformations. A hard contact property is also implemented for the contact behaviour in normal direction between the profile surfaces. As discussed in Chapter 5 (Usefi et al. [22]), the friction between CFS element is not significant and can be ignored in the model.

The designation of master and slave roles can have a substantial impact on the results with surface-to-surface contact. For contact pairs with two deformable surfaces, the following basic principles are used according to the ABAQUS documentation [254]: a) The master surface is selected as the surface of the stiffer element or as the surface with the coarser mesh if the stiffness is similar. B) The smaller surface in the contact region is employed as the slave surface.

When two surfaces are in contact for the duration of the analysis, adjusting the surfaces in a contact pair is needed. The location of the slave surface can be adjusted by assigning an adjustment zone around the master surface. Any nodes on the slave surface that are inside the "adjustment zone" in the primary geometry of the model are moved accurately onto the master surface. In some cases, if the adjustment zone is not defined, the convergence problem occurs. Therefore, an adjustment zone of 0.02 is set for all contacts between elements.

A summary of the contact details for modelling is provided in

Table 7.1. Also, Figure 7.1 shows the different locations in the experimental specimen, where the contact modelling for the numerical method is required. Figure 7.2 illustrates the schematic of contact models in the numerical method.

Table 7.1. Contact details of hybrid wall components

Contact region	Master	Slave	Detail
Hold-down to SHS	Hold-down vertical surface	SHS surface	To prevent penetration of hold-down in SHS
Hold-down to track	Hold-down bottom surface	Track web surface	To prevent penetration of hold-down in track
SHS end-edge to track	Track web	SHS end-edge region	To prevent penetration of SHS end-edge in track web
Bottom track to bottom reaction beam	Top surface of the bottom reaction beam	Track web surface	To prevent penetration of track in bottom reaction beam
Top track to loading beam	Loading beam web surface	Track web surface	To prevent penetration of track in loading beam
Stud to track	Track flange surface	Stud flange surface	To prevent penetration of stud in track
Stud to stud (noggings)	Stud flange surface	Stud flange surface	To prevent penetration of stud in noggings
Stud end to track	Track web surface	Stud end region	To prevent penetration of stud end in track web
SHS to track	SHS surface	Track flange surface	To prevent penetration of SHS in track flange
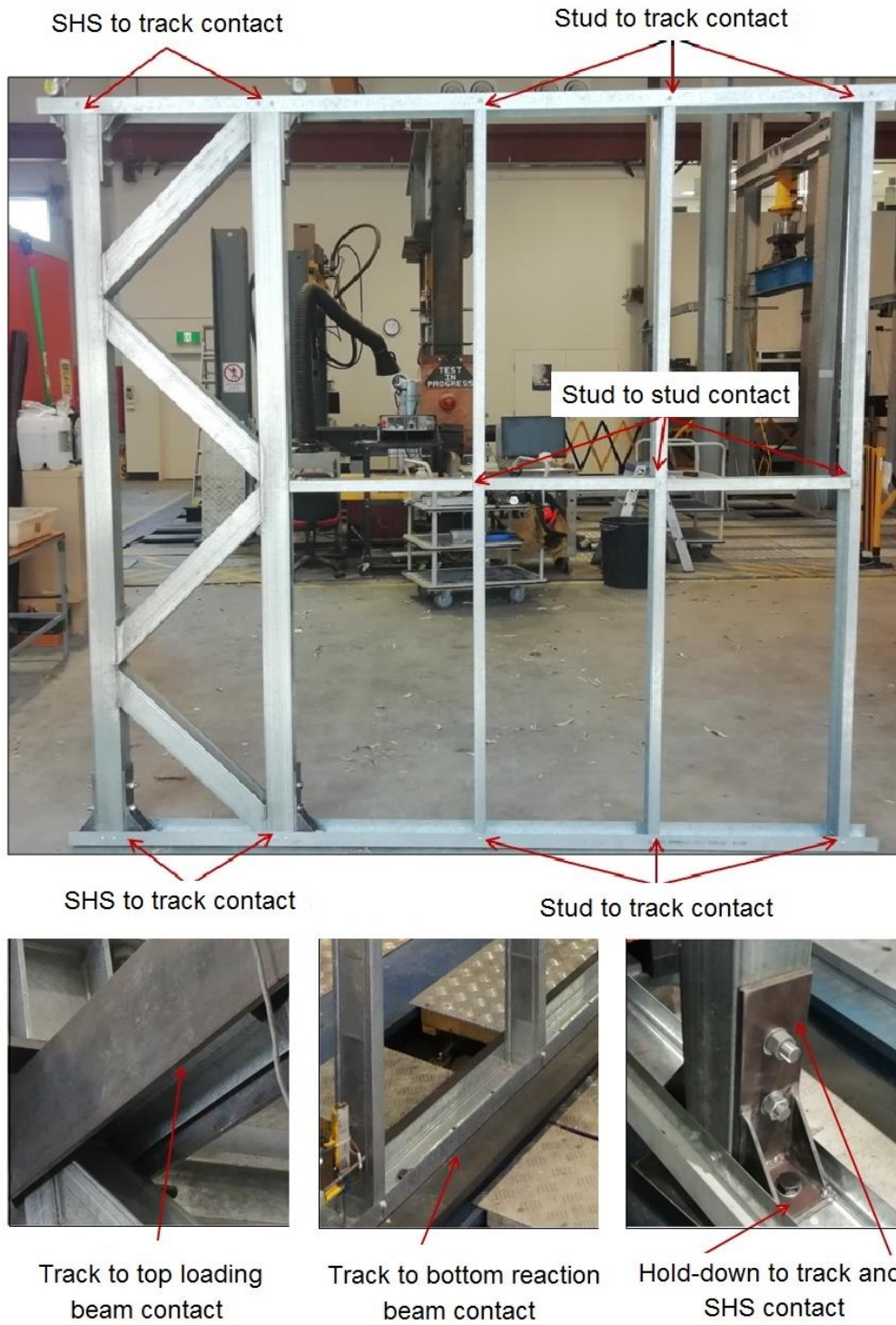
Figure 7.1. Contact locations which need to be assigned for modelling of hybrid walls
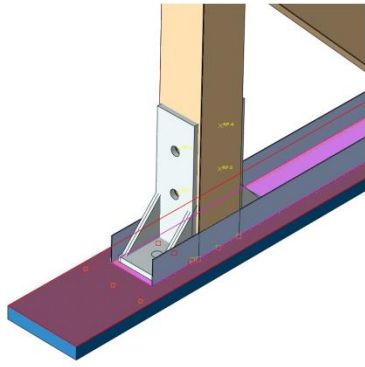
Track to reaction beam contact
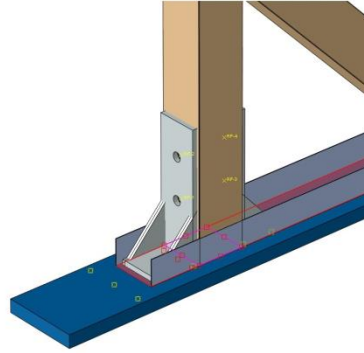
SHS end to track contact
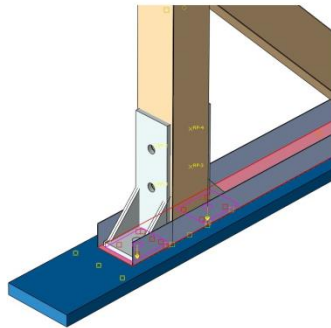
Hold-down to track contact
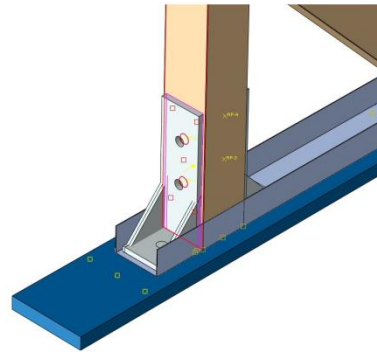
Hold-down to SHS contact

Top track to loading beam contact
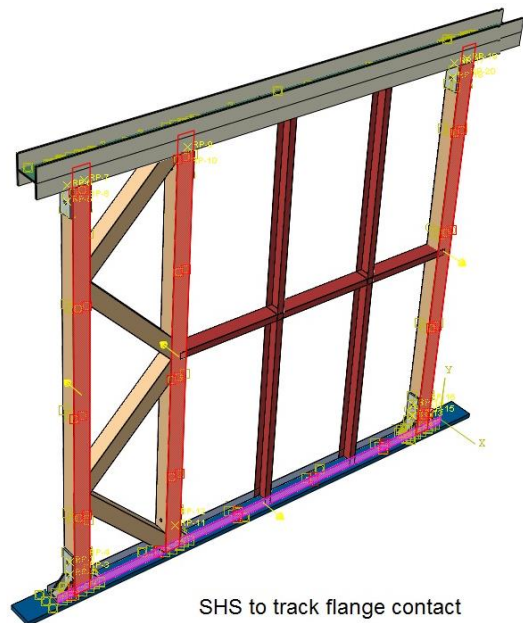
SHS to track flange contact

Figure 7.2. Master and slave modelling for contacts of elements in wall panel

7.2.3 Connection

One of the predominant parameters significantly affecting the numerical results of hybrid CFS walls under lateral load is the modelling the connections. If the real behaviour of the bolts and screws is not properly considered in the modelling, the strength of the wall may be overestimated, and therefore, the results of the model analysis will not represent the actual performance of the wall. Hybrid CFS wall comprises three types of connections:

a) *Connection of hold-down to loading and reaction beams (Bolt connection)*

A surface-based tie constraint is used for simulation of bolt connection of hold-down to loading and reaction beams. Based on the experimental observations in Chapter 3 [256], no slippage was observed at the location of bolts during the experimental test. Therefore, the translational and rotational movement, as well as all other active degrees of freedom of hold-downs, can be considered as equal to the loading and reaction beams at the position of the bolts. Loading and reaction beams' surfaces are designated to be the master surfaces, and the hold-down bottom surface is considered as the slave surface.

b) *Connection of SHS elements to CFS members, and CFS members to each other (Screw connections)*

For connection of SHS elements to track flange as well as CFS connections (stud to track and noggings to stud), a point-based mesh-independent fastener connection is employed. This method uses distributed coupling constraints to connect the wall faces regardless of mesh formation. The desired radius of influence is specified based on the screw diameter used in the experimental test. The face-to-face projection method, used for nearly parallel surfaces, is employed to fasten the surfaces together. Deformable characteristic of the connector is specified by Cartesian behaviour that can indicate the performance of a real screw. Cartesian behaviour provides a connection between two nodes, where the change in translational degrees of freedom at both nodes is measured in three local connection directions. Rotational degrees of freedom are ignored as the screws do not prevent the rotation of components. The schematic of the screw simulation is shown in Figure 7.3.

c) *Connection of hold-down to SHS elements (bolt connection)*

In the experiment of specimens HW4 and HW5, no slippage was observed at the bolt location connecting SHS to hold-down, which indicates that translational and rotational degrees of freedom of the hold-down at the location of bolts is equal to SHS element, until the end of the test. Hence, the structural coupling method, which couples the translation and rotation of SHS at the location of the bolt to the translation and the rotation motion of the group of nodes on the hold-down, is employed to simulate the bolt connection at the hold-down location. Two coupling procedure is required at the location of each bolt. First, the region covered by the bolt on the hold-down is coupled to a reference point. Then, the SHS region covered by the nut is coupled to the same reference point. The reference point is considered at the centre of the hole at bolt location or both SHS and hold-down. Using this method, the hold-down and SHS are entirely engaged to the end of the simulation. Figure 7.3 shows the coupling method applied for hybrid wall models.
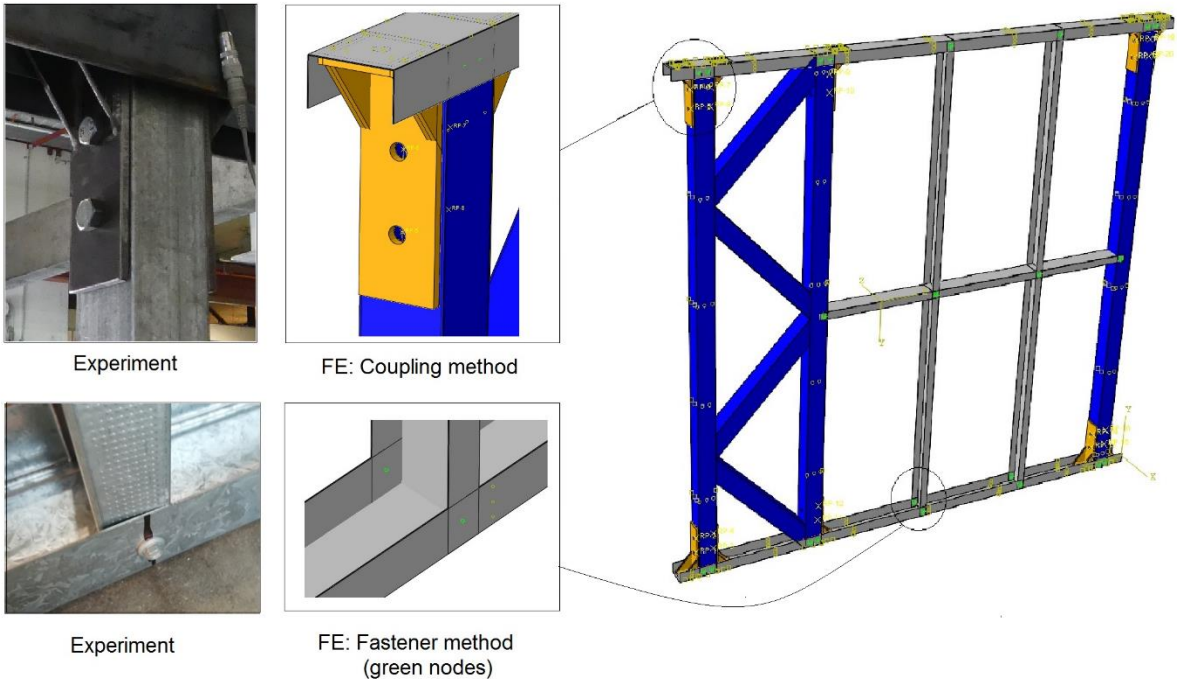
Figure 7.3. Simulation of connections in hybrid wall models

7.2.4 Boundary condition and loading

The boundary condition and applying load in a numerical model should represent the experimental test. However, some simplifications can be assigned for applying load or fixity of shear wall, which can result in a level of inaccuracy in the final results. Different

157

methods have been used for simulation of constrains, loading beam and applying load conditions, which are explained in details in Chapter 5 (Usefi et al. [22]). In most of the previous studies on the CFS shear walls, the reaction and loading beam (top and bottom beam) is not modelled, and only their corresponding effect is stimulated [22]. However, in this study, because of different factors including connection types, failures in bottom track during the test, load distribution pattern of the hybrid panel as well as accurately considering the overturning of the wall, both loading and reaction beams are simulated.

Since no slippage or deformation was observed in the reaction beam during the test, in this study, the reaction beam is fixed in all degree of freedoms. The load is applied to the top left of the loading beam, similar to the experimental condition with a displacement method regime. An ultimate displacement of 90 mm is considered for the applying load. The loading beam is also laterally restrained to simulate the real condition of the experimental test. Figure 7.4 shows the experimental boundary condition which is applied to the numerical modelling.

It is notable that the overall response and trend of the experimental specimens under monotonic loading, as explained in Chapter 3 [256], was similar to that obtained from cyclic loading, as presented in chapter 4 [257]. Therefore, the monotonic investigation of the wall panels is only investigated in this numerical study. Besides, detailed numerical modelling of CFS walls under cyclic loading has some limitations in capturing pinching behaviour [22]. Hence, due to the lack of a proper model for simulation of pinching behaviour in ABAQUS, monotonic loading is employed for this numerical study, like almost all previous micro modelling studies on the CFS wall panels [22].
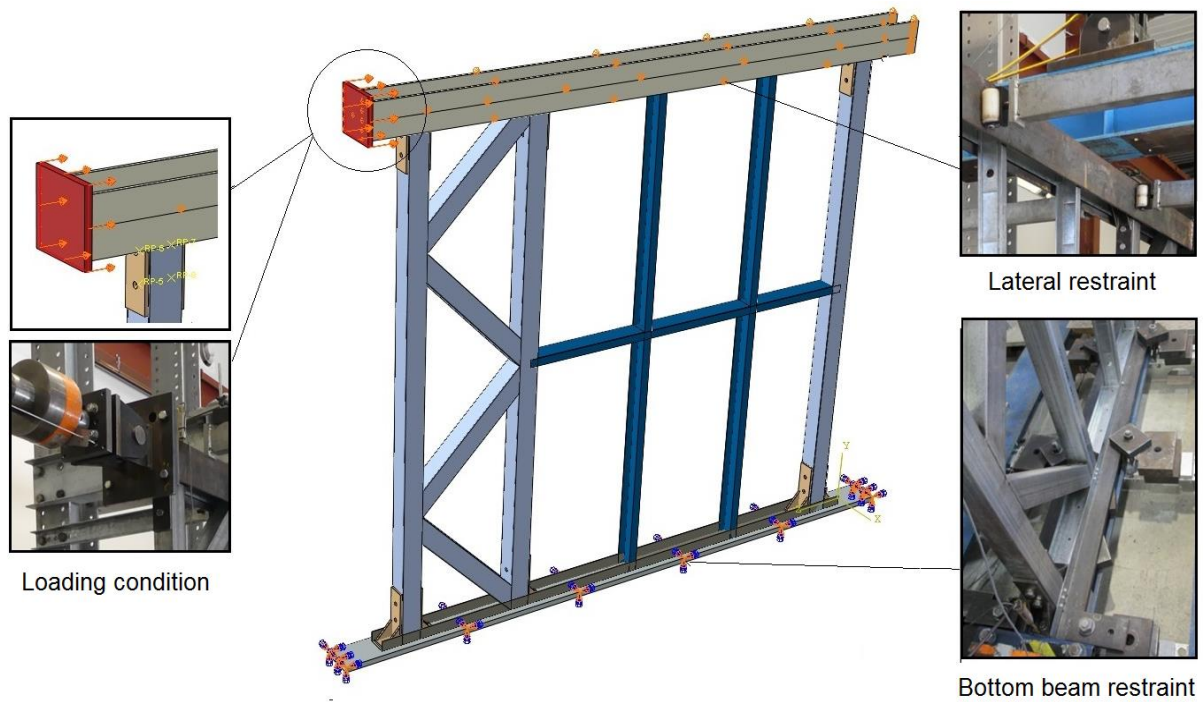
Figure 7.4. Experimental boundary condition applied to the numerical modelling

7.2.5 Solver

A static load-displacement nonlinear analysis is used for the numerical method, as the inertia effects can be neglected. The convergence and integration accuracy are significant factors in a numerical analysis, particularly for modelling of hybrid wall panels with thin sections and large displacement. When there are some localised instabilities, due to large-displacement effects, Abaqus/Standard offers the stabilization option through applying damping factor. The damping value should be reasonable to avoid unfavourable buckling or collapse, and does not considerably influence the behaviour of the model. The adaptive automatic stabilisation scheme, in which the damping factor can vary spatially and with time, is employed in this study. A damping coefficient of 2.0E4, as well as the adaptive automatic stabilisation scheme with default accuracy tolerance of 0.05, are found to be sufficient for solving the convergence problem [118].

After applying the automatic damping factor, this adaptive stabilisation scheme is controlled by two methods. First, the viscous forces are compared with the overall forces in the analysis output and found that the viscous forces are relatively small compared with the overall forces in the model. Then, the ratio of the energy dissipated

by viscous damping to the total strain energy of the system is calculated, which is below 0.5% for the performed analyses and ensured that the ratio is reasonable and does not exceed the dissipated energy fraction.

7.2.6 Element types and mesh density

The four-node shell element with reduced integration scheme, which is known as the S4R element is employed for the numerical approach [22, 258]. This element comprises three translational and three rotational degrees of freedom at each node, and also considers the change in the shell thickness. The element accounts for finite membrane strains and arbitrarily large rotations [254, 259, 260], which is suitable for this study with large-strain phenomena and geometrically nonlinear problem. Using sensitivity analysis, it is observed that quad dominated meshes with dimensions of 18 mm are deemed satisfactory for SHS elements, loading and reaction beams, as well as stud and tracks. For the hold-down devices, a finer mesh size of 14 mm is employed. Figure 7.5 shows the meshing scheme of the hybrid wall components and the results of mesh sensitivity analysis.

| (a) | (b) |
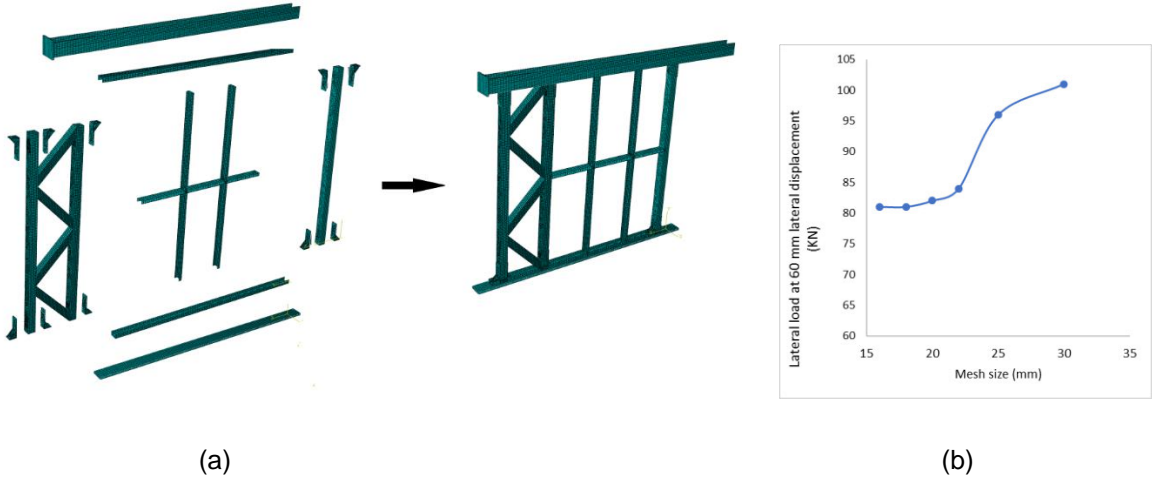
Figure 7.5. a) Mesh density of the hybrid components and wall, b) Mesh sensitivity analysis

7.3 Validation of the numerical method

The proposed numerical method needs to be validated in different conditions (walls with and without brace) in order to be more reliable for further developing of the numerical simulations. Hence, experimental results obtained from specimen HW4 with truss-brace (asymmetric configuration), as well as HW5 without brace (symmetric

configuration) (experimental results of chapter 3 [256]), are used to evaluate the validity and accuracy of the numerical method.

Figure 7.6 shows the comparison of the load-displacement curves of the experimental specimens against the numerical models. As illustrated in this figure, numerical results are in good agreement with experimental data. The discrepancy between the numerical and the experimental results in the initial elastic stage can be attributed to the simplified simulation of bolts in the numerical model as well as the friction between all members, which is ignored in the modelling. As discussed in Section 3.2, one of the critical reasons for the difference between experimental and numerical results is the friction between the interfaces of the elements in the test i.e. hold-down to SHS interaction, which is normally ignored in the numerical methods. Nevertheless, this negligible difference does not impact the overall accuracy of the numerical method.
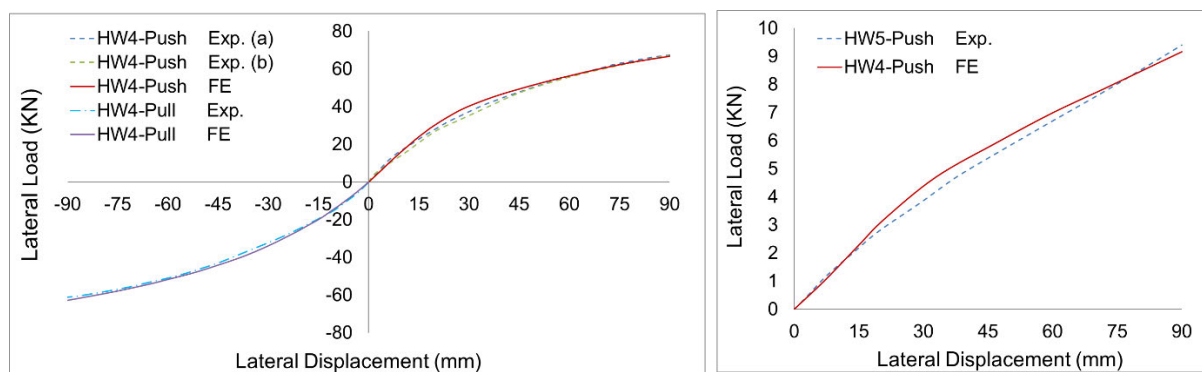
Figure 7.6. Comparison of the load-displacement curves of the hybrid wall panels

Performance of numerical models is also quantitatively evaluated by considering three parameters: maximum strength (at 90 mm lateral displacement), strength at 2.5% storey drift (at 60 mm lateral displacement) and elastic stiffness. From Table 7.2, it can be seen that the numerical and experimental peak load and the load at 2.5% drift are in good agreement with each other. Although the initial stiffness of the model is lower than the initial stiffness of experimental test, the total secant stiffnesses, obtained by numerical analysis, are higher than those of the experimental method.

Table 7.2. Comparison of numerical and experimental results

Specimen	Peak load (at 90 mm displacement)			Load at 2.5% allowable drift (at 60 mm displacement)			Elastic Stiffness		
	FE	Exp.	FE/Exp.	FE	Exp.	FE/Exp.	FE	Exp.	FE/Exp.
HW4-Push (a)	66.7	67.4	0.98	56.4	56.1	1.01	1.5	1.4	1.07
HW4-Push (b)	66.7	67.2	0.99	56.4	55.8	1.02	1.5	1.4	1.07
HW4- Pull	62.8	61.2	1.02	52.1	51.3	1.02	1.3	1.2	1.01
HW5	9.2	9.4	0.97	6.9	6.7	1.03	0.15	0.12	1.25

Figure 7.7 also illustrates the final deformation of the specimen HW4 under pushing phase for both the experimental specimen and numerical model. The local buckling at the bottom track, local damages at hold-down to SHS connection, as well as the overall deformation can also be captured by numerical method, as shown in Figure 7.8.
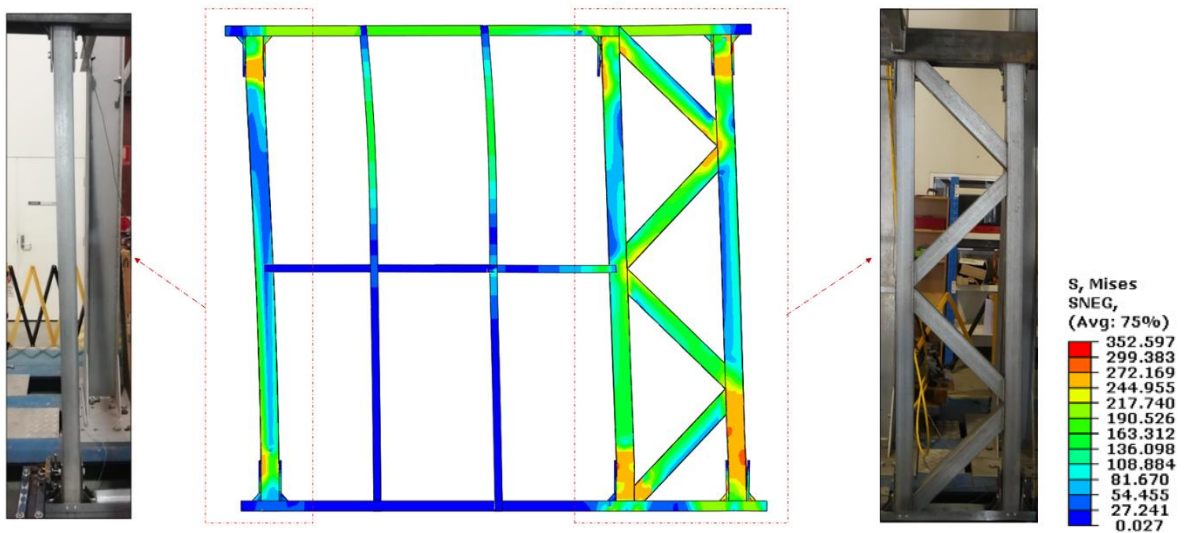
Figure 7.7. Comparison of ultimate deformation pattern between the experimental specimen and numerical model
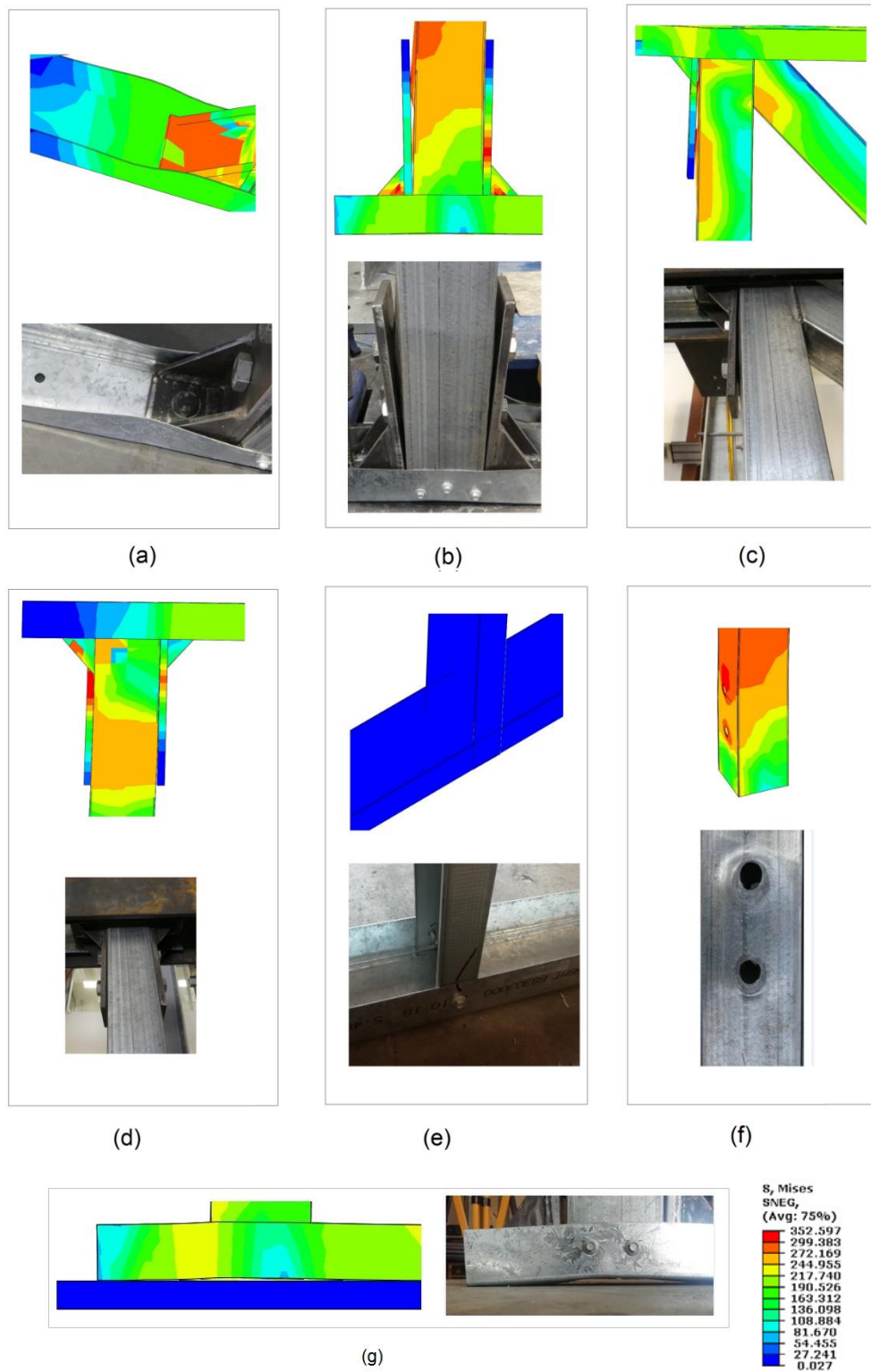
Figure 7.8. Comparison of local failures at different locations for numerical model and experimental specimen: a) buckling of the bottom track, b) hold-down to SHS truss at bottom tension side, c) hold-down to SHS truss at top tension side, d) hold-down to single SHS at the end of the wall, e) stud to track, f) localizes failure in SHS truss, g) uplift in tension side of SHS truss

Comparing numerical and experimental results, with respect to the load-displacement curve, strength, stiffness, ultimate deformation and local failures indicates that the numerical model is able to accurately estimate the overall behaviour of the actual hybrid wall. Therefore, the numerical modelling method looks to be reliable enough to be used for a further study for investigating the performance of different SHS truss brace configuration and their effects on the behaviour of hybrid walls.

7.4 Hybrid panels with different configuration

Using the validated FE method, a numerical model is developed to investigate the lateral performance of 20 new hybrid CFS walls with different SHS brace configuration. The aim is to determine the configuration providing the best lateral performance. Figure 7.9 illustrates the new hybrid wall panels and their configuration. The configuration of each model is selected based on the different types of bracing systems (i.e. knee brace, K brace, V brace, X brace) available in the CFS industry or the previous studies. Some models are also arbitrarily selected to provide a comprehensive comparison between all configurations. The new hybrid CFS models are similar to specimen HW4, where the only difference is with the SHS brace configuration of the wall. The frame size, the diameter of the bolts and screws used in different locations, location of screws, stud spacing, loading and reaction beams, and the dimension of the hold-downs are kept the same as the HW4 frame. In addition, the element type, mesh size, material properties, contact details, modelling of the bolts and screw, boundary conditions and loading scenario are also consistent with those mentioned in section 3. Figure 7.10 also illustrates the hold-down locations at the base of the frame (bottom reaction beam) for all models. The same arrangement is also used for the top of the frame (top loading beam). As shown in this figure, two hold-downs are employed wherever diagonal braces do not frame into the vertical element, while only one hold-down is utilised when braces frame into the vertical post.
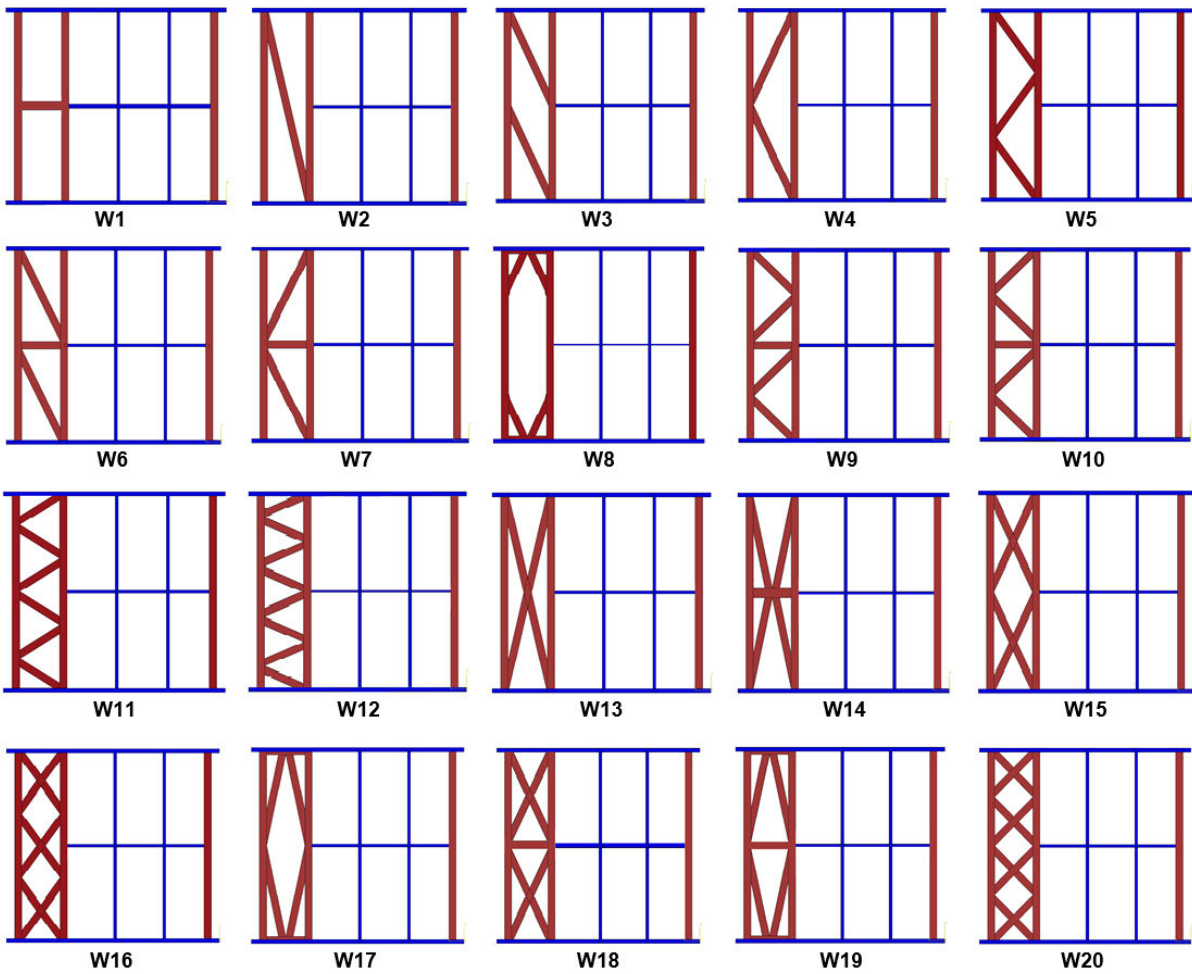
Figure 7.9. Hybrid wall models with different truss-braced configuration
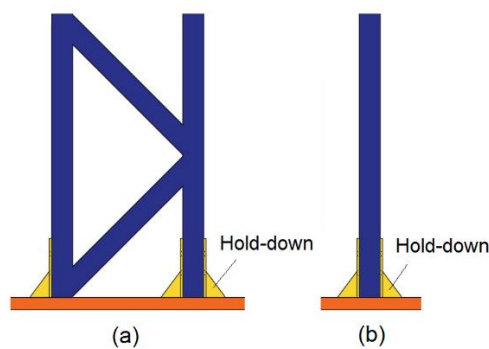
Figure 7.10. Hold down locations at the bottom of the wall: a) truss frame, b) Single SHS post

The new hybrid wall models are analysed, and the results are compared with respect to load-displacement curve, ultimate deformation mode, energy absorption, stiffness ductility ratio and strength to weight ratio. For a better comparison, experimental results of specimen HW4 is also utilised in order to justify the superiority of some of the

numerical hybrid wall panels.

7.4.1 Load-displacement curves

In the numerical model, the shear load is the load captured by the shear resistance of the bottom bolts at the location of hold-downs, while the displacement values are the lateral displacement of the top track. The load-displacement curves extracted from numerical models are categorised in two groups. The first group refers to the walls having asymmetric truss brace configuration, in which pushing and pulling loading phase are different (W2-W7, W9-W12). The second group shows the hybrid walls with symmetrical truss-brace configuration where the results of pushing and pulling are in good agreement (W1, W8, W13-W20).

7.4.1.1 Walls with asymmetric SHS truss

The main reason for considering asymmetric brace configurations is the modular aspect of these systems. In a module, two asymmetric wall panels can be placed at two sides of a module frame providing a symmetric system. The load–lateral displacement curve for each wall with asymmetric truss brace configuration is shown in Figure 7.11. The frames are loaded laterally until reaching the 90 mm lateral displacement, which is the same as the experimental lateral displacement. Due to the difference in rigidity of the walls under pulling and pushing loads, the load-displacement curve of each specimen is provided for both phases. Generally, for all specimens, the resistance of the wall is increasing without experiencing any severe failure, and the nonlinear behaviour of specimens is mainly due to the ductile deformation of SHS elements, as well as the local failure of the SHS at the hold-down connections.

As shown in Figure 7.11, the difference between pushing and pulling phase in specimens W2 and W3 is more noticeable, compared to the other walls with asymmetric SHS truss brace. This can be justified by the fact that the buckling of long diagonal SHS brace in these models causes an undesirable deformation in the wall, and makes the lateral capacity to drop significantly under the pushing phase. Figure 7.12 also shows a comparison of the experimental specimen (HW4) against the walls with asymmetric SHS truss braced. As indicated in this figure, only numerical models W10, W11 and W12 can provide superior performance compared to the HW4. The ultimate deformation of the wall models in this group is presented in Figure 7.13. Since

the only difference of the wall panels is in their SHS truss part, and also the deformation of the other components is similar to the HW4 specimen, the lateral deformation of SHS truss part is only illustrated in this figure. All walls exhibited elastic deformation in SHS part at small displacement amplitudes. As the lateral displacement increased, based on the visualized results of the model, the typical failure is localized at the connection point of the SHS elements to the hold-down devices for most of the specimens, which is followed by a decrease in stiffness and strength of the wall panel. This type of local failure is similar to the experimental reference test (HW4).
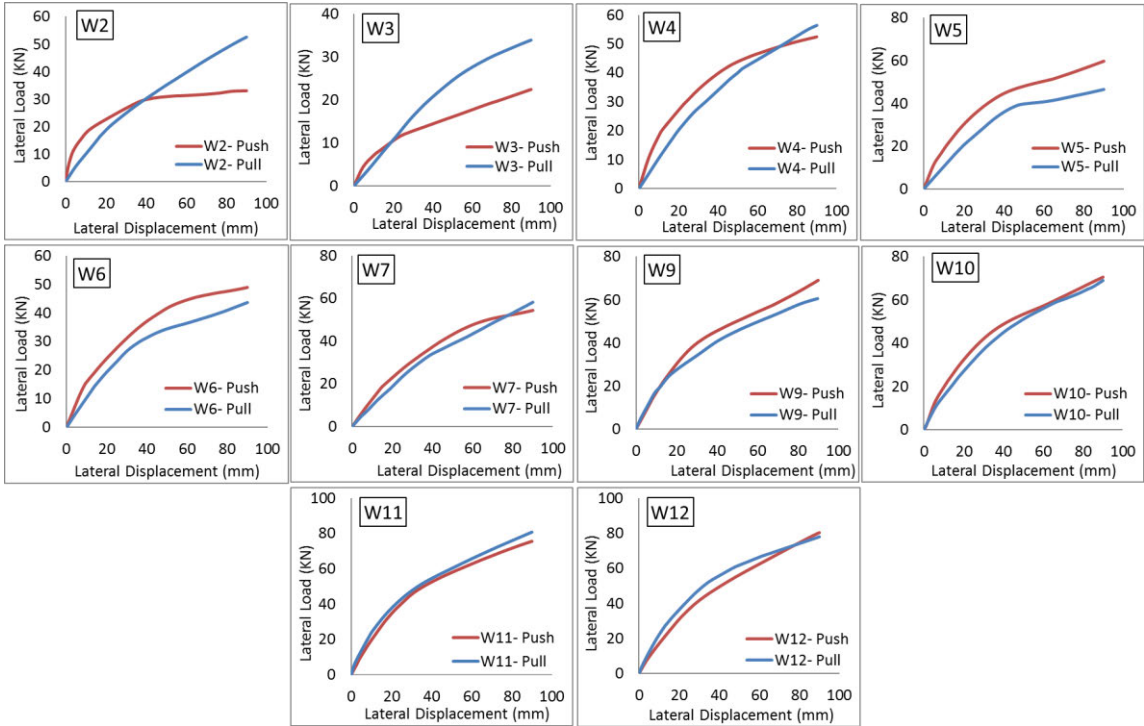
Figure 7.11. Load-displacement curves of the walls with asymmetric SHS configuration
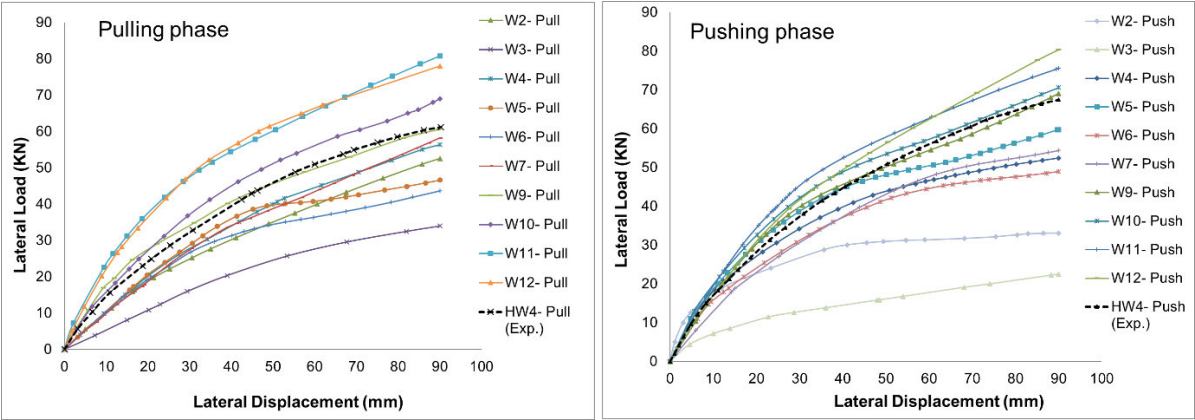
Figure 7.12. Comparison of experimental specimen HW4 against the wall models with asymmetric SHS truss brace
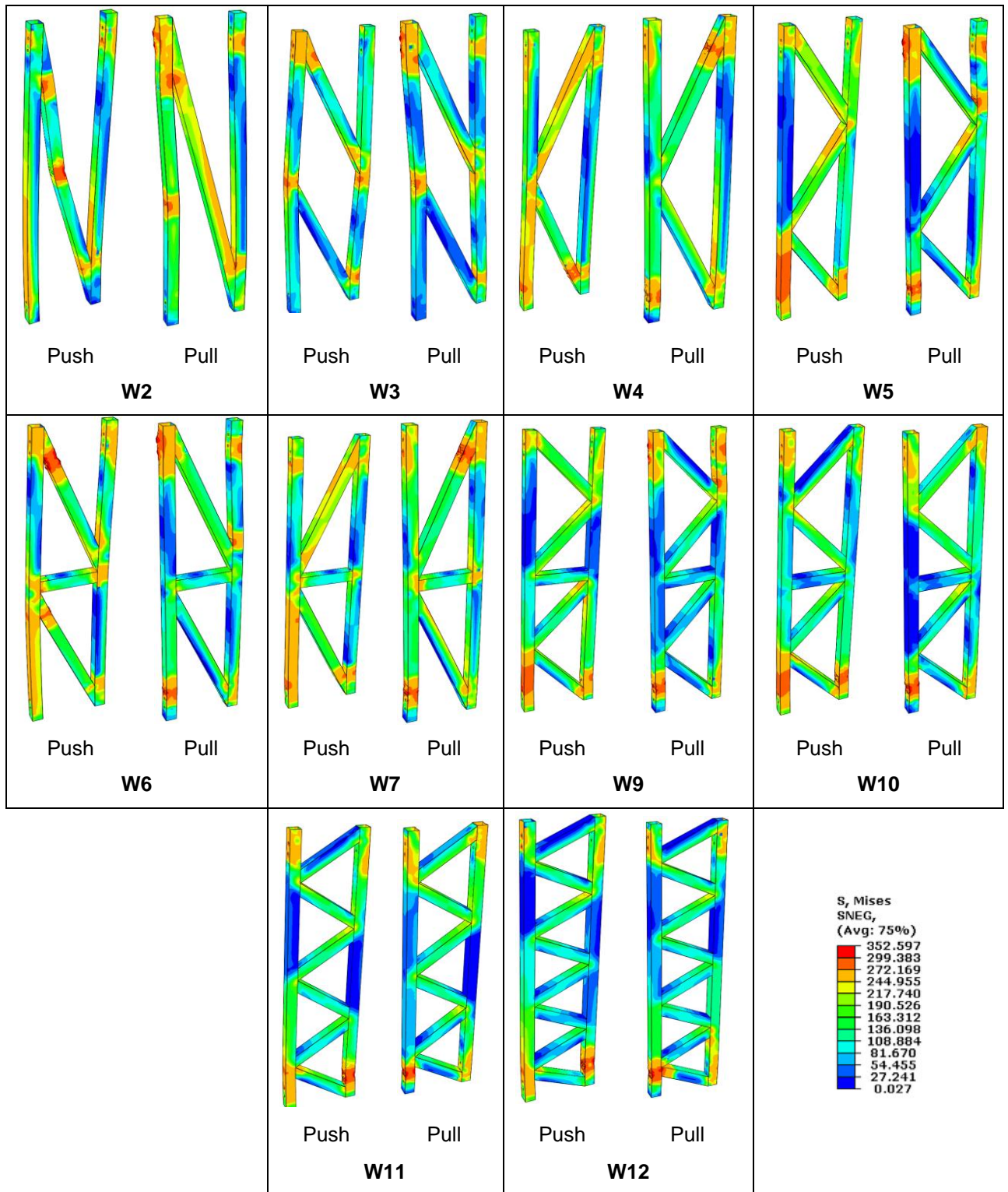
Figure 7.13. Ultimate deformation of hybrid wall models with asymmetric truss brace configuration

7.4.1.2 Walls with symmetric SHS truss

The load-displacement curves for each hybrid model having symmetrical SHS truss

brace, as well as the comparison between the walls and experimental specimen are presented in Figure 7.14. Similar to the wall models with asymmetric truss brace configuration, for all symmetrical walls, there is no drop in the curve until the load reaches the maximum value; i.e. specimens do not lose their bearing capacity till the end of the analysis. It should be noted that while the walls with asymmetric SHS truss configuration exhibit different behaviour under push and pull phases, the corresponding push and pull behaviour in walls with symmetrical SHS truss is about identical. Therefore, the load-displacement curve in the pushing phase is only used for showing the performance of the hybrid walls in this group. The results in Figure 7.14 also indicate that the wall models W13, W15, W16, W18 and W20, can provide higher resistance compared to experimental specimen HW4. Wall model W14 has also offered a general resistance very similar to HW4 with a slightly lower value. For wall models W2, W8, W17 and W19, due to the type of brace configuration, the load-resistance capacities of the walls are much lower than corresponding values for HW4, which indicates that these walls are not suitable to be used for mid-rise structures. The ultimate deformation for specimens having symmetrical SHS truss is also shown in

S, Mises
SNEG,
(Avg: 75%)
352.597
299.383
272.169
244.955
217.740
190.526
163.312
136.098
108.884
81.670
54.455
27.241
0.027
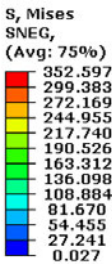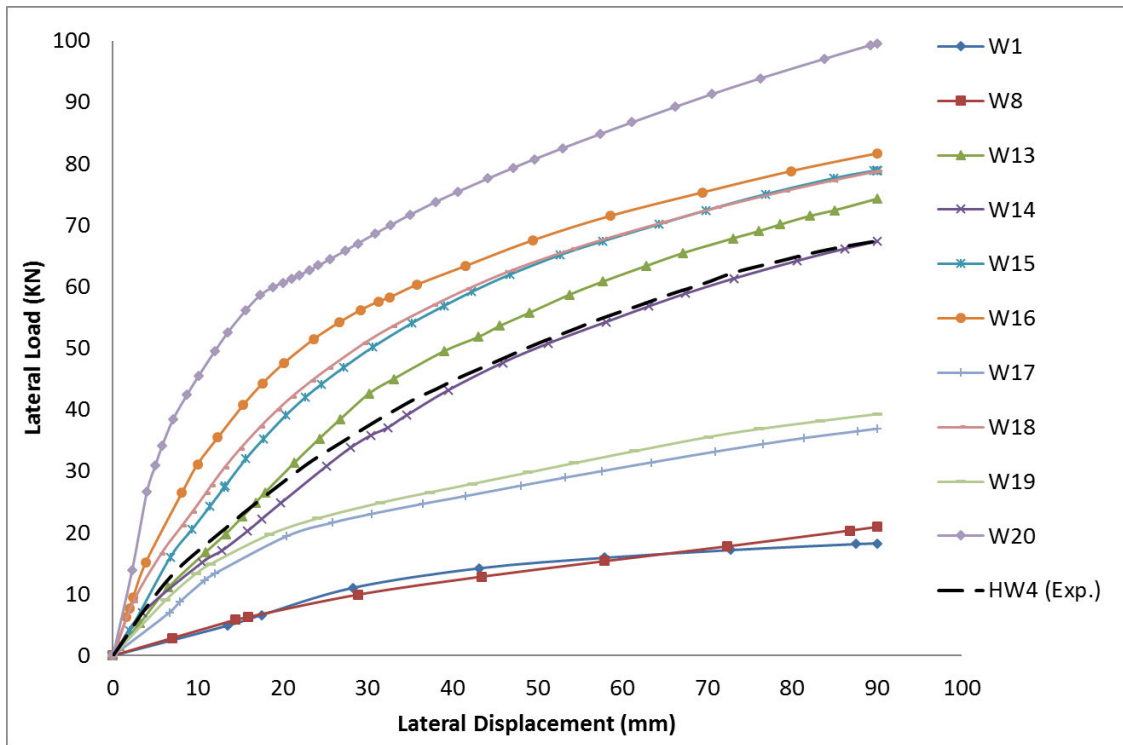
Figure 7.15.

Figure 7.14. Comparison of experimental specimen HW4 against the wall models with symmetrical SHS truss brace

W1   **W8**   **W13**   **W14**   **W15**
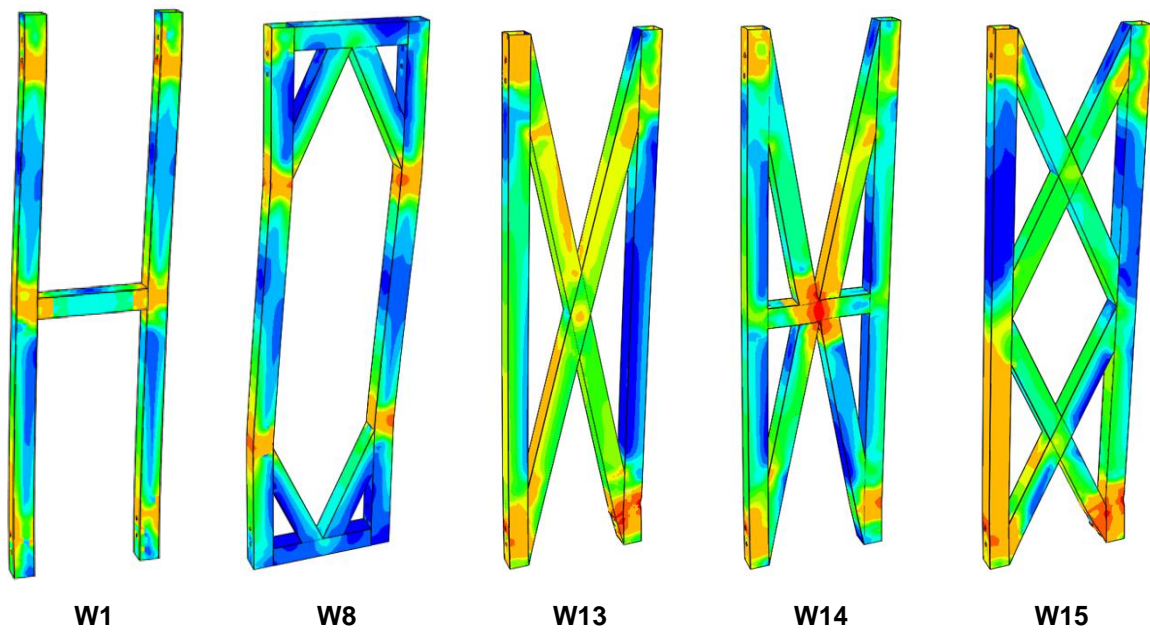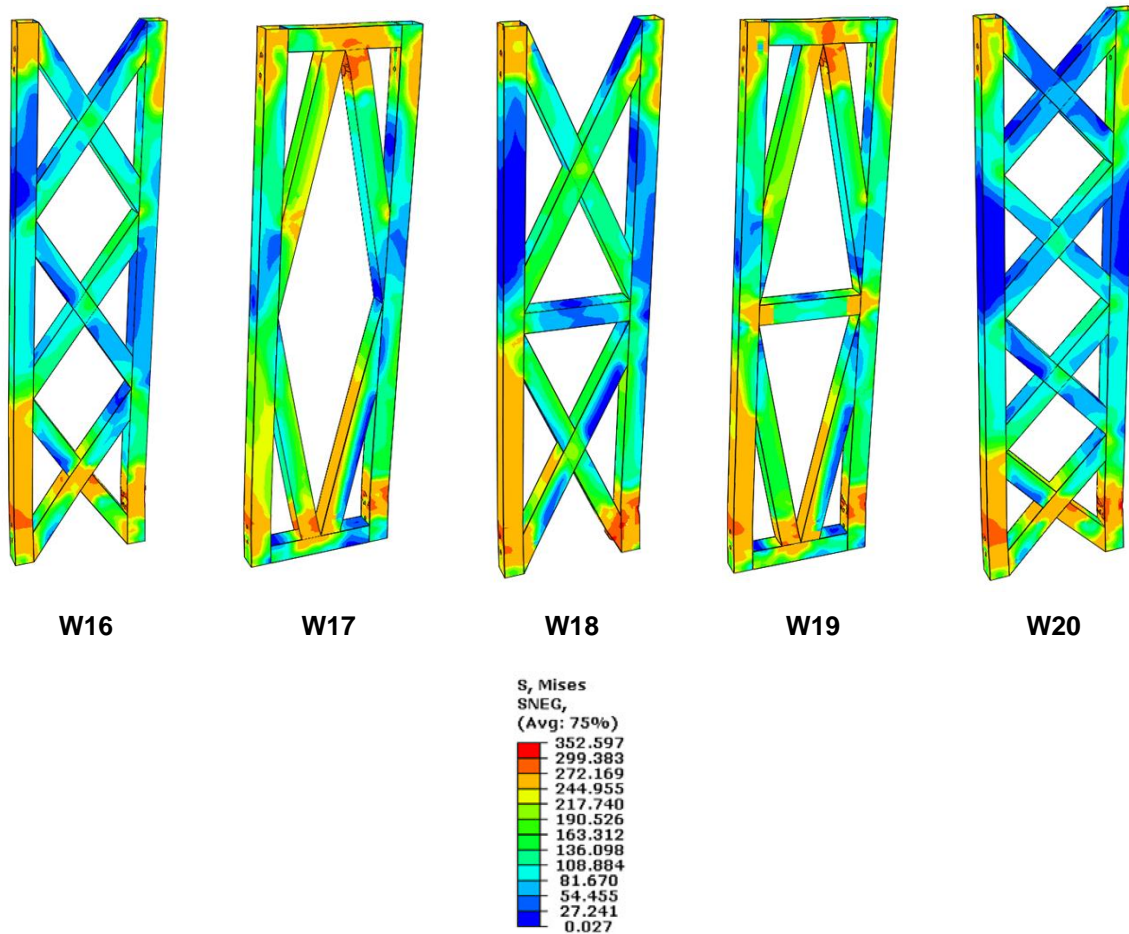
Figure 7.15. Ultimate deformation of hybrid wall models with symmetrical truss brace configuration

7.5 Design values

Using the EEEP method explained in Chapter 3, Section 3.3.2, the design parameters for each wall model can be obtained [261]. According to the many building regulations [109, 261-263], for seismic design, the maximum acceptable inelastic inter-storey drift is equal to 2.5% of the storey height, i.e. 60 mm for a 2400 mm high wall. For this reason, the general calculation procedure for the EEEP curve is modified. The elastic part of the curve remains as is, while the plastic portion of the curve is adjusted based on the 60 mm displacement limit (areas A1 and A2 are equal, as shown in Figure 7.16). It is notable that in some strong CFS shear walls, the ultimate resistance can reach at higher lateral drifts with no drop in resistance and consequently calculating the 80% post-peak load in demand displacement range is not possible. Therefore as stipulated in AISI report [264], the maximum point can be considered as the ultimate point (80%

post-peak load) on the EEEP curve.
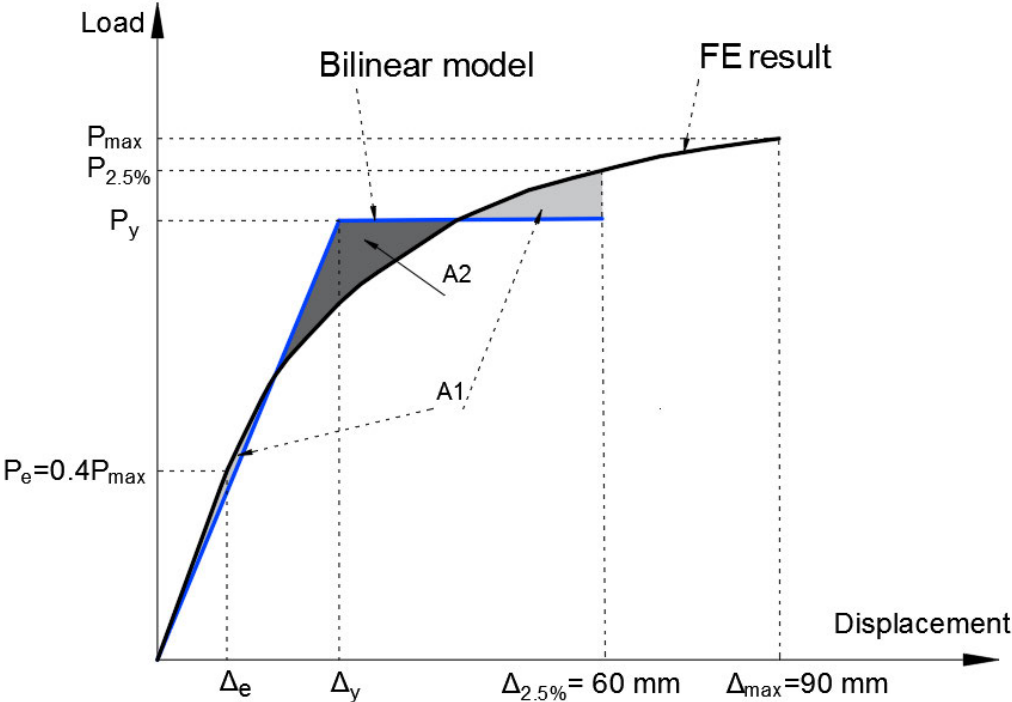
Figure 7.16. EEEP curve and the limitation based on allowable lateral drift of 2.5%

Table 7.3 shows the EEEP results for all specimens calculated based on maximum allowable lateral drift (2.5% or 60 mm lateral displacement). For the wall models with asymmetric SHS truss configuration, the average value for push and pull phases is provided.

Table 7.3. EEEP results for hybrid wall models

Wall	Load type	Δ_e	P_e	Δ_y	P_y	$\Delta_{max}=$ Δ_u	$P_{max}=$ P_u	Maximum Capacity at 90 mm
w1	Push & Pull	17.5	6.6	38.8	14.6	60	16.5	18.2
W2	Push	4.8	12.6	10.2	26.7	60	31.5	33.1
	Pull	16.4	15.8	33.3	32.1	60	39.6	52.6
	Ave.	10.6	14.2	21.7	29.4	60	35.6	42.9
w3	Push	10.0	7.1	19.8	14.1	60	17.8	22.5
	Pull	20.2	10.9	45.6	24.6	60	27.2	34.0
	Ave.	15.1	9.0	32.7	19.3	60	22.5	28.3
w4	Push	10.3	18.6	21.1	38.0	60	46.4	52.4
	Pull	16.9	17.2	36.3	37.0	60	43.1	56.4
	Ave.	13.6	17.9	28.7	37.5	60	44.8	54.4
W5	Push	11.1	20.1	23.9	43.1	60	50.2	60.0
	Pull	15.6	16.4	35.3	37.0	60	40.9	46.6
	Ave.	13.4	18.2	29.6	40.1	60	45.6	53.3

172

w6	Push	12.4	17.9	25.3	36.5	60	44.7	49.0
	Pull	9.0	14.7	16.6	27.2	60	36.8	43.6
	Ave.	10.7	16.3	21.0	31.9	60	40.8	46.3
w7	Push	15.1	18.8	30.8	38.5	60	47.1	54.4
	Pull	18.5	17.4	40.4	37.9	60	43.4	58.2
	Ave.	16.8	18.1	35.6	38.2	60	45.3	56.3
W8	Push & Pull	15.9	6.3	32.3	12.7	60	15.7	20.9
w9	Push	13.3	21.7	28.1	45.9	60	54.3	69.1
	Pull	12.0	19.6	24.5	40.1	60	49.1	60.6
	Ave.	12.7	20.7	26.3	43.0	60	51.7	64.9
w10	Push	12.3	23.0	25.7	48.1	60	57.5	70.6
	Pull	15.5	22.2	33.0	47.2	60	55.4	69.0
	Ave.	13.9	22.6	29.4	47.7	60	56.5	69.8
W11	Push	13.5	25.1	28.5	52.9	60	62.7	75.6
	Pull	11.7	26.4	23.8	53.6	60	65.9	80.8
	Ave.	12.6	25.7	26.1	53.3	60	64.3	78.2
w12	Push	15.5	24.8	32.4	52.0	60	62.1	80.4
	Pull	12.7	26.7	26.3	55.2	60	66.8	78.0
	Ave.	14.1	25.8	29.3	53.6	60	64.5	79.2
w13	Push & Pull	16.8	24.9	36.5	54.0	60	62.2	74.3
W14	Push & Pull	17.5	22.2	37.9	48.1	60	55.5	67.4
w15	Push & Pull	13.1	27.4	27.7	57.9	60	68.4	78.9
w16	Push & Pull	9.1	28.9	18.7	60.2	60	72.3	81.7
w17	Push & Pull	10.8	12.3	22.0	25.1	60	30.7	36.9
w18	Push & Pull	11.5	27.6	22.9	54.9	60	68.9	78.8
w19	Push & Pull	9.8	13.4	19.4	26.4	60	33.4	39.3
w20	Push & Pull	6.2	34.4	12.3	70.40	60	86.2	100.1

A comparison of the ultimate strength (at 90 mm lateral displacement) and the strength at maximum allowable drift (2.5% drift or 60 mm lateral displacement) for all models, as well as the experimental specimen (HW4) is shown in Figure 7.17. It shows that all walls can capture higher resistance after reaching their maximum allowable drift, which can be considered as one advantage of hybrid CFS walls in seismic regions. In addition, except W1-W3, W8, W17 and W19, all other walls can attain reasonable ultimate resistance, though the other parameters need to be also investigated for them.
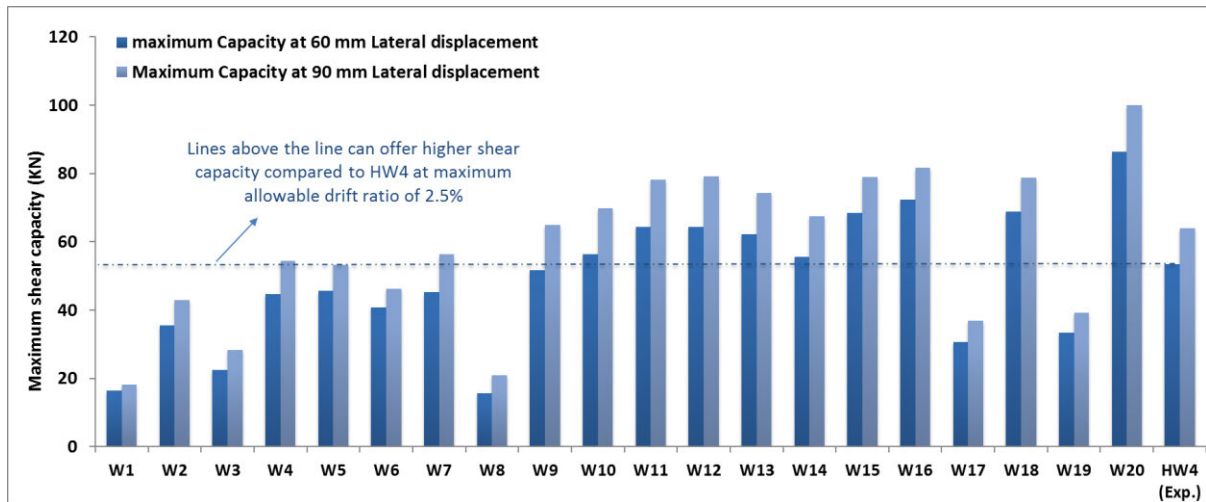
Figure 7.17. Maximum shear capacity of hybrid wall models and experimental specimens HW4

7.5.1 Stiffness, ductility ratio and energy absorption

Stiffness, ductility ratio and energy absorption of the system are also three other parameters that can greatly show the characteristic of the hybrid wall panel.

The stiffness of the models is calculated using secant stiffness at a lateral force equal to 40% of the ultimate strength of each model according to EEEP model. As indicated in Figure 7.18, the secant stiffness of the models W2, W6, W9-W13, W15, W16, W18 and W20 is higher than experimental specimen HW4. Stiffness of models W1, W3 and W8 is significantly lower than HW4, which indicates that these models are not a better alternative for specimen HW4 for mid-rise structures. For model W4, W5 and W19, no considerable improvement is observed on the stiffness of the wall panel. Models W20 and W16 and W20 exhibited the highest stiffness among all proposed hybrid walls, which can be attributed to the X shape bracing system resulting in shorter diagonal elements.

Ductility ratio is another important indicator for evaluation of CFS walls, which means the ratio of the ultimate displacement (Δ_u) to the yield displacement (Δ_y), where the displacements Δ_y and Δ_u are calculated using the EEEP method. It should be noted that the walls do not exhibit brittle behaviour due to truss-bracing configuration, as well as the nature of SHS elements, which prevent from earlier buckling. The calculated ductility ratio of all models is shown in Figure 7.18. According to this figure, it is concluded that all wall panels, except W1, W7, W8, W13 and W14, can provide higher ductility ratio compared to the experimental specimen (HW4). Ductility ratio of the

174

model W2 is relatively high compared to most of the walls. This is mainly because the long diagonal brace is under pure ductile deformation resulting in higher ductility. Interestingly, for specimens W17 and W19, although the stiffness of the system is significantly lower than HW4, the ductility ratio is increased dramatically. Among all these modelled walls, only W4-W6, W9-W12, W15, W16, W18 and W20 can offer both higher stiffness and higher ductility ratio compared to HW4, which indicates their superiority. The values above both blue and red lines in Figure 7.18 show those models with superior performance compared to HW4.
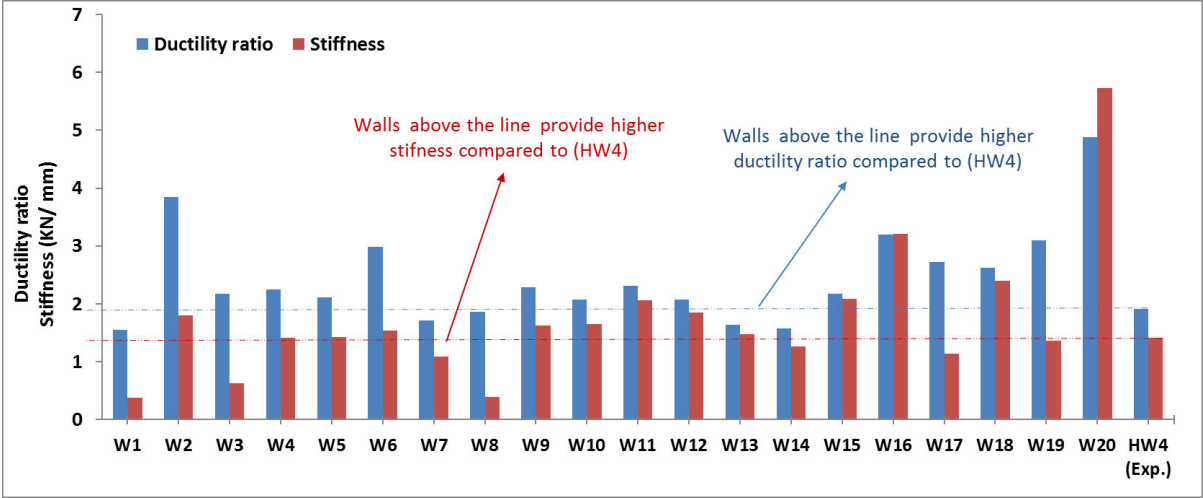
Figure 7.18. Secant stiffness and ductility ratio of the hybrid wall models

The energy absorption can also be determined based on the area under the lateral load-displacement curve. Figure 7.19 compares the energy absorption capacity of the different hybrid walls obtained from numerical models. The energy absorption is calculated based on the maximum allowable drift of 2.5% (60 mm lateral displacement). The energy absorption for wall models with asymmetric SHS truss brace configuration is calculated as the area under the load-displacement curve for pushing and pulling phases separately, and the mean value is then extracted. As illustrated in Figure 7.19, the energy absorption of specimens with shorter diagonal bracing is higher than the energy absorption of specimens with moderate or longer diagonal bracing (W1, W2, W3, W8, W17 and W19), as expected. On the other hands, for the walls with long SHS braced elements the energy absorption is relatively low which is caused by the fact that the shear capacity of the walls decreased rapidly as the local buckling of diagonal brace is observed. The energy absorption capacity of

175

specimens W16 and W20 is higher than all specimens because the energy dissipation mechanisms of these walls are mainly attributed to the deformations in X braced truss members.
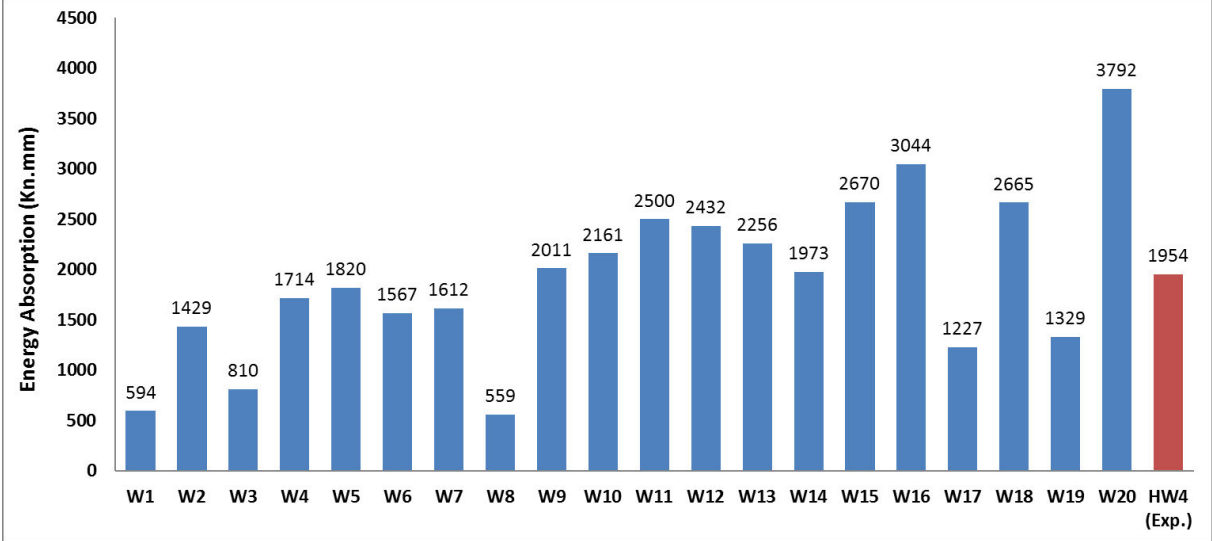
Figure 7.19. Energy absorption of hybrid wall models

The calculated stiffness, ductility ratio and energy absorption are tabulated in

Table 7.4, where the values for wall models with asymmetric truss brace configuration are the average of pushing and pulling phase results.

Table 7.4. Values of stiffness, ductility ratio and energy absorption for hybrid wall models

Wall	Stiffness	Ductility ratio	Energy absorption
W1	0.38	1.55	594
W2	1.80	3.85	1429
W3	0.63	2.17	810
W4	1.41	2.25	1714
W5	1.43	2.11	1820
W6	1.54	2.99	1567
W7	1.09	1.72	1612
W8	0.39	1.86	559
W9	1.63	2.29	2011
W10	1.65	2.07	2161
W11	2.06	2.31	2500
W12	1.85	2.07	2432
W13	1.48	1.64	2256
W14	1.27	1.58	1973
W15	2.09	2.17	2670
W16	3.21	3.22	3044
W17	1.14	2.72	1227
W18	2.40	2.62	2665
W19	1.36	3.10	1329
W20	5.73	4.88	3792
HW4 (Exp.)	1.41	1.91	1954

7.5.2 Strength to weight ratio

The shear resistance of the CFS wall can be increased by increasing the wall weight if the appropriate configuration of the wall components is employed. However, it is important to provide a shear wall with high shear resistance offering the benefits of a light-weight CFS system. Moreover, the higher weight is an obstacle for prefabrication benefits and can also cause some safety issues during lifting and installation of walls.

Strength to weight ratio (S/W) is known to be as one important parameter for comparing the effectiveness of the structural systems and evaluates the system in terms of strength and weight relationship.

Table 7.5 shows the walls' weight, including CFS part and SHS elements, shear strength at 2.5% allowable drift and the S/W of each hybrid wall model. It should be noted that for calculation of wall weight, the mass of the screws, bolts and hold-downs are ignored.

177

Table 7.5. Walls' weight, shear strength and the S/W of the hybrid wall models

Wall	Weight-SHS (Kg)	Weight CFS (Kg)	Total weight (Kg)	maximum Capacity at 60 mm	Strength to Weight ratio (KN/Kg)
W1	40.2		53.5	16.5	0.31
W2	48.3		61.6	35.6	0.58
W3	49.3		62.6	22.5	0.36
W4	49.3		62.6	44.8	0.72
W5	50.4		63.7	45.6	0.72
W6	51.3		64.6	40.8	0.63
W7	51.3		64.6	45.3	0.70
W8	52.1		65.4	15.7	0.24
W9	53.9		67.2	51.7	0.77
W10	53.9		67.2	56.5	0.84
W11	55.2	13.3	68.5	64.3	0.94
W12	59.2		72.5	64.5	0.89
W13	59.4		72.7	62.2	0.86
W14	60.2		73.5	55.5	0.76
W15	60.8		74.1	68.4	0.92
W16	61.5		74.7	72.3	0.97
W17	62.1		75.4	30.7	0.41
W18	62.5		75.8	68.9	0.91
W19	64.1		77.4	33.4	0.43
W20	65.7		79.0	86.0	1.09
HW4 (Exp.)	51.8		65.1	53.5	0.82

A comparison between S/W of wall models in this study and the experimental specimen (HW4) is also presented in

Table 7.5. The S/W of the wall models W1-W9, W14, W17 and W18 is lower than the S/W of experimental specimen HW4. In addition, it should be noted that although W10-W13, W15, W16, W18 and W20 offer higher S/W compared to experimental specimen HW4, their corresponding total weight is around 2-7 Kg higher than those of experimental specimens. The highest S/W ratio is related to W20 followed by W16 and W11, offering 32%, 18% and 15% better S/W compared to HW4, respectively. This indicates that, with the same specimen size and only 14 kg difference in weight, the load-bearing capacity of this wall is high enough to comply with the requirement of many midrise structures. On the contrary, W1, W3 and W8, i.e. hybrid walls without

bracing, capture S/W ratios between 0.24-0.36 KN/Kg, which are relatively low compared to traditional CFS wall. It shows that the truss-braced shape hybrid walls can offer much better structural performance compared to other types when it comes to their applications in mid-rise construction.

As shown in

Table 7.5, the choice of configuration for the walls results in a significant difference in behaviour in terms of shear strength and ductility, in which some hybrid walls with approximately identical weight can capture different shear strength. For example, comparison of the results between specimens W17 and W18 as well as W14 and W15 shows that the strength of walls with a similar steel consumption can be considerably improved by applying a better bracing configuration.

To sum up, the results indicate that the proposed panels in this study offer the benefits of a light-weight CFS system by keeping the weight and size of the walls reasonably low, while offering much better structural performance. Therefore, panels are suitable system for prefabricated construction.

7.6 Conclusion

Numerical models to simulate the lateral response of hybrid CFS wall systems comprising SHS truss brace and open CFS sections were developed in order to investigate the effect of SHS brace configuration on the seismic characteristic of the hybrid wall panel. Hereinto, a comprehensive modelling strategy with the key modelling features, was presented in details, which was calibrated and validated through experimental tests. Using the validated numerical model, a numerical investigation on 20 new hybrid wall panels was conducted to assess the effect of SHS brace configuration on the load-carrying capacity, failure mode, stiffness ductility ratio, energy absorption and strength to weight ratio of the examined hybrid system. Results from the developed numerical models show that the type of SHS configuration can significantly affect the shear performance of the hybrid wall panel. Employing X brace configuration such as W16, W20 dramatically increased the shear strength, ductility, lateral stiffness and energy absorption of the hybrid wall panel compared to experimental specimen HW4. The results also showed that among all proposed hybrid wall models, only W4-W6, W9-W12, W15, W16, W18 and W20 could offer both higher

stiffness and higher ductility ratio compared to HW4, indicating the superiority of these walls compared to the experimental specimen. The overall behaviour of wall models W11, W12, W16, W18 and W20 is reasonably acceptable to be used for mid-rise construction.

The detail numerical model presented in this chapter can also be used as alternative for the time-consuming and expensive experimental tests for the design of hybrid systems, and can be considered as a reference for future numerical studies on hybrid CFS structures. Further studies are also required in order to investigate the effects of connections and the thickness of SHS elements on the hybrid lateral performance.

Chapter 8   Sustainability of hybrid buildings

8.1 Introduction

Apart from its effects on the economy and society, building construction is a key driver of natural resource consumption and emissions to the environment. For a building project to be regarded as sustainable, all the sustainability factors such as environmental, economic and social aspects need to be taken into account [265-268]. Figure 8.1 shows the evolution of sustainable construction concept over the passage of time and illustrates how traditional engineering has been widened since environmental demands were incorporated in the design. Unlike the traditional ideology which would only consider time, cost and quality for construction, in sustainable design, issues such as emission, resource depletion, and conservation of biodiversity has taken a forward step, emerged and are supported by many design standards [269].
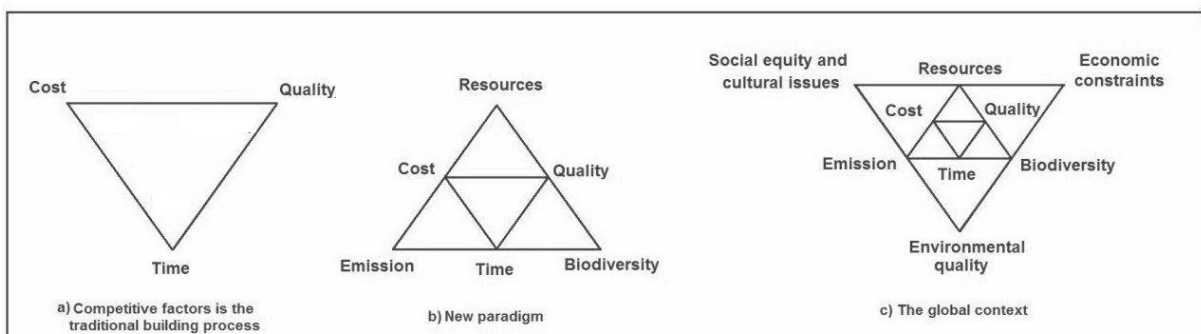
Figure 8.1. Sustainable construction over time [270]

With regards to the economic assessment, the cost has been traditionally considered

as the most influential element in the decision-making process [271-274]. Although in the construction field, the application of life cycle costing is still limited and facing practical problems [275, 276], there is a growing body of research investigating life cycle assessment (LCA) of buildings and structures in terms of environmental impact in Europe and North America as well as in Australia [277-279]. These studies vary remarkably in terms of their method, the building components that are studied, and their degree of complexity. Alongside environmental issues, social costs (traffic, pollution, dust, noise, etc.) of buildings have also increasingly been acknowledged in the literature through a variety of case studies [265, 271, 280, 281].

Each year, the energy used by buildings in North America causes more than 2,200 megatons of CO_2 to be released into the atmosphere. In the United State, buildings account for 39% of primary energy use, 38% of all carbon dioxide emissions, and around 40% of all raw material use annually [282]. The same trend is also reported in Canada which has convinced the enterprises in North America to call for energy performance improvements in the building sector. Over the last two decades, there has been an industry movement towards the design and construction of more energy efficient buildings in North America.

In recent years, several sustainable construction systems have been proposed and developed in using standardised lightweight frames and materials [1, 22, 95, 283, 284]. Hybrid CFS framed structures, are an example of these new construction systems [95, 96, 122]. Despite many advantages of hybrid CFS construction, this system still needs further investigation with regard to the environment, economic and social effects, as well as structural performance in mid-rise construction. Therefore, this chapter examines the application of hybrid CFS structural frame and compares its performance in different terms by an Ordinary Moment Resisting Frames (OMRF) as a representative of conventional HRS structures in North America.

8.2 Limitation of study

Similar to any other research, there have been some limitations related to the analyses approach and the factors influencing the results when it comes to evaluating a new structural system. As the introduced hybrid CFS structure is still in its design stage, and it is not applied to a real construction project yet [95, 96], there are some difficulties for sustainability and social impact assessment of this structural system. A significant

difficulty dealing with this research is data collection for a case study analysis. Full life-cycle assessment of hybrid CFS buildings is another challenging task, primarily due to the lack of cost and environmental impact data for the whole cycle. On the other hand, when a study is intended to be disclosed to the general public, a critical review should be carried out by a number of interested parties. In practice yet, it will be difficult for reviewers to assess any environmental or economic claim of relative values of different sustainability studies. It will be even harder for other stakeholders without lack of information about the study context, to judge the sustainability claim toward the preference or equivalence of one product against a competing product that performs similar or the same function. Therefore, this chapter only evaluates cost, environmental and social impacts for building construction stage (building structural frame) as there is no data available for performing a thorough life cycle assessment. The material production stage is also considered for the environmental assessment as data collection is available for this stage. To that end, two case studies are used to gain a better understanding of the decision-making process for the selection of the most appropriate steel structural frame.

This level of research can be an added value of sustainability for hybrid CFS structures with an important step forward for more future research in this area. Related studies on this field should be accomplished over time, however, it might take a few years to collect an extensive data collection for hybrid CFS structures as this building industry is comparatively new. In future, with the development of hybrid CFS structures, it is expected that researchers will be able to overcome these barriers.

8.3 Case study and design

A designed hybrid CFS building is required to evaluate the system in terms of cost, environmental and social impacts. Therefore, in this study, the methodology for designing a hybrid CFS building presented by Mortazavi et al. [285] is employed (including architectural plan, location of the building, the number of storeys, primary calculations and assumptions and imperfection effects), and then the designed building is utilised for environmental assessment, social impact and cost analysis.

A four-story building located in Los Angles is designed using two structural systems: hybrid CFS and OMRF, with the same architectural plan for a typical mid-rise development, as shown in Figure 8.2. Los Angles is located on one of the most active earthquake regions; thus, the seismic performance of buildings in this zone is of great

importance. The materials and the systems considered in this study specifically complies with the Los Angeles city. The building accommodates four residential units in every level of 21m × 16.2m in plan and 3m in height with the total height of 12m. As shown in Figure 8.2, the building comprises six and three spans in horizontal (X) and vertical (y) directions, respectively.
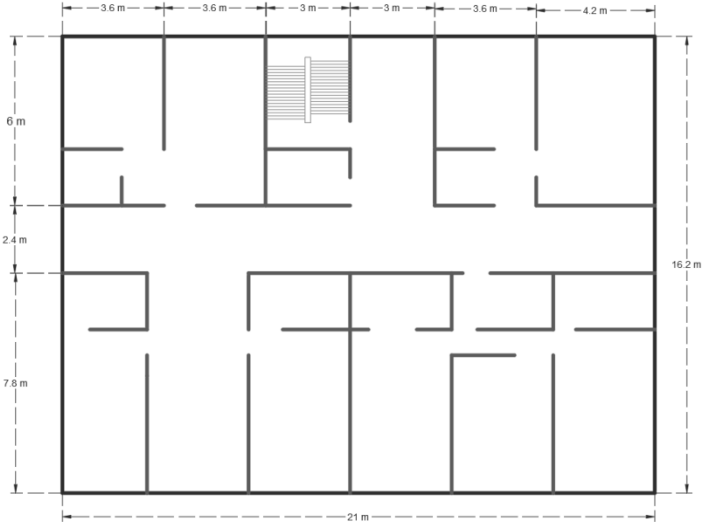
Figure 8.2. Plan layout of the case study building

ETABS Software [286] was utilised for modelling of the building under both gravity and seismic applicable loads according to ASCE7-16 [54]. The analysis involves live load, dead load, super dead load and cladding load. The dead load is a self-weight calculated by ETABS according to the material self-weight. Due to the assumption of the rigid diaphragm for the flooring system, the connection details are not examined in this study. Both buildings were loaded and analysed according to ASCE7-16 [54] and designed according to AISC360-16 [287]. The CFS studs are separately designed according to AISI-S136-16 [288]. The general information, assumptions and primary calculations required for the design of both buildings are given in Table 8.1.

Table 8.1. Primary calculations and assumptions required for the design of the building

Parameter	Location	Type of Building	Soil class	Live load	Superimposed dead load
Detail	Urban California Region	Residential 4-Storey Building	Very Dense Soil and Soft Rock (Class $C)$	1.92 KN/m^2 for typical floors and 0.96 KN/m^2 for roof	1 KN/m^2 to all floors
Parameter	R-factor	Ω_0	C_d	Seismic design category	Risk category factor
Detail	3.5	3	3	D_{max}	I

8.3.1 Design of OMRF system

OMRF has proven to be reliable lateral load resisting systems through a wide range of studies on their seismic behaviour in low-rise to mid-rise structures [289-291], and is easily done in structural engineering practice level. Therefore, as their application is not generally new, the design procedures of this system have also been ignored in this study. The 3D model of the designed OMRF system is shown in Figure 8.3. Different universal beam and column profiles including 200UC60, 150UC30, 200UC46, 250UB37 and 250UB26 were considered for the design of framing members for the OMRF building. The steel decking concrete floor system with 90 mm concrete thickness was employed for the modelling of the floor since this system is being extensively used as one of the conventional flooring methods for the North America buildings and can also be simulated as a rigid diaphragm. It should be mentioned that the steel decking concrete floor is accounted for as one of the lightest flooring systems compared to a composite floor or concrete slab floors.
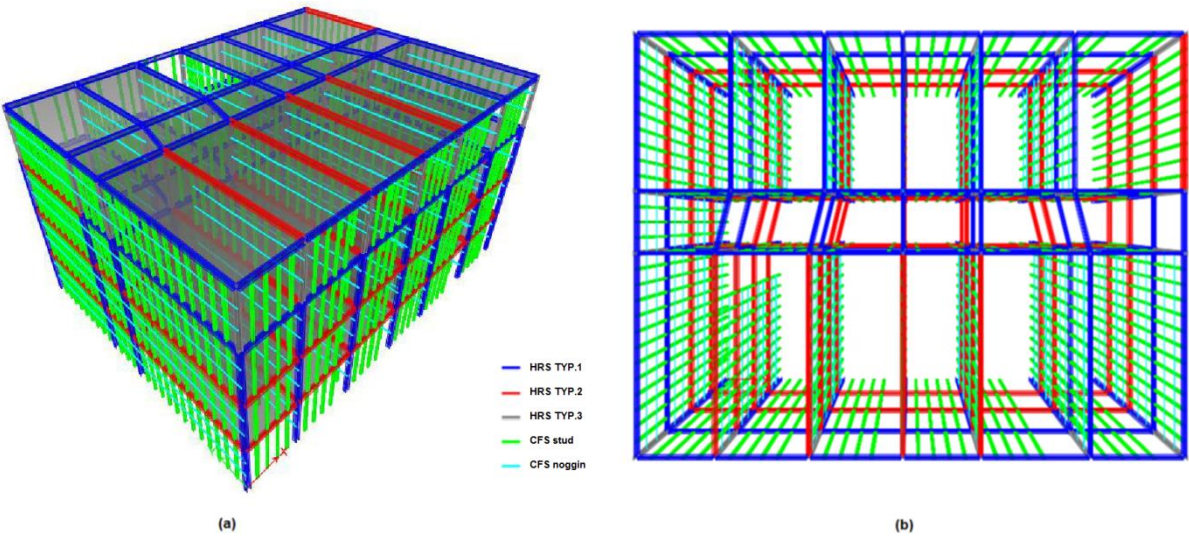
Figure 8.3. 3D model of the conventional OMRF structure   a) 3D view   b) top view

8.3.2 Design of hybrid CFS framed system

The hybrid CFS panel, which its cyclic behaviour was experimentally evaluated by Mortazavi et al. [95], was employed for the design and modelling of hybrid CFS building. The hybrid panel utilises an SHS panel as the main lateral load resisting element connected to CFS panel enduring a major part of gravity loads. In this system, the lateral seismic force is transferred to the SHS part of the panel and the CFS studs

do not provide lateral force resisting capacity. The vertical load can be resisted by either CFS or SHS elements in the wall panel according to their tributary areas.

Having the concept of hybrid CFS wall panel, a 4 storey building is designed and analysed using the hybrid CFS panels as the main LFRS. For building design, the SHS elements have a dimension of 89mm×89mm×6 mm. Figure 8.4 shows the 3D model of the hybrid CFS building with the CFS studs structurally connected to the floors. The section details employed for the hybrid CFS building is also provided in Figure 8.5.
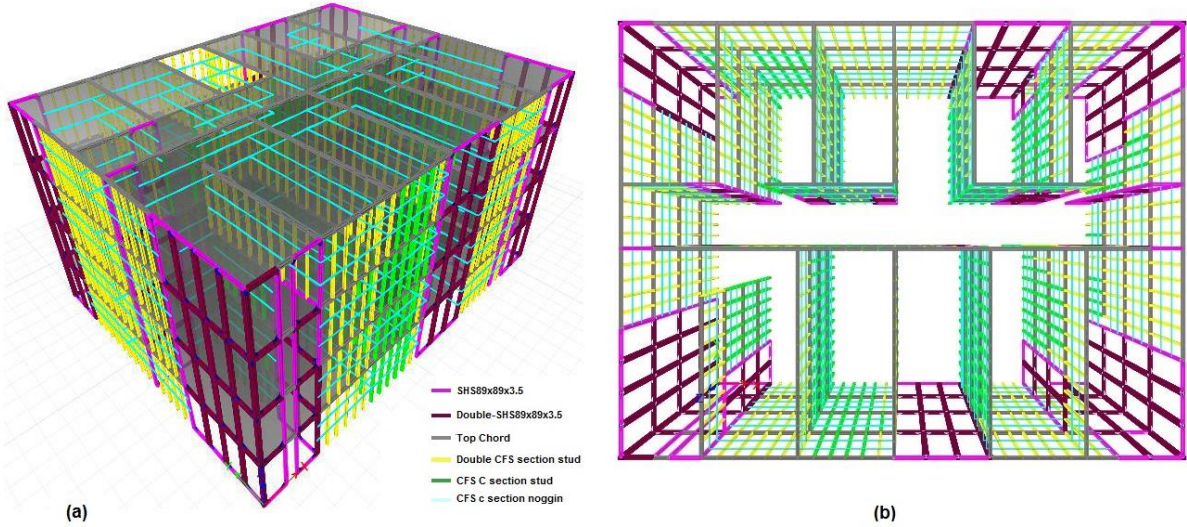
Figure 8.4. Preliminary design and the location of hybrid CFS panels
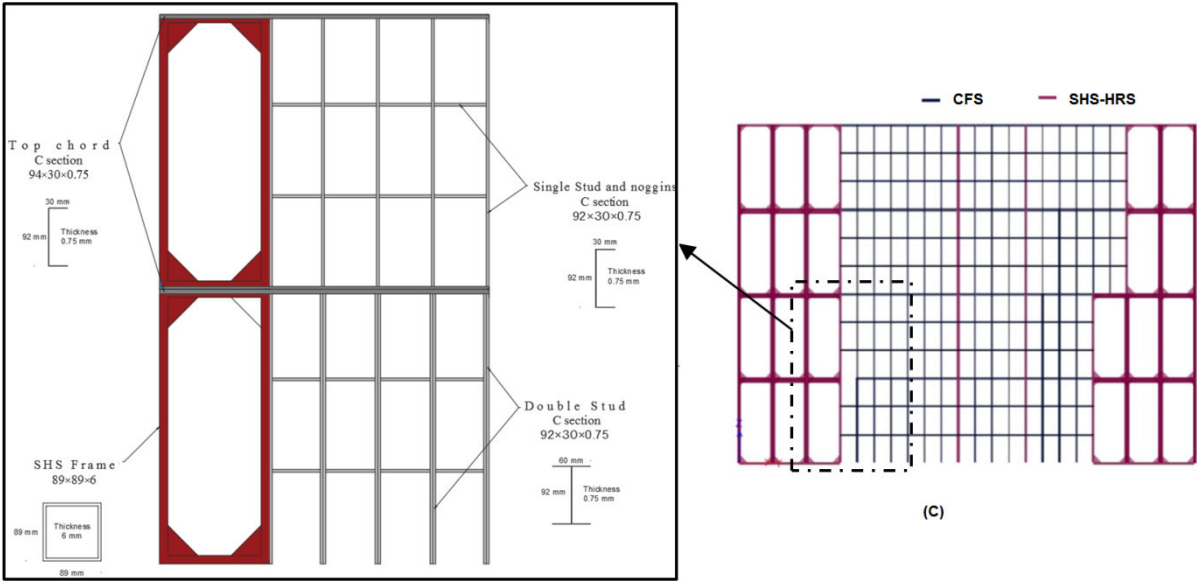
Figure 8.5. Preliminary design and the location of hybrid CFS panels: a) Side view, b) Top view, c) External elevation view and details of the sections

186

CFS composite floor was used for the diaphragm. During recent years, CFS composite floor systems have been increasingly used in residential building in North America [292-297]. The application of this type of floor has been well established in both American and Canadian design codes. Gradually, design procedures for floor systems (commonly used within the North American residential construction industry) were developed for lightweight framing construction systems; however, they have not been adequately adapted for standard structures. It is because the behaviour of the CFS composite floor compare to the HRS framing in the MRF system may not be rigid enough to be considered as a rigid diaphragm in the design procedure. Although this type of flooring system is being extensively used for lightweight buildings in North America, there is a lack of adequate design guidelines for the lightweight CFS floors to be used for standard structures as well as to consider the composite action on the capacity of the diaphragm and its rigidity and vibrations [294-296]. Comprehensive test results are required for better understanding of the performance of CFS lightweight floor systems. Several research have been conducted to better establish the stiffness, strength and ductility capacity of CFS framing diaphragms [96, 298]. The test results recently conducted at WSU indicated that lightweight CFS floors supported by CFS truss joists behave essentially as a one-way slab system and can be also considered as a rigid diaphragm in the modelling [299].

In addition to the dynamic analysis, the imperfection effects need to be considered in the linear elastic analysis. There are different ways of considering imperfection effects in a structural analysis like notional load, probabilistic approaches, fuzzy randomness, etc [300]. The code AISI-S136-16 [288] considers notional loads to be applied to the lateral framing systems to account for the imperfections. In this study, the imperfection effects were considered and applied to the structure. Then, the maximum storey drift, considering the notional loads on the building, is compared to the allowable storey drifts. According to ASCE7-16 [54], for the current four-story building in the risk category I, the allowable story drift was calculated as of $\Delta_a = 0.025h = 0.00714.$, and consequently the maximum story drifts were less than allowable story drift.

Once the hybrid CFS structure is fully designed based on the AISC360-16 [287], the axial forces and the bending moments were extracted from the analysis in order to be used for the design of CFS studs [288].

8.4 Analysis of Structural performance

Having completed the frames' design, the sections employed for each structure with the total weight are shown in Table 8.2. A comparison between the total weight in the 4-storey building (frame and flooring system) for two different construction method is also represented in

Table 8.3 and Figure 8.6. Since lightweight floor system is employed for the hybrid CFS structure, which is being widely used for CFS structures [292-296], the overall building weight is considerably lower than that of the OMRF structure. In addition, as the gravity load is also resisted by CFS studs in the hybrid CFS building, the second-order design leads to members with smaller sections, thus a lighter frame is obtained. It can also be seen that the total steel consumed in the hybrid CFS frames is lower than that used in the OMRF system.

It should be noted that in the OMRF system, the CFS studs are employed to form the interior partition walls or exterior facades; while, the main lateral force resisting system is the steel moment frame. Therefore, the CFS studs are not structurally connected to the frame and make no contribution to the axial force bearing system. The studs instead are aligned laterally every 600mm to provide sufficient support for finishing surfaces of the wall. The reason for considering the CFS studs in the OMRF building is to provide a similar and fair condition for the environmental and economic assessment. In the hybrid CFS structure, the building is prepared for the installation of the sheathing panels on the CFS studs; therefore CFS studs were also taken into account for OMRF building to compare it with a structure similar to hybrid CFS condition.

Table 8.2. Sections designed for the OMRF and hybrid CFS systems

	Section	Weight (KN)		Section	Weight (KN)
Hybrid CFS	SHS89x89x6	117.3	*OMRF*	Double- C section 92-75-30	58
	Double-SHS89x89x6	311.1		Noggin	1.3
	C section 92-75-30	12.7		200UC60	78.2
	Double- C section 92-75-30	21.8		150UC30	80.1
	Top chord	7.9		200UC46	228
	Noggin	1.9		250UB37	253.8
	Light weight floor	1858.7		250UB26	192.2
				Slab floor system	3055.4

Table 8.3. Weight of the structural steel and floor system for both hybrid CFS and OMRF structures

Material Type	Weight (KN)		Floor Area (m²) Hybrid CFS and OMRF	Weight per area (KN/m²)	
	Hybrid CFS	OMRF		Hybrid CFS	OMRF
Column (SHS for hybrid and HRS for OMRF)	311.1	386.3		0.241	0.300
Beam (SHS for hybrid and HRS for OMRF)	117.3	446	1288.8	0.091	0.346
CFS-stud	34.6	58		0.037	0.045
CFS-track and noggin	9.8	1.3		0.008	0.001
Floor	1858.7	3055.4		1.44	2.37
Total	2330.5	3947		1.81	3.062
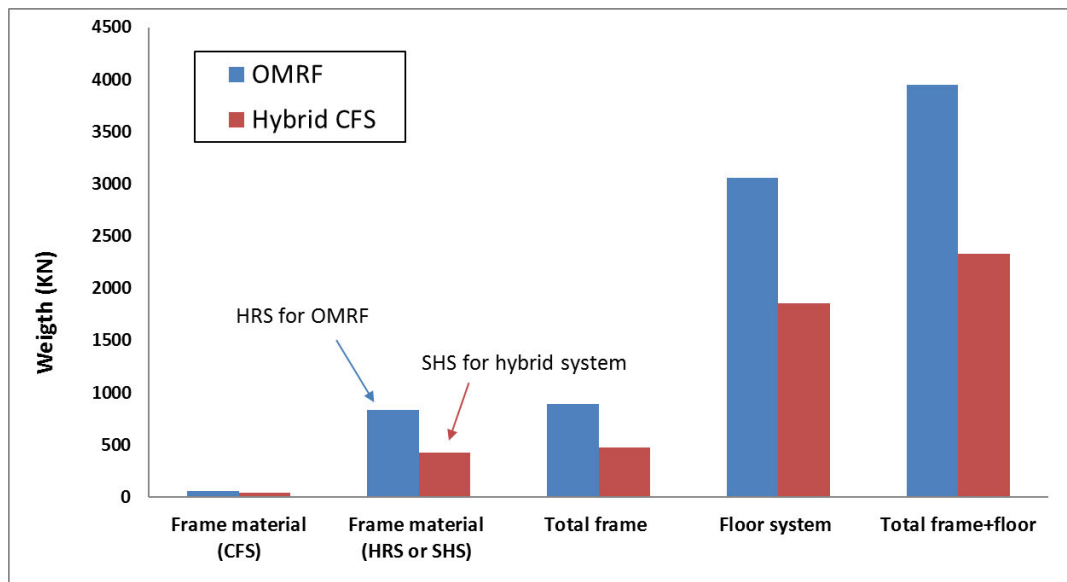
Figure 8.6. Comparison of the total weight of the structure

Having a lighter structure in weight, the hybrid CFS system offers reduced base shear resulting in an efficient LFRS. Table 8.4 and Figure 8.7a illustrate the values of the storey shears. It can be seen from the results that the storey shears for the hybrid CFS are smaller than the OMRF structure. In addition, Table 8.4 and Figure 8.7b illustrate the values of drifts in the X and Y directions, induced by the earthquake loading in X and Y direction, respectively. It is obvious from the results that for the hybrid CFS structure, the drift in X direction is smaller than the drift value in the Y direction. This can be justified by the fact that the number of hybrid CFS panels in X direction is more than Y direction which results in higher building stiffness in this direction. In general,

both structures showed acceptable performance with respect to storey drifts in both directions, while the drift values for the OMRF structure is slightly higher than those for hybrid CFS system. The higher values for storey drifts in OMRF are related to its framing type. Figure 8.8 shows the first three modes of building period for each structure. The modal data of the structures indicates that the frames' period values for the hybrid CFS system are shorter than its counterpart.

Collapse assessment of structural systems and uncertainties involved is also another important aspect in design process [20, 96, 301-303]. However, evaluating the collapse behaviour of this new system needs further details and discussions which are out of the scope of this study, and has been thoroughly discussed by Kildashti et al. [96].

Table 8.4. Drift and shear values of the systems in the X and Y directions

Storey	Direction	Drift		Shear force (KN)	
		Hybrid CFS	OMRF	Hybrid CFS	OMRF
Storey 4	Y	0.006279	0.00658	159.5	235.4
	X	0.006235	0.006476		
Storey 3	Y	0.006977	0.00674	280.5	410.7
	X	0.006169	0.006403		
Storey 2	Y	0.00707	0.006702	358.5	524.8
	X	0.006098	0.006257		
Storey 1	Y	0.005913	0.006308	402.6	576.3
	X	0.005035	0.005652		
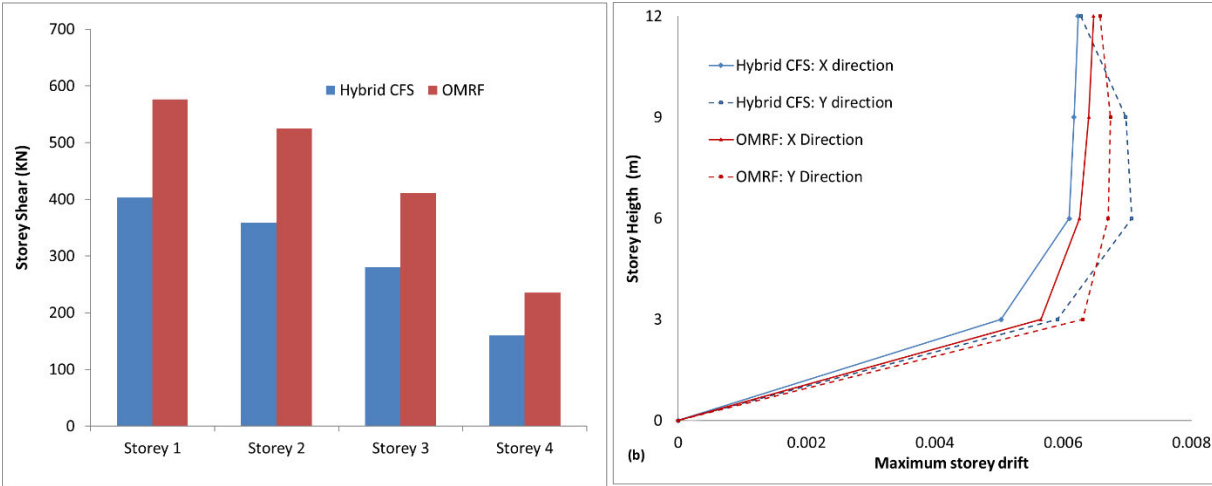
Figure 8.7. a) Storey shear, b) storey drift
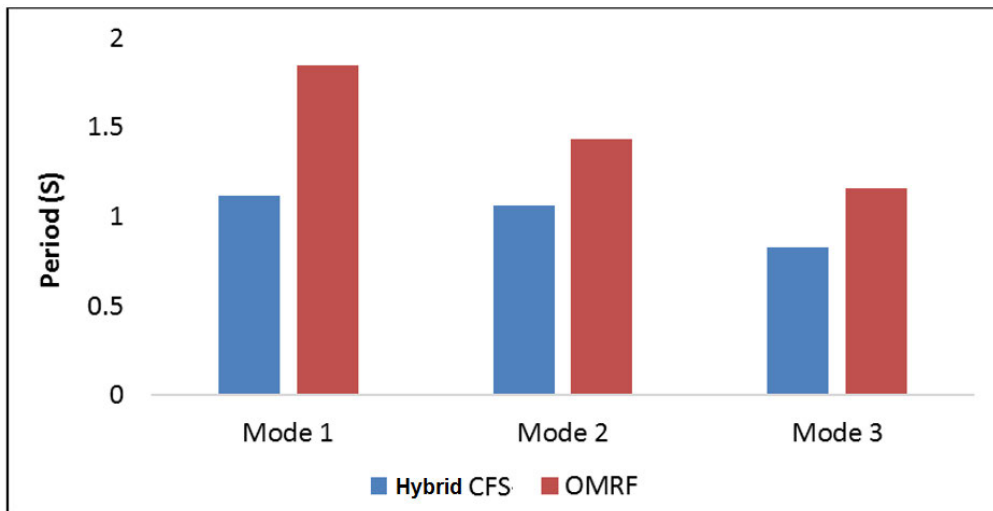
Figure 8.8. The first three modes of building period for each structure

8.5 Environmental assessment

The energy consumption and carbon emission, as the most commonly assessed environmental indicators in the built environment research, are investigated by considering the quantity of energy required or carbon released by all the activities associated with a production process of each system. Employing the existing techniques, the environmental impacts associated with the product of material (such as manufacturing and transport), and construction process (building and transport) are compared for the hybrid CFS and OMRF systems. The impacts associated with the operation, maintenance and eventual deconstruction of the frame are not included in this section due to unavailability of data required.

Being made of non-homogenous components and various materials interlocked within different sub-assemblies, accurate accounting for buildings' environmental impacts at each stage of the raw material acquisition, processing, manufacturing, transportation and construction is not an easy task. To address this challenge, a developing list of computer programs is becoming available to evaluate the environmental impacts of both building materials processes. ATHENA EIE [304] for buildings is a strong computer program to assess the environmental impact of buildings according to internationally recognized LCA approaches. In this study, the ATHENA EIE for Buildings v4.0.64 is utilized to measure the environmental impacts associated with the construction of both case study structures in this study.

191

A summary of the different environmental indicators in the construction of both structural systems in this study is given in Table 8.5. The product of material includes manufacturing plus transportation of material to the factory; while, construction process means the construction-installation process in addition to the transportation of material from the factory to the construction site. It can be seen that the structure of hybrid CFS system (including frame and lightweight floor system), performs considerably better than the conventional OMRF structure across all the environmental impact categories. As indicated in Figure 8.9 and Figure 8.10, hybrid CFS framed system offers 12% less Global Warming Potential (GWP) and 3% less Fossil Fuel consumption impact compared to OMRF system. By application of hybrid CFS frames in design, the total primary energy, non-renewable energy and smog potential are also decreased within a range of 5% to 17%. The highest environmental effect of a hybrid CFS frame is in Non-renewable energy by 17.3% lower effect on ozone compared to that of its counterpart. This is mainly because of the lower weight and consequently lower material usage.

Table 8.5. Environmental effects of the hyrbid CFS and OMRF structures

Environmental parameter	Structure type	Unit	Product (Manufacturing + Transport[*])	Construction Process (Construction-Installation Process + Transport[**])	Total effects (Product and Construction process)
Global Warming Potential	Hybrid CFS	kg CO_2 eq × 10^3	143	26.9	169.9
	OMRF		164	26.1	190
Fossil Fuel Consumption	Hybrid CFS		1560	354	1914
	OMRF		1620	349	1969
Total Primary Energy	Hybrid CFS	MJ × 10^3	2070	363	2433
	OMRF		2480	359	2839
Non-Renewable Energy	Hybrid CFS		2050	361	2411
	OMRF		2470	359	2829
Smog Potential	Hybrid CFS	kg O3 eq × 10^3	8.2	8.5	16.7
	OMRF		9.1	9.9	19
Ozone Depletion Potential	Hybrid CFS	kg CFC-11 eq × 10^{-3}	0.8	0.1	0.9
	OMRF		0.9	0.05	0.9

[*]Transport to factory, [**]Transport from factory to building
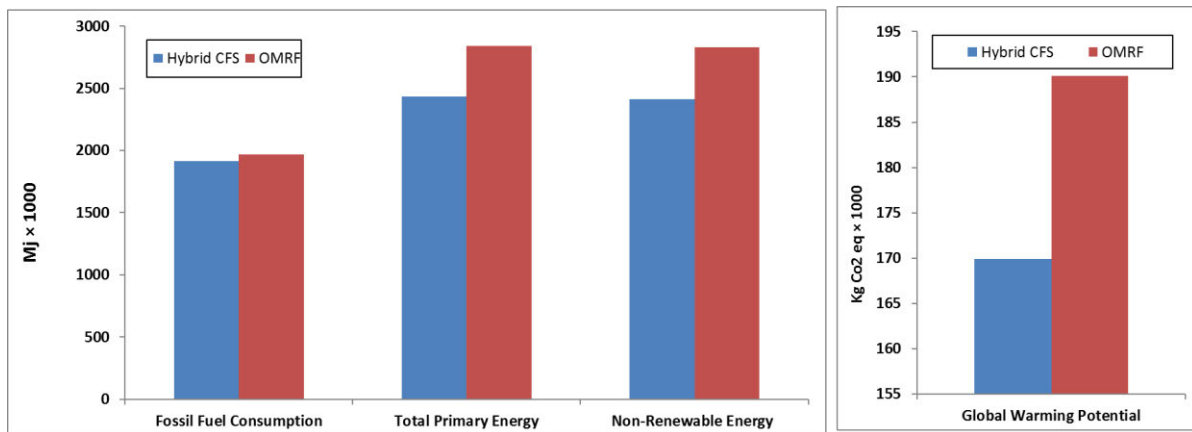
Figure 8.9. Comparison of environmental parameters for both structures
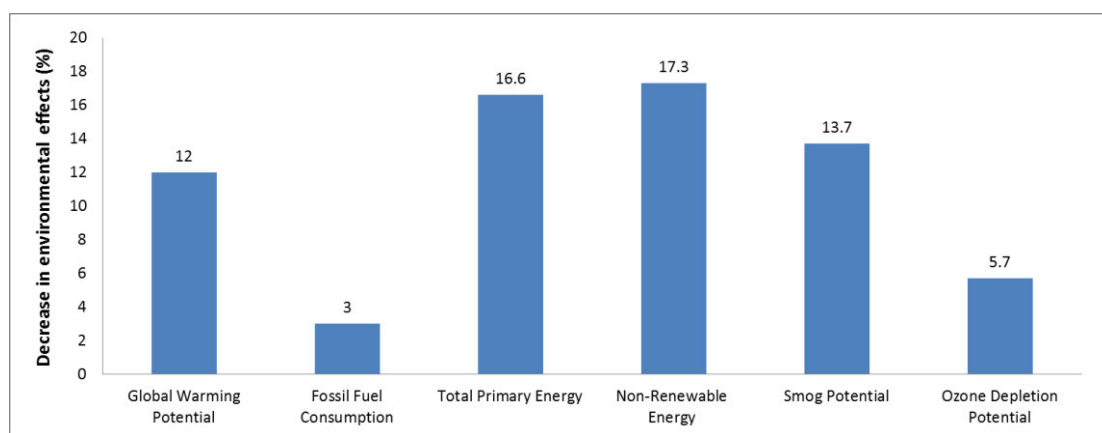
Figure 8.10. Percentage of decreasing environmental effects by application of hybrid CFS frame

Different resources used for the manufacture of material and construction of structure are also listed in Table 8.6. The proportion of the hybrid CFS to OMRF is used for a better comparison of the results. Except for iron ore and coal, all other resources used for hybrid CFS structure are lower in quantity compared to the resources used for its counterpart. Interestingly, the consumption of iron ore in hybrid CFS frame is around twice of OMRF. This is due to the fact that, unlike HRS material, which has a very high recycled content, CFS material usually contains 25% or less recycled content. As described in [305, 306], for manufacturing of CFS virgin materials with a low amount of residual elements such as copper and steel are required. This is mainly because the recycled material can have an adverse impact on the steel properties, restricting it from being rolled into thin sections. Hence, using the recycled material for manufacturing of CFS sections must be restricted. As CFS requires the use of pure material, the higher value in using iron ore for hybrid CFS frame could be expected. Table 8.7 shows the energy consumption by details for the construction of both framed structures. The table

illustrates that by using hybrid CFS instead of OMRF system, significant savings in energy consumption can be achieved. Yet, the hydro, gasoline energy and renewable energy consumption for hybrid CFS system are more than conventional OMRF structure.

Table 8.6. Comparison of resource used for the construction of both structures

Material	Unit	Total = Product +Construction		
		Hybrid CFS	OMRF	$\dfrac{Hybrid\ CFS}{OMRF}$
Carbon dioxide, in air	Kg × 10³	1.8	1.8	1.0
Clay & Shale		2.3	1.3	1.8
Coal		35.1	32.7	1.1
Coarse Aggregate		111.7	255.2	0.5
Dolomite		5.4	6.9	0.8
Ferrous scrap		51.9	108	0.5
Gypsum (Natural)		1.6	1.3	1.2
Iron Ore		39.6	19.8	2.0
Limestone		54.1	46.5	1.2
Natural Gas	m3 × 10³	15.5	16.4	1.0
Crude Oil	L × 10³	6.2	8.6	0.7
Water		1221.4	2044.5	0.6

Table 8.7. Energy Consumption by details for construction of both structures

Energy Source	Total = Product + Construction		
	Hybrid CFS (MJ × 10³)	OMRF (MJ × 10³)	$\dfrac{Hybrid\ CFS}{OMRF}$
Hydro	8.7	2.4	3.6
Non-Hydro Renewable	6.1	1.7	3.6
Coal	882.5	838.8	1.1
Diesel	299.2	319.9	0.9
Gasoline	0.1	0.1	1.4
Heavy Fuel Oil	170.2	177	1.0
LPG	0.3	0.63	0.5
Natural Gas	597.4	636.1	0.9
Nuclear	460.3	853.6	0.5
Wood	9.2	9.7	1.0
Renewable Energy	23.9	13.7	1.7
Primary Energy	2433	2839	0.9
Non-Renewable Energy	2411	2829	0.9
Fossil Fuel	1954	1969	1.0

It should be also mentioned that the environmental effects of a decision often take place many years after the decision was made, and not inevitably in the same region. Environmental decisions, therefore, are identified by noticeable uncertainty at all phases of the decision-making process.

8.6 Economic assessment

In the construction design process, the initial construction cost, so-called capital cost, is a crucial factor while selecting the most economical system. Given that the technology of hybrid CFS structures is in its initial stages, there is not enough real data available for their complete economic assessment. On the other hand, because in this study two types of steel frames are compared against each other, the economic assessment will be mainly limited to the material cost, as the other operational and installation costs are assumed to be the same. It is also assumed that the material maintenance which might be required during the service life of the building due to the weakening of both systems.

Table 8.8 shows the costs associated with the construction of hybrid CFS and OMRF structural frames. The cost estimation was made through the National Construction Estimator package [307] which provides the estimated construction costs for general contractors performing the work with their crews. The prices are estimates of what most contractors who buy in moderate volume will pay suppliers as of mid-2019. Valid industry suppliers were also considered to check the values as the final cost. It should be mentioned that the building costs for each structural system rely on the location where it is constructed. Therefore, for precise cost estimation, Los Angeles location was taken into account as the input of the Estimator package [307]. The suppliers were also chosen from a local industry where the building is located. Figure 8.11 compares the total cost of frames as well as the associated floor system. The results indicate that the hybrid CFS framed construction method is relatively more economical compared to the OMRF structure. Yet, it is not large relative to typical variations that can be found in the cost of home construction. Hence, the qualitative benefits and weaknesses of each construction approach may well govern over the cost-effectiveness of each system in an optimal decision. Components of two structural framing share nearly similar costs, including the manufactured elements, which mean that the cost of the steel frame doesn't differ much in two buildings. The main difference is referred to the cost of the structural steel framing, mainly due to lower steel tonnage for hybrid CFS building.

195

Table 8.8. Estimation of material cost for building both hybrid CFS and OMRF

Section	Material	Cost (USD)	Reference for estimating cost
Hybrid CFS structure			
SHS 89x89x6	SHS	$130,860	[307-309]
Double-SHS89x89x6			
C section 92-75-30	CFS	$13101	[307, 310]
Double-C section 92-75-30			
noggin			
Top chord			
CFS floor system		$38,236	[307, 310, 311]
		Total: $182,197	
OMRF structure			
Double-C	CFS	$3,855	[307, 310]
noggin			
200UC60	HRS	$226,364	[307-309]
150UC30			
200UC46			
250UB37			
250UB26			
Concrete floor and decking		$50,218	[307, 310, 311]
		Total: $280,437	
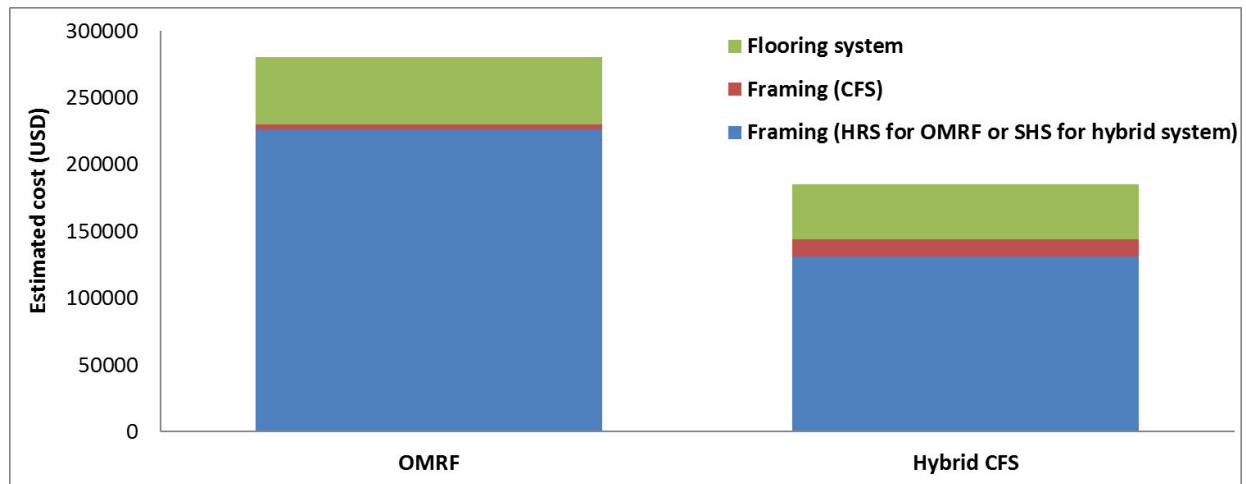
Figure 8.11. Comparison of total estimated material cost for both frames

It can be also claimed that hybrid CFS structural frame requires shallower excavation (due to lower weight) compared to conventional OMRF structure, which also results in lesser construction cost and time. In addition, the difference between construction methods, in terms of the volume of excavation works, leads to a decrease in total

construction cost too. Moreover, conventional OMRF structure requires maintenance in the form of painting, whereas hybrid CFS frame does not; as the galvanised cover insulates the steel against rusting during its service life.

8.7 Social impact assessment

Although the completion of construction projects has a direct positive impact on the society and humans' wellbeing, these buildings, in particular in the urbanised regions, can result in social nuisances for the residents and workers. In the literature, social aspects of construction include issues such as traffic, economic activities, pollution and ecological/social/health [280, 281]. Minimising the impact of such issues, on the society is of great importance. While some studies show that social costs can consider for up to 400% of construction costs on certain projects [312], social costs are not often taken into account during a construction project and design since they cannot be estimated using standard measuring methods. Nowadays, several methods have been introduced for calculating social costs associated with the building industry [281].

Given that both construction methods, being discussed in this study, are in the category of steel structures, their social impacts can be similar in many cases, in particular, when their advantages compared to concrete structures are taken into account [280, 281, 313]. Nevertheless, the ease of prefabrication and offsite activities provide hybrid CFS with some advantages with regard to social impacts. Moreover, being light in weight, hybrid CFS structures require smaller foundations and consequently lower earthworks, i.e. lighter equipment. This will positively affect the on-site vibration noise, dust and air pollution, as well as the risk of injury. Figure 8.12 shows some of the equipment and activities that can potentially make noise and vibration during foundation construction. The decreased time of excavation for foundation and its lower volume of soil excavation in hybrid CFS building contribute low levels of noise and vibration within the construction site and the surrounding area compared to its counterpart building. The shorter time of construction for hybrid CFS structures can also have a positive effect on the construction induced traffic. This causes minor traffic management plan which increases the safety of workers, the safety of motorists and other road users during construction.

Figure 8.12. Equipment and activities creating pollution during excavation and foundation construction

Another positive effect of hybrid CFS structures with respect to the social costs is their impact on the construction by provision of more quickly assembled and affordable houses, because of lower material and construction cost and prefabrication options, as discussed earlier. In general, one can claim that the social impacts related to steel structures can be decreased by employing hybrid CFS systems, mainly due to the lower time of constructing and less volume of material required, and prefabrication-ability. Table 8.9 summarises the social impacts associated with the construction of steel structures as well as the improvements could dealing by using hybrid CFS framed systems.

Table 8.9. Impacts related to steel construction projects in urban environments and improvements by using hybrid CFS frames

General types of social issues related to steel construction projects	Improvements of social issues by using hybrid CFS frames
Traffic	✓ Limited parking space ✓ Increase of fuel consumption ✓ Travel delay ✓ Increased rate of traffic accidents ✓ Road rage ✓ Increase of road deterioration	✓ Less traffic issues and less fuel consumption due to the less time of working and volume of material needed.
Economic activities	✓ Decrease in income ✓ Reduction of productivity ✓ Loss of tax revenues ✓ Property damage	✓ Economic activities face less issues due to the shortening of project time
Pollution	✓ Noise ✓ Dust ✓ Vibration ✓ Air ✓ Water	✓ Less noise and vibration because of using lighter equipment and machinery as well as shorter time of project.
Ecological/social/ health	✓ Treating compromised physical/mental health ✓ Lower life quality ✓ Restoration cost	✓ Safety of adjacent residents and workers is under less risk as the construction work is finishing in shorter time with lighter material and equipment

8.8 Discussion

A majority of the economic, environmental and social impacts of buildings during their

service life are estimated in the early design stages. As much as 80% of the total resources, materials and methods required to construct a building are usually decided in the first 10% of the design process [145, 314]. Adverse impacts from improper building systems compound inefficiency in structure and result in additional initial cost as well as increasing maintenance and operating expenses. In a comprehensive design method, where structural performance and its environmental, economic and social impacts are incorporated into one system, selecting a suitable construction method for a building is extremely important. It is also interesting to mention that for the researchers, comfort is considered the most significant parameter, followed by CO_2 emissions, cost and energy demand [315].

In this study, two steel construction systems (i.e. methods) were evaluated through different control measures in order to develop an effective early-stage decision-making tool. It was shown that in terms of structural performance the hybrid CFS system gives architectural engineers the same design and construction flexibility as OMRF system, while it offers the advantage of lightweight pre-fabrication, manufacturing, transportation and installation. In addition, the hybrid CFS structural frame method is relatively more cost-effective which is mainly because of the lightweight floor system used in hybrid CFS structure. It was also shown that due to the less material used and lighter equipment employed for the hybrid CFS structure the environmental and social issues can also be decreased.

In terms of time-saving it can be said that construction with hybrid CFS systems is more efficient than conventional OMRF systems. This can provide different advantages such as cost savings on site-management and on-site activities, reduction in the cost of finance and earlier return on investment. Since the hybrid CFS panels can be easily manufactured in the factory, their application will come with all the advantages of prefabrication and construction manufacturing. An example is a better quality-control. Panels are almost fully fabricated and built-in production facilities allowing for better quality monitoring control and higher-than-average quality outcomes. The installation of the panels can also be done by labours without a need for heavy cranes, which can accelerate the installation process. Table 8.10 summarises the advantages and disadvantages of the application of hybrid CFS systems in construction industry discussed in this study.

Table 8.10. Advantages and disadvantages of hybrid CFS systems

199

Advantages	Disadvantages
➢ Lighter than conventional HRS structures ➢ Fast constructions work which causes shorter period of project finishing (reduction in project duration) ➢ Needs fewer construction works ➢ Quality control on factory for hybrid CFS panels. ➢ Lower usage of heavy lift cranes (panels can be carried by hand or lift tracks) ➢ Greater economic performance ➢ Better environmental performance ➢ Doesn't need heavy trucks or trains as the weight and length of panels are low and short respectively. ➢ The construction procedure can be conducted at any time because it doesn't need the skilled labour in this field ➢ Shallower excavation due to light frame ➢ Amount of excavation works leads to lessening the intensity of nuisance, vibration and less social impacts ➢ Improvement in social impacts with less sound, vibration and traffic as well as the increase in safety of the workers ➢ Decrease in accident, injuries and fatalities ➢ Prefabrication options, ease of installations and transportation and ease of erection by manual semi-skilled labour ➢ Lower storey drift, shear storey and lower period of the structure ➢ Environmental impacts decreased significantly compared to conventional HRS structure. ➢ Total material cost has been decreased	➢ Large free spans and cantilevers may not be possible by this system ➢ Further design process for CFS parts is needed ➢ Very less or neither numerical/theoretical studies and nor related experimental test data of the hybrid CFS structure exist as a manual for local designer and architecture to develop the systematic lightweight CFS specification ➢ The new framing method is very strange to the general public in term of structure and people still have low confidence about its security, stability and comfort ➢ Recycled content, and use of recycled scrap must be limited as requires the use of virgin materials ➢ Collection challenges and case study buildings are limited for this type of construction therefore complete life-cycle assessment is not possible ➢ Lightweight floor system causes some vibration problems which needs to be further evaluated

It should be noted that both qualitative and quantitative analyses developed in this study are specific to the presented case studies. Although results may be applied for other similar projects, each project has its own circumstances, some of which can significantly change the results. The other limitation of the study is that, because it excludes construction labour work, preparation of the site, foundation and etc, due to the reason that they represent costs related to the site and don't depend on the construction method, the results don't show the complete cost of constructing the building. Furthermore, from region to region and within the literature, there is a considerable difference in the field of energy consumption and carbon CO_2eq, as the approaches, techniques, and energy generation of one region to the next can differ significantly. Therefore, the energy consumption and carbon CO_2eq data, as well as the cost of building in one location, can be completely different, even for the same building material in another location.

The results of this study can be considered by builders and investors to be applied for a general case, when assessing the potential use of hybrid CFS systems, in particular for midrise buildings. However, transforming the conventional building market such as OMRF to hybrid CFS buildings first requires raising the level of knowledge of building design, engineering and construction professionals, building owners and users, investors, building valuation and finance experts, academics, and government officials about the hybrid CFS building and on the other impacts that this system may raise for each of these market actors.

8.9 Conclusion

This chapter comparatively appraised the sustainability of a newly developed hybrid CFS system versus conventional HRS (OMRF) systems using a case study and identified some of the potential advantages and disadvantages of hybrid frames over OMRF systems with regard to their structural performance and environmental, economic and social impacts. The comparative analysis presented here supports the general claim that the cost, environmental and social impacts can be considerably decreased by choosing a more efficient design system such as hybrid CFS. The analyses and investigations showed that the new hybrid system is more economical, more sustainable and structurally stronger in comparison to its conventional counterpart. The calculations of the structures' weight revealed that hybrid frames could be much lighter than OMRF systems, which is basically due to the lightweight floor used in the hybrid system and relatively heavier solid sections used in the conventional HRS construction. The results from the structural analyses also showed that the storey drifts and shears are considerably smaller in the hybrid structure. It was also shown that due to the less material used, better prefabrication-ability and lighter equipment required for the construction of the hybrid structure, it exhibits better performance with regard to the environmental and social impacts. Further research work can be conducted to evaluate the impact of maintenance and material deterioration of both types of structures. As a future research, incorporating the data from building information modelling process into this approach can also result in a more comprehensive tool for the design of hybrid CFS buildings.

Chapter 9   Concluding remarks and recommendations

9.1 Summary and Conclusion

New hybrid CFS wall composed of open CFS sections and SHS was proposed in this study in order to enhance the shear wall resistance by replacing C-shaped CFS section with square steel tube. The study was divided into nine chapters and the major conclusions drawn from this thesis are briefly summarised in the following:

- **Chapter 1** was allocated to the application of CFS components in the lightweight steel buildings and described their current shortcomings. The concept of the proposed hybrid wall panel in this study was described in detail. The significance of the study, the research objectives and the thesis outline were also presented in this chapter.

- **In Chapter 2**, a comprehensive review of the literature was conducted and the current lateral load resisting systems for CFS structures were classified to four groups of: sheathing-braced, strap-braced, mixed of sheathing and strap, and hybrid systems. It was also concluded that the previously proposed CFS walls are not strong enough to be used for mid-rise buildings in high seismic regions. In addition, the parameters that can increase the lateral shear resistance of the CFS wall panels were also provided in this chapter.

- **In Chapter 3,** an experimental program on 11 hybrid CFS under monotonic lateral load was presented. The results showed that employing the SHS truss configuration for one side of the light steel walls can significantly enhance the energy absorption, compared to the traditional CFS walls. The SHS truss also had a considerable effect on decreasing the chance of chord stud buckling; i.e. load-bearing capacity. Specimens sheathed with gypsum board offered higher strength and ductility ratio with a few minor localized failures, compared to specimens without sheathing board. The results also showed that the floor to wall connection (hold-down connection) could significantly affect the performance of the wall panels. Therefore, connection

202

type B provided much higher resistance and allowed shear walls to dissipate more energy in the lateral load path compared to connection type A. The specimen W4 provided higher load capacity and stiffness compared to the specimen HW3, due to implementation of single SHS post at the other end of the wall which controlled the overturning of the wall during the loading procedure.

- **In Chapter 4,** an experimental program on lateral cyclic behaviour of six full-scale hybrid wall panels with truss structural design was presented. This chapter aimed to investigate and characterize the seismic performance of this new CFS solution. The performance of the wall panels was compared in terms of seismic characteristics and response modification factor (R factor). A comprehensive comparison between lateral strength to weight ratio of the hybrid panels of this study and 87 previously tested CFS walls was also carried out to investigate the capability of using hybrid walls in modular lightweight steel buildings. The cyclic results demonstrated that the seismic performance of specimens with appropriate truss frame was satisfactory considering their shear strength, ductility and R factor values. The overall response and trend of the hybrid walls under cyclic loading was similar to that obtained from monotonic loading of chapter 3, both with ascending behaviour. The average R-factor values of 6.1 and 7 were determined for sheathed and unsheathed braced walls, respectively. In addition, specimen HW-C4 with GWB offered a higher R factor value than those CFS walls with sheathing material listed in the CFS codes. The high strength to weight ratio of the hybrid walls of this study compared to the previously tested CFS panels also indicated the hybrid panels are well appropriate for modular lightweight buildings in seismic regions.

- **In Chapter 5,** the numerical methods used for modelling the lateral performance of CFS framed wall structures in the literature were classified and their positive and negative aspects, limitations, their applicable software, and challenges for simulation of different scenarios were studied. The existing models were categorised under micro- and macro- modelling methods, and a summary of the modelling techniques, hysteresis models and the reason for the discrepancy between experimental and numerical results were provided. Then a comparative discussion on both macro and micro categories was carried out in order to evaluate their effectiveness, positive and negative aspects, and their accuracy.

- **In Chapter 6,** advantages and disadvantages of the macro and micro modelling of CFS walls in terms of time of modelling, analysis and accuracy of the results were identified. Macro and micro modelling of CFS shear walls were investigated in a comparative manner. ABAQUS was used for micro modelling and OpenSees for macro modelling of CFS shear walls. Six shear walls with steel and OSB sheathing were modelled in ABAQUS and OpenSees software. Both micro and macro methods were validated by comparing the numerical results with experimental data and the results were compared and discussed. Results showed that both numerical methods have advantages and disadvantages which should be considered in each analysis. Modelling of CFS wall panels in OpenSees, which is used for macro modelling, is very simple and simulation and analysing time is significantly lower than micro modelling in ABAQUS. Moreover, since Pinching4 material is adapted in opensees, this program is able to simulate the behaviour of walls under cyclic loading. ABAQUS results in comparison to the OpenSees results were in better agreement to the experimental data which showed that micro modelling was somewhat more accurate than macro modelling.

- **In Chapter 7,** the lateral response of hybrid CFS wall systems comprising SHS truss brace and open CFS sections were numerically evaluated in order to examine the influence of SHS brace configuration on the lateral performance of the hybrid wall panel. A detailed modelling method was presented, and the numerical approach was verified using experimental tests. Then, a numerical analysis on 20 new hybrid wall panels was performed to evaluate the impact of SHS brace configuration on the load-carrying capacity, failure mode, stiffness ductility ratio, energy absorption and strength to weight ratio of the examined hybrid system. The results of this chapter showed that the type of SHS configuration can meaningfully influence the lateral performance of the hybrid wall panel. Utilizing X brace configuration dramatically increased the shear strength, ductility, lateral stiffness and energy absorption of the hybrid wall panel compared to experimental specimens of Chapter 3. The results of this chapter also showed that among all proposed hybrid wall models, only W4-W6, W9-W12, W15, W16, W18 and W20 could provide both higher stiffness and higher ductility ratio compared to experimental specimen HW4, showing the advantage of these models compared to the experimental specimen. The overall performance of

wall models W11, W12, W16, W18 and W20 is satisfactory to be employed for mid-rise construction. The numerical approach presented in this thesis can also be utilized as an option for the time-consuming and expensive experimental tests.

- **In Chapter 8**, the hybrid CFS systems were evaluated with regard to the sustainability, structural performance, economic cost, and social impacts, and the results were compared with those of Ordinary Moment Resisting Frames (OMRF) as the most popular conventional HRS framed system. The methodology consisted of both qualitative and quantitative analyses that included the overview of the positive and negative points of each construction method in the form of a comparative study. The results of the structural analysis of the two construction systems showed that the hybrid system exhibited better structural performance with regard to the storey shear and drift. It was also shown that in terms of most environmental performance indicators, hybrid CFS framed structures could lead to less environmental impact than OMRF systems. Moreover, the economic assessment demonstrated that hybrid CFS framed structures could save up to the 23% in framing costs, compared to OMRF systems, primarily owing to the fact that lightweight flooring system can be easily incorporated to the design of hybrid CFS structure. Their great potential for prefabrication, on the other hand, makes hybrid CFS a better option with respect to many social compact indicators such as noise, air, vibration and dust pollution and traffic.

9.2 Recommendations for future research

Based on the findings of this study as well as experimental and numerical results of the proposed hybrid system, suggested future works are summarised as follows:

- As shown in Chapter 3 of this study, the floor to wall connections (hold-down connections) could significantly influence the behaviour of the wall panels under lateral load. It is therefore suggested that new connections with different configurations be employed for a deeper understanding of the effect of the connections on the wall performance. The connections can be designed based on capacity-based design principals.

- Capacity-based design approach can also be used for the design of these walls by utilizing a fuse element in the diagonal members of the truss skeleton. This can be achieved either by partially cutting the diagonal element or by using a different steel material (mild steel) in this region. Using this method, more energy dissipation and consequently, more ductility can be obtained for the system.

- A parametric numerical study can be performed in order to investigate the effect of SHS thickness on the performance of the walls. Currently, SHS elements are available in different thicknesses in the market. Therefore, assessing hybrid wall panels with different thickness would provide a better understanding of the strength to weight ratio of this system.

- The effect of the axial gravity load was not considered in this study. Hence, it is worth to experimentally test the proposed hybrid system in a two-storey frame under the combined action of axial and lateral loads. This will provide more realistic results since the overturning of the wall panels are controlled due to applying gravity load. Besides, a two-storey frame would give further information about the behaviour of the connections between two levels.

- In this study (both numerical and experimental approaches), the span of the truss-skeleton was considered as 600 mm; however, an optimization study can also be conducted in order to obtain the optimum span for the truss configuration in a hybrid CFS wall. The optimization needs to be performed based on the idea of achieving "higher strength to weight ratio".

- As shown in Chapter 4, the unique capability of a wall with high lateral capacity and ductility is not necessarily included in the test-based overstrength and ductility reduction factors, respectively. Therefore, the R factor values need to be determined using more sophisticated methods such as FEMA P-695 [135] methodology, which determines the R factor through nonlinear response history analyses.

- The results of this study indicated that the hybrid walls provided a relatively higher strength to weight ratio compared to other previously tested wall panels which satisfy the requirements of the prefabricated and modular buildings. However, the system still needs to be assessed in a module before implementing in modular construction. The proposed system in this study can be positioned in a module and be experimentally tested in order to provide insight into the modular aspect of the proposed system.

References

1. Sharafi, P., et al., *Lateral force resisting systems in lightweight steel frames: Recent research advances.* Thin-Walled Structures, 2018. **130**: p. 231-253.

2. FEMA-450, *NEHRP recommendation provisions for seismic regulations for new buildings and other structures.* 2004, Building Seismic Safety Council, National Institute of Building Science: Washington (DC, USA).

3. TI-809-07, *echnical instructions: Design of cold-formed load bearing steel systems and masonry veneer/steel stud walls.* 2006, US Army Corps of Engineers. Engineering and Construction Division. Directorate of Military Program: Washington (DC, USA).

4. SEI/ASCE-7-02, *Minimum design loads for buildings and other structures.* 2003, American Society of Civil Engineers: Reston (VA, USA).

5. AISI-S100, *North American Specification for the Design of Cold-Formed Steel Structural Members.* 2016, The American Iron and Steel Institute

6. AISI-S110-07/S1-09, *AISI STANDARD Standard for Seismic Design of Cold-Formed Steel Structural Systems - Special Bolted Moment Frames with Supplement No. 1.* 2012, The American Iron and Steel Institute

7. AISI-S202, *Code of Standard Practice for Cold-Formed Steel Structural Framing.* 2015, The American Iron and Steel Institute

8. AISI-S213, *North American Standard for Cold-Formed Steel Framing - Lateral Design.* 2007, The American Iron and Steel Institute

9. AISI-S240, *North American Standard for Cold-Formed Steel Structural Framing.* 2015, The American Iron and Steel Institute

10. AISI-S310, *North American Standard for the Design of Profiled Steel Diaphragm Panels.* 2016, The American Iron and Steel Institute

11. AISI-S400, *North American Standard for Seismic Design of Cold-Formed Steel Structural Systems.* 2015, The American Iron and Steel Institute

12. AISI-S917, *Test Standard for Determining the Fastener-Sheathing Local Translational Stiffness of Sheathed Cold-Formed Steel Assemblies.* 2017, The American Iron and Steel Institute

13. AISI-S918, *Test Standard for Determining the Fastener-Sheathing Rotational Stiffness of Sheathed Cold-Formed Steel Assemblies.* 2017, The American Iron and Steel Institute

14. AUS/NZS-4600, *Cold-formed steel structures.* 2005, Australian/ New Zealand standard: Sydney (NSW, Australia).

15. IBC, *International building code.* 2003, International Code Council: Falls Church (VA, USA).

16. AISI, *North American standard for seismic design of cold-formed steel structural systems.* 2015.

17. Liu, B., et al., *Performance of cold-formed-steel-framed shear walls sprayed with lightweight mortar under reversed cyclic loading.* Thin-Walled Structures, 2016. **98**: p. 312-331.

18. Xu, Z., et al., *Seismic performance of high-strength lightweight foamed concrete-filled cold-formed steel shear walls.* Journal of Constructional Steel Research, 2018. **143**: p. 148-161.

19. Wang, X. and J. Ye, *Reversed cyclic performance of cold-formed steel shear walls with reinforced end studs.* Journal of Constructional Steel Research, 2015. **113**: p. 28-42.

20. Javidan, M.M., et al., *Computationally efficient framework for probabilistic collapse analysis of structures under extreme actions.* Engineering Structures, 2018. **172**: p. 440-452.

21. Mohajeri Nav, F., N. Usefi, and R. Abbasnia, *Analytical investigation of reinforced concrete frames under middle column removal scenario.* Advances in Structural Engineering, 2017. **21**(9): p. 1388-1401.

22. Usefi, N., P. Sharafi, and H. Ronagh, *Numerical models for lateral behaviour analysis of cold-formed steel framed walls: State of the art, evaluation and challenges.* Thin-Walled Structures, 2019. **138**: p. 252-285.

23. Landolfo, R., *Lightweight steel framed systems in seismic areas: Current achievements and future challenges.* Thin-Walled Structures, 2019. **140**: p. 114-131.

24. Wang, X. and J. Ye, *Cyclic testing of two- and three-story CFS shear-walls with reinforced end studs.* Journal of Constructional Steel Research, 2016. **121**: p. 13-28.

25. Karabulut, B. and S. Soyoz, *Experimental and analytical studies on different configurations of cold-formed steel structures.* Journal of Constructional Steel Research, 2017. **133**: p. 535-546.

26. Mohebbi, S., et al., *Experiments on seismic behaviour of steel sheathed cold-formed steel shear walls cladded by gypsum and fiber cement boards.* Thin-Walled Structures, 2016. **104**: p. 238-247.

27. Yu, C., *Shear resistance of cold-formed steel framed shear walls with 0.686 mm, 0.762 mm, and 0.838 mm steel sheet sheathing.* Engineering Structures, 2010. **32**(6): p. 1522-1529.

28. Yu, C. and Y. Chen, *Steel sheet sheathing options for cold-formed steel framed shear wall assemblies providing shear resistance-phase 2.* 2009.

29. Yu, C., et al., *Steel sheet sheathing options for CFS framed shear wall aseemblies providing shear resistance.* 2007.

30. Peck, Q., N. Rogers, and R. Serrette, *Cold-Formed Steel Framed Gypsum Shear Walls: In-Plane Response.* Journal of Structural Engineering, 2012. **138**(7): p. 932-941.

31. Serrette, R. and D.P. Nolan, *Reversed Cyclic Performance of Shear Walls with Wood Panels Attached to Cold-Formed Steel with Pins.* Journal of Structural Engineering, 2009. **135**(8): p. 959-967.

32. Lin, S.-H., C.-L. Pan, and W.-T. Hsu, *Monotonic and cyclic loading tests for cold-formed steel wall frames sheathed with calcium silicate board.* Thin-Walled Structures, 2014. **74**: p. 49-58.

33. Vieira, L.C.M. and B.W. Schafer, *Lateral stiffness and strength of sheathing braced cold-formed steel stud walls.* Engineering Structures, 2012. **37**: p. 205-213.

34. Lange, J. and B. Naujoks, *Behaviour of cold-formed steel shear walls under horizontal and vertical loads.* Thin-Walled Structures, 2006. **44**(12): p. 1214-1222.

35. Nithyadharan, M. and V. Kalyanaraman, *Behaviour of cold-formed steel shear wall panels under monotonic and reversed cyclic loading.* Thin-Walled Structures, 2012. **60**: p. 12-23.

36. Nithyadharan, M. and V. Kalyanaraman, *Modelling hysteretic behaviour of cold-formed steel wall panels.* Engineering Structures, 2013. **46**: p. 643-652.

37. Nithyadharan, M. and V. Kalyanaraman, *Experimental study of screw connections in CFS-calcium silicate board wall panels.* Thin-Walled Structures, 2011. **49**(6): p. 724-731.

38. Hernández-Castillo, L.A., et al., *Fragility curves for thin-walled cold-formed steel wall frames affected by ground settlements due to land subsidence.* Thin-Walled Structures, 2015. **87**: p. 66-75.

39. Fiorino, L., G. Della Corte, and R. Landolfo, *Experimental tests on typical screw connections for cold-formed steel housing.* Engineering Structures, 2007. **29**(8): p. 1761-1773.

40. Fiorino, L., et al., *Experimental study on screwed connections for sheathed CFS structures with gypsum or cement based panels.* Thin-Walled Structures, 2017. **116**: p. 234-249.

41. Bian, G., et al., *Reliability of cold-formed steel framed shear walls as impacted by variability in fastener response.* Engineering Structures, 2017. **142**: p. 84-97.

42. Pan, C.-L. and M.-Y. Shan, *Monotonic shear tests of cold-formed steel wall frames with sheathing.* Thin-Walled Structures, 2011. **49**(2): p. 363-370.

43. Peterman, K.D., N. Nakata, and B.W. Schafer, *Hysteretic characterization of cold-formed steel stud-to-sheathing connections.* Journal of Constructional Steel Research, 2014. **101**: p. 254-264.

44. Baran, E. and C. Alica, *Behavior of cold-formed steel wall panels under monotonic horizontal loading.* Journal of Constructional Steel Research, 2012. **79**: p. 1-8.

45. Restrepo, J.I. and A.M. Bersofsky, *Performance characteristics of light gage steel stud partition walls.* Thin-Walled Structures, 2011. **49**(2): p. 317-324.

46. Xu, L. and J. Martínez, *Strength and stiffness determination of shear wall panels in cold-formed steel framing.* Thin-Walled Structures, 2006. **44**(10): p. 1084-1095.

47. Fülöp, L.A. and D. Dubina, *Performance of wall-stud cold-formed shear panels under monotonic and cyclic loading: Part I: Experimental research.* Thin-Walled Structures, 2004. **42**(2): p. 321-338.

48. Fülöp, L.A. and D. Dubina, *Performance of wall-stud cold-formed shear panels under monotonic and cyclic loading: Part II: Numerical modelling and performance analysis.* Thin-Walled Structures, 2004. **42**(2): p. 339-349.

49. Swensen, S., G.G. Deierlein, and E. Miranda, *Behavior of Screw and Adhesive Connections to Gypsum Wallboard in Wood and Cold-Formed Steel-Framed Wallettes.* Journal of Structural Engineering, 2016. **142**(4): p. E4015002.

50. Shamim, I., J. DaBreo, and C.A. Rogers, *Dynamic Testing of Single- and Double-Story Steel-Sheathed Cold-Formed Steel-Framed Shear Walls.* Journal of Structural Engineering, 2013. **139**(5): p. 807-817.

51. Shamim, I. and C.A. Rogers, *Steel sheathed/CFS framed shear walls under dynamic loading: Numerical modelling and calibration.* Thin-Walled Structures, 2013. **71**: p. 57-71.

52. Shamim, I. and C.A. Rogers, *Numerical evaluation: AISI S400 steel-sheathed CFS framed shear wall seismic design method.* Thin-Walled Structures, 2015. **95**: p. 48-59.

53. DaBreo, J., et al., *Steel sheathed cold-formed steel framed shear walls subjected to lateral and gravity loading.* Thin-Walled Structures, 2014. **74**: p. 232-245.

54. Attari, N.K.A., S. Alizadeh, and S. Hadidi, *Investigation of CFS shear walls with one and two-sided steel sheeting.* Journal of Constructional Steel Research, 2016. **122**: p. 292-307.

55. Shakibanasab, A., N.K.A. Attari, and M. Salari, *A statistical and experimental investigation into the accuracy of capacity reduction factor for cold-formed steel shear walls with steel sheathing.* Thin-Walled Structures, 2014. **77**: p. 56-66.

56. Esmaeili Niari, S., B. Rafezy, and K. Abedi, *Seismic behavior of steel sheathed cold-formed steel shear wall: Experimental investigation and numerical modeling.* Thin-Walled Structures, 2015. **96**: p. 337-347.

57. Landolfo, R., L. Fiorino, and G.D. Corte, *Seismic Behavior of Sheathed Cold-Formed Structures: Physical Tests.* Journal of Structural Engineering, 2006. **132**(4): p. 570-581.

58. Mohebbi, S., et al., *Experimental work on single and double-sided steel sheathed cold-formed steel shear walls for seismic actions.* Thin-Walled Structures, 2015. **91**: p. 50-62.

59. Ye, J., et al., *Cyclic performance of cold-formed steel shear walls sheathed with double-layer wallboards on both sides.* Thin-Walled Structures, 2015. **92**: p. 146-159.

60. Liu, P., K.D. Peterman, and B.W. Schafer, *Impact of construction details on OSB-sheathed cold-formed steel framed shear walls.* Journal of Constructional Steel Research, 2014. **101**: p. 114-123.

61. Mowrtage, W., *Cyclic lateral load behavior of CFS walls sheathed with different materials.* Thin-Walled Structures, 2015. **96**: p. 328-336.

62. Mowrtage, W., et al., *Load carrying capacity enhancement of cold formed steel walls using shotcreted steel sheets.* Thin-Walled Structures, 2012. **60**: p. 145-153.

63. Kim, T.-W., et al., *Shaketable tests of a cold-formed steel shear panel.* Engineering Structures, 2006. **28**(10): p. 1462-1470.

64. Kim, T.-W., J. Wilcoski, and D.A. Foutch, *Analysis of Measured and Calculated Response of a Cold-formed Steel Shear Panel Structure.* Journal of Earthquake Engineering, 2007. **11**(1): p. 67-85.

65. Zhang, W., et al., *Experiments and Simulations of Cold-Formed Steel Wall Assemblies Using Corrugated Steel Sheathing Subjected to Shear and Gravity Loads.* Journal of Structural Engineering, 2017. **143**(3): p. 04016193.

66. Zhang, W., et al., *Seismic Performance Evaluation of Cold-Formed Steel Shear Walls Using Corrugated Steel Sheathing.* Journal of Structural Engineering, 2017. **143**(11): p. 04017151.

67. Gao, W.C. and Y. Xiao, *Seismic behavior of cold-formed steel frame shear walls sheathed with ply-bamboo panels.* Journal of Constructional Steel Research, 2017. **132**: p. 217-229.

68. Telue, Y. and M. Mahendran, *Behaviour of cold-formed steel wall frames lined with plasterboard.* Journal of Constructional Steel Research, 2001. **57**(4): p. 435-452.

69. Telue, Y. and M. Mahendran, *Behaviour and design of cold-formed steel wall frames lined with plasterboard on both sides.* Engineering Structures, 2004. **26**(5): p. 567-579.

70. Yu, C. and Y. Chen, *Detailing recommendations for 1.83 m wide cold-formed steel shear walls with steel sheathing.* Journal of Constructional Steel Research, 2011. **67**(1): p. 93-101.

71. Stojadinovic, B. and S. Tipping, *Structural testing of corrugated sheet steel shear walls.* 2008.

72. Yu, C. and G. Yu, *Experimental Investigation of Cold-Formed Steel Framed Shear Wall Using Corrugated Steel Sheathing with Circular Holes.* Journal of Structural Engineering, 2016. **142**(12): p. 04016126.

73. Javaheri-Tafti, M.R., et al., *An experimental investigation on the seismic behavior of cold-formed steel walls sheathed by thin steel plates.* Thin-Walled Structures, 2014. **80**: p. 66-79.

74. Zeynalian, M. and H.R. Ronagh, *Seismic performance of cold formed steel walls sheathed by fibre-cement board panels.* Journal of Constructional Steel Research, 2015. **107**: p. 1-11.

75. Dastjerdi, M.Z. and H.R. Ronagh, *Seismic performance of steel sheathed cold-formed steel shear walls.* 2012.

76. Gad, E.F., et al., *Lateral Behavior of Plasterboard-Clad Residential Steel Frames.* Journal of Structural Engineering, 1999. **125**(1): p. 32-39.

77. Gad, E.F., et al., *Lateral performance of cold-formed steel-framed domestic structures.* Engineering Structures, 1999. **21**(1): p. 83-95.

78. Moghimi, H. and H.R. Ronagh, *Better connection details for strap-braced CFS stud walls in seismic regions.* Thin-Walled Structures, 2009. **47**(2): p. 122-135.

79. Iuorio, O., et al., *Seismic response of Cfs strap-braced stud walls: Experimental investigation.* Thin-Walled Structures, 2014. **85**: p. 466-480.

80. Macillo, V., et al., *Seismic response of Cfs strap-braced stud walls: Theoretical study.* Thin-Walled Structures, 2014. **85**: p. 301-312.

81. Pastor, N. and A. Rodríguez-Ferran, *Hysteretic modelling of x-braced shear walls.* Thin-Walled Structures, 2005. **43**(10): p. 1567-1588.

82. Pourabdollah, O., F. Farahbod, and F.R. Rofooei, *The seismic performance of K-braced cold-formed steel shear panels with improved connections.* Journal of Constructional Steel Research, 2017. **135**: p. 56-68.

83. Zeynalian, M., H.R. Ronagh, and S. Hatami, *Seismic characteristics of K-braced cold-formed steel shear walls.* Journal of Constructional Steel Research, 2012. **77**: p. 23-31.

84. Zeynalian, M. and H.R. Ronagh, *A numerical study on seismic characteristics of knee-braced cold formed steel shear walls.* Thin-Walled Structures, 2011. **49**(12): p. 1517-1525.

85. Zeynalian, M. and H.R. Ronagh, *An experimental investigation on the lateral behavior of knee-braced cold-formed steel shear walls.* Thin-Walled Structures, 2012. **51**: p. 64-75.

86. Zeynalian, M. and H.R. Ronagh, *A numerical study on seismic performance of strap-braced cold-formed steel shear walls.* Thin-Walled Structures, 2012. **60**: p. 229-238.

87. Berman, J.W., O.C. Celik, and M. Bruneau, *Comparing hysteretic behavior of light-gauge steel plate shear walls and braced frames.* Engineering Structures, 2005. **27**(3): p. 475-485.

88. Fiorino, L., M.T. Terracciano, and R. Landolfo, *Experimental investigation of seismic behaviour of low dissipative CFS strap-braced stud walls.* Journal of Constructional Steel Research, 2016. **127**: p. 92-107.

89. Al-Kharat, M. and C.A. Rogers, *Inelastic performance of cold-formed steel strap braced walls.* Journal of Constructional Steel Research, 2007. **63**(4): p. 460-474.

90. Accorti, M., et al., *Response of CFS Sheathed Shear Walls.* Structures, 2016. **7**: p. 100-112.

91. Gerami, M. and M. Lotfi, *Analytical Analysis of Seismic Behavior of Cold-Formed Steel Frames with Strap Brace and Sheathings Plates.* Advances in Civil Engineering, 2014. **2014**: p. 22.

92. Serrette, R. and K. Ogunfunmi, *Shear Resistance of Gypsum-Sheathed Light-Gauge Steel Stud Walls.* Journal of Structural Engineering, 1996. **122**(4): p. 383-389.

93. Yu, C., C. Li, and C. Elliott. *Behavior and Design of Cold-Formed, Steel-Framed Shear Walls using Structural Composite Panels.* in *Structures Congress 2014.* 2014.

94. Xu, Z., Z. Chen, and S. Yang, *Seismic behavior of cold-formed steel high-strength foamed concrete shear walls with straw boards.* Thin-Walled Structures, 2018. **124**: p. 350-365.

95. Mortazavi, M., et al., *Lateral behaviour of hybrid cold-formed and hot-rolled steel wall systems: Experimental investigation.* Journal of Constructional Steel Research, 2018. **147**: p. 422-432.

96. Kildashti, K., et al., *Seismic collapse assessment of a hybrid cold-formed hot-rolled steel building.* Journal of Constructional Steel Research, 2019. **155**: p. 504-516.

97. Tian, Y.S., J. Wang, and T.J. Lu, *Racking strength and stiffness of cold-formed steel wall frames.* Journal of Constructional Steel Research, 2004. **60**(7): p. 1069-1093.

98. Mojtabaei, S.M., et al., *Analytical and experimental study on the seismic performance of cold-formed steel frames.* Journal of Constructional Steel Research, 2018. **143**: p. 18-31.

99. Moghimi, H. and H.R. Ronagh, *Performance of light-gauge cold-formed steel strap-braced stud walls subjected to cyclic loading.* Engineering Structures, 2009. **31**(1): p. 69-83.

100. Macillo, V., L. Fiorino, and R. Landolfo, *Seismic response of CFS shear walls sheathed with nailed gypsum panels: Experimental tests.* Thin-Walled Structures, 2017. **120**: p. 161-171.

101. Serrette, R., et al., *Cold-Formed Steel Frame Shear Walls Utilizing Structural Adhesives.* Journal of Structural Engineering, 2006. **132**(4): p. 591-599.

102. Tian, H.-W., Y.-Q. Li, and C. Yu, *Testing of steel sheathed cold-formed steel trussed shear walls.* Thin-Walled Structures, 2015. **94**: p. 280-292.

103. ASTM, I., *Standard test methods and definitions for mechanical testing of steel products.* ASTM A370, 2012.

104. Iron, A. and S. Institute, *North American specification for the design of cold-formed steel structural members.* 2016: American Iron & Steel Institute, Committee of Steel Plate Producers ....

105. Standard, A., *Cold-formed structural steel hollow sections*, in *AS 1163.* 2016, Standards association of Australia.

106. Standard, A., *Steel sheet and strip–hot-dipped zinc-coated or aluminium/zinc-coated– AS 1397.* Sydney (Australia): Standards Association of Australia, 2011.

107. Pehlivan, B.M., E. Baran, and C. Topkaya, *Testing and analysis of different hold down devices for CFS construction.* Journal of Constructional Steel Research, 2018. **145**: p. 97-115.

108. F3125M, A.F., *Standard Specification for High Strength Structural Bolts and Assemblies.* 2019, American Society for Testing Material.

109. Council, B.S.S., *NEHRP recommended provisions for seismic regulations for new buildings and other structures (FEMA 450).* Washington, USA, 2003.

110. AISI-S213, *North American standard for cold-formed steel framing-lateral design 2007 edition*. 2007, American Iron and Steel Institute: Washington, USA.

111. Santos, V., *Higher Capacity Cold-formed Steel Sheathed and Framed Shear Walls for Mid-rise Buildings*. 2018, AISI Report RP 17-6.

112. *FEMA 365, Prestandard and Commentary for the Seismic Rehabilitation of Buildings in Rehabilitation Requirements*. 2000, Federal Emergency Management Agency. Washington, D.C.

113. *FEMA P-1050, NEHRP Recommended Seismic Provisions for New Buildings and Other Structures Volume I: Part 1 Provisions, Part 2 Commentary* 2015, Building Seismic Safety Council, Washington, DC, 515 pp.

114. iccons, *Screw Technical Guide*. 2017: Australia.

115. *ASTM E2126, Standard test methods for cyclic (reversed) load test for shear resistance of vertical elements of the lateral force resisting systems for buildings*. 2019, ASTM International West Conshohocken, PA.

116. Shariati, M., et al., *Estimation of moment and rotation of steel rack connections using extreme learning machine*. Steel and Composite Structures, 2019. **31**(5): p. 427-435.

117. Shariati, M., et al., *A novel approach to predict shear strength of tilted angle connectors using artificial intelligence techniques*. Engineering with Computers, 2020: p. 1-21.

118. Mohammadi, M., et al., *Experimental and numerical investigation of an innovative buckling-restrained fuse under cyclic loading*. Structures, 2019. **22**: p. 186-199.

119. Ayatollahi, S.R., et al., *Performance of gypsum sheathed CFS panels under combined lateral and gravity loading*. Journal of Constructional Steel Research, 2020. **170**: p. 106125.

120. Sharafi, P., et al., *Identification of Factors and Decision Analysis of the Level of Modularization in Building Construction*. 2018. **24**(2): p. 04018010.

121. Dubina, D., *Behavior and performance of cold-formed steel-framed houses under seismic action*. Journal of Constructional Steel Research, 2008. **64**(7): p. 896-913.

122. Mortazavi, M., et al., *Prefabricated hybrid steel wall panels for mid-rise construction in seismic regions*. Journal of Building Engineering, 2020. **27**: p. 100942.

123. Accorti, M., et al., *Reprint of Response of CFS Sheathed Shear Walls*. Structures, 2016. **8**: p. 318-330.

124. Balh, N. *Development of seismic design provisions for steel sheathed shear walls*. in *Masters Abstracts International*. 2010.

125. DaBreo, J., et al., *Steel sheathed cold-formed steel framed shear walls subjected to lateral and gravity loading*. Thin-Walled Structures, 2014. **74**: p. 232-245.

126. Ong-Tone, C., *Tests and Evaluation of Cold-formed Steel Frame*. 2009: Department of Civil Engineering and Applied Mechanics, McGill University.

127. Serrette, R., K. Morgan, and M. Sorhouet, *Performance of cold-formed steel-framed shear walls: Alternative configurations*. Final Report: LGSRG-06-02, Santa Clara University, Santa Clara, CA, 2002.

128. Liu, P., K. Peterman, and B. Schafer, *Test report on cold-formed steel shear walls*. 2012.

129. *Uniform building code*. 1997, International Conference of Building Officials, Whittier.

130. *International building code*. 2018: International Code Council

131. *ASCE/SEI 7, Minimum design loads and associated criteria for buildings and other structures,* . 2017. American Society of Civil Engineers Reston, VA.

132. *National Building Code of Canada.* 2015, National Research Council of Canada.

133. *Eurocode 8: Design of structures for earthquake resistance.* 2005, European Committee for Standardization.

134. *AS/NZS 4600, Cold-formed steel structures.* 2018, Standards Australia.

135. *FEMA P695, Quantification of Building Seismic Performance Factors* 2009, Federal Emergency Management Agency, Washington, D.C.

136. Kaveh, A. and P. Sharafi, *Charged System Search Algorithm for Minimax and Minisum Facility Layout Problems.* Asian Journal of Civil Engineering, 2011. **12**(6): p. 703-718

137. Kaveh, A. and P. Sharafi, *Nodal ordering for bandwidth reduction using ant system algorithm.* Engineering Computations, 2009. **26**(3): p. 313-323.

138. Kaveh, A. and P. Sharafi, *Optimal priority functions for profile reduction using ant colony optimization.* Finite Elements in Analysis and Design, 2008. **44**(3): p. 131-138.

139. Majidi, L., N. Usefi, and R. Abbasnia, *Numerical study of RC beams under various loading rates with LS-DYNA.* Journal of Central South University, 2018. **25**(5): p. 1226-1239.

140. Usefi, N., F.M. Nav, and R.J.G. Abbasnia, *Finite element analysis of RC elements in progressive collapse scenario.* Gradevinar, 2016. **68**(12): p. 1009-1022.

141. Ishizaki, T., et al., *Model Reduction and Clusterization of Large-Scale Bidirectional Networks.* IEEE Transactions on Automatic Control, 2014. **59**(1): p. 48-63.

142. Qu, Z.Q., *Model Order Reduction Techniques with Applications in Finite Element Analysis.* 2013: Springer London.

143. Usefi, N., et al. *Macro/micro analysis of cold-formed steel members using ABAQUS and OPENSEES.* in *13th International Conference on Steel, Space and Composite Structures (SS18).* 2018. The University of Western Australia, Perth, Australia.

144. Sharafi, P., et al., *Interlocking system for enhancing the integrity of multi-storey modular buildings.* Automation in Construction, 2018. **85**: p. 263-272.

145. Sharafi, P., et al., *Automated spatial design of multi-story modular buildings using a unified matrix method.* Automation in Construction, 2017. **82**: p. 31-42.

146. Wang, M. and W. Yang, *Equivalent constitutive model of steel plate shear wall structures.* Thin-Walled Structures, 2018. **124**: p. 415-429.

147. Rezai, M., *Seismic behaviour of steel plate shear walls by shake table testing.* 1999, PhD Thesis, University of British Columbia: Canada.

148. Elgaaly, M., V. Caccese, and C. Du, *Postbuckling Behavior of Steel Plate Shear Walls under Cyclic Loads.* Journal of Structural Engineering, 1993. **119**(2): p. 588-605.

149. Thorburn, L.J., C. Montgomery, and G.L. Kulak, *Analysis of steel plate shear walls.* 1983: Department of Civil Engineering, University of Alberta.

150. Shishkin, J.J., R.G. Driver, and G.Y. Grondin, *Analysis of Steel Plate Shear Walls Using the Modified Strip Model.* Journal of Structural Engineering, 2009. **135**(11): p. 1357-1366.

151. Guo, L., et al., *Hysteretic Analysis of Steel Plate Shear Walls (SPSWs) and a Modified Strip Model for SPSWs.* Advances in Structural Engineering, 2012. **15**(10): p. 1751-1764.

152. Gad, E.F., *Performance of brick-veneer steel-framed domestic structures under earthquake loading*. 1997, PhD Thesis, University of Melbourne, Australia.

153. Carr, A.J., *RUAUMOKO-Inelastic dynamic analysis program*. Department of Civil Engineering, University of Canterbury, Christchurch, New Zealand, 2008.

154. Stewart, W., *The seismic design of plywood sheathed shear walls*. 1987, University of Canterbury.

155. Boudreault, F., *Seismic analysis of steel frame/wood panel shear walls*. 2005, Master Thesis, Department of Civil Engineering and Applied Mechanics, McGill University, Montréal, Que.

156. Boudreault, F., C. Blais, and C. Rogers, *Seismic force modification factors for light-gauge steel-frame-wood structural panel shear walls*. Canadian Journal of Civil Engineering, 2007. **34**(1): p. 56-65.

157. Fulop, L.A. and D. Dubina, *Seismic performance of wall-stud shear walls*, in *16th International Specialty Conference on Cold-Formed Steel Structures*. 2002: Missouri University of Science and Technology.

158. Prakash, V., G.H. Powell, and S. Campbell, *Drain-3DX: Base Program Description and User Guide: Version 1.10*. 1994: Department of Civil Engineering, University of California.

159. Lee, M.-S. and D.A. Foutch, *Performance evaluation of cold-formed steel braced frames designed under current U.S. seismic design code*. International Journal of Steel Structures, 2010. **10**(3): p. 305-316.

160. Allahabadi, R. and G.H. Powell, *DRAIN-2DX user guide*. Vol. 88. 1988: University of California, Earthquake Engineering Research Center, College of Engineering.

161. Shamim, I., *PhD Thesis, Seismic design of lateral force resisting cold-formed steel framed (CFS) structures*. Department of Civil Engineering and Applied Mechanics, McGill University, Canada, 2013.

162. Rogers, C., et al. *Development of seismic design provisions for steel sheet sheathed shear walls*. in *Structures Congress* 2011.

163. Shamim, I. and C. Rogers, *Numerical modelling and calibration of CFS framed shear walls under dynamic loading*, in *21st International Specialty Conference on Cold-Formed Steel Structures*. 2012: Missouri University of Science and Technology.

164. Mazzoni, S., et al., *The open system for earthquake engineering simulation (OpenSEES) user command-language manual*. 2006.

165. Lu, S., *Influence of gypsum panels on the response of cold-formed steel framed shear walls*. 2015, Master Thesis, McGill University Libraries.

166. Wang, X., J. Ye, and Q. Yu, *Improved equivalent bracing model for seismic analysis of mid-rise CFS structures*. Journal of Constructional Steel Research, 2017. **136**: p. 256-264.

167. Leng, J., et al., *Modeling seismic response of a full-scale cold-formed steel-framed building*. Engineering Structures, 2017. **153**: p. 146-165.

168. Schafer, B.W., et al., *Seismic Response and Engineering of Cold-formed Steel Framed Buildings*. Structures, 2016. **8**: p. 197-212.

169. Leng, J., B. Schafer, and S. Buonopane. *Seismic computational analysis of CFS-NEES building*. in *21st international specialty conference on coldformed steel structures*. 2012. Missouri University of Science and Technology.

170. Leng, J., B. Schafer, and S. Buonopane. *Modeling the seismic response of cold-formed steel framed buildings: model development for the CFS-NEES building.* in *Proceedings of the Annual Stability Conference-Structural Stability Research Council, St. Louis, Missouri.* 2013. Citeseer.

171. Leng, J., *Simulation of cold-formed steel structures.* 2015, PhD Thesis, Hopkins University.

172. Yu, C., G. Yu, and J. Wang, *Innovative cold-formed steel framed shear wall sheathed with corrugated steel sheets: experiments and dynamic analysis,* in *22nd International Specialty Conference on Cold-Formed Steel Structures.* 2014: Missouri University of Science and Technology.

173. Zhang, W., M. Mahdavian, and C. Yu, *Lateral strength and deflection of cold-formed steel shear walls using corrugated sheathing.* Journal of Constructional Steel Research, 2018. **148**: p. 399-408.

174. FEMA, P., *Commentary for the seismic rehabilitation of buildings.* FEMA-356, Federal Emergency Management Agency, Washington, DC, 2000.

175. Fiorino, L., V. Macillo, and R. Landolfo, *Shake table tests of a full-scale two-story sheathing-braced cold-formed steel building.* Engineering Structures, 2017. **151**: p. 633-647.

176. Fiorino, L., et al., *Seismic response of CFS shear walls sheathed with nailed gypsum panels: Numerical modelling.* Thin-Walled Structures, 2018. **122**: p. 359-370.

177. Fiorino, L., et al., *Behaviour factor (q) evaluation the CFS braced structures according to FEMA P695.* Journal of Constructional Steel Research, 2017. **138**: p. 324-339.

178. Campiche, A., et al., *Seismic Behaviour of Sheathed CFS Buildings: Shake Table Tests and Numerical Modelling.* Ing. Sismica, 2018. **35**(2): p. 106-123.

179. Macillo, V., et al., *Development and calibration of a hysteretic model for CFS strap braced stud walls.* Int. J. Adv. Steel Constr, 2018. **14**(3).

180. Scotta, R., et al., *Light steel-timber frame with composite and plaster bracing panels.* Materials, 2015. **8**(11): p. 7354-7370.

181. Morello, D., *Seismic Performance of Multi-storey Structures with Cold-formed Steel Wood Sheathed Shear Walls.* 2009, Master Thesis, McGill University.

182. Pei, S. and J. van de Lindt, *User's manual for SAPWood for Windows: Seismic analysis package for woodframe structures.* NEEShub (nees. org), 2010.

183. Balh, N., *Development of seismic design provisions for steel sheathed shear walls.* 2010, Master Thesis, McGill University.

184. AISI-S213, *North American Standard for Cold-Formed Steel Framing–Lateral Design.* 2007, American Iron and Steel Institute Washington, DC, USA.

185. NBC, *National building code of Canada.* 1990: Associate Committee on the National Building Code, National Research Council.

186. Comeau, G., K. Velchev, and C. Rogers, *Development of seismic force modification factors for cold-formed steel strap braced walls.* Canadian Journal of Civil Engineering, 2010. **37**(2): p. 236-249.

187. Velchev, K., *Inelastic performance of screw connected cold-formed steel strap braced walls.* 2008, Master Thesis, mcgill university.

188. Bourahla, N., et al., *Post elastic modeling techniques and performance analysis of cold formed steel structures subjected to earthquake loadings Paper Title Line,* in *15 World conference on Earthquake Engineering.* 2012: Lisbon, Portuga.

189. Dao, T.N. and J.W.v.d. Lindt, *Seismic Performance of an Innovative Light-Gauge Cold-Formed Steel Mid-Rise Building*, in *Structures Congress 2012*. 2012.

190. Dao, T.N. and J.W.v.d. Lindt, *Seismic Performance of an Innovative Light-Frame Cold-Formed Steel Frame for Midrise Construction.* Journal of Structural Engineering, 2013. **139**(5): p. 837-848.

191. Folz, B. and A. Filiatrault, *Cyclic Analysis of Wood Shear Walls.* Journal of Structural Engineering, 2001. **127**(4): p. 433-441.

192. Shahi, R., *Performance evaluation of cold-formed steel stud shear walls in seismic conditions.* 2015, PhD Thesis, University of Melbourne.

193. Shahi, R., et al., *Seismic Performance Behavior of Cold-Formed Steel Wall Panels by Quasi-static Tests and Incremental Dynamic Analyses.* Journal of Earthquake Engineering, 2017. **21**(3): p. 411-438.

194. Kechidi, S. and N. Bourahla, *Deteriorating hysteresis model for cold-formed steel shear wall panel based on its physical and mechanical characteristics.* Thin-Walled Structures, 2016. **98**: p. 421-430.

195. Kechidi, S., et al., *Seismic risk assessment of cold-formed steel shear wall systems.* Journal of Constructional Steel Research, 2017. **138**: p. 565-579.

196. Kechidi, S., N. Bourahla, and J.M. Castro, *Seismic design procedure for cold-formed steel sheathed shear wall frames: Proposal and evaluation.* Journal of Constructional Steel Research, 2017. **128**: p. 219-232.

197. Zeynalian, M., A.Z. Shahrasbi, and H.T. Riahi, *Seismic Response of Cold Formed Steel Frames Sheathed by Fiber Cement Boards.* International Journal of Civil Engineering, 2018. **16**(11): p. 1643-1653.

198. Jiang, L. and J. Ye, *Impact of Wall Configurations on Seismic Fragility of Steel-Sheathed Cold-Formed Steel-Framed Buildings.* Advances in Civil Engineering, 2018. **2018**.

199. Ye, J. and L. Jiang, *Simplified Analytical Model and Shaking Table Test Validation for Seismic Analysis of Mid-Rise Cold-Formed Steel Composite Shear Wall Building.* Sustainability, 2018. **10**(9): p. 3188.

200. Bian, G., et al., *Fastener-based computational models with application to cold-formed steel shear walls*, in *22nd International Specialty Conference on Cold-Formed Steel Structures*. 2014: Missouri University of Science and Technology.

201. Bian, G., et al. *OpenSees modeling of cold-formed steel framed wall system*. in *Proceedings of 8th International Conference on Behavior of Steel Structures in Seismic Areas*. 2015. Shanghai, China.

202. Bian, G., et al. *OpenSees modeling of wood sheathed cold-formed steel framed shear walls*. in *Proceedings of the Annual Stability Conference*. 2015. Structural Stability Research Council, Nashville, Tennessee.

203. Buonopane, S., T. Tun, and B. Schafer. *Fastener-based computational models for prediction of seismic behavior of CFS shear walls*. in *Proceedings of the 10th National Conference in Earthquake Engineering*. 2014. EERI Anchorage, AK.

204. Buonopane, S.G., et al., *Computationally efficient fastener-based models of cold-formed steel shear walls with wood sheathing.* Journal of Constructional Steel Research, 2015. **110**: p. 137-148.

205. Bian, G., *Modeling cold-formed steel members and systems.* 2017, PhD Thesis, Johns Hopkins University.

206. Padilla-Llano, D.A., *A framework for cyclic simulation of thin-walled cold-formed steel members in structural systems*. 2015, PhD Thesis, Virginia Polytechnic Institute and State University.

207. Yanagi, N. and C. Yu, *Effective Strip Method for the Design of Cold-Formed Steel Framed Shear Wall with Steel Sheet Sheathing.* Journal of Structural Engineering, 2014. **140**(4): p. 04013101.

208. Santos, V., *Higher Capacity Cold-formed Steel Sheathed and Framed Shear Walls for Mid-rise Buildings*. 2018, PhD Thesis, McGill University Libraries.

209. Brière, V., V. Santos, and C.A. Rogers, *Cold-formed steel centre-sheathed (mid-ply) shear walls.* Soil Dynamics and Earthquake Engineering, 2018. **114**: p. 253-266.

210. BRIERE, V., *Higher capacity cold-formed steel sheathed and framed shear walls for mid-rise buildings: Part 2*. 2017, PhD Thesis, McGill University.

211. Ye, J. and X. Wang, *Piecewise Function Hysteretic Model for Cold-Formed Steel Shear Walls with Reinforced End Studs.* Applied Sciences, 2017. **7**(1): p. 94.

212. Pang, W.C., et al., *Evolutionary Parameter Hysteretic Model for Wood Shear Walls.* Journal of Structural Engineering, 2007. **133**(8): p. 1118-1129.

213. Folz, B. and A. Filiatrault, *CASHEW—Version 1.0: A computer program for cyclic analysis of wood shear walls.* Richmond, California, 2000.

214. Folz, B. and A. Filiatrault, *SAWS—Seismic analysis of woodframe structures*. 2002.

215. Lowes, L.N., N. Mitra, and A. Altoontash, *A Beam-column Joint Model for Simulating the Earthquake Response of Reinforced Concrete Frames*. 2004: Pacific Earthquake Engineering Research Center, College of Engineering, University of California.

216. Robert K. Dowell, F.S. and L.W. Edward, *Pivot Hysteresis Model for Reinforced Concrete Members.* Structural Journal, 1998. **95**(5).

217. Ariyanayagam, A.D. and M. Mahendran, *Numerical modelling of load bearing light gauge steel frame wall systems exposed to realistic design fires.* Thin-Walled Structures, 2014. **78**: p. 148-170.

218. Gunalan, S. and M. Mahendran, *Finite element modelling of load bearing cold-formed steel wall systems under fire conditions.* Engineering Structures, 2013. **56**: p. 1007-1027.

219. Kyvelou, P., L. Gardner, and D.A. Nethercot, *Finite element modelling of composite cold-formed steel flooring systems.* Engineering Structures, 2018. **158**: p. 28-42.

220. Selvaraj, S. and M. Madhavan, *Investigation on sheathing effect and failure modes of gypsum sheathed cold-formed steel wall panels subjected to bending.* Structures, 2018.

221. Hibbitt, Karlsson, and Sorensen, *ABAQUS/Explicit: user's manual.* Vol. 1. 2001: Hibbitt, Karlsson and Sorenson Incorporated.

222. DeSalvo, G.J. and J.A. Swanson, *ANSYS user's manual.* Swanson Analysis Systems, 1989.

223. CSI, S.V., *8, 2002. Integrated Finite Element Analysis and Design of Structures Basic Analysis Reference Manual.* Computers and Structures, Inc., Berkeley, California, USA, 2010.

224. Borzoo, S., et al., *Nonlinear finite element modeling of steel-sheathed cold-formed steel shear walls.* Steel and Composite Structures, 2016. **22**(1): p. 79-89.

225. Hatami, S., et al., *A Numerical Study on Response Modification Factor of CFS Walls Sheathed with Steel Sheets.* Journal of Engineering Science & Technology Review, 2017. **10**(2).

226. Dai, X., *Numerical modelling and analysis of structural behaviour of wall-stud cold-formed steel shear wall panels under in-plane monotonic loads.* Journal of Civil Engineering Research, 2012. **2**(5): p. 31-41.

227. Dai, X., *Structural Behaviour of Cold-formed Steel Cassette Wall Panels Subject to In-plane Shear Load.* Journal of Civil Engineering Research, 2013. **3**(2): p. 65-74.

228. Ngo, H.H., *Numerical and experimental studies Of wood sheathed cold-formed steel framed shear walls.* 2014: Master Thesis, Johns Hopkins University.

229. Ding, C., *Monotonic and Cyclic Simulation of Screw-Fastened Connections for Cold-Formed Steel Framing.* 2015, Master Thesis, Virginia Polytechnic Institute and State University.

230. Henriques, J., et al., *Structural performance of light steel framing panels using screw connections subjected to lateral loading.* Thin-Walled Structures, 2017. **121**: p. 67-88.

231. Gad, E., et al. *Modelling of plasterboard lined domestic steel frames when subjected to lateral loads.* in *Proceedings of the 15th Australasian Conference on the Mechanics of Structures and Materials, University of Melbourne, Australia.* 1997.

232. Fülöp, L.A. and D. Dubina, *Design Criteria for Seam and Sheeting-to-Framing Connections of Cold-Formed Steel Shear Panels.* Journal of Structural Engineering, 2006. **132**(4): p. 582-590.

233. Xuhong, Z., et al. *Study On Shear Resistance Of Cold-Formed Steel Stud Walls In Residential Structure.* 2006. Dordrecht: Springer Netherlands.

234. Hatami, S., et al., *A parametric study on seismic characteristics of cold-formed steel shear walls by finite element modeling.* Advanced Steel Construction, 2014. **10**(1): p. 53-71.

235. Zeynalian, M., *Numerical Study on Seismic Performance of Cold Formed Steel Sheathed Shear Walls.* Advances in Structural Engineering, 2015. **18**(11): p. 1819-1829.

236. Zeynalian, M., *Structural performance of cold-formed steel-sheathed shear walls under cyclic loads.* Australian Journal of Structural Engineering, 2017. **18**(2): p. 113-124.

237. Abu-Hamd, M., M. Abdel-Ghaffar, and B. El-Samman, *Computational Study of Cold-Formed-Steel X-Braced Shear Walls.* Advances in Civil Engineering, 2018. **2018**: p. 11.

238. Martínez-Martínez, J. and L. Xu, *Simplified nonlinear finite element analysis of buildings with CFS shear wall panels.* Journal of Constructional Steel Research, 2011. **67**(4): p. 565-575.

239. Martinez Martinez, J., *Seismic performance assessment of multi-storey buildings with cold formed steel shear wall systems.* 2007, PhD Thesis, University of Waterloo: Canada.

240. Dolan, J.D. and R.O. Foschi, *Structural Analysis Model for Static Loads on Timber Shear Walls.* Journal of Structural Engineering, 1991. **117**(3): p. 851-861.

241. Serrette, R.L., et al., *Static Racking Behavior of Plywood, OSB, Gypsum, and FiberBond Walls with Metal Framing.* Journal of Structural Engineering, 1997. **123**(8): p. 1079-1086.

242. Selvaraj, S. and M. Madhavan, *Studies on Cold-Formed Steel Stud Panels with Gypsum Sheathing Subjected to Out-of-Plane Bending.* Journal of Structural Engineering, 2018. **144**(9): p. 04018136.

243. Javaheri-Tafti, M.R., et al., *An experimental investigation on the seismic behavior of cold-formed steel walls sheathed by thin steel plates.* 2014. **80**: p. 66-79.

244. Kamaya, M. and M. Kawakubo, *True stress–strain curves of cold worked stainless steel over a large range of strains.* Journal of Nuclear Materials, 2014. **451**(1): p. 264-275.

245. Cabezas, E.E. and D.J. Celentano, *Experimental and numerical analysis of the tensile test using sheet specimens.* Finite Elements in Analysis and Design, 2004. **40**(5): p. 555-575.

246. Pham, C.H. and G.J. Hancock, *Numerical simulation of high strength cold-formed purlins in combined bending and shear.* Journal of Constructional Steel Research, 2010. **66**(10): p. 1205-1217.

247. Laím, L. and J.P.C. Rodrigues, *Numerical analysis on axially-and-rotationally restrained cold-formed steel beams subjected to fire.* Thin-Walled Structures, 2016. **104**: p. 1-16.

248. Schafer, B.W. and T. Peköz, *Computational modeling of cold-formed steel: characterizing geometric imperfections and residual stresses.* Journal of Constructional Steel Research, 1998. **47**(3): p. 193-210.

249. Ranawaka, T. and M. Mahendran, *Numerical modelling of light gauge cold-formed steel compression members subjected to distortional buckling at elevated temperatures.* Thin-Walled Structures, 2010. **48**(4): p. 334-344.

250. Quach, W.M., J.G. Teng, and K.F. Chung, *Residual stresses in steel sheets due to coiling and uncoiling: a closed-form analytical solution.* Engineering Structures, 2004. **26**(9): p. 1249-1259.

251. Wang, H. and Y. Zhang, *Experimental and numerical investigation on cold-formed steel C-section flexural members.* Journal of Constructional Steel Research, 2009. **65**(5): p. 1225-1235.

252. Zhang, J.-H. and B. Young, *Numerical investigation and design of cold-formed steel built-up open section columns with longitudinal stiffeners.* Thin-Walled Structures, 2015. **89**: p. 178-191.

253. Sadovský, Z., et al., *Computational modelling of geometric imperfections and buckling strength of cold-formed steel.* Journal of Constructional Steel Research, 2012. **78**: p. 1-7.

254. Hibbit, D., B. Karlsson, and P. Sorensen, *ABAQUS/Standard analysis user's manual, version 6.13.* Providence, RI: Dassault Systèmes/Simulia, 2013.

255. Usefi, N., et al. *Macro/micro analysis of cold-formed steel members using ABAQUS and OPENSEES.* in *Volume of Abstracts, Proceedings of the 13th International Conference on Steel, Space and Composite Structures (SS18).* 2018.

256. Usefi, N., H. Ronagh, and P. Sharafi, *Lateral performance of a new hybrid CFS shear wall panel for mid-rise construction.* Journal of Constructional Steel Research, 2020. **168**: p. 106000.

257. Usefi, N. and H. Ronagh, *Seismic characteristics of hybrid cold-formed steel wall panels.* Structures, 2020. **Doi:10.1016/j.istruc.2020.06.033**

258. Shariati, M., et al., *Numerical study on the structural performance of corrugated low yield point steel plate shear walls with circular openings.* Steel and Composite Structures, 2019. **33**(4): p. 569-581.

259. Taheri, E., et al., *Investigation of a Method for Strengthening Perforated Cold-Formed Steel Profiles under Compression Loads.* Applied Sciences, 2019. **9**(23): p. 5085.

260. Taheri, E., et al., *Experimental and Numerical Investigation of a Method for Strengthening Cold-Formed Steel Profiles in Bending.* 2020. **10**(11): p. 3855.

261. *AISI-S400, North American standard for seismic design of cold-formed steel structural systems,.* 2015, American Iron and Steel Institute.

262. *FEMA P-58-5, Seismic Performance Assessment of Buildings, Volume 5 – Expected Seismic Performance of Code-Conforming Buildings.* 2018, Federal Emergency Management Agency.

263. *ASCE/SEI 7, Minimum design loads and associated criteria for buildings and other structures.* 2016, American Society of Civil Engineers.

264. Brire, V., *Higher Capacity Cold-Formed Steel Sheathed and Framed Shear Walls for Mid-Rise Buildings: Part 2, Research report RP17-6.* 2018: American Iron and Steel Institute.

265. Rohden, A.B. and M.R. Garcez, *Increasing the sustainability potential of a reinforced concrete building through design strategies: Case study.* Case Studies in Construction Materials, 2018. **9**: p. e00174.

266. Ighravwe, D.E. and S.A. Oke, *A multi-criteria decision-making framework for selecting a suitable maintenance strategy for public buildings using sustainability criteria.* Journal of Building Engineering, 2019. **24**: p. 100753.

267. Awadh, O., *Sustainability and green building rating systems: LEED, BREEAM, GSAS and Estidama critical analysis.* Journal of Building Engineering, 2017. **11**: p. 25-29.

268. Balasbaneh, A.T., A.K.B. Marsono, and S.J. Khaleghi, *Sustainability choice of different hybrid timber structure for low medium cost single-story residential building: Environmental, economic and social assessment.* Journal of Building Engineering, 2018. **20**: p. 235-247.

269. CIB, A., *on Sustainable Construction.* CIB Report Publication. **237**.

270. Bourdeau, L., *Sustainable development and the future of construction: a comparison of visions from various countries.* Building Research & Information, 1999. **27**(6): p. 354-366.

271. An, J.H., et al., *Sustainable design model for analysis of relationships among building height, CO2 emissions, and cost of core walls in office buildings in Korea.* Building and Environment, 2019. **150**: p. 289-296.

272. Dwaikat, L.N. and K.N. Ali, *Green buildings life cycle cost analysis and life cycle budget development: Practical applications.* Journal of Building Engineering, 2018. **18**: p. 303-311.

273. Morrissey, J. and R.E. Horne, *Life cycle cost implications of energy efficiency measures in new residential buildings.* Energy and Buildings, 2011. **43**(4): p. 915-924.

274. Alsayed, M.F. and R.A. Tayeh, *Life cycle cost analysis for determining optimal insulation thickness in Palestinian buildings.* Journal of Building Engineering, 2019. **22**: p. 101-112.

275. Flanagan, R. and C. Jewell, *Whole life appraisal for construction.* 2008: John Wiley & Sons.

276. Sterner, E., *Reconciling theory and practice of life-cycle costing AU - Cole, Raymond J.* Building Research & Information, 2000. **28**(5-6): p. 368-375.

277. Ahmed, I.M. and K.D. Tsavdaridis, *Life cycle assessment (LCA) and cost (LCC) studies of lightweight composite flooring systems.* Journal of Building Engineering, 2018. **20**: p. 624-633.

278. Sharif, S.A. and A. Hammad, *Simulation-Based Multi-Objective Optimization of institutional building renovation considering energy consumption, Life-Cycle Cost and Life-Cycle Assessment.* Journal of Building Engineering, 2019. **21**: p. 429-445.

279. Panteli, C., et al., *A framework for building overhang design using Building Information Modeling and Life Cycle Assessment.* Journal of Building Engineering, 2018. **20**: p. 248-255.

280. Gilchrist, A. and E.N. Allouche, *Quantification of social costs associated with construction projects: state-of-the-art review.* Tunnelling and Underground Space Technology, 2005. **20**(1): p. 89-104.

281. Çelik, T., S. Kamali, and Y. Arayici, *Social cost in construction projects.* Environmental Impact Assessment Review, 2017. **64**: p. 77-86.

282. Van, K. and L. Xu, *A life-cycle assessment of cold-formed steel enclosures verses alternative enclosures in commerical buildings.* 2010.

283. Usefi, N., et al. *Macro/micro analysis of cold-formed steel members using ABAQUS and OPENSEES.* in *Volume of Abstracts: 13th International Conference on Steel, Space and Composite Structures (SS18), 31 January-2 February 2018, The University of Western Australia, Perth, Australia.* 2018.

284. Shafaei, S., H. Ronagh, and N. Usefi. *Experimental evaluation of CFS braced-truss shear wall under cyclic loading.* in *Advances in Engineering Materials, Structures and Systems: Innovations, Mechanics and Applications: Proceedings of the 7th International Conference on Structural Engineering, Mechanics and Computation (SEMC 2019), September 2-4, 2019, Cape Town, South Africa.* 2019. CRC Press.

285. Mortazavi, M., *Lateral capacity and seismic characteristic of hybrid cold formed and hot rolled steel systems.* 2019.

286. Wilson, E.L., J. Hollings, and H.H. Dovey, *ETABS: Three Dimensional Analysis of Building Systems (extended Version).* 1979: National Information Service for Earthquake Engineering/Computer ….

287. *American National Standard Institute/American Institute of Steel Construction (ANSI/AISC) ANSI/AISC360-16: Specification for Structural Steel Buildings.* 2016: 130 East Randolph Street, Chicago, Illinois, USA.

288. Kanyilmaz, A., et al., *Experimental assessment of the seismic behavior of unbraced steel storage pallet racks.* Thin-Walled Structures, 2016. **108**: p. 391-405.

289. Mahmoudi, F., et al., *Experimental study of steel moment resisting frames with shear link.* Journal of Constructional Steel Research, 2019. **154**: p. 197-208.

290. Asgarian, B., A. Sadrinezhad, and P. Alanjari, *Seismic performance evaluation of steel moment resisting frames through incremental dynamic analysis.* Journal of Constructional Steel Research, 2010. **66**(2): p. 178-190.

291. Ahmadi, O., J.M. Ricles, and R. Sause, *Modeling and seismic collapse resistance study of a steel SC-MRF.* Soil Dynamics and Earthquake Engineering, 2018. **113**: p. 324-338.

292. Zhou, X., et al., *A simplified method to evaluate the flexural capacity of lightweight cold-formed steel floor system with oriented strand board subfloor.* Thin-Walled Structures, 2019. **134**: p. 40-51.

293. Dizdar, Ç., E. Baran, and C. Topkaya, *Strength and stiffness of floor trusses fabricated from cold-formed steel lipped channels.* Engineering Structures, 2019. **181**: p. 437-457.

294. Zhang, S. and L. Xu, *Determination of equivalent rigidities of cold-formed steel floor systems for vibration analysis, Part I: Theory.* Thin-Walled Structures, 2018. **132**: p. 25-35.

295. Xu, L., S. Zhang, and C. Yu, *Determination of equivalent rigidities of cold-formed steel floor systems for vibration analysis, Part II: evaluation of the fundamental frequency.* Thin-Walled Structures, 2018. **132**: p. 1-15.

296. Kyvelou, P., L. Gardner, and D.A. Nethercot, *Design of Composite Cold-Formed Steel Flooring Systems.* Structures, 2017. **12**: p. 242-252.

297. Lakkavalli, B.S. and Y. Liu, *Experimental study of composite cold-formed steel C-section floor joists.* Journal of Constructional Steel Research, 2006. **62**(10): p. 995-1006.

298. Majdi, Y., C.-T.T. Hsu, and M. Zarei, *Finite element analysis of new composite floors having cold-formed steel and concrete slab.* Engineering Structures, 2014. **77**: p. 65-83.

299. *In-Plane Behaviour Of Composite Cold-Formed Truss Floors.* 2018 [cited 2018; Available from: https://www.westernsydney.edu.au/cie/research/Student_Project_In-Plane_Behaviour_Of_Composite_Cold-Formed_Truss_Floors.

300. Javidan, M.M. and J. Kim, *Variance-based global sensitivity analysis for fuzzy random structural systems.* Computer-Aided Civil and Infrastructure Engineering. **0**(0).

301. Shayanfar, M.A. and M.M. Javidan, *Progressive Collapse-Resisting Mechanisms and Robustness of RC Frame Shear Wall Structures.* Journal of Performance of Constructed Facilities, 2017. **31**(5): p. 04017045.

302. Ahmadi, R., et al., *Experimental and Numerical Evaluation of Progressive Collapse Behavior in Scaled RC Beam-Column Subassemblage.* Shock and Vibration, 2016. **2016**: p. 17.

303. Javidan, M.M. and J. Kim, *Seismic Retrofit of Soft-First-Story Structures Using Rotational Friction Dampers.* Journal of Structural Engineering, 2019. **145**(12): p. 04019162.

304. Athena, S., *Impact Estimator for Buildings.* Available fromathenasmi. org/our-software-data/overview, 2009.

305. MacLeay, I., *Digest of United Kingdom energy statistics 2010.* 2010: The Stationery Office.

306. Johnston, R.P.D., et al., *Sustainability of Cold-formed Steel Portal Frames in Developing Countries in the Context of Life Cycle Assessment and Life Cycle Costs.* Structures, 2018. **13**: p. 79-87.

307. Ogershok, D., G. Moselle, and R. Pray, *National construction estimator.* 2019: Craftsman Book Co.

308. *Metal Supermarkets.* Available from: https://ecommerce.metalsupermarkets.com.

309. *OnlineMetals.* Available from: Available from: https://www.onlinemetals.com.

310. *Home Depot Product.* Available from: http://www.homedepot.com.

311. Sharafi, P., et al., *Form finding for rectilinear orthogonal buildings through charged system search algorithm.* International Journal of Optimization in Civil Engineering, 2017. **7**(1): p. 129-142.

312. Rahman, S., D.J. Vanier, and L.A. Newton, *MIIP Report: Social Cost Considerations for Municipal Infrastructure Management*, in *Client Report (National Research Council Canada. Institute for Research in Construction); no. B-5123.8*. 2005, National Research Council Canada.

313. Burgan, B.A. and M.R. Sansom, *Sustainable steel construction.* Journal of Constructional Steel Research, 2006. **62**(11): p. 1178-1183.

314. Sharafi, P., M.N. Hadi, and L.H. Teh, *Optimum column layout design of reinforced concrete frames under wind loading*, in *Topics on the Dynamics of Civil Structures, Volume 1*. 2012, Springer. p. 327-340.

315. Invidiata, A., M. Lavagna, and E. Ghisi, *Selecting design strategies using multi-criteria decision making to improve the sustainability of buildings.* Building and Environment, 2018. **139**: p. 58-68.